Effect of Fuel Chemistry and Physical Influences on Low Temperature Heat Release

A thesis submitted in partial fulfilment of the requirements for the degree of Doctor of Philosophy

Samuel Philip White

Keble College

Supervisor: Professor Felix C P Leach

Department of Engineering Science

University of Oxford

Hilary Term 2024

Abstract

Most passenger vehicles are powered by internal combustion engines (ICE), which emit CO_2 and contribute to global warming. Despite this, ICEs are forecasted to be used for decades to come, hence their CO_2 impact must be reduced urgently. Three viable options for achieving this are extending the knocking limit, using advanced combustion strategies and using low carbon fuels.

Low Temperature Heat Release (LTHR) is the phenomenon in which some of the fuel-air mixture undergoes a slower, exothermic reaction at relatively lower temperatures, producing intermediate species prior to the main combustion event. LTHR can be seen in fuels that exhibit two-stage autoignition, due to their negative temperature coefficient characteristics. It has mostly be studied in homogeneous charge compression ignition (HCCI) engines, but recently it has been observed in spark ignition (SI) engines where it is termed pre-spark heat release (PSHR). Understanding and controlling LTHR has the potential to contribute to extending the knocking limit and enabling advanced combustion strategies though this would be highly dependant on fuel choice and its individual LTHR behaviour.

This thesis presents a methodology to isolate LTHR in SI engines, paving the way for new studies of many parameters that previously were not accessible. The effect of pressure, temperature and engine speed on isolated LTHR were investigated. For LTHR to occur, cylinder pressures must be high enough, cylinder temperatures must fall within the LTHR region and engine speed must be low enough to provide enough time for LTHR to occur. The effect of equivalence ratio on LTHR is also investigated. Heat released from LTHR in a direct injection engine is found to increase linearly with equivalence ratio, up until the point where charge cooling reduced cylinder temperatures below the LTHR threshold.

The LTHR behaviour of binary blends of n-heptane, iso-octane and ethanol is explored. Ethanol is shown to strongly inhibit LTHR by increasing competition for hydroxyl radicals which would otherwise initiate the low temperature oxidation of n-heptane or iso-octane. Combustion residuals, specifically nitric oxide is shown to strongly inhibit LTHR in iso-octane. It is also found that popular chemical kinetic mechanisms were unable to model the behaviour of nitric oxide and iso-octane at temperature relevant to LTHR.

Finally, an optically accessible SI engine is used to show formaldehyde planar laser-induced fluorescence (PLIF) signal intensity under motored conditions is well correlated to cumulative isolated LTHR intensity. An alternative ignition method using four side-mounted spark plugs is implemented to generate end gas close to the cylinder axis. This enabled measurement of LTHR within the end gas during the deflagration process of a SI engine, demonstrating the utility of formaldehyde PLIF to optically measure LTHR under conditions where pressure-based diagnostics cannot isolate the contribution of LTHR.

Contents

Nomenclature

°CA	Crank angle degrees
CA50	CA location at 50% heat release point
CI	Compression ignition
CO	Carbon monoxide
EGR	Exhaust gas recirculation
GDI	Gasoline direct injection
HCCI	Homogenous charge compression ignition
HTHR	High temperature heat release
ICE	Internal combustion engine
KLSA	Knock-limited spark advance
LTHR	Low temperature heat release
MON	Motor octane number
NO	Nitric oxide
NO_2	Nitrogen dioxide
NO_x	Oxides of nitrogen
NTC	Negative temperature coefficient
PLIF	Planar laser-induced fluorescence
PRF	Primary reference fuel
PSHR	Pre-spark heat release
RON	Research octane number
SI	Spark ignition
TDC	Top dead centre
ϕ	Fuel-air equivalence ratio

Acknowledgements

First and foremost, my sincere thanks go to Professor Felix Leach for his advice, guidance, expertise, and mentorship not just over the course of this project but also since I joined the university as an undergraduate in 2016. I am particularly grateful for his extraordinarily speedy and helpful feedback on the thesis and paper drafts. It goes without saying that this project would not have been possible without his support.

Secondly, my thanks go to Abdullah Bajwa, a colleague, friend and collaborator. Many of the experiments in this project would not have been possible without his help. Likewise, I would like to thank Chris Willman for experimental support, sharing his expertise on optics and beyond—and for guidance as cover supervisor.

Within the TPSRG, I would like to give special thanks to Varun, Sam Baker, Tejo, Ruixuan, Qichi, Dan and Priyav for the encouragement, support and for the many friendships that have formed. I would also like to thank Kharthik, Maruthi, Hannah, Niko, Sam Shen, Leo and Laurent for their advice throughout this project.

I am grateful to Professor Richard Stone for sharing his expertise, and wisdom and providing practical support with experiments—even into his retirement. Our research group is very lucky to have him. I would also like to thank Professor Ben Williams for advice and support on optical diagnostic matters and Professor Martin Davy for his role in running the research group.

I am grateful for the support I have received from staff in the Department of Engineering Science, in particular Dave Ilsley, Greg Maddock, and all of the Maintenance team; Duncan Constable and Lewis Burke in the workshop and Sukarni Wheeler for her friendly and efficient administrative support.

I would like to thank the Engineering and Physical Sciences Research Council and JLR (formerly Jaguar Land Rover), for providing the funding and opportunity to undertake the DPhil. I would also like to express my thanks to the Keble Association and Edgell Sheppee Fund for funding conference travel, giving me the opportunity to present my work, build my network and further my career. I would like to acknowledge the John Fell Oxford University Press Research Fund for funding some of the equipment required for my experimental work. I am grateful to Keble College, Balliol College, Jesus College and New College for fantastic and generous opportunities to teach alongside my research.

I would like to thank all of my friends from school, my time at university and beyond. Last but not least, I would like to thank my Mum, Dad and brother Ben, for all of their support and encouragement, and Emily for her unwavering support, enthusiasm and patience at every stage of the journey.

Chapter 1

Introduction

1.1 Background and Motivations

1.1.1 CO_2 Emissions From Internal Combustion Engines

Global warming, contributed to by CO_2 emissions from burning fossil fuels poses a significant threat to society. Despite this fossil fuel-powered vehicles make up the vast majority of light-duty passenger vehicles around the world[1]. Carbon dioxide (CO_2) is a product of complete combustion of hydrocarbon fuels; it is a greenhouse gas, and accumulates in the atmosphere, contributing to global warming[2,3]. CO_2 emissions cannot be removed from the tailpipe of ICEs without moving to carbon-free fuels such as hydrogen or ammonia; nevertheless, CO_2 emissions should be reduced as much as possible, by reducing energy demand from vehicles and improving the efficiency of ICEs. In recent years, the EU has mandated reductions in fleet CO_2 emissions, encouraging higher efficiency vehicles[4].

In the face of growing electric vehicle sales, and increasingly bad press, it is important to justify the continued development of the ICEs and their fuels. Its low cost, development history and use of energy-dense fuels mean that the internal combustion engine is not going away. Aside from the decline caused by the global pandemic, global passenger vehicle sales continue to grow, with the vast majority containing an internal combustion engine. This is particularly relevant in low- and middle-income countries, where electric vehicle subsidies are not available and ICE vehicles are the only feasible choice[1].

Looking ahead, BloombergNEF predicts the global passenger vehicle fleet to contain around 900 million ICE powered vehicles in 2040[5]. Furthermore, the cars sold in 2040 will have a lasting legacy. In the EU, the average age of the passenger car fleet is currently 11.5 years[6], with some vehicles on the road being significantly older. In the UK the current fleet of personal vehicles has an average age of 8 years, with each vehicle being scrapped, on average, after 14 years[7]. Despite their current environmental impact, liquid-fuelled ICEs are likely to be around for the long run; the need to further improve them is clear.

The pressing need to reduce the environmental impact of the existing ICE fleet has given rise to a global sentiment of a shift away from fossil-derived liquid hydrocarbon fuels to alternative fuels, which can be produced synthetically or from biomass. With this shift, the chemical composition of fuel blends will inevitably change, giving rise to an opportunity to optimise the choice of fuel, fuel properties and ICE design to maximise overall efficiency. Choosing the right fuel requires a complete and fundamental understanding of fuel behaviours and fuel properties. This work aims to further the current understanding in this area.

1.1.2 Recent Improvements to Internal Combustion Engines

Throughout history, engineers and researchers have continuously sought to improve the efficiency of internal combustion engines and reduce emissions. This section will outline various techniques employed so to do and will focus specifically on gasoline-powered ICEs, for light-duty vehicles.

A combination of boosting and downsizing has become increasingly widespread in recent years. Downsizing involves achieving a given load for a smaller displacement engine; this moves the operating point to higher in the engine map, opening up the throttle for a given torque requirement, avoiding losses associated with throttling. To achieve successful downsizing, a form of boosting is often employed[3,8]. This is where inlet air is compressed into order to increase mass flow rate of air into the cylinder. Increasing the amount of air in the cylinder allows for an accompanying increase in fuel available for a given equivalence ratio, enabling increased power output for the same displacement[3,9]. Boosting is achieved with either a supercharger a turbocharger (or in some cases, both). Superchargers are directly connected to the engine, whilst turbochargers use a turbine to recover energy from hot exhaust gases at a cost of increased back pressure and hence increased pumping work[3]. Boosting alone can often lead to efficiency gains (though it is not guaranteed) since not all losses are proportional to power output.[8,10]

Historically, internal combustion engines used carburettors to prepare the charge mixture. Since then, fuel injection has become widely adopted, with a recent shift to direct injection in contrast to port fuel injection in order to increase performance and fuel economy. With direct injection, only air is drawn into the cylinder during the compression stroke, this improves volumetric efficiency. The injection also has a cooling effect, ultimately resulting in reduced end-gas temperature during combustion and reduced likelihood of knocking[3]. The injection process introduces charge motion in the cylinder, allowing for improved mixing, leading to reduced combustion variability. The improved control of direct injection allows for charge stratification in the cylinder, which can enable efficiency improvements and or pollutant emissions reductions. Throttling is reduced to give an overall lean mixture, whilst ignitability is preserved by increasing the equivalence ratio near to the spark[11]. Direct injection can be affected by deposit build-up on the injector, resulting in poorer control of the charge. Additionally, if these deposits ignite before the spark, the system may be subject to low speed preigni-

tion. Poor atomisation can lead to increased soot and particulate emissions, though this can often be mitigated with increased injection pressure.[11,12]

Increasing the expansion ratio of an engine allows for more work to be extracted from the expansion stroke. However, in a traditional Otto cycle engine, the expansion ratio is equal to the compression ratio, which is typically knock-limited and requires a non-negligible amount of compression work. In 1882 James Atkinson designed a cycle with unequal compression and expansion ratios. This can be emulated in a modern ICE by employing unconventional valve timing. Early or late intake valve closure both have the effect of reducing the volume of air trapped in the cylinder[13]. This process is also referred to as a miller cycle when boosting is employed[14]. Whilst this method ultimately reduces power output, it increases efficiency, making it suitable for lower loads.

More recently, cylinder deactivation techniques have been employed in consumer vehicles. Cylinder deactivation increases efficiency by increasing specific load and hence the operating point on the remaining cylinders, leading to reduced throttling losses and reduced engine friction[8]. Some implementations of cylinder deactivation uses a solenoid actuator to switch the cam profile of certain cylinders, effectively closing the valves, whilst other techniques involve dynamically skipping different cylinders every cycle according to real-time demand.[15]

Over the last two decades, hybrid vehicles have become increasingly widespread, to the point where many manufacturers offer some form of hybrid version of the majority of their fleet. As well as hybrid vehicle's ability to utilise energy from regenerative breaking, the electric motors allow the vehicle to decouple the drive cycle from the engine, narrowing the operating range that the engine is exposed to, and enabling the engine to run at a higher efficiency operating point for a given set of conditions[8].

Exhaust Gas Recirculation (EGR) can be employed to reduce emissions and reduce part load fuel consumption. Recirculating some of the exhaust gases back to the intake dilutes the oxygen and provides inert gas for the next combustion cycle[16]. The dilution lowers flame temperatures and therefore reduces NO_x emissions; a small EGR percentage (5-10%) can half NO_x emissions in some cases[3]. EGR is often cooled to increase its density so that the same volume fraction makes up a greater mass-wise portion of the charge. EGR changes the ratio of specific heats for the working gas. EGR slows combustion speeds, so it is typically limited by combustion stability. EGR can increase wear rates, especially in the absence of a low sulphur fuel[17,18].

To summarise, the internal combustion engine has already undergone an enormous amount of development. However, there is still a clear need to transition away from fossil fuels, and minimise their consumption in the meantime. As fuels and fuel blends change, it is important to ensure that the latest ICE technologies—such as those highlighted in this section—are compatible with and optimised for the alternative fuels of the future.

1.2 Reducing CO_2 Emissions of Internal Combustion Engines

It is evident that enormous progress has been made on ICE efficiency to this date, but further improvements are essential to help reduce its contribution to global warming as rapidly as possible. The overall CO_2 emissions of gasoline-powered light-duty vehicles can be reduced by increasing ICE efficiency, either with advanced combustion techniques or extending the knocking limit, and using fuels and fuel sources that are less carbon-intensive[19]. This section will elaborate on these three strategies.

1.2.1 Low Carbon Fuels

There is a vast range of alternative ICE fuels, each with its own strengths and challenges. This section will discuss the most important factors to consider when choosing and comparing alternative fuels and outline some possible alternatives to fossil fuels.

Choosing the Right Fuel

Cost is very often the deciding factor for the selection of energy source when working on large scales, however, it is very difficult to use price to quantify and compare fuels. A huge number of factors influence the consumer price of fuel, including taxes and duties, transport costs, short timescale supply and demand fluctuations as well as political and economic reasons. The wholesale price of oil is no better an indicator of true cost, as it is subject to many of the same forces as pump price.

The compatibility of any potential alternative fuel with current ICEs is another important factor, due to their prevalence and the decades of research behind them. Any cost or complexity of conversion to an alternative fuel represents a boundary to widespread adoption. So-called drop-in fuels, fuels that can be used interchangeably or blended with current fuels in existing engines, are desirable as they ease the transition away from fossil fuels without forcing consumers to commit to a new type of fuel. Factors that affect fuel compatibility typically include flammability, resistance to knocking (covered in greater detail in Section 1.2.3), emissions performance and effects on component wear. Energy density (both by mass and by volume) is another highly important factor when determining which fuel, or energy carrier, to use in automotive applications. Whilst, per joule, electricity can be cheaper than liquid fuels, gasoline and diesel's high energy densities explain why they have dominated the automotive market for nearly a century—they are easy to transport both to, and on-board, the vehicle.

Finally, supply and infrastructure are important considerations when choosing an energy source. There must be a stable and sufficient supply of the fuel. Supply of the feedstock should not impact land usage for growing food crops, for example. Infrastructure is essential to enable consumption of the fuel; hydrogen fuel cell use is held back by the lack of refuelling stations, for example.

Since ICEs are capable of being fuelled by an almost infinite number of different fuels and fuel blends, the considerations above can be used to narrow down the choice of a future fuel to something feasible and compatible with production and practical applications. With the above considerations in mind, two important streams of alternative fuels are outlined below.

Biofuels

Biofuels are fuels derived from biomass (which can be anything from sugar crops to used cooking oil to waste from agriculture[20]) and contains carbon originating from CO_2 absorbed from the atmosphere during photosynthesis. Whilst biofuels are often thought to be carbon neutral due to the CO_2 absorbed by biological processes, any additional processing will require energy and therefore potentially net CO_2 emissions, which must be taken into account. Examples of commercially used biofuels include biodiesel (which is primarily fatty acid methyl esters), biomethane (for compressed or liquefied natural gas engines) and alcohols[20].

Ethanol is the most most commonly used biofuel in spark ignition engines, it can be derived from biomass feedstock sources, typically plants such as wheat, sugar beet, corn, straw, and wood[21]. Its uptake is increasing due to its ability to aid decarbonisation and reduce fossil fuel reliance in the existing vehicle fleet, for example in the UK where standard gasoline moved from E5 to E10 (i.e. 5 to 10% vol ethanol) in 2021, with many modern SI vehicles capable of accepting higher. In some markets, levels up to 85% (E85) are accepted in so-called flex fuel vehicles and in Brazil 100% ethanol is common. Despite its slightly lower energy density, ethanol is a suitable candidate for a drop-in fuel blend component, up to a certain volume, it can displace crude oil fractions thanks to its high octane rating and lower combustion temperatures—this allows for higher efficiency through the use of high compression ratios and optimised ignition timing, and reduced emissions[19,22,23].

E-fuels

E-fuels are synthetic fuels that can be created using excess renewable energy from the fluctuations in supply from electrical grid; they are effectively an energy storage mechanism in the form of a drop-in fuel. The term e-fuel covers a broad range compounds, from hydrogen and methane to butanol. E-fuels benefit from the flexibility in their synthesis, fuels can be created that perform better than fossil derived fuels across a variety of parameters. For example, a recent synthetic fuel developed by Porsche nearly eliminated soot formation[24]. However, e-fuels suffer from the high energy requirements of their production, leading to poor overall conversion efficiency, especially when compared to battery or fuel cell vehicles[25].

The need to reduce CO_2 emissions is clear, and whilst fossil fuels are being phased out, ICEs will be around for decades to come. The ICE has been thoroughly developed this will continue as sources of fuels change.

This change in fuels and fuel sources opens up an opportunity for ICE development that use techniques that previously weren't suitable for legacy fuels.

1.2.2 Advanced Combustion Techniques

This section introduces combustion techniques that are more complex than spark ignition and compression ignition operation that have recently been or are currently being investigated for their potential efficiency or pollutant emissions performance. The focus of the selection of techniques presented reasonable compatibility with gasoline or gasoline-like fuels.

Homogeneous Charge Compression Ignition

(HCCI) uses autoignition to ignite a near-homogeneous mixture. HCCI engines were developed with the aim to improve efficiency and emission over typical SI (spark ignition) and CI (compression ignition) engines by limiting throttling losses and soot emissions The lower flame temperature of HCCI operation leads to reduced production of soot and NO_x emissions compared to standard diesel CI. HCCI operations requires careful control of peak temperatures and pressures. As well as non-homogeneous mixing, residuals are used to limit peak temperature and pressure.

The main drawback of HCCI is that it is very difficult to control the point of ignition, as it lacks a fully controllable external trigger such as spark timing or injection timing. There are a number of ways that ignition can be influenced. Control of charge temperature at induction can be effective however it is impractical in real-world applications. Air to fuel ratio can be controlled. Compression ratio can be controlled, either with a variable compression chamber, or controlling inlet valve timing. Valve timing can also be used to control levels of residuals and hence the reactivity and temperature of the mixture [3]. The high level of residuals required for HCCI operation limit the load, and therefore its effectiveness in real-world applications that require a wide range of operating conditions.

Reactivity controlled compression ignition (RCCI) is an extension of HCCI that uses an injection of high reactivity fuel to initiate combustion. It is effectively HCCI with a pilot injection of a fuel such as diesel that is used to give far greater control over combustion phasing, temperatures, power output and emissions [26].

Controlled End Gas Autoignition

Autoignition can be taken advantage of when used in conjunction with spark ignition. End-gas is the last portion of unburned fuel in a combustion chamber. When the mixture is lean or stratified, the end-gas can be difficult to ignite—this is where autoignition can be exploited if controlled effectively.

Whilst not an advanced combustion technique in its own right, many modern advanced combustion techniques increasingly rely on controlled autoignition of the unburnt mixture (end gas), which is often triggered by initial deflagration from spark ignition [27–30], this goes by many names though it is perhaps most commonly referred to as spark-assisted compression ignition (SACI). For optimum combustion, and to avoid knocking, these techniques rely on curating specific thermodynamic and chemical conditions in the end gas [31].

Partial Fuel Stratification is a similar technique that can also rely on end-gas autoignition to improve overall efficiency. In one example, a spray-guided direct injection SI engine several initial injections were combined with a pilot injection to initiate a three-stage combustion mechanism for gasoline and E85, under certain conditions [32]. Intake temperature, combustion phasing and equivalence ratio were then controlled to induce a third combustion stage, where increased temperature and pressure induced a level of end-gas autoignition that increased combustion and therefore thermal efficiency, without causing knock [32,33].

Autoignition plays an important role in enabling successful high efficiency combustion technique. Section 1.3 of this introduction will explore the current understanding and gaps in understanding, of autoignition and in particular, its relationship to fuel properties.

1.2.3 Extending the Knocking Limit

Knocking, the unwanted and uncontrolled autoignition of end gas (the portion of the fuel-air mixture ahead of the flame), is one of the main factors currently limiting engine operation and efficiency [34]. The high-frequency, high-pressure oscillations associated with the occurrence of knock can cause significant damage to many different engine components, hence it must be avoided. Knocking can occur when the pressure and temperature of the end gas spend enough time above a certain threshold, leading to spontaneous autoignition [35]. The specific delay time, pressure and temperature at which autoignition occurs depends on the composition of the mixture and therefore the choice of fuel and any intermediate reactions that have occurred in the meantime.

Extending the knocking limit improves Otto cycle efficiency, η_{Otto}, by allowing for higher compression ratios (and therefore expansion ratio), r, as demonstrated by Equation 1 where γ is the ratio of specific heats.

$$\eta_{\text{Otto}} = 1 - \frac{1}{r^{\gamma-1}} \tag{1}$$

Extending the knocking limit also improve efficiency by enabling more optimal ignition timing, so that combustion peak pressure occurs closer to top dead centre. This maximises the pressure exerted on the pistons, allowing for more extraction of useful work.

1.3 Low Temperature Heat Release

This section introduces the main topic of this thesis—Low Temperature Heat Release. Before examining the details of LTHR, the concept of autoignition and negative temperature coefficient behaviour must be looked at in depth.

1.3.1 Autoignition

Autoignition is when pressure and temperature conditions cause charge to ignite without an external ignition source. Depending on the combustion mechanism, this effect can be desired or actively avoided; it causes ignition in diesel engines and unwanted knocking in SI engines.

The ignition delay, τ is the time it takes for a certain charge mixture to undergo autoignition. It is highly dependant on temperature, pressure and the fuel in question. It can be modelled by an Arrhenius-type expression as in Equation 2. In many cases, temperature and pressure vary with time, so to predict when a mixture undergoes autoignition one must examine the thermodynamic state history of the charge. The Livengood-Wu integral (Equation 3) describes how temperature and pressure history contributes to causing autoignition, in a similar fashion to cumulative fatigue damage in materials[3]. Figure 1 visualises this concept[36] showing how, when the integration of the ignition delay (which changes as the temperature of the mixture changes)—represented by the area under the curve—is approximately equal to 1, knock is predicted to occur.

$$\tau = Ap^{-n}\exp\left(\frac{B}{T}\right) \tag{2}$$

$$\int_0^{t_{\text{ai}}} \frac{1}{\tau} dt = 1 \tag{3}$$

Whilst autoignition is desirable and in fact necessary in a compression ignition engine, it is almost always avoided in standard spark ignition engines. When autoignition occurs unintentionally, it can have damaging consequences; this is known as knock—the rapid pressure rise caused by spontaneous ignition of unburned gasses[3].

Fuel Properties and Autoignition

This section will explain how autoignition behaviour is quantified in order to compare differences across fuels.

Knock, a result of autoignition, is a complex phenomenon which depends on fuel chemistry, combustion chamber design and engine operating conditions. To attempt to quantify a fuel's resistance to knocking, octane numbers were introduced. Research Octane Number (RON) and Motor Octane Number (MON) tests quantify

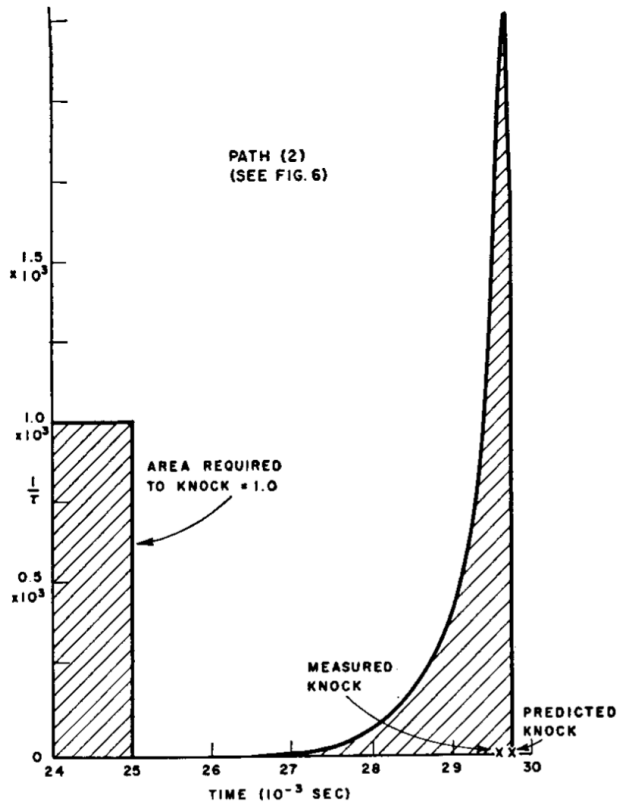

Figure 1: Graphical illustration of the Livengood-Wu integral[36]

a fuel's anti-knock quality by comparing its performance to a blend of primary reference fuels (PRF), which are based on a blend of 2,2,4-Trimethylpentane (commonly known as iso-octane), which has good knocking resistance and n-heptane, which has relatively poor knocking resistance[37,38]. PRF x is a blend of $x\%$ isooctane and $(100 - x)\%$ n-heptane as is assigned the octane number of x in both RON and MON scales.

The RON and MON scales represent two different sets of conditions. To be assigned a RON of 90 a fuel would begin to knock at the same compression ratio as PRF 90 under RON conditions. Standardised tests for RON and MON are carried out in a single cylinder, Cooperative fuels research (CFR) engines with a knockmeter. In the test, the fuel-air mixture is varied until knocking intensity is maximised. The cylinder height, which correlates with compression ratio is then adjusted until a standard reading of knocking intensity is achieved. Test fuels are then bracket between two primary reference fuels, from which octane number can be interpolated using the difference in compression ratios. Extrapolation can be used to award octane numbers of above 100, previously based on PRFs blends of iso-octane and tetraethyllead[37,38].

Fuels respond differently to changes in pressure and temperature conditions and often have differing values on the RON and MON scales. The difference in RON and MON scores is defined at Sensitivity S.

$$S = \text{RON} - \text{MON} \tag{4}$$

Kalghatgi defined Octane Index (OI) to specify the anti-knock quality of a fuel in a given operating condition.

K is an experimentally derived constant for a given set of conditions[39] such that OI is a linear combination of RON and MON.

$$\text{OI} = (1 - K)\,(\text{RON}) + K\,(\text{MON}) \tag{5}$$

$$\text{OI} = \text{RON} - KS \tag{6}$$

K depends on engine operating conditions and in some cases, K is negative so that for a given RON, a fuel with higher sensitivity (lower MON) has better anti-knock quality. The value of K decreases as the engine becomes more prone to knock i.e. as its octane requirement increases. In terms of the end-gas properties, K decreases as the temperature decreases for a given pressure[39]. In some markets, AKI (Anti-knock index) is used, which is OI for $K = 0.5$.

$$\text{AKI} = \frac{\text{RON} + \text{MON}}{2} \tag{7}$$

It has since been found that the K weighting factor between RON and MON is not universally applicable. In recent work, alternative definitions were tested to improve descriptions of knocking trends across various conditions but as of yet, no robust correlation has been found[40]. Whilst it is clear than octane numbers are hard to predict accurately over a range of operating conditions, the next will provide some of the explanation as to why certain fuels behave differently so as to cause their RON and MON differ.

1.3.2 NTC Behaviour

Low temperature heat release originates from fuels that exhibit negative temperature coefficient (NTC) behaviour. A fuel mixture that exhibits NTC behaviour has a non-monotonically decreasing relationship between ignition delay time and mixture temperature at certain pressures. In certain temperature ranges (depending on fuel) mixture reactivity decreases due to unfavourable equilibrium rates of radical forming reactions, ultimately leading to an ignition delay time that increases with temperature causes mixtures that exhibit it to have two stages of autoignition[41].

Figure 2 shows the results from a low temperature autoignition studies in a static reactor, where fuel and oxidiser were added to heated reaction vessel and time required for autoignition was measured.[41]. Until 600K, there is a monotonic decrease in autoignition time, which is consistent with classic Arrhenius kinetics. Between 600K and 650K, autoignition times increase with; here, reaction rates decrease with increasing temperature, hence the term 'negative temperature coefficient'.

Two-stage ignition is synonymous with NTC behaviour and can be observed in a rapid compression machine,

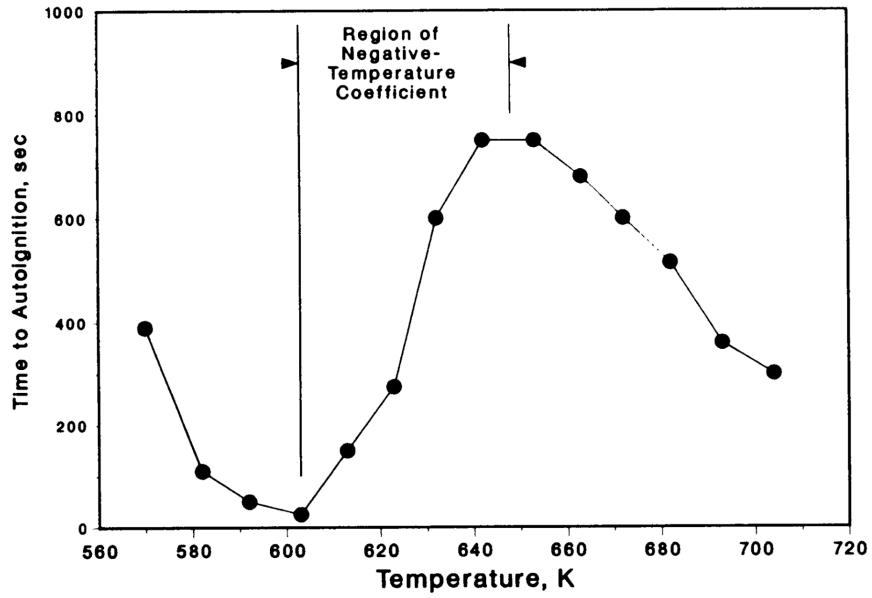

Figure 2: Propane exhibiting NTC behaviour between 600K and 650K [41]

as in Figure 3. Compression occurs until point A, and the region A–B is the induction time during which autoignition chemistry is building to the point of releasing detectable energy. There is significant energy release during the region B–C, which causes a rapid increase in temperature and pressure, until point C where the chemistry enters the NTC region and rate of pressure rise is significantly decreased. At point D, NTC behaviour ends and autoignition occurs [41].

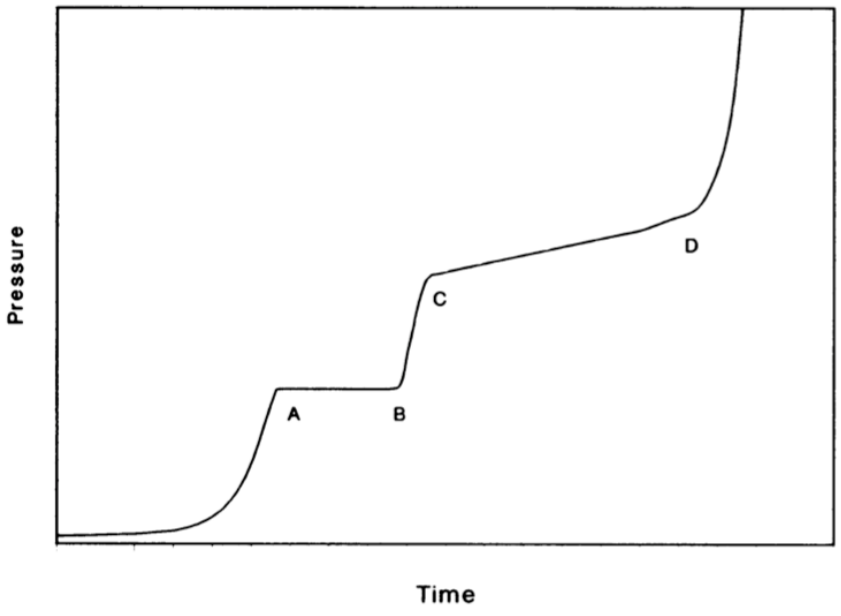

Figure 3: NTC behaviour seen between C and D in a rapid compression machine. [41]

LTHR is the heat released from the first stage of two-stage autoignition (i.e. region B–C in Figure 3) and it involves a significant change in composition of the mixture, due to the reactions that occur. NTC behaviour and hence LTHR is most often observed in fuels with low octane sensitivity, particularly straight chain alkanes such

as propane and n-heptane, unlike alkenes and aromatics which have different low temperature chemistry [41–43].

1.3.3 Low Temperature Oxidation of Primary Reference Fuels

The low temperature reaction pathways that cause LTHR in the two primary reference fuels, iso-octane and n-heptane, were examined in depth by Curran et al in comprehensive modelling studies [44,45]. The reaction pathway is depicted in Figure 4 and each reaction is outlined below, working vertically from the top to the bottom of the figure.

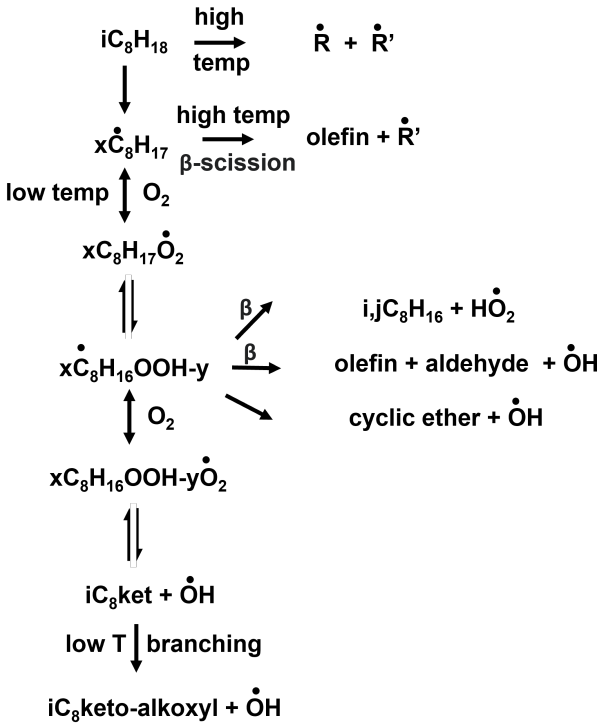

Figure 4: iso-octane oxidation pathways [44]

1. The first step is hydrogen abstraction of iso-octane, usually by a hydroxyl (OH) radical to form iso-octanyl radical plus water.
2. Then, at low temperature, the first addition of O_2 to the iso-octanyl radical occurs to create an iso-octylperoxy radical.
3. The iso-octylperoxy radical undergoes isomerisation to form a hydroperoxyalkyl radical.
4. There is a second O_2 addition to form peroxy-alkylhydroperoxide.
5. Next, isomerisation of the peroxy-alkylhydroperoxide forms an OH radical alongside a carbonyl-hydroperoxide molecule.
6. The carbonyl-hydroperoxide molecule subsequently decomposes to the form a carbonyl radical and a second OH radical.

Overall, two OH radicals are formed from one OH radical reacting with a stable molecule. This leads to the chain branching process, where the low temperature oxidation of a single iso-octane molecule provides enough radicals to initiate the low temperature oxidation of two further iso-octane molules, and so on. Alongside the above steps, beta-decomposition of the various intermediate species leads to the formation of smaller hydrocarbon species, including formaldehyde.

1.3.4 Ignition Delay Contours

The relationship between pressure, temperature and ignition delay for a given fuel can be summarised by an ignition delay contour, such as in Figure 5. They offer an effective method of illustrating the changing relationship between ignition delay and temperature as pressure rises and help explain the link between engine conditions and LTHR behaviour. The negative temperature coefficient behaviour is described in Section 1.3.2 can be seen in Figure 5 at pressures of 18 bar and above.

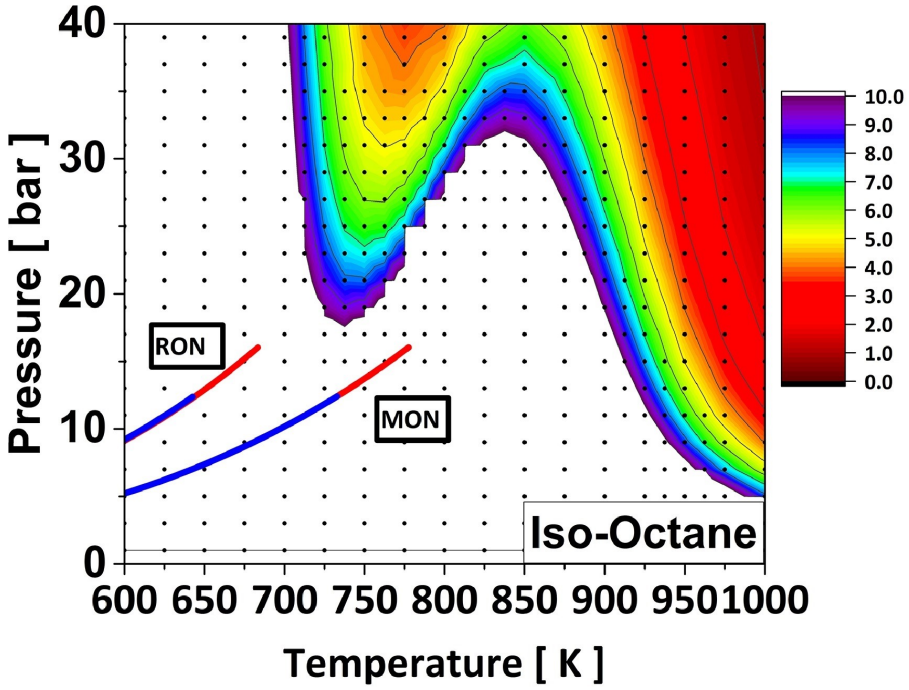

Figure 5: An example ignition delay contour for iso-octane, illustrating ignition delay time in ms [40].

Ignition delay contours are constructed from ignition delay time data either from experiments or simulations where a fuel-air mixture experiences a given combination of pressure and temperature as initial conditions and time until ignition is measured—this can be defined by a temperature inflection point, or a constant temperature rise. As explained in Section 1.3.1, ignition delay is a function of pressure and temperature history, so (for a system where pressure and temperature are not constant, i.e. and engine) it is useful to present the history (or trajectory) of pressure and temperature (PT) on the contour. The PT trajectories of RON and MON conditions (discussed in Section 1.3.1) are included in Figure 5 for additional context.

PT trajectories of cylinder contents in engines are primarily affected by inlet conditions (i.e. initial pressure

and temperature), mixture properties (such as the ratio of specific heats), compression ratio and heat transfer effects. Many modern ICEs are boosted and therefore experience relatively higher pressures throughout the compression cycle. These conditions are commonly referred to as "beyond RON" because, for a given temperature, they experience higher pressures than the RON PT trajectory.

1.3.5 LTHR in engines

Until recently, LTHR in an engine context was mostly confined to homogeneous charge compression ignition (HCCI) engines because of higher compression ratio and therefore cylinder pressures [46–49] In HCCI engines, LTHR appears as a distinct heat release event occurring before the much larger heat release from HTHR—this is visualised in Figure 6 in the apparent heat release rate trace from an HCCI engine exhibiting a clear LTHR event around 20°CA before top dead centre.

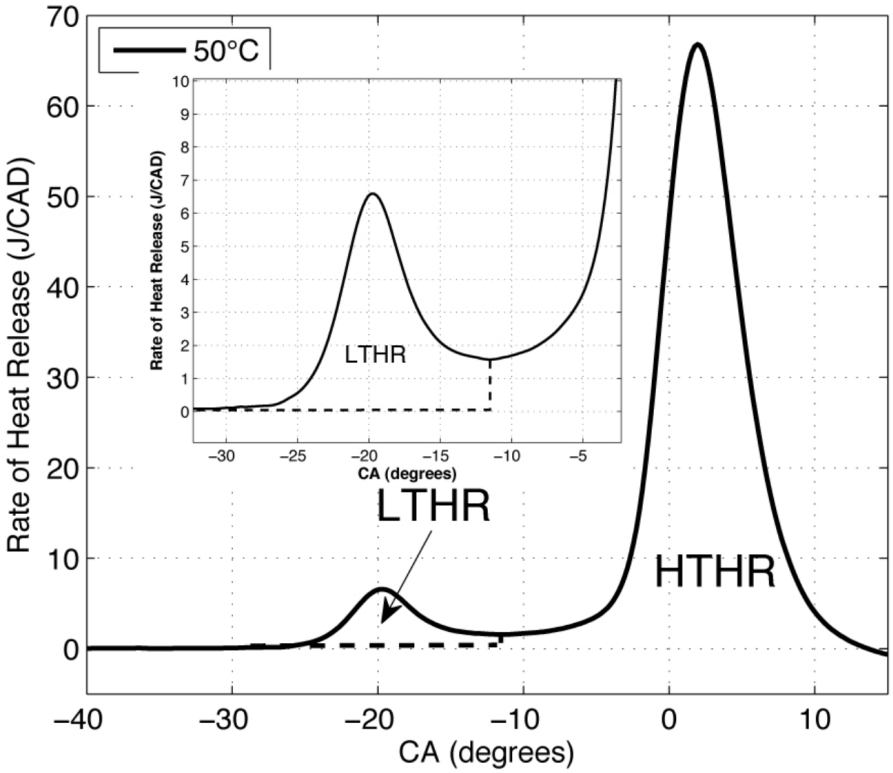

Figure 6: LTHR in an HCCI engine [49].

In these engines, the occurrence of LTHR has been taken advantage of to control combustion heat release rate via partial fuel stratification [50]. Furthermore, LTHR has been studied in reactivity controlled compression ignition (RCCI) engines, where the low temperature reactions can have an important role in curating varying degrees of charge reactivity and therefore help control high temperature heat release [51–53].

More recently, LTHR has been shown in spark ignition (SI) engines with low octane sensitivity fuels at high load conditions with elevated inlet temperatures [54–56] where it is seen before the spark and hence termed pre-spark heat release (PSHR). In these studies, PSHR was induced by retarding spark timing, revealing in LTHR

around top dead centre (TDC) before a spark discharge triggers deflagrative combustion[57,58].

Szybist and Splitter observed that PSHR was more likely to be seen in fuels with low octane sensitivity and at high load conditions with elevated inlet temperatures[40]. Furthermore, Splitter *et al.* used elevated intake temperatures to show PSHR is related to knocking chemistry[57].

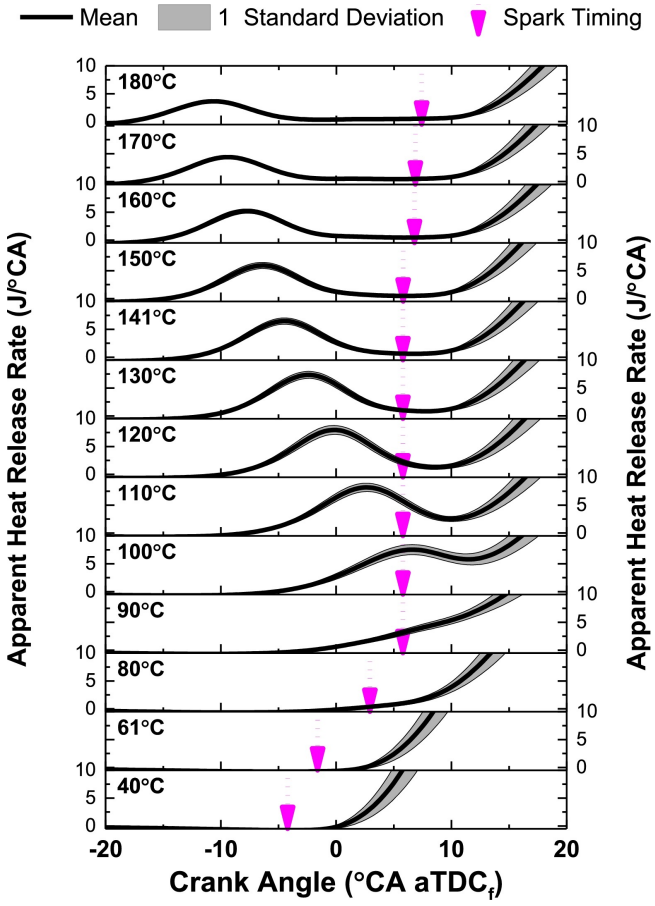

Figure 7: Pre-spark Heat Release affecting knock limited spark advance as intake temperature increases[59]

Results from Splitter *et al.*'s study (Figure 7) showed that, for conditions without PSHR (40–80°C intake temp), knock-limited spark advance (KLSA) required nearly linear retarding with increasing inlet temperature, however once PSHR was observed (intake temperature above 90°C) KLSA is nearly constant, hence the occurrence of LTHR effectively allowed more advanced knock-limited combustion phasing[59]. It was theorised that when LTHR occurred, it modified the thermodynamic state of the unburned mixture, moving it into the NTC region and therefore causing it to have a long ignition delay and hence low reactivity—this in turn inhibited knocking[57].

Meanwhile, in a different study where intake temperature was varied, increasing intake temperature encouraged autoignition to occur, but in a controlled manor[32]. In another study, the frequency and intensity of low speed pre-ignition have been found to correlate with LTHR magnitude[60], and LTHR has more recently been modelled at boosted conditions[61,62]. It has also been hypothesised that LTHR-induced changes in mixture composition increase its laminar flame speed, which accelerates combustion[63], this could ultimately lead to

improved combustion efficiency, particularly for lean operation where low flame speeds can be a limiting factor.

1.3.6 LTHR: Research Questions

With the phenomena of PSHR only recently being discovered, there are many aspects of LTHR, particuarly in SI engines, that are not fully understood. Whilst results from the studies above involving SI engine LTHR suggest that it is most prevalent with low octane sensitivity fuels at high inlet pressures and temperatures, factors such as the impact of individual components in fuel blends, equivalence ratio and residuals have not been investiated in much depth if at all.

Furthermore, Splitter *et al.* used ignition delay analysis in a PSHR study to show that it is possible that, for some conditions that do not exhibit PSHR, as deflagration occurs the end gas region will traverse the same region in pressure-temperature space as cases that do exhibit PSHR, suggesting that bulk gas LTHR reactions in the end gas is probable[57]. Since these reactions change the species composition ahead of the flame, understanding them could be critical for understanding knocking behaviour in SI engines. However, conventional pressure-based heat release analysis techniques are unable to experimentally observe end gas LTHR as its contribution to pressure rise would be indistinguishable from that of the heat released from deflagration.

Finally, the cylinder contents with the altered knocking characteristic as a result of PSHR reactions are difficult to study because they are consumed by the subsequent deflagration (or HTHR in HCCI engines).

Summary

Section 1.1 outlined the pressing issue with CO_2 emissions from ICEs, and explained recent developments to ICE that began to deal with the problem. Section 1.2 outlined three ways in which the CO_2 impact of ICEs could be further improved: low carbon fuels, using advanced combustion strategies and extending the knocking limit. Section 1.3 Introduced LTHR and highlighted how it directly relates to the knocking limit, as well as potentially enabling better control for advanced combustion strategies. LTHR is also relevant to low carbon fuels as it needs to be understood in the context of the next generation of fuels and engines. The work carried out in this thesis focuses on LTHR, and aims to further understanding of it, addressing the topics raised in Section 1.3.6.

1.4 Thesis Overview

Integrated Thesis Format

This document is an integrated thesis—it is presented as a paper-based thesis containing six closely linked studies that were all part of the same project. As such, the research chapters (Chapters 2 3 and 4) are presented in the format in which they were published or submitted for publication. The papers in these chapters also contain a comprehensive literature review (in addition to Sections 1.1 to 1.3) throughout their introduction sections. These chapters also include additional context, usually relating to the other studies in this thesis, intended to aid the reading of the thesis as a single, coherent document. Finally the studies are further brought together by the overall discussion conclusions in Chapter 5.

1.4.1 Thesis Objectives

There were two overarching objectives of the work in this thesis:

1. To study low temperature heat release in engines by isolating the behaviour and examining including all the parameters that affect it.

2. To develop a new technique, that does not rely on pressure-derived apparent heat release measurements, to observe LTHR in SI engines—then apply it to a fired engine where LTHR is possible but unobservable with current techniques.

The six papers are deeply linked and within the topic of LTHR fit into three themes: physical effects, chemical effects (though of course, these are interdependent) and planar laser-induced fluorescence. The studies in the first two chapters broadly cover the first objective, and were also carried out to inform the methodology and conditions for the final study, which addresses the second objective. Table 1 gives an overview of every topic covered within the six studies in this thesis, and identifies the papers that cover them. The publications included in this thesis are listed in the following section, and identified by their section number that they referenced by in the table.

1.4.2 Publications

- **Section 2.1:** White, S. P., Bajwa, A. U. & Leach, F. C. P. Isolated low temperature heat release in spark ignition engines. *SAE International Journal of Advances and Current Practices in Mobility* (2024)

- **Section 2.2:** Bajwa, A. U., White, S. P. & Leach, F. C. P. Low temperature heat release and phi-sensitivity characteristics of iso-octane/air mixtures. *Combustion Science and Technology* (2023)

- **Section 3.1:** White, S. P. & Leach, F. C. P. Isolated low temperature heat release from binary blends of iso-octane, n-heptane and ethanol in a spark ignition engine. In *Proceedings of the ASME 2024 ICE Forward Conference*, Internal Combustion Engine Division Fall Technical Conference (2024)

- **Section 3.2:** White, S. P., Bajwa, A. U. & Leach, F. C. P. Effect of ethanol and iso-octane blends on isolated low temperature heat release in a spark ignition engine. *SAE International Journal of Fuels and Lubricants* (2024)

- **Section 3.3:** White, S. P., Bajwa, A. U. & Leach, F. C. Effects of nitric oxide on isolated low temperature heat release in spark ignition engines. *Combustion and Flame* **273**, 113921 (2025)

- **Section 4.1:** White, S. P., Willman, C. & Leach, F. C. Observing simultaneous low temperature heat release and deflagration in a spark ignition engine using formaldehyde planar laser induced fluorescence. *Applications in Energy and Combustion Science* **21**, 100321 (2025)

Table 1: Summary of everything covered in this thesis, by paper. Key: ○ covered in paper, ⋆ principal subject of paper.

Chapter		**Physical Effects**		**Chemical Effects**			**PLIF**
Paper (by section)		2.1	2.2	3.1	3.2	3.3	4.1
Topics	Isolating LTHR	⋆	○	○	○	○	○
	Temperature Effects	⋆	○		○		
	Pressure Effects	⋆					
	Speed Effects	⋆					
	Equivalence Ratio		⋆				
	iso-Octane	○	○	⋆	⋆	○	○
	n-Heptane	○		⋆			○
	Ethanol			⋆	⋆		
	Residuals			⋆		⋆	
	LTHR Phasing	○	○		○	○	
	LTHR Indicators	○		○	○		○
	LTHR Products			⋆			
	Simultaneous LTHR & Delfagration						⋆
Techniques	Pressure-derived Measurement	⋆	○		○		○
	Exhaust Emission Measurement		○	⋆	○	○	
	PLIF						⋆
	Ignition Delay Analysis	⋆	○	○	○	○	
	0D Engine Modelling			○		○	
	Mechanism Sensitivity Analysis				⋆	⋆	

Chapter 2

Physical Effects on Low Temperature Heat Release

2.1 Isolated Low Temperature Heat Release in Spark Ignition Engines

This is the first paper in the series of six. It builds upon previous experimental work on pre-spark heat release, such by Splitter and Szybist[40,59] discussed in Section 1.3.5. Since, in their studies, LTHR was occurring before the spark, the logical step for attempting to isolate it was disabling the ignition system. This procedure was developed into the isolated LTHR methodology that is reported in this paper. Preliminary experiments highlighted the necessity to curate the inlet conditions to encourage LTHR to occur (and, equally importantly, to avoid HTHR knocking and damaging the engine when using low-octane fuels). This was developed into a study on the effect of temperature, pressure and engine speed (some of the fundamental physical parameters for engines) on LTHR behaviour. For simplicity, single components fuels were used, leaving scope to explore the effect of different fuel blends in later studies (discussed in Chapter 3).

Upon being submitted to the 2023 SAE International WCX event, this work was selected to be included in SAE International Journal of Advances and Current Practices in Mobility for being one of the best papers of the WCX event. Furthermore, this work won the 2023 SAE International Award for the Outstanding Student Paper honoring Phil Myers.

Contributions

- A new methodology for isolating low temperature heat release in spark ignition engines is introduced and used to realise isolated LTHR in n-heptane and in iso-octane in two different SI engines.
- Isolated LTHR is presented in contrast with high temperature heat release in spark ignition engines.

- The effects of pressure, temperature and engine speed on LTHR behaviour is investigated.
- Ignition delay and Livengood-Wu analyses are used to explain the effects of the above parameters.

2023-01-0235 Published 11 Apr 2023

Isolated Low Temperature Heat Release in Spark Ignition Engines

Samuel White, Abdullah Bajwa, and Felix Leach University of Oxford

Citation: White, S., Bajwa, A., and Leach, F., "Isolated Low Temperature Heat Release in Spark Ignition Engines," SAE Technical Paper 2023-01-0235, 2023, doi:10.4271/2023-01-0235.

Received: 25 Oct 2022 Revised: 09 Jan 2023 Accepted: 30 Jan 2023

Abstract

Low temperature heat release (LTHR) has been of interest to researchers for its potential to mitigate knock in spark ignition (SI) engines and control auto-ignition in advanced compression ignition (ACI) engines. Previous studies have identified and investigated LTHR in both ACI and SI engines before the main high temperature heat release (HTHR) event by appropriately curating the in-cylinder thermal state during compression, or in the case of SI engines, timing the spark discharge late to reveal LTHR (sometimes referred to as pre-spark heat release). In this work, LTHR is demonstrated in isolation from HTHR events. Tests were run on motored single-cylinder engines and inlet air temperatures and pressures were adjusted to realise LTHR from n-heptane and iso-octane (2,2,4-trimethylpentane) without entering the HTHR regime. LTHR was observed for a lean n-heptane-air mixture at inlet temperatures ranging from 60°C to 100°C and inlet pressures of 0.9 bar (absolute). For temperatures below 60°C LTHR was not detected and for temperatures above 100°C measurements could not be taken due to the presence of HTHR. No LTHR was detected for iso-octane at 0.9 bar inlet pressures for the same conditions. Following predictions from chemical kinetics modelling in CHEMKIN (and previous studies), intake pressures were increased to 1.1 bar and 1.5 bar, which successfully led to the realisation of LTHR from iso-octane. The effect of temperature, pressure, and engine speed on the presence, intensity and phasing of LTHR are presented alongside pressure-temperature trajectories of the in-cylinder gases to explain the trends.

Introduction

Ever-increasing global CO_2 emissions mean that every effort must be made to reduce them as swiftly as possible. One technique, which can increase the efficiency of internal combustion engines (ICEs) by 10-20%, is lean operation - where the air: fuel ratio is weak of stoichiometric [1]. This improves the ratio of specific heats and leads to an efficiency improvement, provided the fuel-air mixture can still be ignited successfully. However, NO_x emissions need to be addressed either in-cylinder [2] or by exhaust aftertreatment (both of which can come with an efficiency penalty). One potential enabler for this technology, improving the ignition of the fuel-air mixture, is low temperature heat release (LTHR).

Certain fuels are known to possess two-stage autoignition (AI) chemistry, with non-monotonic relationships between mixture temperature and ignition delay due to negative temperature coefficient (NTC) behaviour [3]. The first heat release (HR) stage for such fuels, commonly referred to as low temperature heat release as it occurs at relatively low temperatures (< 850 K), has garnered interest recently because of its potential to promote clean and efficient combustion. Straight chain fuels like n-heptane and n-hexane exhibit stronger LTHR behaviour than branched chain species like iso-octane [4].

LTHR has been observed in internal combustion engines such as in controlled autoignition engines, where thermal conditions and fuel metering were managed to realise LTHR before the main volumetric autoignition stage [5, 6]. LTHR has also been observed in spark ignition (SI) engines as 'pre-spark heat release' (PSHR) induced by retarding spark timing, resulting in LTHR around top dead centre (TDC) before a spark discharge triggers deflagrative combustion [5, 7, 8].

A notable challenge in conducting experimental LTHR research is the coupled nature of low and high temperature heat release (HTHR) stages, whereby the former is obscured (to varying degrees) by the more dominant HTHR stage under

'firing' engine conditions. It has been suggested that LTHR could occur during deflagration [7], though distinguishing it from concurrent HTHR would require methods beyond pressure-based heat release analysis.

Strategies have been devised to bridge this gap: heuristic post-processing approaches have been used to isolate LTHR and HTHR portions from concurrent LTHR-HTHR data. Splitter et al. [7] used 'spline fitting' to estimate LTHR and HTHR contributions in an SI engine undergoing intermediate HR (when LTHR is partially revealed and lacks a distinct NTC drop). Waqas et al. [5] used heat release rate thresholds to define 'early heat release' in a controlled auto ignition (CAI) engine undergoing intermediate HR.

LTHR could potentially be controlled and harnessed to improve overall efficiency of internal combustion engines via the following methods:

- Improved understanding of end gas AI chemistry can help avoid abnormal combustion events like knocking and low-speed pre-ignition (stochastic pre-ignition) in spark ignition (SI) engines. This can enable engine operation at high boost levels, allow design of high compression ratio engines, and permit engine operation at thermodynamically efficient (advanced) spark timings. For fuels with significant NTC behaviour LTHR has been found to make knock onset less sensitive to inlet temperature by moving the mixture's thermodynamic state into a long-ignition-delay region [7]. Moreover, low-speed pre-ignition frequency and intensity have been found to be correlated to LTHR magnitude [9].
- Control of advanced compression ignition combustion by utilising the thermal and chemical couplings between LTHR and HTHR processes in CAI engines, Shibata et al. [6] found LTHR and HTHR 50% mass fraction burned points (CA50) to be linearly related. Controlled autoigition has been shown to enable stable ultra-lean combustion [10] and so better control of autoignition using through improved understanding of the LTHR chemistry could expand the range of fuels and scenarios where ultra lean combustion can be utilised.
- Combustion efficiency improvements by tailoring end gas conditions to consume fuel via LTHR. It has also been hypothesised that LTHR-induced changes in mixture composition increase its laminar flame speed, which accelerates combustion [11]. This, if found to be true, can be another mechanism through which LTHR can improve combustion efficiency. Such improvements can promote ultra-lean combustion in spark ignition engines.

Isolated LTHR investigations can offer the following benefits:

- Chemical kinetics model validation and development to better represent the thermokinetics of LTHR reactions as emissions measured from isolated LTHR experiments will not be confounded by HTHR reactions. DelVescovo et al. [8] reported that existing chemical mechanisms have high levels of discrepancy even for a well-studied fuel such as iso-octane.
- Using appropriate ignition delay (ID), pressure and temperature surfaces, pressure-temperature (P-T) trajectories that lead to anomalous HTHR events can be studied and the underlying thermodynamic reasons for the breaches can be investigated.
- Relatively extreme LTHR conditions, which if accompanied by HTHR can be detrimental in SI engines, can be investigated. Improved understanding of chemical and thermodynamic conditions in the lead up to damaging HTHR events.
- For conditions where LTHR is weak, heat release based indexing of LTHR (for example, finding the crank angle at 2% mass fraction burned [7]) may not be sensitive enough to detect its onset. Studying LTHR in isolation allows weak LTHR to be detected using alternative methods, such as measurements of emissions or exhaust temperature.
- By separating LTHR from autoignition and deflagration, it can be investigated with minimal chemical and charge heating effects from residual gases.

This work demonstrates an experimental technique that decouples the two heat release regimes and allows the realisation of LTHR without a following HTHR stage. This is achieved by motoring a relatively low compression ratio gasoline direct injection (GDI) engine at elevated intake temperatures and, if need be, pressures to induce LTHR reactions.

Methodology

Quantifying LTHR

To measure and quantify the amount of energy release from low temperature heat release, net apparent heat release rate (AHRR), $\frac{dQ_n}{d\theta}$ (defined as the heat release rate $\frac{dQ_{hr}}{d\theta}$ less the heat transfer rate $\frac{dQ_{ht}}{d\theta}$) was calculated in MATLAB using the crank angle (θ) based pressure p and volume V (calculated from engine geometry) traces according to Equation 1 [12], using a constant ratio of specific heats $\gamma = 1.35$:

$$\frac{dQ_n}{d\theta} = \frac{dQ_{hr}}{d\theta} - \frac{dQ_{ht}}{d\theta} = \frac{\gamma}{\gamma - 1} p \frac{dV}{d\theta} + \frac{1}{\gamma - 1} V \frac{dp}{d\theta} \quad (1)$$

To isolate heat release Q_{hr} measurements originating from LTHR from heat transfer Q_{ht} effects and other assumptions, the calculated AHRR trace for a corresponding unfuelled, motored case was subtracted from the fuelled case. Start of LTHR (SoLTHR) was determined by finding points around top dead centre (TDC) where either the AHRR of the fuelled and unfuelled cases deviated from each other or there was a noticeable inflection in the fuelled curve indicating HR onset. End of LTHR (EoLTHR) was identified as the point where the fuelled and unfuelled AHRR curves intersected again. The

difference in AHRR was then integrated between these boundaries to find the total heat release in Joules per cycle, as shown in Figure 1.

Cylinder temperature was calculated using the ideal gas law with measurements of cylinder pressure, cylinder volume and estimations of cylinder contents.

Experimental Facility

The experimental work was conducted on two single cylinder internal combustion engines, one naturally aspirated, and another with the capability for boosted inlet air.

Single Cylinder Engine with Optical Access For naturally aspirated inlet pressure conditions, a single cylinder, GDI research engine with the capability for optical access was used. The engine is referred to as the 'optical engine' due to the engine's capabilities, despite the fact that no optical diagnostic techniques were used in this work; its technical specifications are summarised in Table 1 and the engine has been fully described in previous work [13]. The engine was coupled with a Control Techniques motoring dynamometer, to control engine speed. Fuel was injected at 160 bar, with injection timing and duration controlled by a Berkeley Nucleonics BNC725 unit. Ignition was disabled by disconnecting the ignition coil's power supply and control signal. The optical engine uses polyamide-imide piston rings to achieve an oil-free combustion chamber; engine coolant was controlled to its standard operating temperature of 45°C (to minimise the risk of melting the piston rings). The inlet air heater was controlled using a relay connected to a West 6100+ temperature controller; the inlet temperature fluctuated by up to ± 3°C at the higher temperature operating points. The test cell was controlled by a Taylor DynPro2 system, which was also used for continuous data logging at 1 Hz. Cylinder pressure data was measured using a Kistler Type 6041A high speed pressure transducer, at a resolution of 0.1 °CA (crank angle), recorded with an AVL X-ion high speed data acquisition system. The cylinder pressure signal was pegged every cycle to a barrel pressure transducer, which was exposed to the combustion chamber around TDC. High speed data was collected for 300 cycles, with three independent runs conducted per operating point. If the live pressure trace readings indicated HTHR via visibly high peak pressures, fuel injection was disabled immediately to avoid engine damage.

FIGURE 1 The difference between the apparent heat release rate fuelled and unfuelled test, with the quantity of LTHR highlighted in the shaded region

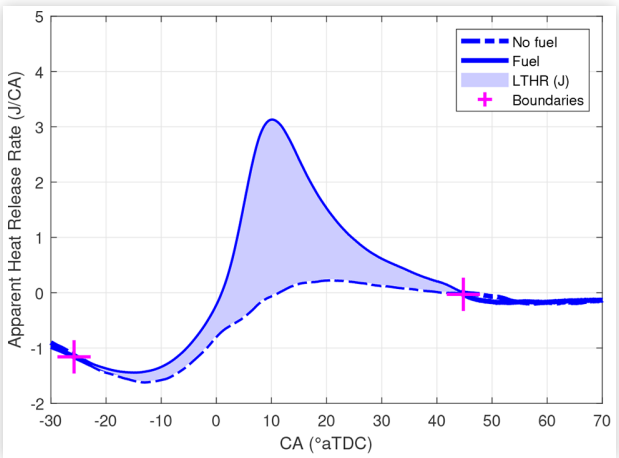

TABLE 1 Engine specifications.

Parameters	Optical	Thermal
Bore [mm]	89.0	83.0
Stroke [mm]	90.3	92.0
Displacement [cm^3]	561.9	500.0
Compression ratio	11.1:1	10.56:1
Valves per cylinder	2 intake, 2 exhaust	
Fuel injection system	Direct injection	Direct injection production injector centrally mounted in cylinder head

Single Cylinder Engine For studying high inlet pressure conditions, a single cylinder, GDI engine based on a Ricardo Hydra bottom end was used. The engine is referred to as the 'thermal engine' and its technical specifications are summarised in Table 1. The engine was coupled to a 57 kW AC motoring dynamometer (Vascat MAC-Q with ABB power electronics) that maintained required speed (± 1 rpm). Fuel injection settings (timing, duration, rail pressure) were controlled by a Schaeffler Protronic ECU via an ETAS INCA interface. As with the optical engine study, ignition was disabled. The engine was operated at wide open throttle and intake pressure was increased to desired levels using a closed loop external boosting rig. Intake air was heated using a 10 kW electric heater (OSRAM Sylvania) installed upstream of the throttle valve and intake plenum.

The test cell has been fully described in previous publications [14, 15, 16]. Inlet pressure was measured around 35 cm upstream of the inlet ports using a Druck UNIK 5000 series sensor and logged at a frequency of 1 Hz using a Sierra-CP CADET engine control system. Temperatures (measured using 3mm k-type thermocouples), fuel flow rate (measured using a coriolis flow meter, Siemens FC Mass 2100), air flow rate (measured using a hot wire flow meter, Sierra-CP Airtrak 628S), and exhaust composition (measured using a Horiba MEXA-ONE) were also recorded at 1 Hz. Cylinder pressure was measured using a water-cooled piezoelectric transducer (Kistler-6041B) and was logged, along with other high-speed measurements (manifold pressures, valve lift), at a resolution of 0.1°CA using a high-speed data acquisition system (AVL Indiset). Data post-processing was performed using AVL Concerto and custom MATLAB scripts.

Engine coolant and oil temperatures were maintained at 90°C during experiments using closed loop temperature control systems within 2 and 1°C, respectively. Slow and high-speed data were recorded for 30 seconds and 300 cycles, respectively.

Operating Conditions

N-Heptane Tests Engine parameters used are listed in Table 2. Inlet temperature sweeps were carried out with inlet pressure and injection duration held constant. As a result air mass flow rate and hence equivalence ratio varied with inlet temperature. Equivalence ratio (ϕ) was estimated by using fuel flow rate measurements from a calibration of the injector, using a lambda sensor close to its stoichiometric operating point.

Iso-Octane Tests Tests were performed with iso-octane at a constant equivalence ratio of 0.5 at three speeds, four inlet temperatures and two inlet pressures (Table 2). Equivalence ratios, calculated from fuel and air flow measurements and verified from exhaust emissions using the 'Spindt' method [17], were maintained between 0.48 and 0.5. Inlet temperatures were maintained within ± 2°C and pressure within ± 0.01 bar.

Modelling

Ignition delay simulations were performed in CHEMKIN, using the closed homogeneous ignition delay model with a constant volume. The simulations modelled 200 ms of reactions, and reported ignition delay defined by a 50 K rise in temperature, in order to detect the relatively small changes in temperature due to LTHR. Mixtures of air and both n-heptane and iso-octane were modelled at an equivalence ratio of 0.5 using a reduced Lawrence Livermore National Laboratory gasoline surrogate mechanism [18].

TABLE 2 Engine settings.

Parameters	Optical	Thermal
IVO [°CA aTDC]	-336	-352
IVC [°CA aTDC]	-86	-165
EVO [°CA aTDC]	116	159
EVC [°CA aTDC]	366	359
Speed [rpm]	1100	1000, 1500, 2000
Injection pressure [bar]	160	140
Injection timing [°CA aTDC]	-270	-300
Inlet temperature [°C]	40, 60, 80, 100	60, 80, 100, 120
Inlet pressure [bar (absolute)]	0.9	1.1, 1.5
Equivalence ratio (ϕ)	0.5	0.5
Fuel	n-heptane (>99% purity)	iso-octane (>99% purity)

Results and Discussion

Isolated LTHR

Isolated LTHR from n-heptane the optical engine is shown Fig. 2. The figure shows calculated apparent heat release rate for the optical engine with heated intake at 100°C for cases with and without n-heptane injected. Heat release for the case with n-heptane deviates from the motored air case, exceeding 4 J/°CA around 8 °after TDC (aTDC). Fig. 3 shows the pressure rise due to the heat release, from which AHRR was calculated. Peak cylinder pressure was only marginally higher than the non-fuelled case, but occurred at a later crank angle. There was no evidence of HTHR, i.e. there were no rapid pressure rises and the overall magnitude of heat release remained low.

FIGURE 2 AHRR traces for an engine motored with and without n-heptane, with inlet air heated to 100°C

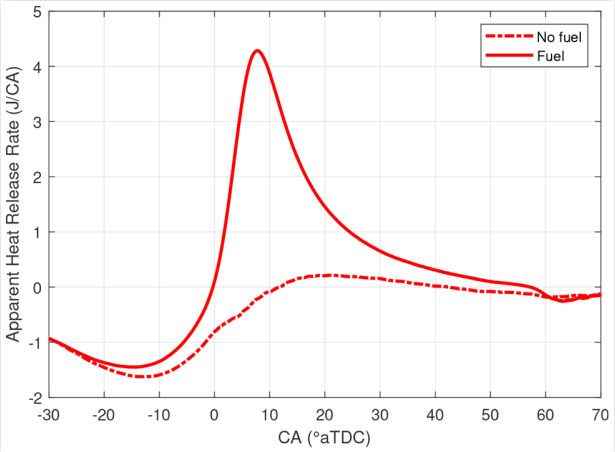

FIGURE 3 Pressure traces for an engine motored with and without n-heptane, with inlet air heated to 100°C

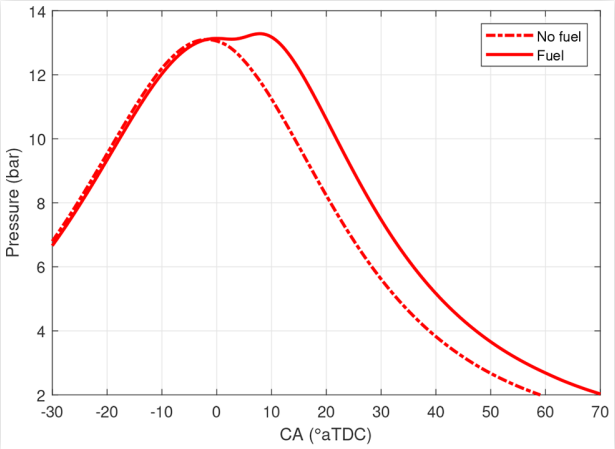

Temperature Effects on LTHR in N-Heptane

LTHR was virtually non-existent when near-ambient (40°C) inlet temperatures (T_{in}) were used at the same conditions as in Fig. 2 and Fig. 3; This can be seen in Fig. 4 where the heat release trace of the fuelled case closely follows the non-fuelled case, and in Fig. 5 where the cylinder pressure was lower in the fuelled case. The slight difference in pressure may be accounted for by charge cooling effects of the direct injected fuel.

The effect of inlet temperature on the pressure traces of mixtures exhibiting LTHR can be examined in Fig. 6. The T_{in} = 40°C case, and to a lesser extent the T_{in} = 60°C case resemble a typical unfuelled, motoring pressure; however, as inlet temperature increases, the traces deviate from motoring after TDC, as a result of the pressure rise due to the heat released by low temperature reactions. The effect of LTHR on pressure traces is most noticeable for the T_{in} = 100°C case, where pressure rises and peaks after TDC.

FIGURE 4 AHRR traces for an engine motored with and without n-heptane, with inlet air heated to 40°C

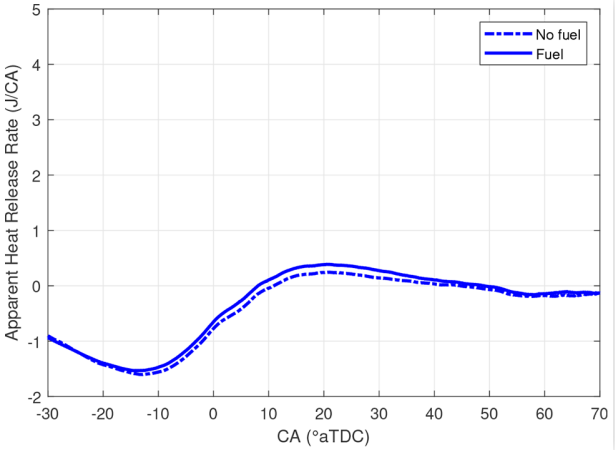

FIGURE 5 Pressure traces for an engine motored with and without n-heptane, with inlet air heated to 40°C

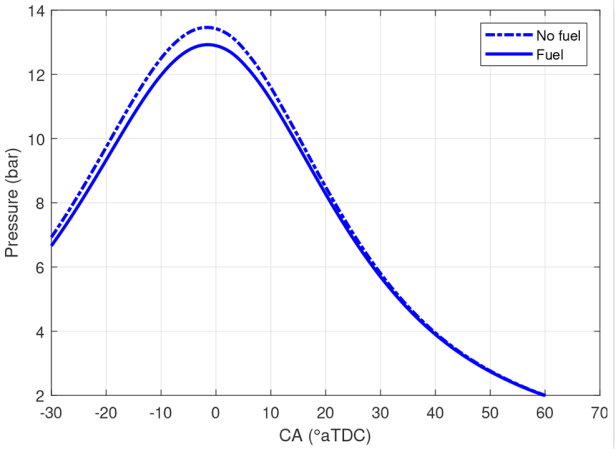

FIGURE 6 Pressure traces for an engine motored with n-heptane at range of inlet temperatures

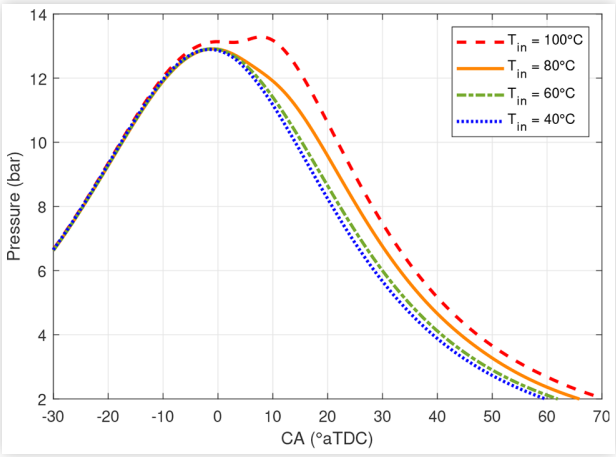

FIGURE 7 Temperature traces for an engine motored with n-heptane at range of inlet temperatures

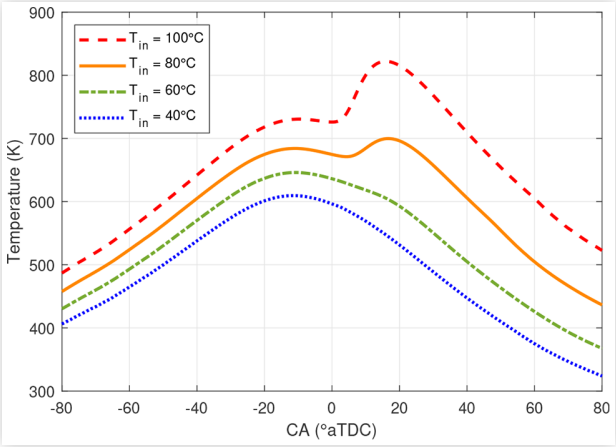

Cylinder temperature traces are shown for the increasing inlet temperatures in Fig. 7. For the cases T_{in} = 100°C and T_{in} = 80°C, a second peak in cylinder temperature occurs after TDC, caused by LTHR.

Fig. 8 shows the clear effect of increasing inlet temperature on LTHR. The graph shows the difference in heat release rate compared to an unfuelled, motored case at the different inlet conditions. The magnitude of heat release increases from negligible at T_{in} = 40°C to 4.5 J/°CA at the highest inlet temperature. The integral of apparent heat release rate, cumulative heat release (CHR) is shown in Fig. 9, which gives an indication of the increased magnitude of heat release from LTHR and advanced LTHR phasing as inlet temperature increases.

The effect of inlet temperature on on total heat release from LTHR is shown in Fig. 10. There is a clear trend in increasing quantity of heat release with increasing inlet temperature, from near zero at T_{in} = 40°C to around 65 J per

FIGURE 8 Apparent heat release rate traces for an engine motored with n-heptane at range of inlet temperatures

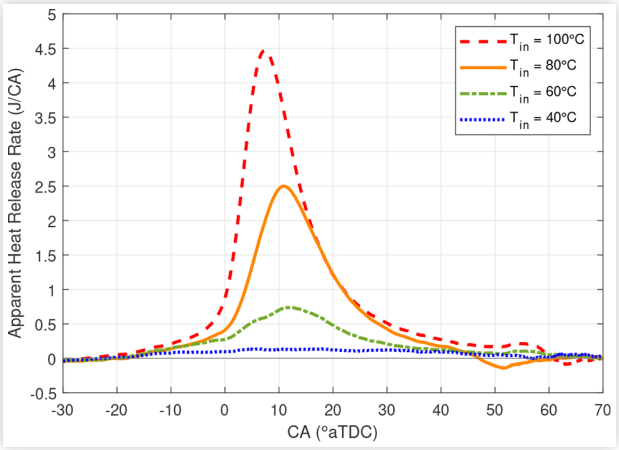

FIGURE 9 Cumulative heat release traces for an engine motored with n-heptane at range of inlet temperatures

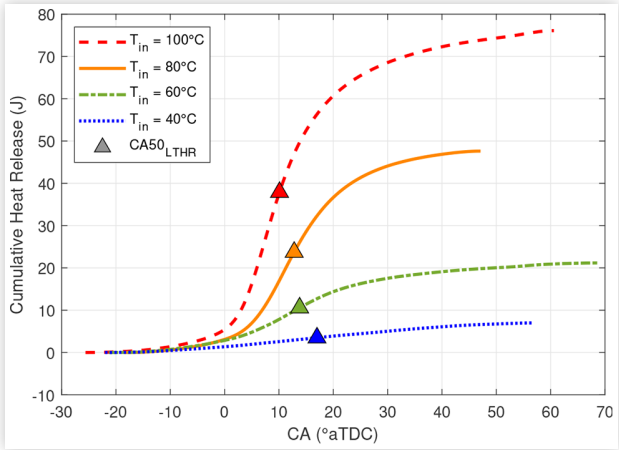

FIGURE 10 Amount of LTHR per cycle from n-heptane against inlet temperature

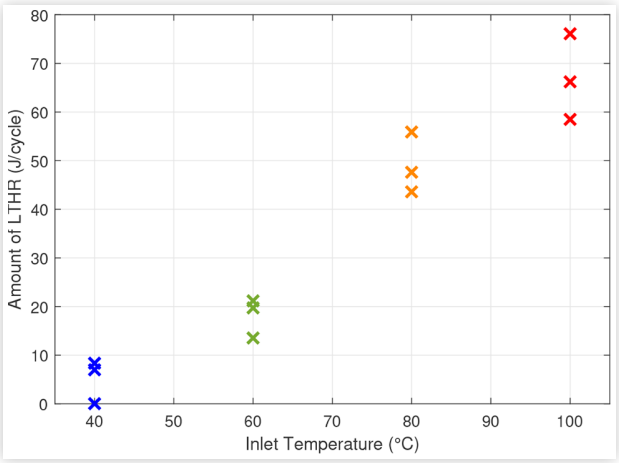

FIGURE 11 Pressure-temperature trajctories of cycles from an engine motored with n-heptane at range of inlet temperatures superposed onto an ignition delay contour for n-heptane, defined by 50 K rise in temperature

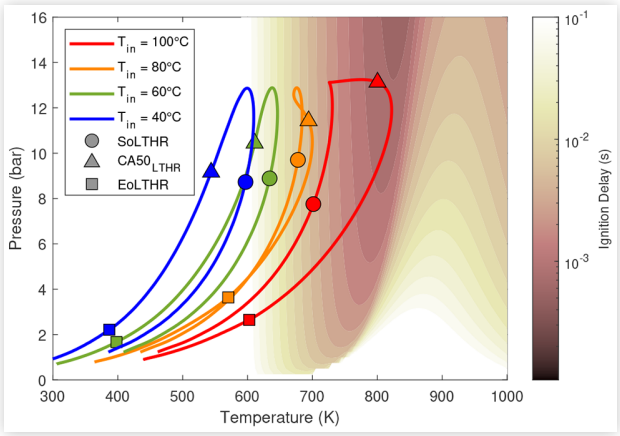

cycle for T_{in} = 100°C. This can be explained by the analysing pressure-temperature (P-T) trajectories through the ignition delay contour in Fig. 11, which shows a contour of n-heptane ignition delay as defined by a 50K rise in temperature [7]. For the T_{in} = 40°C case, the P-T trajectory only traverses portions of the ignition delay contour with ignition delay less than 0.1 s for a brief period, and in that brief period the value of the ignition delay is relatively long. As inlet temperature increases, the respective P-T trajectories shift right into higher temperature regions where ignition delay is reduced. The longer the time the mixture's thermodynamic state resides in the shorter ignition region, the more opportunity there is for chemical reactions that result in LTHR. The compression trajectory of the T_{in} = 100°C case takes it into regions of very short ignition delay, explaining the earlier and greater LTHR. The effect of LTHR on the trajectory can be seen in the plots: there is a clear rise in temperature at near constant pressure for the T_{in} = 100°C case and a more delayed and gradual rise in temperature for the T_{in} = 80°C case as pressure decreases during its expansion stroke.

The time (t) spent traversing through the contour of varying ignition delay (τ) can be summarised by the Livengood-Wu (LW) integral, to give an estimate of overall progression towards the ignition delay time (Equation 2).

$$\mathrm{LW} = \int_0^t \frac{dt}{\tau\left(T(t),P(t)\right)} \tag{2}$$

This is represented by the solid lines in Fig. 12. A LW score of above unity suggests that, on average, the mixture reached its ignition point (as defined by a 50 K rise in temperature) and measurable heat release as a result would be likely. The two cases where the LW score did not reach 1 (T_{in} = 60°C and T_{in} = 40°C) also exhibited some heat release; this may be explained by two factors: temperature stratification and the possibility of autoignition reactions that lead to a temperature rise of less than 50 K that are not accounted for by the

FIGURE 12 Livengood-Wu (LW) integral score traces for an engine motored with n-heptane at range of inlet temperatures

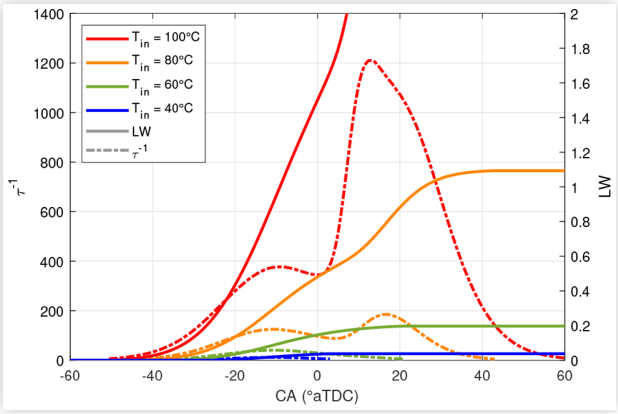

ignition delay contour upon which the calculation is based. The dashed lines represent the reciprocal of instantaneous ignition delay of the mixture, $(\frac{1}{\tau})$ and give an indication of when during the cycle the mixture was traversing through regions of short ignition delay.

The effect of inlet temperature on LTHR phasing can be shown in Fig. 13. One of the data points for T_{in} = 40°C is omitted as no LTHR was detected. Increased inlet temperature resulted in more advanced phasing of the 50% LTHR point (the point at which half of the energy from LTHR has been released). This can be explained by analysing P-T trajectories through the ignition delay contour in Fig. 11 and by $\frac{1}{\tau}$ in Fig. 12; the thermodynamic state of the mixtures that began with higher inlet temperatures reach the short ignition delay region sooner and therefore LTHR begins sooner, when compared to the lower inlet temperature cases.

LTHR vs HTHR

Data collection was hindered for inlet temperatures above 100°C due to the onset of high temperature heat release. Fuel injection had to be cut to avoid damage to the apparatus. However, some cycles were captured for a case (T_{in} = 140°C) at the same inlet pressure and with shorter injection duration compared to the rest of the data (0.85 ms versus 1 ms) that contain a period of around 60 consecutive HTHR cycles amongst 300 LTHR cycles. Figs. 14, 15 and 16 show the cycles plotted separately alongside a corresponding unfuelled case, and highlights the difference between the two phenomena. The two distinct periods of heat release, peaking at -12 °CA and 10 °CA can be seen in the HTHR + LTHR trace in Fig. 14; these separate heat release events originated from a single fuel injection and no external ignition source. HTHR + LTHR trace closely resembles traditional HCCI heat release behaviour from Urushihara et. al [19]. The phasing of the LTHR was earlier in the cycles where HTHR was present (-12 °CA vs 3 °CA); reasons for this could include higher cylinder temperatures from previous HTHR cycles, or residual combustion products changing the chemical pathways and accelerating the LTHR onset. The temperature traces in Fig. 16 clearly show the two-stage autoignition behaviour commonly exhibited by alkane fuels such as n-heptane; two rapid rises in temperature can be seen at -12 °CA and 10 °CA, with the NTC region occurring at 925 K. Fig. 15 shows the pressure traces for the two cases, with peak pressure for LTHR only occurring approximately 2 °CA after the unfuelled case at 14.5 bar, whilst the HTHR case peaked much later at 14 °CA with a peak pressure of 21.5 bar. The onset and retreat of HTHR cycles were both sudden. The sudden onset was likely caused by minor variations in residuals and slightly unsteady inlet air temperature which led to the initial cylinder temperature crossing an HTHR threshold during a given cycle. This may have become unsustainable when HTHR stopped due to the unsteady inlet air temperatures decreasing again.

FIGURE 13 Phasing of 50% LTHR from n-Hepate against inlet temperature

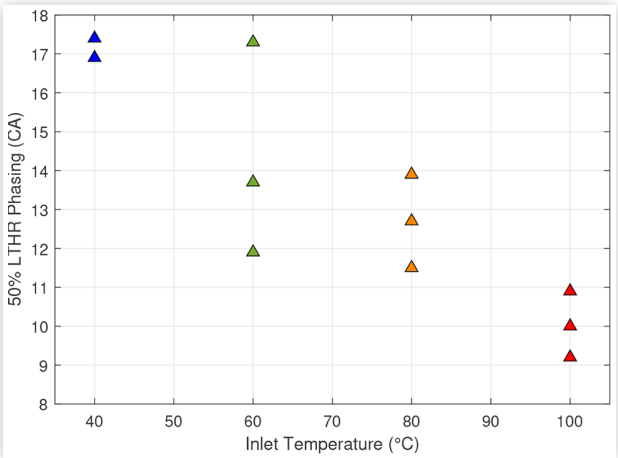

FIGURE 14 AHRR traces of HTHR vs isolated LTHR

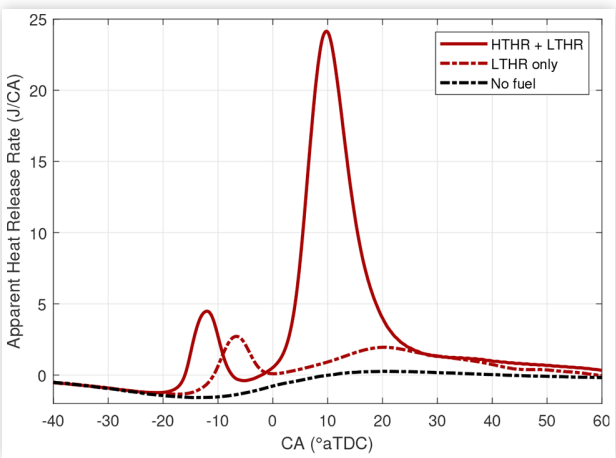

8 ISOLATED LOW TEMPERATURE HEAT RELEASE IN SPARK IGNITION ENGINES

FIGURE 15 Pressure traces of HTHR vs isolated LTHR

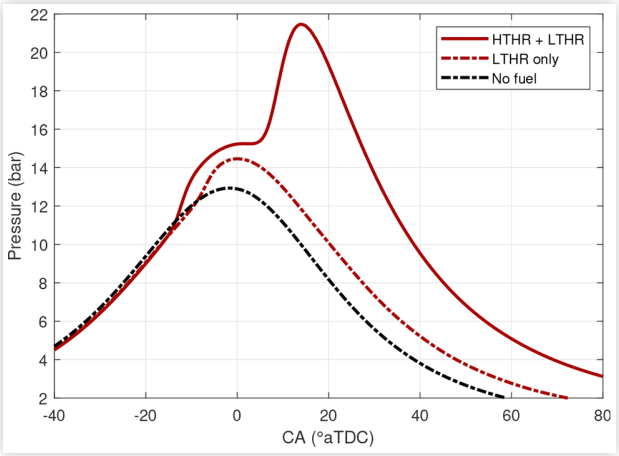

FIGURE 16 Temperature traces of HTHR vs isolated LTHR

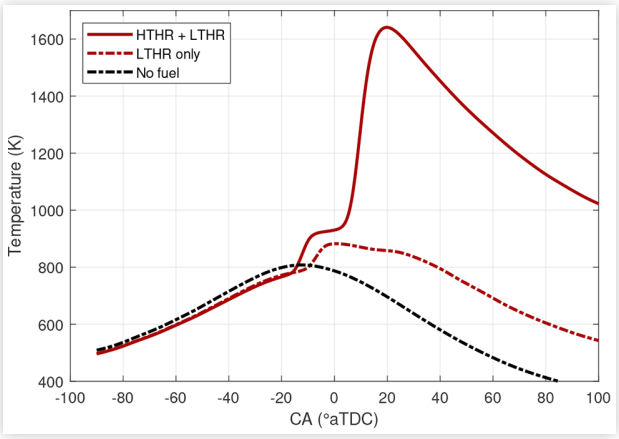

FIGURE 17 Pressure traces for the thermal engine motored with and without isooctane at T_{in} = 60°C

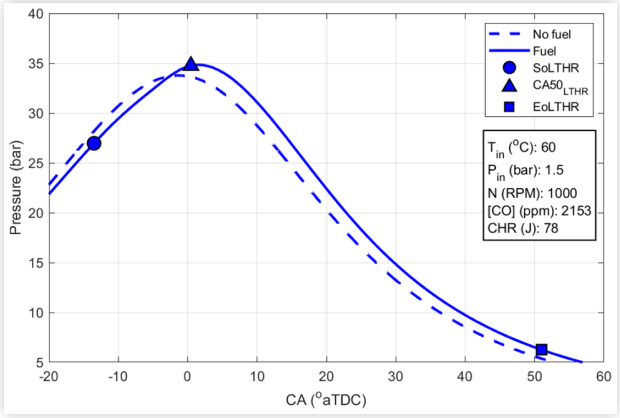

FIGURE 18 AHRR traces for the thermal engine motored with and without isooctane at T_{in} = 60°C

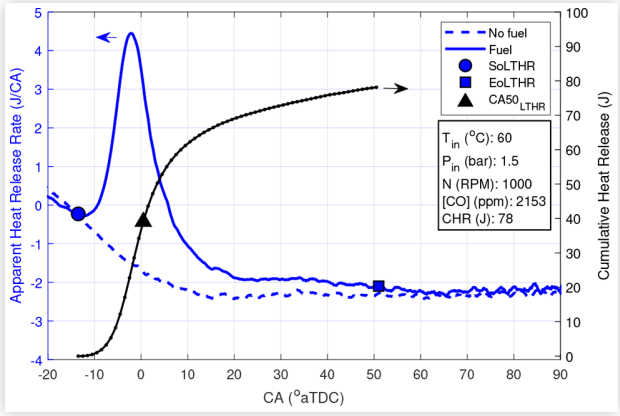

Isolated LTHR with Iso-Octane

Isolated LTHR was successfully observed with iso-octane on the thermal engine at 1000 rpm with boosted inlet conditions (1.5 bar) at an inlet temperature of 60°C. Sample LTHR results are shown in Fig. 17 and Fig. 18 as cylinder pressure and heat release curves, respectively.

Estimated cylinder temperature and measured pressure for the above data point are shown in Fig. 19 with various LTHR milestones marked. The cylinder mixture's thermal state rests in the LT region (first region of short ID, T < 800 K) at the start of HR. The P-T trajectory shows that ID initially decreases but progressive HR causes it to increase despite the accompanying rise in cylinder temperature (i.e. NTC behaviour), which eventually causes HR to cease. In following sections, the effect of changing engine inlet conditions and speed on iso-octane LTHR is discussed by analysing shifts in P-T trajectories.

FIGURE 19 P-T trajectories of cycles from the thermal engine motored with and without iso-octane at T_{in} = 60°C

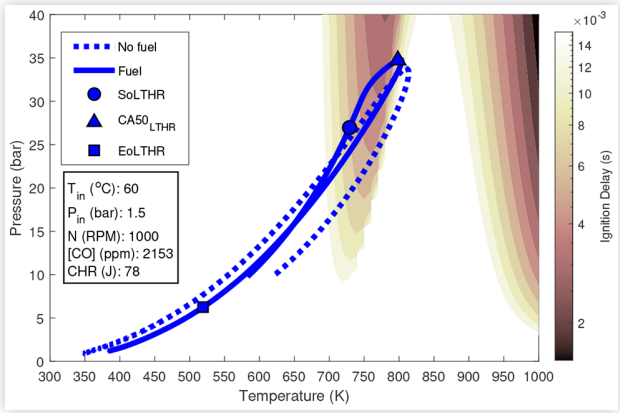

LTHR Vs HTHR LTHR experiments at 1000 rpm and boosted conditions were prone to extreme and inconsistent HTHR events, especially as inlet temperatures increased beyond 70°C. Sample HTHR results are shown in Fig. 20, which contains 25 consecutive HTHR cycles and 25 HTHR-preceding LTHR cycles. Once HTHR started, combustion did not return to the LTHR regime and fuel injection had to be stopped to prevent damage to the engine. Therefore, only a limited amount of iso-octane LTHR data is available at 1000 rpm, which is used in the next section to to discuss the effects of time availability on LTHR.

The occurrence of HTHR can be attributed to the simultaneous (volumetric) HR across the cylinder for a relatively long period of time that increased cylinder temperature sufficiently to shift the mixture state rightward in the P-T space from the LT to the HT region. It can be speculated that after the onset of HTHR, compression P-T trajectories shifted to further higher temperatures because of the presence of hot residual gases. This might explain the apparent irreversible nature of the shift from LTHR to HTHR. Chemical reformation during the relatively long LTHR period could have also changed mixture ID characteristics and contributed to HTHR occurrence. The observed extreme HTHR cycles can be categorised as low-speed pre-ignition, which is known to exhibit LTHR [9] and will be investigated further in future studies using engine chemical kinetics simulation models. LTHR experiments at 1000 rpm in Splitter et al. [7] were also limited to 90°C T_{in} by pre-ignition events.

Temperature Effects on LTHR in Iso-Octane

Inlet temperatures were swept from 60 to 120°C at an inlet pressure of 1.5 bar and engine speed of 1500 rpm. Increasing inlet temperatures increased compression temperatures and decreased compression pressures as shown in Fig. 21 and Fig. 22, respectively. Consequently, the mixture's P-T trajectories moved rightward (Fig. 23) and entered the LTHR short ID region earlier as marked by the red line in Fig. 21. The compression P-T trajectories for the high temperature cases, however, had longer effective ID (i.e. low LW score), which pushed their SoLTHR points close to the NTC region, causing them to land in the NTC region relatively quickly. Resultantly, the amount of energy released via LTHR at high inlet temperatures was limited as shown in the CHR results in Fig. 24. The measured increase in exhaust temperature, shown collectively for two inlet pressures in Fig. 25, demonstrates the same trends. The LTHR intensity trends are consistent with chemical kinetics modelling results from Pan et al. [20] that studied LTHR for n-heptane at different initial temperatures.

Figure 24 also shows that increasing inlet temperatures advances LTHR phasing (CA location at 50% heat release point - CA50). This observation is consistent with iso-octane PSHR experiments by Szybist and Splitter [21] in which relatively advanced LTHR, characterised by a distinct NTC drop

FIGURE 20 Sample iso-octane HTHR results at T_{in} = 80°C, P_{in} = 1.5 bar, and ϕ = 0.75. Bottom subplot is a magnified version to highlight LTHR cycles

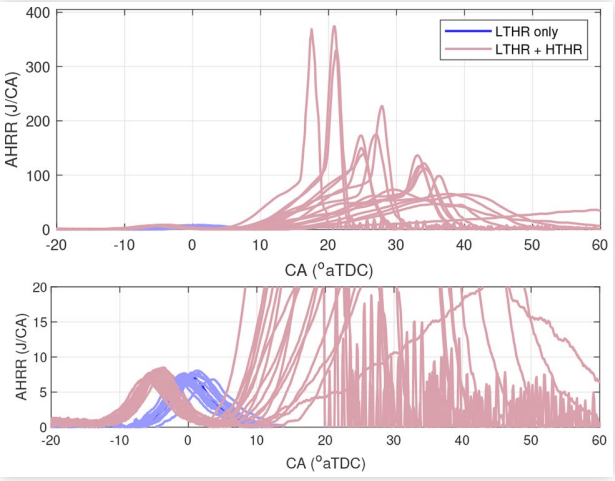

FIGURE 21 Cylinder temperature during compression and initial portion of LTHR at four inlet temperatures (P_{in} = 1.5 bar, 1500 rpm, ϕ = 0.5)

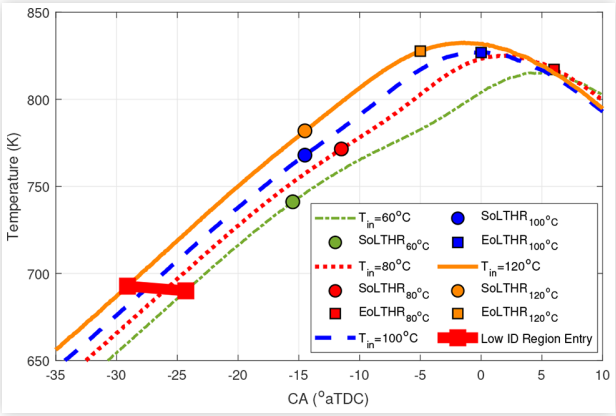

FIGURE 22 Cylinder pressure during compression and initial portion of LTHR at four inlet temperatures (P_{in} = 1.5 bar, 1500 rpm, ϕ = 0.5)

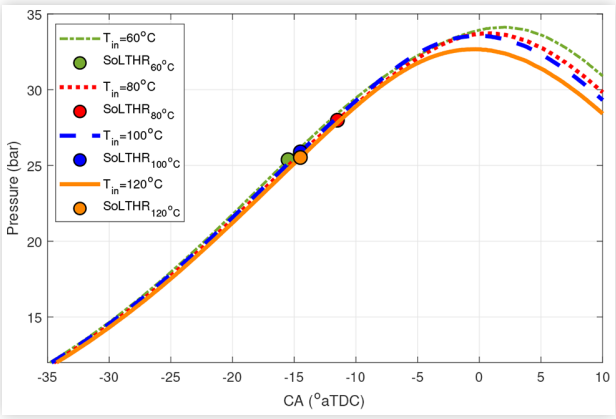

FIGURE 23 P-T trajectories during LTHR at four inlet temperatures (P_{in} = 1.5 bar, 1500 rpm, ϕ = 0.5)

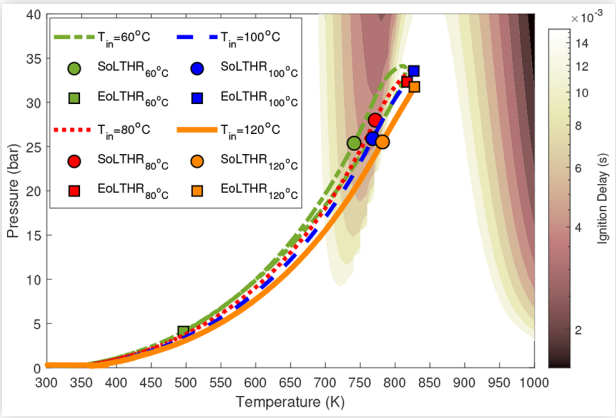

FIGURE 24 Cumulative (left) and rate of apparent heat release (right) at four inlet temperatures (P_{in} = 1.5 bar, 1500 rpm, ϕ = 0.5)

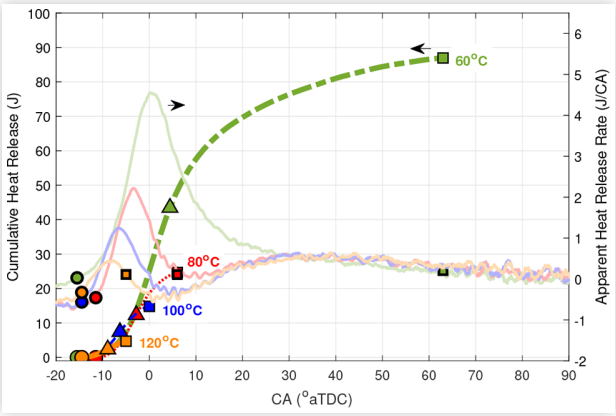

FIGURE 25 Change in LTHR strength (indexed by increase in exhaust temperature) with inlet temperature changes (P_{in} = 1.1 and 1.5 bar, 1500 rpm, ϕ = 0.5)

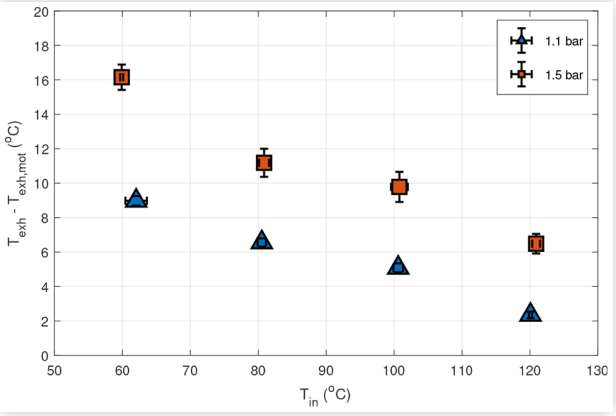

and absence of merged LT-HT HR (intermediate HR), was observed at inlet temperatures above 90°C. The trends regarding the magnitude of LTHR (LTHR weakening at higher temperatures) are, however, opposite. This could be because in the PSHR experiments, a portion of LTHR was obscured by deflagrative HR. In a following study by Splitter et al. [7], inlet temperatures were increased to 180°C, and LTHR intensity was found to reduce beyond 120°C while the advancement of LTHR phasing continued. Waqas et al. [5] reported decreasing LTHR with increasing inlet temperature from 52 to 80°C in a cooperative fuel research engine at relatively low LTHR pressures (< 15 bar) for a PRF-90 fuel (a mixture of 10% (v/v) n-heptane and 90% iso-octane). At elevated temperatures (T_{in} > 60°C), SoLTHR temperatures are nearly constant (Fig. 23). Temperatures at end of heat release are in close proximity as well. These observations might provide support to the idea that fuels with two-stage chemistry 'self-regulate' temperature rise during LTHR, which reduces SI engine knocking sensitivity to inlet temperature [7]. More data including at higher CHR levels will be needed to investigate this thoroughly.

Pressure Effects on LTHR in Iso-Octane

Inlet temperature sweep was repeated at an inlet pressure of 1.1 bar to assess the low pressure limits of iso-octane LTHR. LTHR was still observed but with significantly diminished intensity as shown in Fig. 25 and Fig. 26 by exhaust temperature and CHR results, respectively. The LTHR weakening can be attributed to elongation of the effective ID time (low LW scores) resulting from lowering of the P-T trajectories to low ID regions in Fig. 27. The trends with inlet temperature variations are the same as for 1.5 bar and can be explained using the same line of reasoning. At 120°C, no HR was detected from HR analysis but exhaust temperature results (Fig. 25) indicate weak signatures of LTHR, pointing at the limitations of AHRR based LTHR indexing. Exhaust based measurements and

FIGURE 26 Cumulative LTHR at four inlet temperatures at P_{in} = 1.1 bar, 1500 rpm, and ϕ = 0.5.

Note: The Motoring AHRR Difference Based Method Produced Unrealistic Results At Such Weak LTHR Conditions, Therefore, Only The Firing Cycles Were Used In CHR Computation.

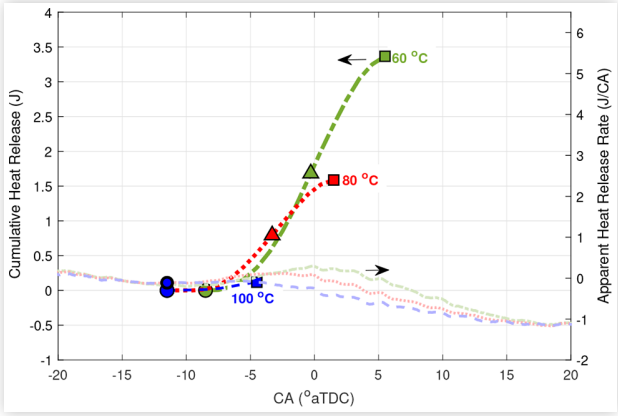

FIGURE 27 P-T trajectories during LTHR or compression in cases with no LTHR at four inlet temperatures (P_{in} = 1.1 bar, 1500 rpm, ϕ = 0.5)

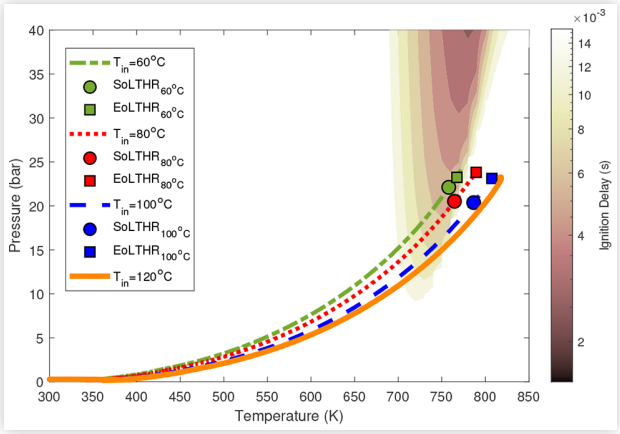

'effective' ID time metrics like the LW score can potentially help provide higher resolution LTHR strength indexing.

Engine Speed Effects on LTHR in Iso-Octane

Tests were performed at 1.5 bar inlet pressure and inlet temperatures of 60 and 80°C at 1000, 1500 and 2000 rpm.

Fig. 28 and Fig. 29 show the cylinder temperature and pressure for the three speed points, respectively. Increasing engine speed increased cylinder temperature because of reduced wall heat losses. The effect on pressure was less pronounced because of accompanying reductions in volumetric efficiency. The resulting effect on the mixture thermal state in the P-T space (Fig. 30) was a rightward shift whereby the compression P-T trajectories entered the LTHR short ID region earlier in the cycle (marked by the red line in Fig. 28). However, the time spent in the LTHR ID region was shorter for the higher speed cases

FIGURE 28 Cylinder temperature during compression and initial portion of LTHR at three engine speeds (P_{in} = 1.5 bar, T_{in} = 60°C, ϕ = 0.5)

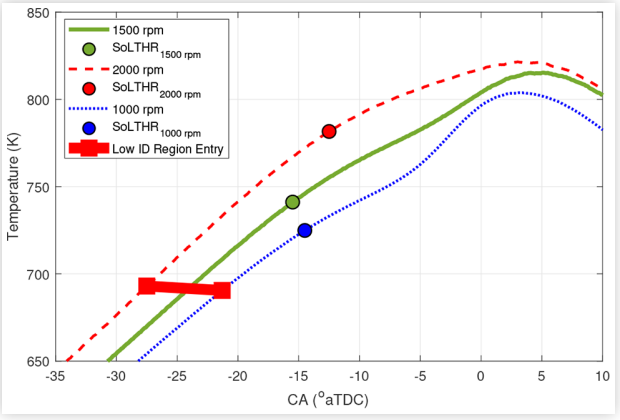

FIGURE 29 Cylinder pressure during compression and initial portion of LTHR at three engine speeds (P_{in} = 1.5 bar, T_{in} = 60°C, ϕ = 0.5)

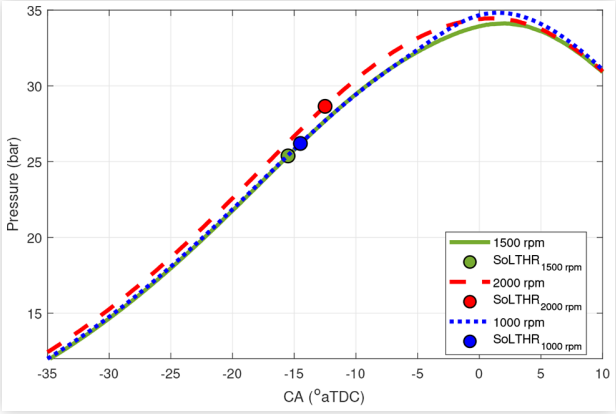

FIGURE 30 P-T trajectories during LTHR at three engine speeds (P_{in} = 1.5 bar, T_{in} = 60°C, ϕ = 0.5)

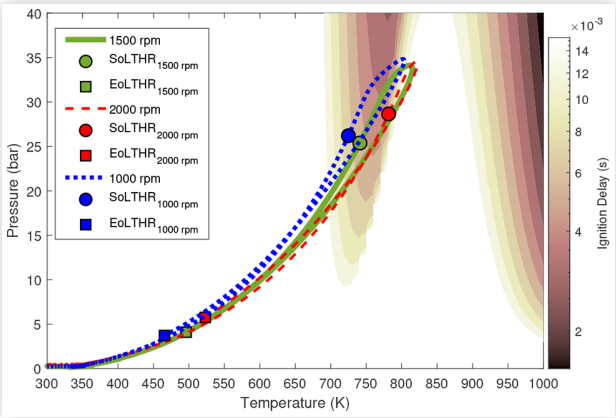

which caused SoLTHR to occur at higher temperatures despite the mixture state traversing the low ID contours that initiated LTHR at 1000 rpm. In other words, though the cylinder mixture's thermal state existed in relatively low ID regions, it did not rest there long enough for sufficient LT reactions to 'build up' to yield sensible LTHR, i.e. the LW score was low.

The location of the SoLTHR points in Fig. 30 for the high speed cases was closer to the NTC region edge, and their respective post-SoLTHR P-T trajectories traversed relatively long ID regions. Resultantly, the total heat release amount was reduced, as can be seen from the AHRR results in Fig. 31. The LTHR intensity observations are also supported by measured rise in exhaust temperatures relative to motoring temperatures (Fig. 32). Such independent experimental indexing of LTHR strength is not possible in combined LTHR-HTHR experiments. Fig. 32 also contains results for 80°C inlet temperature experiments, which indicate a weakening effect of inlet temperatures increase on LTHR as discussed above. The retardation of LTHR phasing (CA50 in Fig. 31) with speed increase can also be explained by the differences in the effective ID times for the three speeds.

FIGURE 31 Cumulative (left) and rate of apparent heat release (right) at three engine speeds (P_{in} = 1.5 bar, T_{in} = 60°C, ϕ = 0.5)

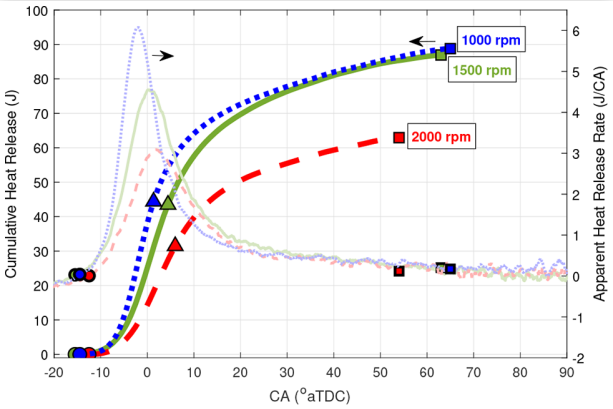

FIGURE 32 Change in LTHR strength (indexed by increase in exhaust temperature) with engine speed changes (P_{in} = 1.5 bar, T_{in} = 60°C and 80°C, ϕ = 0.5)

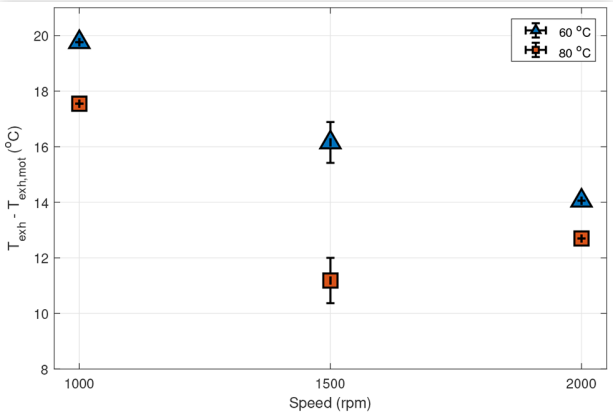

Conclusions

This work has presented, for the first time, LTHR decoupled from HTHR using iso-octane and n-heptane as fuels in two different gasoline direct injection engines. The results showed the following:

1. It is possible to observe LTHR for n-heptane, a low octane number fuel in gasoline direct injection engines, without subsequent HTHR, when inlet heating is utilised.
2. With inlet heating and boosting, isolated LTHR can also be observed for iso-octane, a high octane number fuel.
3. The magnitude of heat release originating from LTHR can be measured by comparing the pressure derived AHRR measurements from a fuelled LTHR case to an unfuelled, motored case.
4. The effect of inlet temperature on isolated LTHR depends on the specific fuel's ignition delay characteristics, and the pressure and temperature conditions that the mixture traverses throughout its cycle. The more time the mixture resided in the short ignition delay (by 50 K rise) region, the more energy was released by LTHR.
5. The net effect of increasing inlet temperature for n-heptane and iso-octane were strengthening and weakening of LTHR, respectively. The changes in LTHR intensity for iso-octane are opposite to what has been reported in PSHR studies.
6. Increasing engine speed and decreasing inlet pressure reduced the amount of energy released through LT reactions because the changes in mixture's state reduced the effective low-ID region residence time.
7. Isolating LTHR allowed indexing of LTHR strength using out-of-cylinder measurements such as exhaust temperature.

References

1. Senecal, K. and Leach, F., *Racing toward Zero: The Untold Story of Driving Green* (SAE International, Jun 2021)
2. Attard, W.P. and Blaxill, H., "A Lean Burn Gasoline Fueled Pre-chamber Jet Ignition Combustion System Achieving High Efficiency and Low Nox at Part Load," in *SAE 2012 World Congress and Exhibition*, SAE International, apr 2012.
3. Leppard, W.R., "The Chemical Origin of Fuel Octane Sensitivity," International Fuels and Lubricants Meeting and Exposition, SAE International, oct 1990.
4. Saisirirat, P., Foucher, F., Chanchaona, S., and Mounaïm-Rousselle, C., "Effects of Ethanol, n-Butanol — n-Heptane Blended on Low Temperature Heat Release and HRR Phasing in Diesel-HCCI," in *9th International Conference on Engines and Vehicles*, Consiglio Nazionale delle Ricerche, sep 2009.
5. Waqas, M.U., Hoth, A., Kolodziej, C.P., Rockstroh, T. et al., "Detection of Low Temperature Heat Release (Lthr) in the Standard Cooperative Fuel Research (Cfr) Engine in both Si and Hcci Combustion Modes," *Fuel* 256 (2019): 115745.
6. Shibata, G., Oyama, K., Urushihara, T., and Nakano, T., "Correlation of Low Temperature Heat Release with Fuel Composition and HCCI Engine Combustion," SAE Technical Paper 2005-01-0138, 2005, https://doi.org/10.4271/2005-01-0138.
7. Splitter, D.A., Gilliam, A., Szybist, J., and Ghandhi, J., "Effects of Pre-Spark Heat Release on Engine Knock Limit,"

Proceedings of the Combustion Institute 37, no. 4 (2019): 4893-4900.

8. DelVescovo, D.A., Splitter, D.A., Szybist, J.P., and Jatana, G.S., "Modeling Pre-Spark Heat Release and Low Temperature Chemistry of Iso-Octane in a Boosted Spark-Ignition Engine," *Combustion and Flame* 212 (2020): 39-52.
9. Splitter, D., Kaul, B., Szybist, J., and Jatana, G., "Engine Operating Conditions and Fuel Properties on Pre-Spark Heat Release and Spi Promotion in Si Engines," *SAE International Journal of Engines* 10, no. 3 (2017): 1036-1050.
10. Hu, Z., Zhang, J., Sjöberg, M., and Zeng, W., "The Use of Partial Fuel Stratification to Enable Stable Ultra-Lean Deflagration-Based Spark-Ignition Engine Operation with Controlled End-Gas Autoignition of Gasoline and e85," *International Journal of Engine Research* 21, no. 9 (2020): 1678-1695.
11. Yamakawa, M., Youso, T., Fujikawa, T., Nishimoto, T. et al., "Combustion Technology Development for a High Compression Ratio Si Engine," *SAE International Journal of Fuels and Lubricants* 5, no. 1 (2012): 98-105.
12. Stone, C.R., *Introduction to Internal Combustion Engines*, 4th ed. (Macmillan International Higher Education, 2012)
13. Leach, F., Stone, R., Davy, M., and Richardson, D., "Comparing the Effect of Different Oxygenate Components on PN Emissions from GDI Engines," 12 2015.
14. Leach, F.C., Davy, M., and Terry, B., "Combustion and Emissions from Cerium Oxide Nanoparticle Dosed Diesel Fuel in a High Speed Diesel Research Engine under Low Temperature Combustion (LTC) Conditions," *Fuel* 288 (2021): 119636.
15. Papaioannou, N., Leach, F.C., Davy, M.H., Weall, A. et al., "Evaluation of Exhaust Gas Recirculation Techniques on a High-Speed Direct Injection Diesel Engine Using First Law Analysis," *Proceedings of the Institution of Mechanical Engineers, Part D: Journal of Automobile Engineering* 233, no. 3 (2019): 710-726.
16. Leach, F., Ismail, R., Davy, M., Weall, A., and Cooper, B., "Comparing the Effect of Fuel/Air Interactions in a Modern High-Speed Light-Duty Diesel Engine," *13th International Conference on Engines and Vehicles*, SAE International, sep 2017.
17. Bresenham, D., Reisel, J., and Neusen, K., "Spindt Air-Fuel Ratio Method Generalization for Oxygenated Fuels," *SAE Transactions* 107 (1998): 2154-2171.
18. Wu, Y., Pal, P., Som, S., and Lu, T., "A Skeletal Chemical Kinetic Mechanism for Gasoline and Gasoline/Ethanol Blend Surrogates for Engine CFD Applications," 5 2017.
19. Urushihara, T., Nakano, T., Shibata, G., and Oyama, K., "Correlation of Low Temperature Heat Release with Fuel Composition and Hcci Engine Combustion," in *SAE 2005 World Congress and Exhibition, SAE International*, apr 2005.
20. Pan, J., Zhao, P., Law, C.K., and Wei, H., "A Predictive Livengood–Wu Correlation for Two-Stage Ignition," *International Journal of Engine Research* 17, no. 8 (2016): 825-835.
21. Szybist, J.P. and Splitter, D.A., "Pressure and Temperature Effects on Fuels with Varying Octane Sensitivity at High Load in Si Engines," *Combustion and Flame* 177 (2017): 49-66.

Contact Information

Felix Leach
Department of Engineering Science,
University of Oxford,
Parks Rd,
Oxford,
OX1 3PJ,
UK
felix.leach@eng.ox.ac.uk

Acknowledgements

This research was funded in whole or in part by the Engineering and Physical Sciences Research Council Prosperity Partnership, grant number EP/T005327/1. For the purpose of Open Access, the author has applied a CC BY public copyright licence to any Author Accepted Manuscript (AAM) version arising from this submission. The Prosperity Partnership is a collaboration between Jaguar Land Rover, Siemens Digital Industries Software, the University of Bath, and the University of Oxford. The authors would also like to thank the Dept. of Engineering Science technicians and maintenance teams for facilities support. Due to confidentiality agreements with research collaborators, data supporting this paper can only be made available to bona fide researchers subject to a non-disclosure agreement. Details of the data and how to request access are available from the "Oxford Research Archive" repository at https://ora.ox.ac.uk/.

Abbreviations

$\frac{dQ_{hr}}{d\theta}$ - Heat release rate

$\frac{dQ_{ht}}{d\theta}$ - Heat transfer rate

$\frac{dQ_{n}}{d\theta}$ - Net apparent heat release rate

γ - Ratio of specific heats

ϕ - Equivalence ratio

τ - Ignition delay

θ - Crank angle

ACI - Advanced Compression Ignition

AHRR - Apparent heat release rate

AI - Auto-ignition

aTDC - After top dead centre

CA - Crank angle

CA50 - CA location at 50% heat release point

CAI - Controlled auto-ignition

CHR - Cumulative heat release

EoLTHR - End of LTHR

GDI - Gasoline direct injection

HR - Heat release

HTHR - High temperature heat release

ICE - Internal combustion engine
ID - Ignition delay
LT - Low temperature
LTHR - Low temperature heat release
LW - Livengood-Wu
NO_x - Oxides of nitrogen
NTC - Negative temperature coefficient
P - Pressure
PRF - Primary reference fuel
PSHR - Pre-spark heat release
Q_{hr} - Heat release
Q_{ht} - Heat transfer
rpm - Revolutions per minute
SI - Spark ignition
SoLTHR - Start of LTHR
T - Temperature
t - Time
T_{in} - Inlet air temperature
TDC - Top dead centre
V - Volume

ISSN 0148-7191

Statement of Authorship for joint/multi-authored papers for PGR thesis

To appear at the end of each thesis chapter submitted as an article/paper

The statement shall describe the candidate's and co-authors' independent research contributions in the thesis publications. For each publication there should exist a complete statement that is to be filled out and signed by the candidate and supervisor **(only required where there isn't already a statement of contribution within the paper itself).**

Title of Paper	Isolated low temperature heat release in spark ignition engines
Publication Status	Published
Publication Details	White, S. P., Bajwa, A. U. & Leach, F. C. P. Isolated low temperature heat release in spark ignition engines. SAE International Journal of Advances and Current Practices in Mobility (2024).

Student Confirmation

Student Name:	Samuel P. White		
Contribution to the Paper	• Idea • Experimental design • Implementation (optical engine and computational modelling) • Data analysis (ignition delay modelling and n-heptane tests) • Writing • Conference presentation		
Signature 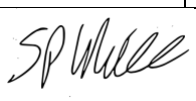		Date	12 April, 2024

Supervisor Confirmation

By signing the Statement of Authorship, you are certifying that the candidate made a substantial contribution to the publication, and that the description described above is accurate.

Supervisor name and title: Felix Leach, Associate Professor of Engineering Science		
Supervisor comments I agree with Sam's comments.		
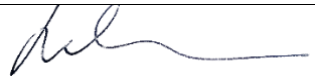	Date	12-4-24

This completed form should be included in the thesis, at the end of the relevant chapter.

The above paper introduced the islated LTHR methodology, a valuable tool for studying LTHR in engines and this is used in the five remaining papers in this thesis. The conclusions on the effects of temperature, pressure and speed on LTHR are used in subsequent work to help determine which parameters to modify to induce LTHR in various scenarios (different compression ratios, boosting capacities, etc.). Furthermore, this study introduced ignition delay analysis, including the Livengood-Wu integral, to isolated LTHR experiments to explain the causes of the physical effects observed in the experiments.

2.1.1 Limitations of the AHRR Technique for Measuring LTHR

As presented in the paper, an AHRR based method, assuming a constant ratio of specific heats (γ) was applied to measure LTHR. Heat transfer effects were imperfectly accounted for by measuring AHRR for the equivalent motoring case of a given test point and subtracting the motoring measurement from the fuelled measurement. In reality, γ is not constant—in fact it changes with the mixture composition (and therefore factors such as equivalence ratio), temperature and, critically, changes as LTHR progresses due to the chemical reactions occurring. The specific composition of intermediate species that were generated was not known and therefore an accurate γ could not be determined. Additionally, the physical differences in heat transfer behaviour between the cylinder wall and just air, compared to the wall and a mixture of air and fuel, are not able to be taken into account with this method.

This method was chosen for its simplicity and because it did a satisfactory job of measuring LTHR. Ultimately, in this work the method only needed to demonstrate the existence of LTHR and be rigorous enough for comparing similar test points—which it was. Whilst the methodology was being developed, more complicated iterations of the technique, which used variable γ, were trialled but were unsuccessful. If an accurate, quantified LTHR was required, further work and different techniques and instrumentation would be required to improve confidence in the precise measurement. Alternatively, a LTHR indicator that is unaffected by the uncertainties in the heat transfer effects could be discovered and applied.

2.1.2 Measurement Uncertainty

The figures containing ignition delay contours and pressure-temperature trajectories are subject to a level of measurement uncertainty that is not fully elucidated in the paper (or any of the subsequent papers in this thesis). The trajectories are comprised of data points, each with a measured pressure and an associated calculated temperature. The cylinder pressure was measured with highly precise instrumentation, with an error of 0.3%. Meanwhile, the temperature calculation used the ideal gas law, which incorporated the same pressure measurement, the volume of the cylinder calculated using knowledge of its geometry, and an estimation of the trapped mass inside the cylinder. The trapped mass estimation was based on relatively precise measurements of fuel

flow rate and air flow rate, but also included a term estimating the residual mass fraction, which was based on previous work carried out at similar engine conditions; this estimate is likely to be the largest single source of error. The uncertainty in the temperature estimates for the pressure-temperature plots is hence a compound of the individual uncertainties of the various measurements and assumptions that it is comprised of. It would be beneficial for future reports on this topic to contain error bars or regions to represent the level of uncertainty in the plotted pressure-temperature trajectories.

2.2 Low Temperature Heat Release and φ-Sensitivity Characteristics of Iso-Octane/Air Mixtures

This paper builds upon the work in Section 2.1 by exploring a physical effect not covered in the previous paper—equivalence ratio. The study uses the methodology from Section 2.1 and builds upon the LTHR measuring technique with exhaust CO measurements that were available in the test cell that was used for these tests, which was also chosen for its relatively high inlet air boosting capacity and fine control and measurement of equivalence ratio by measuring air and fuel flow rates (as opposed to lambda sensor which is designed to be operated around stoichiometric firing).

Contributions

- The relationship between equivalence ratio and isolated LTHR intensity is investigated experimentally and computationally.
- Exhaust carbon monoxide measurements from isolated LTHR are presented as an effective indicator for LTHR intensity.
- The relationship between heat release phasing from LTHR and equivalence ratio is explored.

Taylor & Francis
Taylor & Francis Group

Combustion Science and Technology

ISSN: (Print) (Online) Journal homepage: https://www.tandfonline.com/loi/gcst20

Low Temperature Heat Release and φ-Sensitivity Characteristics of Iso-Octane/Air Mixtures

Abdullah U. Bajwa, Samuel P. White & Felix C. P. Leach

To cite this article: Abdullah U. Bajwa, Samuel P. White & Felix C. P. Leach (05 Sep 2023): Low Temperature Heat Release and φ-Sensitivity Characteristics of Iso-Octane/Air Mixtures, Combustion Science and Technology, DOI: 10.1080/00102202.2023.2245635

To link to this article: https://doi.org/10.1080/00102202.2023.2245635

Published online: 05 Sep 2023.

COMBUSTION SCIENCE AND TECHNOLOGY
https://doi.org/10.1080/00102202.2023.2245635

Low Temperature Heat Release and ϕ-Sensitivity Characteristics of Iso-Octane/Air Mixtures

Abdullah U. Bajwa, Samuel P. White, and Felix C. P. Leach

Department of Engineering Science, University of Oxford, Oxford, UK

ABSTRACT

Chemical energy release from high octane number fuels via low temperature heat release (LTHR) can help develop high-efficiency gasoline engines by promoting ultra-lean combustion in spark ignition engines and improving combustion control in gasoline compression ignition engines. A recently developed experimental technique that permits isolated LTHR investigations in motored engines was used to characterize the LTHR behavior of iso-octane/air mixtures ranging in strength from $\phi \approx 0.02$ to 1.6 at multiple inlet temperature conditions (60 to 120°C). LTHR changes were studied by observing variations in exhaust CO emissions and exhaust temperature increase. Observed heat release results were explained using cylinder mixture pressure-temperature histories alongside supporting chemical kinetics modeling estimates of mixture reactivity in the form of chemical ignition delay (ID) time. The effects of fuel enrichment on iso-octane/air mixture reactivity were found to be non-uniform and dependent on mixtures' thermal state trajectories in the LTHR ID peninsula. LTHR intensity measurements were used to discuss changes in mixture ϕ−sensitivity at different engine inlet conditions. It was shown that by appropriately adjusting mixture thermal conditions via charge cooling from direct fuel injection and intake air heating, reactivity enhancements could be exploited maximally; and strong, positive, linear ϕ−sensitivity of around 10 J per 0.1 increase in ϕ could be realized across a wide range of equivalence ratios from 0.05–1.2. It was also found that dominance of charge cooling effects at rich conditions resulted in negative and zero ϕ−sensitivity regions.

ARTICLE HISTORY
Received 2 May 2023
Revised 11 July 2023
Accepted 27 July 2023

KEYWORDS
Low temperature heat release; ϕ-sensitivity; HCCI; ultra-lean combustion

Introduction

Certain fuels exhibit two-stage auto-ignition (**AI**) chemistry, where mixture temperature and ignition delay (**ID**) are non-monotonically related due to the existence of a negative temperature coefficient (**NTC**) thermal band (Leppard 1990). In internal combustion engines, such fuels release energy through low (<850 K), intermediate (850–1200 K) and high temperature (>1200 K) reactions (Waqas et al. 2019). Heat released via low temperature reactions is known as low-temperature heat release (**LTHR**) and depends on the reacting mixture's NTC characteristics. The two-stage chemistry of straight chain, diesel-like, low octane number fuels such as n-heptane (Pan et al. 2016; Saisirirat et al. 2009) is well established and LTHR has been

CONTACT Samuel P. White samuel.white@eng.ox.ac.uk Department of Engineering Science, University of Oxford, Parks Road, Oxford OX1 3PJ, UK

demonstrated to improve emissions and performance of controlled auto-ignition (**CAI**) engines fueled by such fuels (Bajwa, Leach, and Davy 2023), for example by serving as an ignition trigger and promoting main heat release (Borgqvist, Tunestal, and Johansson 2013), making combustion more resilient to changes in charge state (Sjöberg and Dec 2006), or smoothing heat release and reducing NO_x emissions via staged AI (Sjöberg and Dec 2006; Yang et al. 2011).

Similar benefits can be extended to engines fueled by high octane number, gasoline-like fuels if LTHR can be reliably realized and controlled. This is, however, difficult to achieve as such fuels generally exhibit weak two-stage AI chemistry at typical engine inlet conditions (Saisirirat et al. 2009). If realized, the benefits of LTHR can be exploited in various gasoline-based engines ranging from conventional spark ignition (**SI**) engines to different gasoline fueled CAI embodiments like partially premixed compression ignition (Kalghatgi, Risberg, and Ångström 2007) and spark-assisted compression ignition engines (Olesky et al. 2013). Gasoline LTHR can help improve combustion control and extend operating envelopes of CAI engines, and enable thermally efficient ultra-lean operation in SI engines because of its low temperature and spatially distributed ("volumetric") nature (Collin et al. 2003). Approximately 80% of the global light-duty vehicle fleet is powered by gasoline engines (Senecal and Leach 2021, Ch. 9), therefore, the potential for reducing road transport CO_2 and pollutant emissions is significant. Some benefits of gasoline LTHR have already been demonstrated for SI engines by pre-spark heat release studies as improved knock resistance (Splitter et al. 2019; Szybist and Splitter 2017), and the promise of improved combustion control for gasoline CAI engines has been explored through ϕ-sensitivity studies (Alemahdi et al. 2022; Dec, Yang, and Dronniou 2011; Pintor, Dec, and Gentz 2019).

This paper investigates the LTHR characteristics of iso-octane, used often as a gasoline surrogate (DelVescovo et al. 2020; Pintor, Dec, and Gentz 2019), to help advance the understanding of low-temperature chemistry of such fuels under engine-like conditions. The LTHR potential for different gasoline fuels can vary depending on the particular fuel's octane sensitivity (Alemahdi et al. 2022; Szybist and Splitter 2017), which indirectly captures the extent of its underlying two-stage chemistry (NTC) characteristics. Iso-octane, being a primary reference fuel (**PRF**), has zero octane sensitivity by definition, and possesses relatively pronounced, for a high octane number fuel, NTC characteristics. Its NTC and reactivity (**ID**) attributes are similar to those of conventional gasoline fuels (Pintor, Dec, and Gentz 2019). Other reference fuels like ethanol or toluene-ethanol blended reference fuels have non-zero octane sensitivities and exhibit weaker LTHR (Alemahdi et al. 2022; Shahanaghi et al. 2022).

Previous engine studies using iso-octane have identified the following effects of changes in compressed mixture thermal and chemical states on LTHR behavior:

(i) Increasing compression pressure generally supports LTHR onset and increases its intensity by making the mixture's thermal state traverse low ID regions (Szybist and Splitter 2017; White et al. 2023).
(ii) Depending on the operating pressure and equivalence ratio, which determines the mixture's thermal state relative to the NTC region, increasing compression temperature can weaken (White et al. 2023) or strengthen LTHR (Szybist and Splitter 2017) even though the effect of solely changing mixture temperature is to increase reactivity (Pintor, Dec, and Gentz 2019).

(iii) Increasing compression time by reducing engine speed strengthens LTHR by allowing more time for chain-branching exothermic reactions to occur, and can even lead to high temperature heat release if the mixture state resides in low ID regions for a prolonged period (Shahanaghi et al. 2022; Splitter et al. 2019; White et al. 2023).
(iv) Under suitable thermal conditions, increasing the fuel-air equivalence ratio (ϕ) enhances mixture kinetics (i.e. shortens ID) and increases LTHR (Dec and Sjöberg 2004; Pintor, Dec, and Gentz 2019; Sjöberg and Dec 2006).

This enhancement is weaker than for lower octane number fuels. Another factor that can influence LTHR is the presence of residual gases, which can have varied net effects depending on the interplay between their diluting, heat capacity, chemical, and charge heating influences. DelVescovo et al. (2020) predicted that the presence of NO in residual gases can significantly strengthen iso-octane LTHR.

A mixture property which has been used to study the effects of changing ϕ on reactivity is ϕ-sensitivity, which can be expressed in general terms as:

$$\phi - \text{sensitivity} = \frac{d(ReactivityIndex)}{d(\phi)} \tag{1}$$

The Reactivity Index can be any quantifier of a mixture's propensity to combust in an engine, e.g. ignition delay computed from chemical kinetics models (Pintor, Dec, and Gentz 2019), or empirically determined auto-ignition or combustion indices like crank angle location of 10% (Dec, Yang, and Dronniou 2011; Yang et al. 2011) or 50% (Sjöberg and Dec 2006) mass fraction burned point, pressure at start of heat release (Alemahdi, García, and Tunér 2022), or compression ratio in a cooperative fuel research engine needed to keep combustion phasing constant for different ϕ mixtures (Alemahdi et al. 2022).

Dec and Sjöberg (2004) attempted to smooth heat release in gasoline CAI engines by using ϕ-sensitivity to create a LTHR intensity distribution corresponding to a mixture ϕ distribution generated via partial fuel stratification. It was hypothesized that richer strata would have significantly enhanced reactivity and would thus release more energy via "pre-ignition" reactions (i.e. LTHR), compared to leaner, less reactive strata. Consequently, LTHR would take place in stages across the cylinder ("sequential auto-ignition") and cumulative heat release would be milder. Desired smoothing was achieved for a two-stage AI chemistry fuel (PRF-73, a mixture of 73% iso-octane and 27% n-heptane), but not for iso-octane, which at the naturally aspirated conditions studied did not exhibit NTC behavior. This led the authors to conclude that mixtures exhibiting single-stage AI chemistry could not sequentially auto-ignite as their reactivity did not increase appreciably with ϕ, i.e. they had weak ϕ-sensitivity. For the iso-octane mixtures, the thermal effects of increased direct fuel injection (charge cooling and reduction in the compressed mixture's ratio of specific heats, γ) dominated the mild chemical effects.

Later studies by Dec and coworkers (Dec, Yang, and Dronniou 2011; Pintor, Dec, and Gentz 2019) on boosted CAI engines found that weak NTC fuels like iso-octane exhibited noticeable ϕ-sensitivity when compression pressures were increased, and could thus potentially be used for sequential auto-ignition. The ϕ-sensitivity of gasoline and iso-octane was reported to increase significantly as inlet pressures were increased to 2.5 bar. Chemical

kinetics modeling using a detailed (2027 species) Lawrence Livermore National Laboratory (**LLNL**) mechanism revealed that highest ϕ-sensitivities existed in the NTC region, especially near the "cold side of the NTC zone." The emergence of ϕ-sensitivity at high pressures was, however, attributed to intermediate (850–1200 K), not low, temperature heat release reactions based on a categorization approach that used H_2O_2 as a combustion tracer.

This work will explore, in-depth, the reactivity effects of iso-octane and the potential for promoting LTHR via fuel enrichment, as well as managing the intensity and phasing of LTHR by controlling mixture thermal conditions. Previous iso-octane LTHR and ϕ-sensitivity studies (Alemahdi et al. 2022; Dec and Sjöberg 2004; Sjöberg and Dec 2006; Yang et al. 2011) have been limited in their explorations by difficulties in observing reactivity effects on LTHR in isolation because of confounding effects of high-temperature reactions, which change the thermal and chemical properties of the compressed mixture. Dec and Sjöberg (2004) used a sequenced firing technique to partially isolate chemical kinetics effects from thermal effects where every 19^{th} cycle had a richer mixture than the preceding 18 cycles. Previous studies have experimentally looked at mixture strengths up to $\phi \approx 0.47$ (Sjöberg and Dec 2006; Yang et al. 2011), likely because of high-temperature heat release intensity and pressure rise rate limitations.

A recently developed experimental technique (White, Bajwa, and Leach 2023) that enables isolated investigation of LTHR is used here to study the LTHR and ϕ-sensitivity characteristics of iso-octane/air mixtures ranging in strength from $\phi = 0.02$ - 1.6. The technique realizes isolated LTHR by motoring a moderate compression ratio gasoline direct injection engine at elevated intake temperatures and, if need be, pressures to induce LTHR reactions without triggering high temperature heat release. It thus captures the net effects of the mixture's thermal state and chemical reactivity on LTHR. The contributions of the two changes are then isolated by using chemical kinetics simulations to compute mixture ID and cylinder pressure measurements to estimate the compressed mixture's pressure-temperature (**P-T**) histories.

Methodology

Experimental facility

A single cylinder, gasoline direct injection engine based on a Ricardo Hydra bottom end was used for the experimental investigations. Its technical specifications are summarized in Table 1. The engine was coupled to a 57 kW AC motoring dynamometer (Vascat MAC-Q) that maintained the required speed (±1 rpm). Fuel injection settings (timing, duration, rail pressure) were controlled by a Schaeffler Protronic ECU via an ETAS INCA interface. Ignition was disabled during the

Table 1. Engine specifications.

Bore [mm]	83.0
Stroke [mm]	92.0
Displacement [cm^3]	497.8
Compression ratio	10.56:1
Fuel injection system	Production direct injector centrally mounted in cylinder head

LTHR testing using the ECU. The engine was operated at wide open throttle and intake pressure was maintained at desired levels using an external boosting rig. Intake air was heated using an electric heater installed upstream of the throttle valve and intake plenum. Engine coolant and oil temperatures were maintained at 90°C during experiments using closed loop temperature control systems.

Inlet pressure and temperature were measured around 35 cm upstream of the inlet ports using a flexible silicon pressure sensor (Druck UNIK 5000) and a 3 mm k-type thermocouple, respectively. Fuel and air flow rates were measured using a Coriolis (Siemens FC Mass 2100) and a hot wire (Sierra-CP Airtrak 628S) flow meter, respectively. A Horiba MEXA-ONE emissions analyzer was used to measure exhaust composition. These "slow-speed" parameters were recorded at a frequency of 1 Hz using a Sierra-CP CADET system. A water-cooled piezoelectric transducer (Kistler-6041B) was used to measure cylinder pressure, which was logged at a resolution of 0.1°CA using an AVL Indiset data acquisition system. Slow speed data was logged for 30 seconds, while high-speed measurements were recorded for 300 cycles. AVL Concerto and custom MATLAB scripts were used for data post-processing. More details about the test cell can be found in previous publications (Leach, Davy, and Terry 2021; Papaioannou et al. 2019).

Operating conditions

Tests were performed at a constant speed of 1500 rpm, with the exception of some preliminary test points to demonstrate the difference between LTHR and HTHR that were at 1000 rpm (Figures 2 and 3). The inlet pressure was maintained at 1.5 bar (absolute), and mixture strengths were varied from very lean ($\phi \approx 0.02$) to very rich ($\phi = 1.2$–1.6) conditions at five inlet temperatures (40–120°C). Equivalence ratios were calculated from fuel and air flow measurements, and verified from exhaust emissions using the "Spindt" method (Bresenham, Reisel, and Neusen 1998) up to $\phi \approx 0.55$. Beyond that, the unburned hydrocarbon sensor started to saturate and only the air and fuel flow measurements were used for determining ϕ. Inlet temperature was maintained within ±2°C and pressure within ±0.01 bar. Engine settings are listed in Table 2 and a summary of all the test points (174 in total) is shown in Figure 1.

Table 2. Engine settings.

Parameters	Values
IVO [°CA aTDC]	−352
IVC [°CA aTDC]	−165
EVO [°CA aTDC]	159
EVC [°CA aTDC]	359
Speed [rpm]	1500
Injection pressure [bar]	140
Injection timing [°CA aTDC]	−300
Inlet temperature [°C]	40, 60, 80, 100, 120
Inlet pressure (Pin) [bar]	1.5
Equivalence ratio (**Φ**)	0.02–1.6
Fuel	iso-octane (>99% purity)

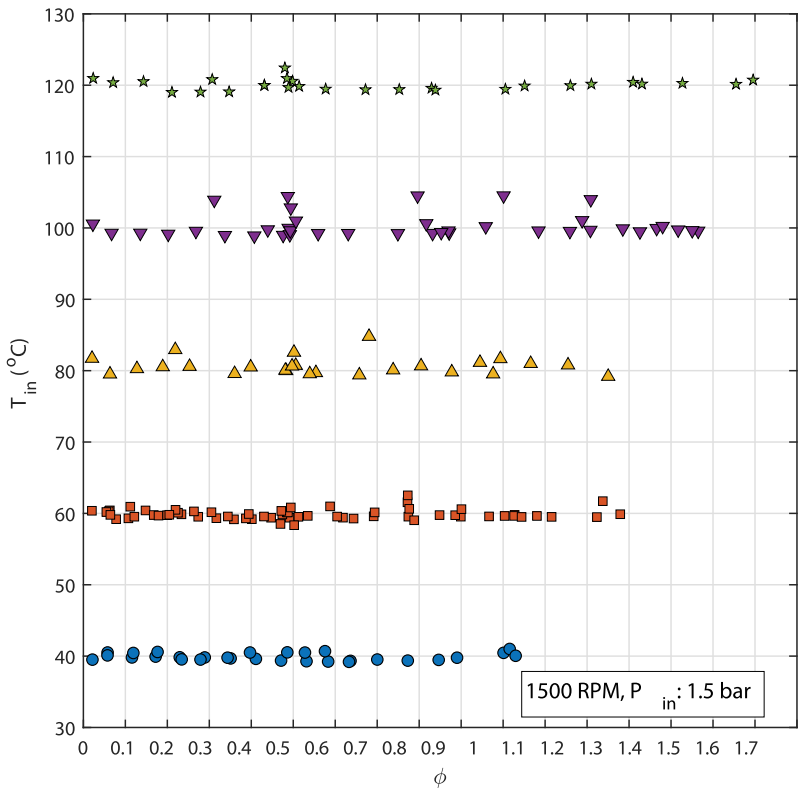

Figure 1. Summary of experimental test points.

Apparent heat release analysis

Net apparent heat release rate **(AHRR)** was calculated from measured cylinder pressure as described in (White, Bajwa, and Leach 2023). A heuristic feature identification-based method, adapted from Saisirirat et al. (2009), was then to determine LTHR duration, magnitude, and phasing. Start of LTHR (**SoLTHR**) was defined as the positive inflection point in the AHRR curve and end of LTHR (**EoLTHR**) was defined as the point when AHRR returned to the SoLTHR level. Start of high-temperature heat release (**SoHTHR**) was determined similarly. LTHR duration was defined as the difference between EoLTHR and SoLTHR, and the center of combustion (median of LTHR crest, **CA50**) was used to index LTHR phasing.

Modelling

Ignition delay simulations were performed in CHEMKIN using the closed homogeneous ignition delay model with a constant volume. The simulations modeled 200 ms of reactions, and reported ID defined by a 50 K rise in temperature in order to detect the relatively small rises in temperature caused by LTHR. The approach has been successfully used in previous engine LTHR studies (Splitter et al. 2019; Szybist and Splitter 2017) for indexing LTHR ID times. Note, however, that the LTHR ID calculated here is slightly different from the first-stage

ID calculated in the literature from the temperature rise rate (Pan et al. 2016; Tao et al. 2019). The LTHR ID definition was selected to manage the computational expense of indexing low temperature reactivity at the wide range of mixture temperature, pressure, and ϕ points studied. Mixtures of air and iso-octane were modeled at multiple equivalence ratios ranging between 0.064 and 1.3 using a reduced Lawrence Livermore National Laboratory (LLNL) gasoline surrogate mechanism with 165 species and 839 reactions (Wu et al. 2017).

P-T trajectories were generated using measured cylinder pressure and calculated average cylinder temperature. The cylinder temperature was calculated using the ideal gas law with measured cylinder pressure, calculated cylinder volume, and estimated trapped cylinder mass.

Results

Low vs high temperature heat release

Figure 2 shows pressure-temperature (P-T) traces on an ID map for two types of LTHR cycles – one (the orange solid line) which led to high-temperature heat release (HTHR) and one which terminated after LTHR, i.e. exhibited isolated LTHR (the blue dashed line). The corresponding AHRR curves are shown in Figure 3. The results demonstrate the distinct nature of the two heat release stages, whereby the first stage exists in the LTHR band (700–800 K), referred to here as the LTHR peninsula; and the high temperature stage takes place in the so-called HTHR peninsula. The end of LTHR and the subsequent start of HTHR in the HTHR cycle are characterized by the NTC-induced drop in cylinder pressure, followed by a rapid rise in mixture temperature resulting from high temperature combustion. Whereas, for the isolated LTHR cycle, the pressure and temperature drop after the end of LTHR because of expansion. Based on these distinct LTHR and HTHR characteristics it is reasoned that the measurements from isolated LTHR experiments carry signatures of only LTHR. Note that the results in Figures 2 and 3 are from

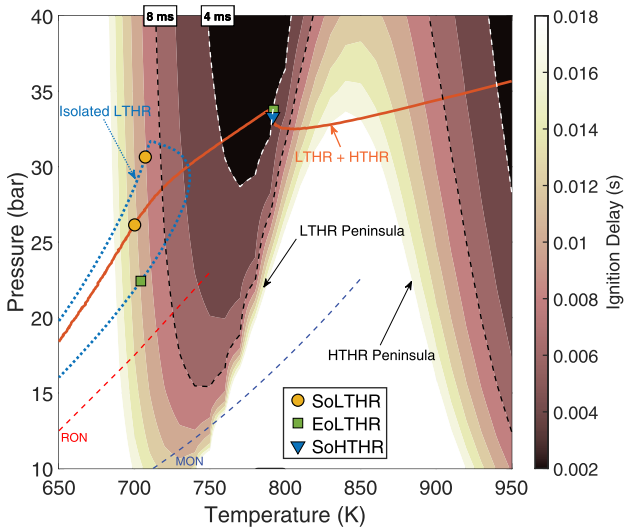

Figure 2. P-T trajectory for $\phi = 0.7$ mixtures at $T_{in} = 60$°C and 1000 rpm undergoing isolated LTHR and LTHR + HTHR with research octane number (RON) and motor octane number (MON) trajectories shown for reference.

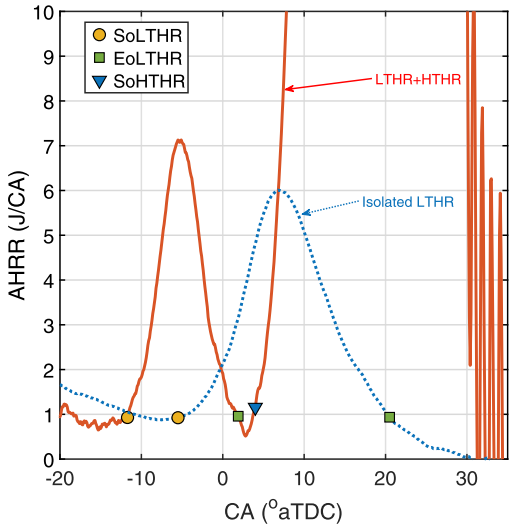

Figure 3. Apparent rate of heat release for $\phi = 0.7$ mixtures at $T_{in} = 60$°C and 1000 rpm undergoing isolated LTHR and LTHR + HTHR.

a 1000 rpm case because HTHR was not observed at higher speeds, as has been discussed in White, Bajwa, and Leach (2023).

LTHR strength indices

To discuss the effects of changes in mixture state and reactivity on the strength of LTHR, high sensitivity heat release indicators are needed. The isolated LTHR experimental approach makes available multiple parameters to choose from – some directly measured ones like exhaust gas temperature (**EGT**), exhaust emissions, engine torque and indicated mean effective pressure (**IMEP**); and some indirectly computed ones like cumulative heat release (**CHR**) and integrated Livengood-Wu (**LW**) type progress variables (Pan et al. 2016).

The following parameters were compared using the entire experimental data set (Figure 1) to select appropriate LTHR indicators: IMEP, CHR, EGT rise relative to motored EGT, and exhaust CO, CO_2, NO_x, and O_2 concentrations. LW scores, which have been shown to be high-sensitivity indicators of LTHR intensity (Pan et al. 2016; White, Bajwa, and Leach 2023), were not considered because their computation requires accurate quantification of cylinder temperature, which was difficult to accomplish for the current engine because of uncertainty associated with its residual gas fraction. Rough bulk cylinder temperatures computed using an estimated residual gas fraction of 10% are, however, used throughout the paper for qualitative discussions of "effective" ID times. These discussions assume that the shorter the effective ID for a given process, as computed by the LW progress variable score ($\int \frac{dt}{ID(P,T,\phi)}$), the stronger will be the resulting LTHR.

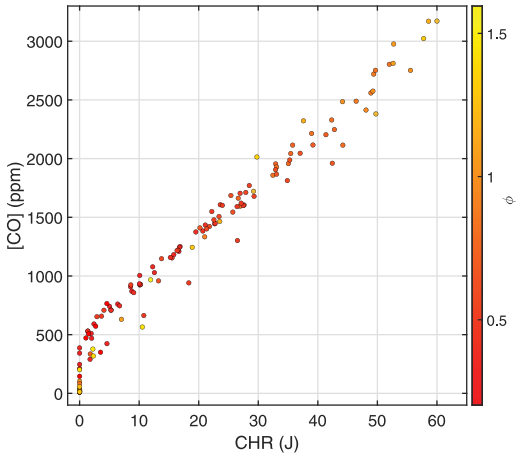

Figure 4. LTHR indexing using CHR and exhaust CO concentration.

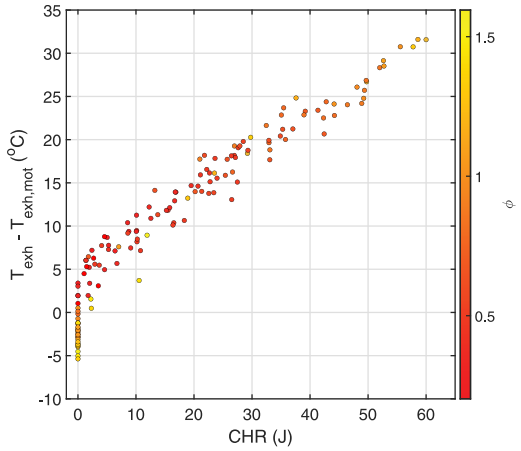

Figure 5. LTHR indexing using CHR and EGT rise.

Exhaust CO and temperature rise exhibited consistent trends with and high sensitivity to changing LTHR intensity, as shown in Figures 4 and 5, respectively, which makes them promising LTHR intensity indicators. Both increased monotonically with CHR beyond an initial weak LTHR region (CHR <3 J) at approximate rates of 40 ppm/J and 0.5°C/J, respectively. The initial CHR insensitivity to heat release intensity highlights limitations of the apparent heat release rate based LTHR indexing method used when very small quantities of energy are released.

EGT rise results presented a wider spread in the weak LTHR (CHR = 0) band because, unlike exhaust CO, the effects of evaporative cooling from fuel vaporization (charge cooling) were directly captured. These effects were particularly pronounced for the very rich cases (see color bar to right) where there was no sensible LTHR as per the CO and CHR results. EGT results can also be influenced by variations in heat release phasing as they

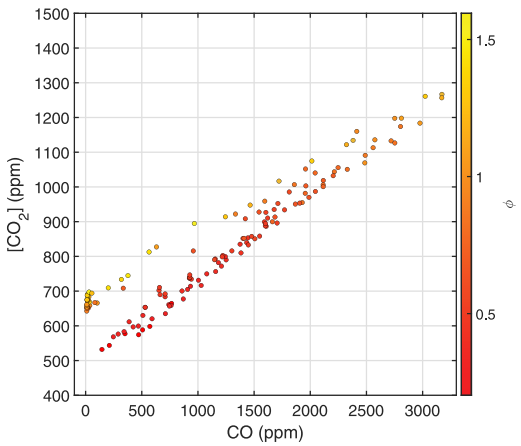

Figure 6. LTHR indexing using exhaust CO_2 and CO concentration.

depend on the cylinder temperature and pressure at the point of exhaust valve opening, whereas post-LTHR CO concentrations can be assumed to be "frozen." Therefore, CO was considered to be a more robust LTHR indicator and is thus preferred in the following discussion.

Exhaust CO_2 also captures LTHR intensity changes as can be seen from the exhaust CO_2 vs CO scatter plot in Figure 6. It, however, has lower sensitivity than CO (11 vs 40 ppm/J) and is, therefore, a weak LTHR indicator. An inconsistency in trends can be observed at rich cases in the CO_2 results, whereby CO_2 concentrations do not return to motoring levels (440–470 ppm) even when CO results indicate cessation of LTHR reactions. This likely represents a limitation, for very rich mixtures, of the non-dispersive infrared type analyzer used. Notwithstanding this, all LTHR indicators considered (CO, CO_2, CHR, EGT rise) showed consistent trends between $0.2 < \phi < 1$ and had correlation coefficients greater than 92%.

Equivalence ratio effects

LTHR intensity effects

The effects of changing ϕ on LTHR intensity are shown in Figure 7 by exhaust CO concentration measurements at the constant inlet temperature of 60°C. LTHR can be observed at very lean conditions, outside of the typical lean flammability limits of deflagrative combustion, which for iso-octane/air mixtures have been reported to range between $\phi = 0.55$ and 0.625 (Liu, Akram, and Wu 2020). CO concentration of 75 ppm was recorded at $\phi = 0.055$, which is indicative of oxidation reactions taking place in the very lean mixture. LTHR at such lean conditions can be attributed to its occurrence at low temperatures and its volumetric nature, whereby oxidation reactions take place in the dilute homogeneous fuel-air mixture throughout the combustion chamber and cumulatively generate sensible heat release signatures.

In Figure 7, increasing ϕ up to around 0.7 gradually strengthens LTHR, beyond which LTHR weakens rapidly reaching near-motoring levels for stoichiometric mixtures. These

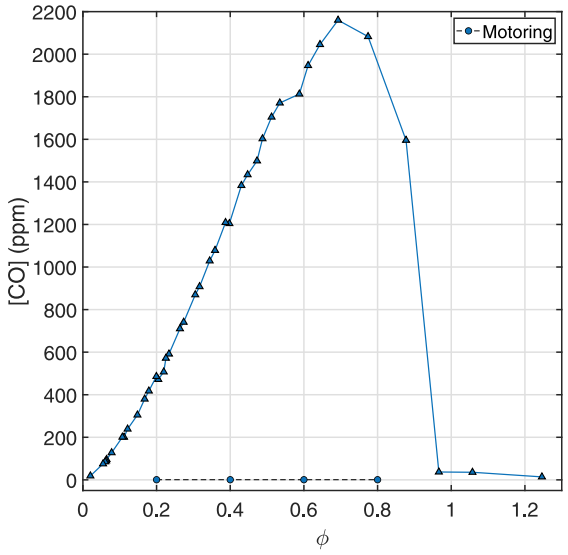

Figure 7. Exhaust CO concentration at $T_{in} = 60$°C.

observations can be explained by the differences in the ID of the various ϕ mixtures and their respective compression P-T histories. ID differences represent the effects of changes in AI chemistry of the mixture, specifically its reactivity, while the P-T trajectories represent thermal conditions.

ID effects

Figure 8 presents selected ID contours at different ϕ levels to illustrate the increase in mixture reactivity accompanying mixture enrichment. 8 and 4 ms ID contours are selected to, respectively, represent contours close to the periphery and the core of the LTHR

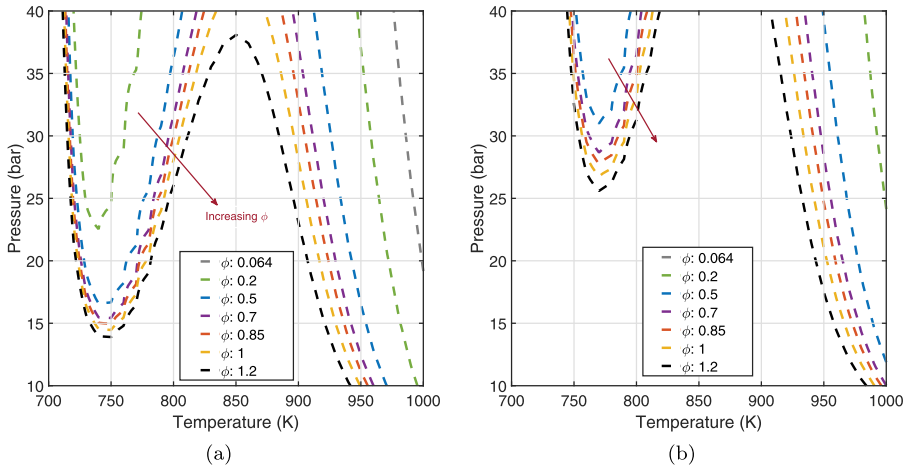

Figure 8. (a) 8 ms and (b) 4 ms ignition delay contours at various equivalence ratios (T_{in}= 60^{o}C).

peninsula. Doing so permits direct comparison of reactivity across different ϕ levels. Figure 2 provides an example of a complete ID map at a constant ϕ value. The contours in Figure 8 show that increasing ϕ expands the LTHR peninsula, potentially enabling mixtures at lower pressure and temperature to undergo LTHR. The rightward expansion also increases the likelihood of LTHR reactions for higher temperature mixtures. The reactivity enhancement is more pronounced toward the high temperature (right) edge of the LTHR peninsula. This is consistent with detailed chemical kinetics modeling results from (Zhao and Law 2013) and (Pintor, Dec, and Gentz 2019). Another observation from Figure 8 is that relativity low marginal reactivity enhancement takes place for mixtures richer than $\phi \approx 0.5$, i.e. ϕ-sensitivity decreases for relatively rich mixtures.

The thermal effects of fuel enrichment result primarily from increased charge cooling as greater quantities of fuel are injected, and secondarily from reduction in the compressed mixture's ratio of specific heats, γ. The charge cooling effects are expected to be less significant in non direct injection engines. Both of the fueling effects lower the cylinder pressure and temperature during compression, and move P-T trajectories leftward in the P-T space. This can be seen in Figure 9 in which the ID contours from Figure 8 are overlaid with P-T trajectories for various ϕ cases. The leftward movement of the P-T traces from $\phi = 0.064$ to 0.85 moves the mixture thermal states closer to the low ID core of the LTHR peninsula, thus reducing the effective ID; plus, it permits increased exploitation of the rightward LTHR peninsula expansion (i.e. the high ϕ-sensitivity region). The initial increase in LTHR intensity reported in Figure 7 is the combined result of these thermal and chemical influences of increased fueling. Additional fuel enrichment increases the effective ID because the compression P-T traces are shifted further left and brought close to the left edge of the LTHR peninsula where mixture reactivity is not enhanced appreciably (i.e. low ϕ-sensitivity region).

LTHR based $\phi-$sensitivity characterization

Figure 7 results can be used to describe $\phi-$sensitivity behavior of the various compressed mixtures by using LTHR intensity as a reactivity index. At the selected inlet temperature

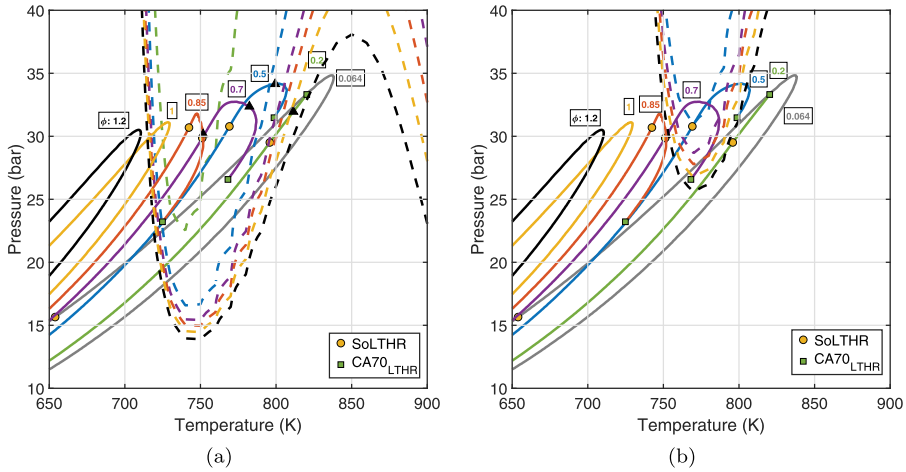

Figure 9. Changes in P-T trajectories at different equivalence ratios shown using (a) 8 ms and (b) 4 ms ignition delay contours (T_{in}= 60°C).

and engine conditions, the near-linear increase in LTHR intensity up to $\phi = 0.7$ corresponds to a constant $\phi-$sensitivity of around 420 ppmCO/0.1$\phi_{increase}$, which translates to 10 J/0.1$\phi_{increase}$ using Figure 4, i.e. an additional 10 J of heat is released per cycle via low temperature reactions for every 0.1 increase in ϕ. This is followed by a period negative $\phi-$sensitivity up to $\phi \approx 1$. Further fuel addition renders the mixture $\phi-$insensitive. The negative ϕ-sensitivity region represents the relatively rich conditions where fuel injection induced P-T lowering effects dominate over mixture reactivity enhancement from mixture enrichment. Other LTHR strength indices discussed earlier can also be used as reactivity indices to describe $\phi-$sensitivity changes.

LTHR phasing effects

The effects of ϕ changes on heat release phasing with respect to the total amount of heat released are shown in Figure 10 for mixtures in which heat release was detected using the AHRR technique employed. Combustion phasing and duration changes are summarized in Figure 11. Upon mixture enrichment, combustion phasing is initially retarded from around – 7 CA°aTDC to 6 CA°aTDC as LTHR intensity increases up to $\phi \approx 0.8$; after which, as LTHR weakens upon further fuel addition, combustion phasing retards at a much slower rate before settling at around 8 CA°aTDC for the richest cases. The retardation of combustion phasing is largely caused by combustion duration elongation as LTHR strengthens. Therefore, the combustion duration increases by almost the same number of degrees as the center of combustion retards. The slight decrease in combustion duration at $\phi > 0.8$ results from charge cooling induced LTHR weakening. The SoLTHR is slightly delayed upon mixture enrichment from – 6 to – 12 CA°aTDC (yellow circles in Figure 10), which contributes minimally

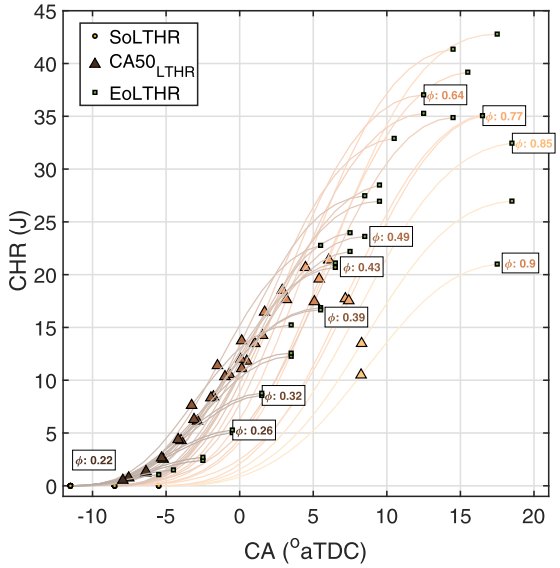

Figure 10. Changes in LTHR intensity and phasing with changing ϕ at $T_{in} = 60$°C. Colour map is scaled from $\phi = 0.9$ (lightest) to $\phi = 0.22$ (darkest).

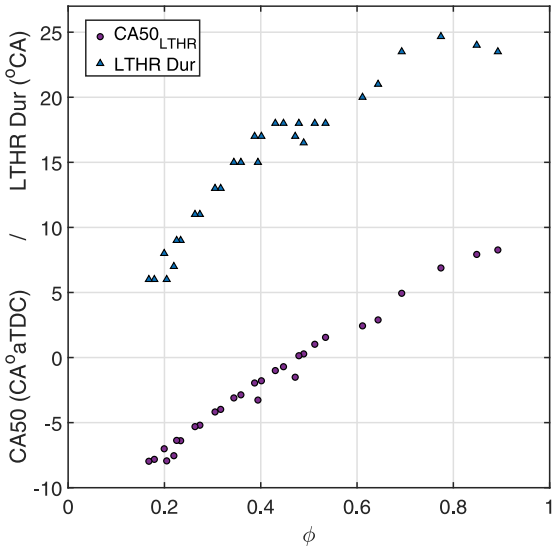

Figure 11. Changes in LTHR phasing and duration with changing ϕ at $T_{in} = 60$°C.

to LTHR phasing retardation. The low sensitivity of SoLTHR to ϕ is similar to results from (Pintor, Dec, and Gentz 2019) who, for a firing CAI engine, found the start of LTHR to be ϕ-insensitive but that of main combustion (HTHR) to be ϕ-sensitive. The current isolated-LTHR results show that even in the absence of hot combustion residuals, SoLTHR is ϕ-insensitive. Therefore, charge enrichment or heating alone cannot be used to control SoLTHR. Other means of decreasing effective ID before SoLTHR would be needed, e.g. increasing pressure was shown to advance SoLTHR in (White, Bajwa, and Leach 2023).

The LTHR phasing results also have the same trends as those from Yang et al. (2011) who reported that CA10 ("hot-ignition timing;" similar to CA50 here) for iso-octane/air mixtures retarded as mixtures became richer. The phasing shift was attributed to reduction in compression temperatures and absence of two-stage AI chemistry at the engine inlet conditions (1 bar, 174°C). The reasons for CA50 retardation for the current boosted engine are, however, different as the iso-octane/air mixtures do exhibit NTC behavior leading to a significant reactivity enhancement (positive ϕ-sensitivity), and resulting in stronger and longer LTHR with later LTHR centers. This, then, leads to an advantage of direct quantification of LTHR, directly coupled to the NTC characteristics of the reacting mixture and thus prevents obfuscation by the "main" heat release.

A practical implication of the AHRR results is that the SoLTHR cannot serve as a LTHR ϕ-sensitivity indicator, whereas, LTHR phasing and duration, both of which increase as LTHR strengthens (Figure 7), can be used for characterizing ϕ-sensitivity in AHRR-sensible regions.

Temperature effects

It was concluded from Figures 9 and 10 results that the increase in LTHR upon fuel enrichment was limited by the thermal cooling effects of fuel injection which shifted the compressed mixture's thermal state leftward to the low ϕ-sensitivity region. It is hypothesized that if the P-T trajectories can somehow be translated rightward, the high ϕ-sensitivity region can be exploited to overpower the reactivity diminishing thermal effects of fueling. This is attempted by increasing inlet temperature to raise the compression temperatures.

Inlet temperature is varied from 40 to 120°C in 20°C increments. The resulting effects on LTHR intensity are shown in Figure 12 at different ϕ levels. Increasing inlet temperature raises the peak LTHR intensity and delays the following charge cooling drop to richer equivalence ratios. This is shown separately in Figure 13. The peak LTHR intensity nearly doubles as the inlet temperatures rise from 40°C to 120°C and the corresponding ϕ (ϕ_{max})

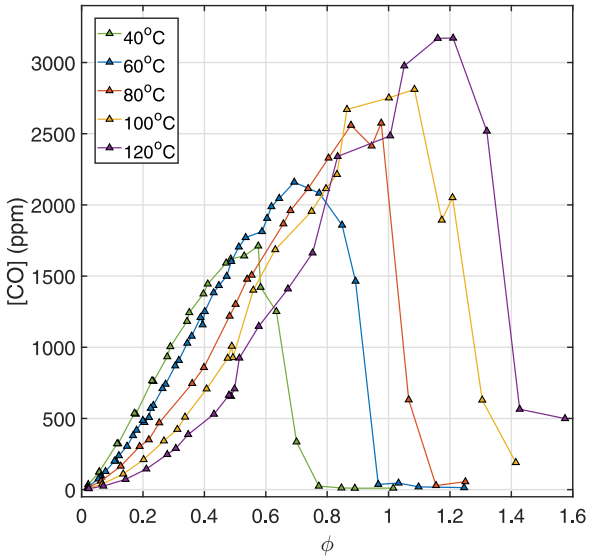

Figure 12. Exhaust CO concentration at $T_{in} = 40 - 120$°C.

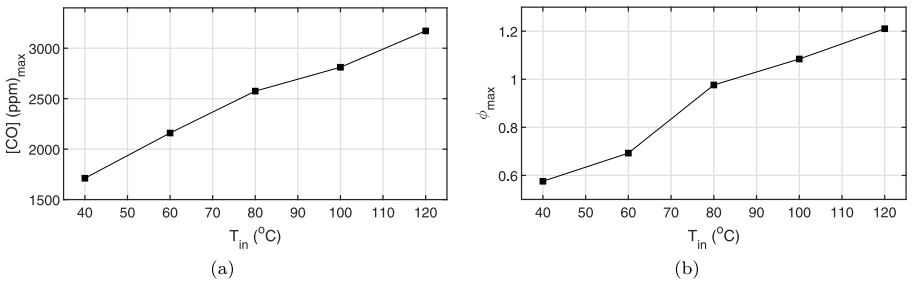

Figure 13. (a) Maximum exhaust CO concentration and (b) corresponding ϕ at different inlet temperatures.

shifts from 0.53 to 1.16. ϕ_{max} marks the equivalence ratio where ϕ-sensitivity changes from positive to negative.

These trends can be explained by looking at the respective thermal state histories to deduce the effective ID times. Figure 14 shows an ID map for $\phi = 0.5$ mixtures with P-T traces at different inlet temperatures overlaid. At such relatively lean conditions, charge cooling effects are weak and the LTHR peninsula is relatively narrow. Hence, increasing the inlet temperature significantly shifts the P-T traces from the LTHR peninsula core rightward across the high-temperature edge, leading to an increase in the effective ID time. Consequently, at very lean conditions ($\phi < 0.5$), inlet heating has the net effect of weakening LTHR as confirmed by the measured LTHR results in Figure 12.

As mixtures become richer, charge cooling and specific heat ratio effects become more pronounced as can be seen by the leftward shift in the P-T trajectories (relative to leaner mixtures at the same temperatures) for $\phi = 0.7$ mixtures shown in Figure 15. This decreases the effective ID time for inlet temperature cases of 60°C and higher, and thus strengthens LTHR. For the 40°C case, however, the excessive leftward shift increases the effective ID time and weakens LTHR (Figure 12). Figure 16 shows P-T traces for the stoichiometric case and the same trends continue, whereby the high temperature cases (80–120°C) experience increased reactivity while for the two low-temperature cases, LTHR is quenched as they are shifted to the low temperature, long ID region. Thus, for relatively rich mixtures, increasing inlet temperature strengthens LTHR because the thermal effects of fueling shift the compression P-T histories to high reactivity regions. These trends are consistent with those reported by Szybist and Splitter (2017) for stoichiometric iso-octane/air mixtures with similar compression P-T histories ("condition C").

The increase in the peak LTHR magnitude with inlet heating (Figure 13a) is the net result of the interplays between the two competing thermal influences (charge cooling from

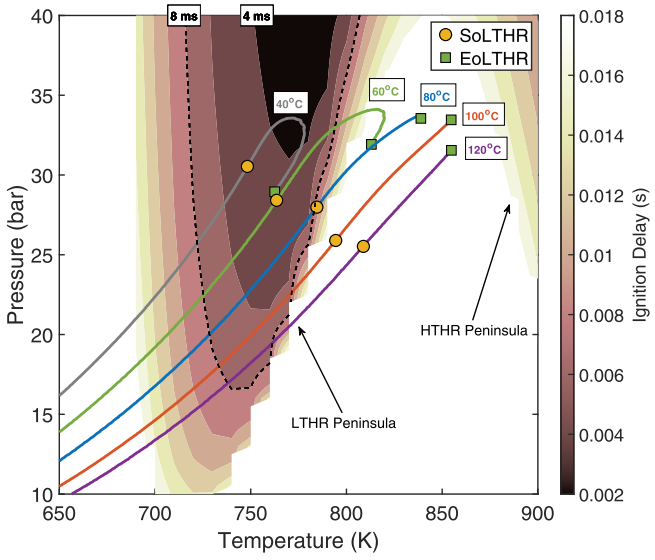

Figure 14. P-T trajectories for $\phi = 0.5$ mixtures at $T_{in} = 40 - 120$°C.

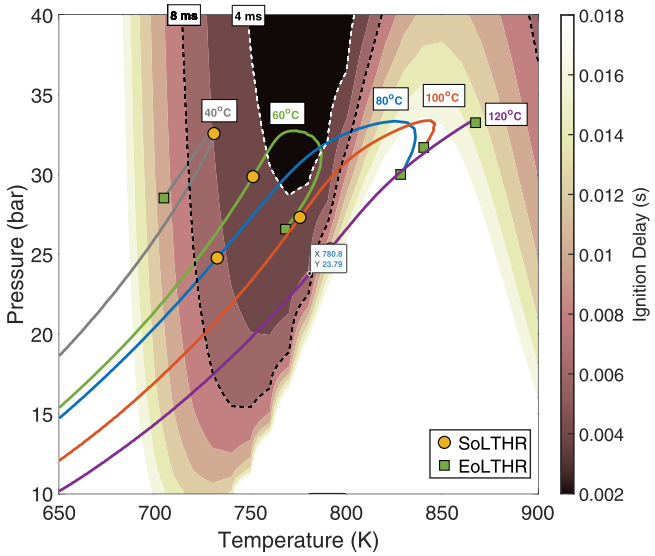

Figure 15. P-T trajectories for $\phi = 0.7$ mixtures at $T_{in} = 40 - 120$°C.

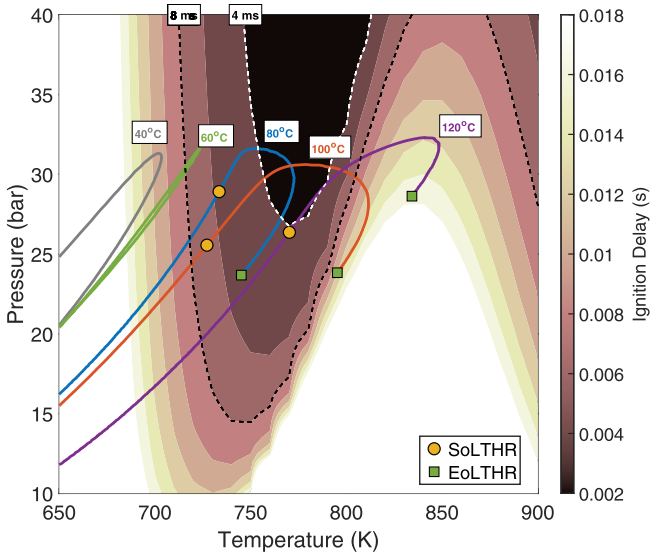

Figure 16. P-T trajectories for $\phi = 1$ mixtures at $T_{in} = 40 - 120$°C.

fueling, and inlet heating), and the chemical effects of asymmetric LTHR ID peninsula expansion discussed above.

Another observation from the ID maps of the rich mixtures (Figures 15, 16) is that for these high reactivity mixtures, the highest inlet temperatures mixtures benefit from two regions of ID decrease – first as the thermal states pass through the LTHR

peninsula core during compression (ID decreases from > 18 to <4 ms), and then toward the end of LTHR as mixture states start encroaching into the high temperature heat release region. Higher inlet temperatures (and/or lower pressures) that cause flattening of the P-T curves beyond the 120°C curve can lead to HTHR events. This was experienced sporadically during $\phi > 0.7$ experiments at 120°C, likely triggered by momentary excursions in inlet pressures and temperatures and/or presence of rich fuel pockets.

In closing, the hypothesis posited at the start of this section is shown to be correct, i.e. inlet heating can be used to create appropriate thermal conditions to maximize the exploitation of the high ϕ-sensitivity region. As can be inferred from Figure 12, strong, positive, linear $\phi-$sensitivity of around 10 J/0.1$\phi_{increase}$ can be realized for mixtures ranging in strength from very lean ($\phi = 0.05$) to rich ($\phi = 1.2$) by increasing mixture temperature. The magnitude of the ϕ-sensitivity does not change significantly for the various mixture temperatures as they are richened, but the onset of negative sensitivity is delayed by increasing temperatures.

Discussion

Some potential implications of the observed iso-octane LTHR behavior and the underlying thermo-chemical influences on engine combustion and control are briefly discussed next.

LTHR reactions are often precursors to high-temperature AI reactions – end gas AI in SI engines or controlled auto-ignition – and LTHR intensity can thus be treated as a predictor of high-temperature AI. Some support for this can be found from non-isolated-LTHR experimental studies by Kalghathi and co-workers (2013, 2003) in which fuels with higher ID-based LW scores (i.e. shorter effective ID times) were reported to have a higher propensity to knock in SI engines and promote AI in CAI engines; and from Shibata et al. (2005) who found LTHR and HTHR 50% mass fraction burned points in a CAI engine to be linearly related. This is not to imply that end gas AI always leads to knocking. Optical studies have demonstrated that if in-cylinder thermal states are maintained at relatively mild levels, by e.g. managing in-cylinder flows, end gas AI without high frequency pressure fluctuations typical of knocking can take place (Iijima et al. 2013), which is the basis of spark-assisted CAI engines. In fact, LTHR can also have a knock inhibiting effect if it is staged appropriately to exploit the temperature drop induced by NTC reactions (Splitter et al. 2019). Thus, depending on the intensity and phasing of LTHR reactions relative to main heat release, they can act to promote, moderate, or inhibit high-temperature AI.

Iso-octane LTHR characterization data at different thermal and chemical conditions presented above (Figures 10, 12) can be used to avoid regions of high-intensity LTHR in SI engines to *prevent knock* or to control AI in CAI engines. The existence of strong, positive $\phi-$sensitivity and the possibility of extending it via mixture heating can help realize staged combustion via *chemical stratification* in gasoline engines. The negative $\phi-$sensitivity region at relatively rich conditions can potentially also be exploited to moderate combustion. Depending on the mixture temperature, the negative $\phi-$sensitivity region could still be lean of stoichiometric, e.g. 40°C and 60°C cases in Figure 12, potentially making negative $\phi-$sensitivity biased chemical stratification viable from a fuel conversion efficiency perspective.

The occurrence of LTHR at lean conditions could be an enabler for stable *ultra lean* ($\phi < 0.1$ (Hu et al. 2020)) combustion in SI engines, which is prone to combustion instabilities resulting from cyclic variability during early kernel growth and susceptibility of nascent flames to extinction. If compressed mixture reactivity can be tailored to have pre-spark LTHR reactions, the rise in temperature can make deflagrative combustion more resilient by increasing flame speeds.

Ultra lean LTHR can also potentially be used to consume unburned fuel in dilute end gas mixtures if appropriate thermal conditions can be created. This can improve the *combustion efficiency* of ultra-lean SI engines and also compensate for slow combustion rates typical of lean deflagrative combustion. Moreover, because the intensity of LTHR is low at lean conditions (Figure 12), the likelihood of knocking is expected to be low.

Some *control strategies*, in addition to inlet heating and supercharging, that can help create the needed in-cylinder thermal and chemical conditions to tailor mixture reactivity are listed next. Chemical stratification can be achieved via late and/or multiple injection events, e.g. Alemahdi et al. (2022) and Dec, Yang, and Dronniou (2011) achieved partial fuel stratification by injecting the majority (80–90%) of the fuel early during the intake stroke and the rest, late during the compression stroke. Thermal stratification can be created using different combustion product retention strategies like recompression via negative valve overlap or rebreathing via early/late positive valve overlap (Lang et al. 2005). Note, however, that some level of thermal stratification exists naturally in engines because of non-uniformities in energy fluxes, and provides a certain degree of sequential combustion by creating a spatial ID distribution (Dec, Hwang, and Sjöberg 2006). Direct injection-induced thermal effects can be managed by changing injection timings, e.g. retarding injection to reduce charge cooling and specific heat ratio effects, of course with associated effects on mixture homogeneity and volumetric efficiency. In SI and spark-assisted CAI engines, the progression of deflagrative combustion can also be managed to generate desired P-T histories of the end gases (Olesky et al. 2013). Evaporative cooling from water injection can also be used to change the compression P-T states (Golzari et al. 2021). An uncontrollable lever that could impact LTHR in real engines is the occurrence of partially burning cycles, which can increase mixture reactivity in succeeding cycles because of fuel reformation reactions (Sjöberg et al. 2004).

Conclusions

The paper explored the LTHR characteristics of iso-octane/air mixtures at different equivalence ratio levels and inlet air temperatures by monitoring changes in LTHR intensity and its phasing. LTHR intensity was indexed by exhaust CO concentration, which was found to be a high sensitivity and reliability signature of LTHR. Major findings of the experimental study are as follows:

(i) LTHR can take place at very lean ($\phi < 0.05$) conditions. It gains strength as the mixture becomes richer and more reactive. However, beyond a certain ϕ limit, in direct injection engines, the thermal cooling effects of fueling overpower reactivity enhancement, and LTHR is quenched.
(ii) The non-monotonic behavior of LTHR intensity, phasing, and duration can be used to characterize ϕ-sensitivity at different engine inlet conditions.

(iii) Iso-octane/air mixtures exhibit positive or negative ϕ-sensitivities depending on the dominant effect – chemical or thermal. Dominance of the former confers positive sensitivity, while that of the latter produces negative sensitivity and can even render mixtures ϕ-insensitive.
(iv) Increasing mixture temperature counters the thermal effects of fuel enrichment and shifts the positive to negative ϕ-sensitivity transition point to higher equivalence ratios and permits more energy release via low temperature reactions. Peak LTHR intensity nearly doubled as the inlet temperatures were increased from 40°C to 120°C, and ϕ_{max} increased from 0.53 to 1.16.
(v) By appropriately adjusting mixture thermal conditions using thermal control levers (charge cooling and intake heating in this case), strong, positive, linear $\phi-$sensitivity can be realized across a wide range of ϕ levels.

Nomenclature

AHRR	Apparent heat release rate
AI	Auto-ignition
aTDC	After top dead centre
CA	Crank angle
CA50	CA location at 50% heat release point
CAI	Controlled auto-ignition
CHR	Cumulative heat release
EGT	Exhaust gas temperature
EoLTHR	End of LTHR
HTHR	High temperature heat release
ID	Ignition delay
IMEP	Indicated mean effective pressure
LTHR	Low temperature heat release
LW	Livengood-Wu progress variable
mot	Motored (no fuel)
NTC	Negative temperature coefficient
P	Pressure
PRF	Primary reference fuel
SI	Spark ignition
SoHTHR	Start of HTHR
SoLTHR	Start of LTHR
t	time
T	Temperature
γ	Ratio of specific heats
ϕ	Fuel-air equivalence ratio
ϕ_{max}	ϕ for highest intensity LTHR

Acknowledgements

This research was supported by an Engineering and Physical Sciences Research Council Prosperity Partnership, grant number EP/T005327/1. The Prosperity Partnership is a collaboration between Jaguar Land Rover, Siemens Digital Industries Software, the University of Bath, and the University of Oxford. The authors would also like to thank the Dept. of Engineering Science technicians and maintenance teams for facilities support.

Disclosure statement

No potential conflict of interest was reported by the author(s).

Funding

The work was supported by the Engineering and Physical Sciences Research Council [EP/T005327/1].

ORCID

Felix C. P. Leach http://orcid.org/0000-0001-6656-2389

References

Alemahdi, N., A. García, E. Boufaim, G. Aferiat, and M. Tunér. 2022. Development of an empirical test method to quantify the ϕ-sensitivity of liquid fuels. *Energy Convers. Manage.* 254:115257. ISSN: 0196- 8904. https://www.sciencedirect.com/science/article/pii/S019689042200053X. doi:10.1016/j.enconman.2022.115257.

Alemahdi, N., A. García, and M. Tunér. 2022. Understanding the effect of Intake temperature on the ϕ-sensitivity of toluene-ethanol reference fuels and neat ethanol. *Int. J. Engine Res.* (0):14680874221134147. doi:10.1177/14680874221134147.

Bajwa, A. U., F. C. P. Leach, and M. H. Davy. 2023. Prospects of controlled auto-ignition based thermal propulsion units for modern gasoline vehicles. *Energies* 16 (9):3887. ISSN: 1996-1073. doi:10.3390/en16093887.

Borgqvist, P., P. Tunestal, and B. Johansson. 2013. Comparison of Negative Valve Overlap (NVO) and Rebreathing valve strategies on a gasoline PPC engine at low load and idle operating conditions. *SAE Int. J. Engines* 6 (1):366–78. ISSN: 19463936, 19463944. Accessed 11 7, 2022. http://www.jstor.org/stable/26277624.

Bresenham, D., J. Reisel, and K. Neusen. 1998. Spindt air-fuel ratio method generalization for oxygenated fuels. *Sae Trans.* 107:2154–71. ISSN: 0096736X, ISSN: 0096736X. Accessed 09 22, 2022. http://www.jstor.org/stable/44736682.

Collin, R., J. Nygren, M. Richter, M. Aldén, L. Hildingsson, and B. Johansson. 2003. Simultaneous OH- and Formaldehyde-LIF measurements in an HCCI engine. *Sae Trans.* 112:2479–86. ISSN: 0096736X, ISSN: 0096736X. Accessed 12 31, 2022. http://www.jstor.org/stable/44742465.

Dec, J. E., W. Hwang, and M. Sjöberg. 2006. An investigation of Ther- mal stratification in HCCI engines using chemiluminescence imaging. *Sae Trans.* 115:759–76. ISSN: 0096736X, 25771531. Accessed 12 31, 2022. http://www.jstor.org/stable/44687346.

Dec, J. E., and M. Sjöberg. 2004. Isolating the effects of fuel chemistry on combustion phasing in an HCCI engine and the potential of fuel stratification for ignition control. *Sae Trans.* 113:239–57. ISSN: 0096736X, 25771531. Accessed 10 26, 2022. http://www.jstor.org/stable/44740754.

Dec, J. E., Y. Yang, and N. Dronniou. 2011. Boosted HCCI – controlling pressure-rise rates for performance improvements using partial fuel stratification with conventional gasoline. *SAE Int. J. Engines*. 4(1):1169–89. ISSN: 19463936, 19463944. Accessed 12 31, 2022. http://www.jstor.org/stable/26278213.

DelVescovo, D. A., D. A. Splitter, J. P. Szybist, and G. S. Jatana. 2020. Modeling pre-spark heat release and low temperature chemistry of iso- octane in a boosted spark-ignition engine. *Combust. Flame* 212:39–52. ISSN: 0010-2180. https://www.sciencedirect.com/science/article/pii/S0010218019304651. doi:10.1016/j.combustflame.2019.10.009.

Golzari, R., H. Zhao, J. Hall, M. Bassett, J. Williams, and R. Pearson. 2021. Impact of intake port injection of water on boosted downsized gasoline direct injection engine combustion, efficiency and emissions. *Int. J. Engine Res.* 22 (1):295–315. doi:10.1177/1468087419832791.

Hu, Z., J. Zhang, M. Sjöberg, and W. Zeng. 2020. The use of partial fuel stratification to enable stable ultra-lean deflagration-based Spark-Ignition engine operation with controlled end-gas autoignition of gasoline and E85. *Int. J. Engine Res.* 21 (9):1678–95. doi:10.1177/1468087419889702.

Iijima, A., M. Tanabe, K. Yoshida, H. Shoji, N. Itoh, A. Terashima, and T. Tojo. 2013. Visualization and spectroscopic measurement of knocking combustion accompanied by cylinder pressure oscillations in an HCCI engine. *SAE Int. J. Engines* 6 (4):2150–63. ISSN: 19463936, 19463944. Accessed 11 4, 2022. http://www.jstor.org/stable/26272341.

Kalghatgi, G. Oct. 2013. *Fuel/Engine Interactions*. SAE International. doi:10.4271/R-409.

Kalghatgi, G., P. Risberg, and H.-E. Ångstrom. May, 2003. "A method of defining ignition quality of fuels in HCCI engines". In: *2003 JSAE/SAE International Spring Fuels and Lubricants Meeting*. SAE International. doi:10.4271/2003-01-1816.

Kalghatgi, G., P. Risberg, and H.-E. Ångström. Jan, 2007. Partially pre-mixed auto-ignition of gasoline to attain low smoke and low NOx at high load in a compression ignition engine and comparison with a diesel fuel. *2007 Fuels and Emissions Conference*. SAE International. doi:10.4271/2007-01-0006.

Lang, O., W. Salber, J. Hahn, S. Pischinger, K. Hortmann, and C. Bücker. 2005. Thermodynamical and mechanical approach towards a variable valve train for the controlled auto ignition combustion process. *Sae Trans.* 114: 722–34. ISSN: 0096736X, 25771531 Accessed 11 7, 2022. http://www.jstor.org/stable/44722038.

Leach, F. C. P., M. H. Davy, and B. Terry. 2021. Combustion and emissions from cerium oxide nanoparticle dosed diesel fuel in a high speed diesel research engine under low temperature combustion (LTC) conditions. *Fuel* 288:119636. ISSN: 0016-2361 https://www.sciencedirect.com/science/article/pii/S0016236120326326. doi:10.1016/j.fuel.2020.119636.

Leppard, W. R. Oct, 1990. The chemical origin of fuel octane sensitivity. *International Fuels and Lubricants Meeting and Exposition*. SAE International. doi:10.4271/902137.

Liu, F., M. Z. Akram, and H. Wu. 2020. Hydrogen effect on lean flammability limits and burning characteristics of an isooctane–air mixture. *Fuel* 266:117144. ISSN: 0016-2361. https://www.sciencedirect.com/science/article/pii/S0016236120301393. doi:10.1016/j.fuel.2020.117144.

Olesky, L. M., J. B. Martz, G. A. Lavoie, J. Vavra, D. N. Assanis, and A. Babajimopoulos. 2013. The effects of spark timing, unburned gas temperature, and negative valve overlap on the rates of stoichiometric spark assisted compression ignition combustion. *Appl. Energ.* 105:407–17. ISSN: 0306-2619. https://www.sciencedirect.com/science/article/pii/S0306261913000470. doi:10.1016/j.apenergy.2013.01.038.

Pan, J., P. Zhao, C. K. Law, and H. Wei. 2016. A predictive Liven- good–Wu correlation for two-stage ignition. *Int. J. Engine Res.* 17 (8):825–35. doi:10.1177/1468087415619516.

Papaioannou, N., F. C. P. Leach, M. H. Davy, A. Weall, and B. Cooper. 2019. Evaluation of exhaust gas recirculation techniques on a high-speed direct injection diesel engine using first law analysis. *P. I. Mech. Eng.* 233 (3):710–26. doi:10.1177/0954407017749110.

Pintor, D. L., J. E. Dec, and G. R. Gentz. 2019. Φ-sensitivity for LTGC engines: Understanding the fundamentals and tailoring fuel blends to maximize this property. *SAE Technical Paper*. ISSN: 2019-01-0961. https://www.osti.gov/servlets/purl/1576882.

Saisirirat, P., F. Foucher, S. Chanchaona, and C. Mounaïm-Rousselle. Sept. 2009. Effects of Ethanol, n-Butanol — n-Heptane Blended on Low Temperature Heat Release and HRR Phasing in Diesel-HCCI. *9th International Conference on Engines and Vehicles*. Consiglio Nazionale delle Ricerche. doi:10.4271/2009-24-0094.

Senecal, K., and F. C. P. Leach. June, 2021. *Racing toward zero: The untold story of driving green*. SAE International.

Shahanaghi, A., S. Karimkashi, O. Kaario, V. Vuorinen, T. Sarjovaara, and R. Tripathi. 2022. Temperature stratification induced ignition regimes for gasoline surrogates at engine-relevant conditions. *Combust. Sci. Technol* (0):1–41. doi:10.1080/00102202.2022.2124511.

Shibata, G., K. Oyama, T. Urushihara, and T. Nakano. 2005. Correlation of low temperature heat release with fuel composition and HCCI engine combustion. *SAE Technical Paper*. ISSN: 0148-7191. doi:10.4271/2005-01-0138.

Sjöberg, M., and J. E. Dec. 2006. Smoothing HCCI heat-release rates using partial fuel stratification with two-stage ignition fuels. *Sae Trans.* 115:318–34.ISSN: 0096736X, ISSN: 0096736X Accessed 10 26 2022. http://www.jstor.org/stable/44687308.

Sjöberg, M., J. E. Dec, A. Babajimopoulos, and D. Assanis. 2004. Comparing enhanced natural thermal stratification against retarded combustion phasing for smoothing of HCCI heat-release rates. *Sae Trans.* 113:1557–75.ISSN: 0096736X, 25771531 Accessed 10 26, 2022. http://www.jstor.org/stable/44723614.

Splitter, D. A., A. Gilliam, J. Szybist, and J. Ghandhi. 2019. Effects of pre-spark heat release on engine knock limit. *Proc. Combust. Inst.* 37 (4):4893–900. ISSN: 1540-7489. doi:10.1016/j.proci.2018.05.145.

Szybist, J. P., and D. A. Splitter. 2017. Pressure and temperature effects on fuels with varying octane sensitivity at high load in SI engines. *Combust. Flame* 177:49–66. ISSN: 0010-2180. doi:10.1016/j.combustflame.2016.12.002.

Tao, M., P. Zhao, J. P. Szybist, P. Lynch, and H. Ge. 2019. Insights into engine autoignition: Combining engine thermodynamic trajectory and fuel ignition delay iso-contour. *Combust. Flame* 200:207–18. ISSN: 0010-2180 https://www.sciencedirect.com/science/article/pii/S0010218018305091. doi:10.1016/j.combustflame.2018.11.025.

Waqas, M. U., A. Hoth, C. P. Kolodziej, T. Rockstroh, J. Pulpeiro Gonzalez, and B. Johansson. 2019. Detection of low temperature heat release (LTHR) in the standard Cooperative Fuel Research (CFR) engine in both SI and HCCI combustion modes. *Fuel* 256:115745. ISSN: 0016-2361 https://www.sciencedirect.com/science/article/pii/S001623611931097X. doi:10.1016/j.fuel.2019.115745.

White, S., A. U. Bajwa, and F. C. P. Leach. 2023. Isolated low temperature heat release in spark ignition engines. *SAE Int. J. Adv. Curr. Pract. Mobility*. doi:10.4271/2023-01-0235.

Wu, Y., P. Pal, S. Som, and T. Lu. May, 2017. A skeletal chemical kinetic mechanism for gasoline and gasoline/ethanol blend surrogates for engine CFD applications. 10th International Conference on Chemical Kinetics, University of Illinois at Chicago.

Yang, Y., J. E. Dec, N. Dronniou, and M. Sjöberg. 2011. Tailoring HCCI heat-release rates with partial fuel stratification: Comparison of two-stage and single-stage-ignition fuels. *Proc. Combust. Inst.* 33 (2):3047–55. ISSN: 1540-7489. https://www.sciencedirect.com/science/article/pii/S1540748910001999. doi:10.1016/j.proci.2010.06.114.

Zhao, P., and C. K. Law. 2013. The role of global and detailed kinetics in the first-stage ignition delay in NTC-affected phenomena. *Combust. Flame.* 160 (11):2352–58. ISSN: 0010-2180 https://www.sciencedirect.com/science/article/pii/S0010218013002241. doi:10.1016/j.combustflame.2013.06.009.

Statement of Authorship for joint/multi-authored papers for PGR thesis

To appear at the end of each thesis chapter submitted as an article/paper

The statement shall describe the candidate's and co-authors' independent research contributions in the thesis publications. For each publication there should exist a complete statement that is to be filled out and signed by the candidate and supervisor **(only required where there isn't already a statement of contribution within the paper itself).**

Title of Paper	Low temperature heat release and phi-sensitivity characteristics of iso-octane/air mixtures
Publication Status	Published
Publication Details	Bajwa, A. U., White, S. P. & Leach, F. C. P. Low temperature heat release and phi-sensitivity characteristics of iso-octane/air mixtures. Combustion Science and Technology 0, 1–23 (2023).

Student Confirmation

Student Name:	Samuel P. White		
Contribution to the Paper	• Idea • Experimental design (test matrix) • Implementation (computational modelling) • Data analysis (ignition delay modelling) • Writing (computational modelling methodology)		
Signature 		Date	12 April, 2024

Supervisor Confirmation

By signing the Statement of Authorship, you are certifying that the candidate made a substantial contribution to the publication, and that the description described above is accurate.

Supervisor name and title: Felix Leach, Associate Professor of Engineering Science		
Supervisor comments I agree with Sam's comments.		
	Date	12-4-24

This completed form should be included in the thesis, at the end of the relevant chapter.

Chapter Summary

In this Chapter, the effects of physical parameters on LTHR in engines were explored in depth. First, a new method was introduced that successfully isolated LTHR from other combustion (such as HTHR) in a spark ignition engine, paving the way for a broad range of experiments. The two publications in this chapter covered physical effects relatively exhaustively. Increasing cylinder pressure (achieved by increasing inlet pressure for a given compression ratio) encourages LTHR, whilst the effect of temperature more complex—the fuel-air mixture must to spend sufficient time in LTHR temper region for LTHR to occur. Engine speed relates to time the mixture spent at certain conditions, but also affects time available for heat transfer out of the cylinder, and LTHR intensity was shown to be linear with equivalence ratio until thermal effects of charge cooling dominate. Useful analysis techniques and theories surrounding the analysis of isolated LTHR were introduced in the first paper (most notably the ignition delay analysis), paving the way for future investigations on different parameters. Furthermore, Section 2.2 included a demonstration of the linear relationship between exhaust CO concentration and isolated LTHR intensity. This relationship effectively enables the sidestepping of the limitations of the AHRR-based LTHR measurement (as highlighted in Section 2.1.1)—which will prove critical in subsequent studies and will be elaborated on later in this thesis. On completion of the work in this chapter, there was sufficient understanding to turn attention to investigating the effects of chemicals, such as fuels and residuals, on LTHR.

Chapter 3

Chemical Effects on Low Temperature Heat Release

3.1 Isolated Low Temperature Heat Release from Binary Blends of iso-Octane, n-Heptane and Ethanol in a Spark Ignition Engine

Following on from the development of isolated LTHR technique and methodology, this section focuses on chemical effects. Section 2.1 showed that iso-octane required higher pressure conditions than n-heptane to realise LTHR, this study examines blends of the two. As Section 1.2.1 suggests, ethanol is an increasingly prevalent component of market fuels, hence its impact on LTHR behaviour is also investigated by blending it into n-heptane.

To learn more about the chemical products of LTHR, and to help find a suitable indicator for the optical work in Chapter 4.1, an FTIR exhaust analyser was employed to look at the products of LTHR that would otherwise be consumed without the isolated LTHR methodology developed in Section 2.1. Finally, this section begins the work on investigating the effect of residuals on LTHR behaviour, by using a skip-firing methodology to provide firing residuals from the previous cycle at the beginning of an isolated LTHR cycle.

Contributions

- The effect of blending iso-octane and ethanol with n-heptane in binary blends on isolated LTHR intensity is investigated experimentally and computationally.
- Species measurements in exhaust gas from isolated LTHR cycles are presented.
- The effect of combustion residuals on isolated LTHR are investigated by using a skip-firing technique.

Proceedings of the ASME 2024
ICE Forward Conference
ICEF2024
October 20–23, 2024, San Antonio, Texas

ICEF2024-140524

ISOLATED LOW TEMPERATURE HEAT RELEASE FROM BINARY BLENDS OF ISO-OCTANE, N-HEPTANE AND ETHANOL IN A SPARK IGNITION ENGINE

Samuel P. White[1], Felix C. P. Leach[1,*],

[1]Department of Engineering Science, University of Oxford, UK

ABSTRACT

The potential of using low temperature heat release (LTHR) to improve engine efficiency is of particular interest because of its effect on autoignition chemistry in spark ignition (SI) and advanced compression ignition engines (ACI). A recently developed method has been shown to isolate LTHR in SI engine conditions, paving the way for more detailed and sophisticated analyses of LTHR characteristics and chemistry under realistic engine conditions. Previous LTHR modelling work has suggested that residuals and residual chemistry have a significant impact on LTHR characteristics. Until now, studies on isolated LTHR have focused on single-component surrogates.

In this work, the effect of primary reference fuels (PRFs), binary blends of n-heptane and iso-octane (2,2,4-trimethylpentane), alongside blends with ethanol on LTHR characteristics was studied. Tests were conducted on a single-cylinder engine with SI geometry, motored (with the ignition system disabled) but with fuels injected. PRFs containing 50 and 75% isooctane by volume (i.e. PRF50 and PRF75) were tested, as well as pure n-heptane and iso-octane. In addition, blends of n-heptane and ethanol containing 10, 20 and 50% ethanol by volume were also tested. The blends were tested with inlet temperatures of 40°C to 140°C at an inlet pressure of 0.9 bar (absolute).

To simulate the effect of high temperature combustion residuals, a skip spark duty cycle was employed for ignition of a PRF80 blend. A Fourier-Transform Infra-Red (FTIR) exhaust gas measurement system was employed to analyse the change in mixture composition as a result of experiencing LTHR. Ignition delay and homogeneous charge compression ignition (HCCI) simulations were performed with a gasoline surrogate chemical kinetic mechanism on CHEMKIN to assist with analysing the experimental data. At the conditions tested, the presence of iso-octane in the blend strongly reduced the intensity of LTHR whilst neat iso-octane exhibited no signs of LTHR due to its relatively lower reactivity at the conditions tested. Ignition delay contours were used to explain the results observed at the conditions tested and the HCCI modelling showed that as well as the n-heptane portion of the blends being almost entirely consumed during LTHR, significant fractions of iso-octane and ethanol were also consumed alongside it—as opposed to pro-rated consumption or single component consumption of n-heptane. Substituting ethanol into the blend reduced the LTHR intensity more dramatically because of ethanol's interaction with n-heptane's low temperature oxidation reactions. Skip firing was shown to have a small impact on the LTHR characteristics in cycles immediately after high temperature SI combustion cycles.

Keywords: Low Temperature Heat Release, Iso-octane, Ethanol

1. INTRODUCTION

CO_2 emissions from internal combustion engines (ICE) must be reduced as rapidly as possible. This can be achieved by increasing ICE efficiency and by reducing the carbon intensity of the fuel over its life cycle [1]. As liquid hydrocarbon fuels move away from being crude oil-derived to being derived from biomass or produced from carbon capture (e-fuels), their properties are likely to change and hence there is need to fully understand fundamental fuel properties and combustion behaviour, and an opportunity to optimise these properties for maximum engine efficiency. Hence engines and (advanced) combustion modes can be designed in co-operation with the fuels they will use.

One important fuel-related phenomenon that has the potential to increase engine efficiency is low temperature heat release (LTHR); this is the heat released from the fuel-air mixture undergoing a slower, exothermic reaction at relatively lower temperatures, producing intermediate species prior to the main combustion event. LTHR originates from fuels that exhibit negative temperature coefficient (NTC) behaviour. NTC behaviour describes the non-monotonic relationships between mixture temperature and ignition delay (i.e. within a certain temperature range ignition delay increases with increasing temperature due to unfavourable equilibrium rates of radical forming reactions) and causes mix-

*Corresponding author: felix.leach@eng.ox.ac.uk
Documentation for `asmeconf.cls`: Version 1.34, August 16, 2024.

tures that exhibit it to have two stages of autoignition [2]. LTHR is the heat release from the first stage of autoignition and it occurs alongside a significant change in composition of the mixture, due to the reactions that occur. NTC behaviour and hence LTHR is most often observed in fuels with low octane sensitivity, particularly straight chain alkanes such as n-heptane [3]. Until recently, LTHR in an engine context was mostly confined to homogeneous charge compression ignition (HCCI) engines where it appeared as a distinct heat release event occurring before the much larger heat release from HTHR [4]. Understanding and controlling LTHR could lead to higher efficiency by extending the knocking limit or by enabling advanced combustion modes that involved controlled autoignition of end-gas. Recently, LTHR has been observed in spark ignition (SI) engines with low octane sensitivity fuels at high load conditions with elevated inlet temperatures [5–7]. In SI engines, LTHR is referred to as pre-spark heat release (PSHR) when it occurs before ignition. Splitter *et al.* showed that when PSHR occurred it modified the thermodynamic state of the unburnt mixture, moving it into the NTC region and therefore causing it to have a long ignition delay—this in turn inhibited knocking [8]. Modern advanced combustion techniques increasingly rely on controlled autoignition of the unburnt mixture (end gas), which is often triggered by initial deflagration from spark ignition [9–11]. For optimum combustion, and to avoid knocking, these techniques rely on curating specific thermodynamic and chemical conditions in the end gas [12].

Due to its chemical reaction nature, LTHR behaviour is highly dependent on the fuel. In previous work, it took elevated inlet temperatures and boosting to cause iso-octane to undergo LTHR [5, 13], meanwhile, n-heptane underwent LTHR at temperatures and pressures very commonly seen in a naturally aspirated internal combustion engine. The two widespread octane ratings: research octane number and motor octane number (RON and MON) are defined by performance as measured against blends of n-heptane and iso-octane, which define the primary reference fuels (PRFs) [14, 15]. Single-component surrogates make for convenient and repeatable test fuels in engine research, which is why many engine studies are based on PRFs. Meanwhile, ethanol is being increasingly blended into market fuels, for example up to 10% in the UK, with many modern SI vehicles accepting higher. In some markets, levels up to 85% (E85) are accepted in so-called flex-fuel vehicles and in Brazil 100% ethanol is common. Unlike iso-octane and n-heptane, ethanol does not exhibit NTC behaviour and therefore does not exhibit two-stage autoignition [16]. Select blends of iso-octane and ethanol have been examined for LTHR behaviour in an Ignition Quality Tester [17] and very low speed HCCI engine [18], however, despite their widespread use, the effect of blending iso-octane and ethanol into n-heptane on its LTHR behaviour has not been exhaustively studied—and has not at all been studied with LTHR in isolation.

The products of reactions that release LTHR, i.e. first stage autoignition reactions, are of significant interest because not only do they affect the knocking propensity of a mixture (as previously discussed), but they can contribute to the pollutant emissions of an engine when not fully consumed by deflagration or high temperature autoignition. The low temperature oxidation of PRFs involves formation of short-chain hydrocarbons and aldehydes by beta decomposition of longer-chain hydrocarbon species [19, 20] and high concentrations of formaldehyde were observed in an optical study of PRF70 misfiring in an engine [21]. Furthermore, blending ethanol into gasoline is known to cause benzaldehyde, acetaldehyde, formaldehyde and volatile organic compound emissions to increase [22] and Shankar *et al.* suggested that such increased aldehyde emissions associated with ethanol are related to low temperature conditions [23]. Measuring the productions of LTHR in isolation is therefore vital to the understanding of overall engine emissions.

Recent studies attempting to model LTHR have found that residuals, and the species that make them up, have a significant impact on the LTHR behaviour in engines. Guo *et al.* found that, when simulating LTHR in 3D CFD, the well-stirred reactor model had to remain active throughout the entire simulation (i.e. not just between intake valve closing and exhaust valve opening) [24, 25]. Furthermore, DelVescovo *et al.* reported that NO concentration has a significant effect on the LTHR magnitude, and a small effect on LTHR phasing in a zero-dimensional, two-zone Spark Ignited (SI) engine model with detailed chemistry [26]. Studies examining the effect of residual components on ignition delay time (which in turn affects LTHR propensity) reported mixed effects. Yang *et al.* found that for a mixture of n-heptane and air at $\phi = 0.5$, the effect of NO_x addition varied with temperature, and in a low temperature region ($T < 1250$ K), NO_x addition shortened ignition delay time, with the effect increasing with NO_x concentration [27]. Meanwhile, Fang *et al.* reported both promoting and inhibiting effects of NO addition on the ignition delay time of iso-octane ignition, with the effects being temperature dependent [28]. Whilst it is clear that residuals have a significant impact on LTHR behaviour, it is not clear what that impact would be in an engine context, hence there is a need to experimentally examine the effect of residuals on LTHR in an engine cycle.

Recent work by White *et al.* [13] introduced a methodology to isolate LTHR in a spark ignition engine that maintained LTHR- and PSHR-susceptible inlet conditions whilst avoiding HTHR by disabling the ignition system. This methodology results in LTHR products (that would ordinarily react with or be entirely consumed by concurrent or subsequent deflagration) remaining in the exhaust gas. Hence, these products can be analysed to validate and inform chemical kinetic mechanisms.

In this study, we seek to expand the understanding of the occurrence of LTHR in SI engines through examining the effect of primary reference fuels (PRFs), binary blends of n-heptane and iso-octane (2,2,4-trimethylpentane), alongside blends with ethanol. PRFs containing 50 and 75% isooctane by volume (i.e. PRF50 and PRF75) are tested, as well as pure n-heptane and iso-octane. In addition, blends of n-heptane and ethanol containing 10, 20 and 50% ethanol by volume are studied. A Fourier Transform Infrared Spectroscopy (FTIR) emissions analyser is used to examine the products of isolated LTHR from these blends for the first time. In addition to the established LTHR methodology, a PRF blend is tested in a skip-fired engine, using an ignited (HTHR) cycle to generate residuals and conditions from firing cycles whilst maintaining the isolated LTHR method to investigate the effect of these residuals on LTHR with these fuels.

2. METHODOLOGY

2.1 Experimental Facility

2.1.1 Single Cylinder Engine. A single cylinder, Gasoline Direct Injection (GDI) research engine was employed for this study; the engine's technical specifications are summarised in Table 1. Engine speed was controlled by a Control Techniques motoring dynamometer. Fuel was injected at 160 bar. Injection timing and duration were precisely controlled by a Berkeley Nucleonics BNC725 Multi-trigger digital delay generator. A West 6100+ temperature controller was used to control the inlet air heater, and the inlet temperature fluctuated by up to 3 °C at the highest temperature operating point. Engine coolant was controlled to its standard operating temperature of 45 °C to minimise the risk of melting its piston rings (the engine was equipped with polyamide-imide piston rings to achieve an oil-free combustion chamber for optical access, though this was not used in this study).

The engine test cell was controlled by a Taylor DynPro2 system, which also continuously recorded data at 1 Hz. Cylinder pressure was measured at a resolution of 0.1°CA using a Kistler Type 6041A high speed pressure transducer and recorded with an AVL X-ion high speed data acquisition system. To correct for drift, the cylinder pressure signal was pegged to a barrel pressure transducer (which was exposed to the combustion chamber around BDC) measurement, every cycle. Data was collected for 300 consecutive cycles, with at least three independent repeats conducted per operating point.

TABLE 1: ENGINE SPECIFICATIONS

Bore [mm]	89.0
Stroke [mm]	90.3
Displacement [cm^3]	561.9
Compression ratio	11.1:1
Fuel injection system	Direct injection

2.1.2 Exhaust Gas Analyser. A Fourier transform infrared spectroscopy (FTIR) gas analyser (AVL SESAM FTIR i-60) was used to measure engine-out emissions. The specifications of the FTIR can be found in Table 2 and the relevant measured emissions can be found in Table 3. The FTIR analyser sampled and recorded the exhaust gas at 5 Hz. It had a gas cell capacity of 200 mL, and operated with a sample flow rate of 8 L/min. The analyser and sample line were heated to prevent losses from adsorption and condensation. A heated pre-filter removed particulate matter to prevent optical cell contamination. Before each test, the analyser was purged with nitrogen gas and a background absorbance spectrum was collected. Note that, in this study, the FTIR was occasionally used to measure concentrations beyond its certified range which slightly reduces its performance relative to the specifications in Table 2, however the authors still had confidence in these measurements unless otherwise stated in the results.

2.2 Operating Conditions

Engine operating parameters used are listed in Table 4. Inlet temperature sweeps were carried out with inlet pressure and injection duration held constant. As a result air mass flow rate and hence equivalence ratio varied slightly with inlet temperature. The equivalence ratio (ϕ) was estimated by using fuel flow rate measurements from a calibration of the injector. Inlet temperature was measured in the plenum and hence represents an upper bound on the initial cylinder temperature. A method recently introduced by White *et al.* [13] was employed to isolate LTHR from HTHR by disabling the ignition system. An equivalence ratio of 0.5 was chosen to give the best opportunity to observe LTHR in all of the fuels tested and hence enable better comparisons. In the direct injection engine used in this study, increasing the equivalence ratio to around stoichiometric would likely reduce LTHR, primarily for physical reasons, with charge cooling reducing mixture temperatures due to the latent heat of vaporisation of the fuels [29, 30].

TABLE 2: FTIR SPECIFICATIONS

Sampling Rate	5 Hz
Operating Temperature	191 °C
Operating Pressure	800 hPa
Repeatability	0.5%
Zero Drift	1.0%
End Point Drift	1.0%
Noise	1.0%
Rise Time ($T_{10\text{-}90}$)	1.5 s

TABLE 3: FTIR MEASUREMENT RANGES

Name	Molecular Formula	Certified Range (ppm)
Carbon Monoxide	CO	0-8000
Carbon Dioxide	CO_2	0-200000
Water	H_2O	0-300000
Formaldehyde	CH_2O	0-1000
Ethene	C_2H_4	0-1000
Propene	C_3H_6	0-1000
1,3-Butadiene	C_4H_6	0-1000
Ethanol	C_2H_5OH	0-1000

2.2.1 Skip Firing. To investigate the effect of HTHR combustion residuals on LTHR, a skip firing methodology was employed. The BNC725 was used in duty cycle mode to trigger ignition every third cycle, with fuel injection maintained throughout to produce HTHR every third cycle with two isolated LTHR cycles in between—a cycle denoted "1 after", affected by residuals and a further cycle denoted "2 after" that would not be expected to be affected by residuals. To minimise the likelihood of knocking, PRF80 was selected; the equivalence ratio was increased until ignition was reliable at approximately $\phi = 0.9$ at $T_{in} = 140$ °C.

2.3 Fuels

The fuel blends tested are listed in Table 5. These were chosen to explore the full dynamic range of PRFs (from 0 to 100) with PRF0 expected to exhibit high levels of LTHR and PRF100 low to no LTHR at the engine operating conditions in this work. In addition, binary blends of ethanol and n-heptane (referred to in this paper as EH*xx*) were tested in order to explore the expected

TABLE 4: ENGINE SETTINGS

IVO [°CA aTDC]	-336
IVC [°CA aTDC]	-86
EVO [°CA aTDC]	116
EVC [°CA aTDC]	366
Speed [rpm]	1100
Injection pressure [bar]	160
Injection timing [°CA aTDC]	-270
Inlet temperature [°C]	40, 60, 80, 100, 120, 140
Inlet pressure [bar (absolute)]	0.9
Equivalence ratio (ϕ)	0.5

inhibiting effect of ethanol on LTHR when blended with a fuel with a relatively high LTHR propensity.

TABLE 5: FUELS TESTED IN THIS WORK

Component	n-heptane		iso-octane		ethanol	
Percentage	vol%	mol%	vol%	mol%	vol%	mol%
PRF0	100	100	0	0	0	0
PRF50	50	53.1	50	46.9	0	0
PRF75	25	27.4	75	72.6	0	0
PRF100	0	0	100	100	0	0
EH10	90	78.2	0	0	10	21.8
EH20	80	61.5	0	0	20	38.5
EH50	50	28.5	0	0	50	71.5

2.4 Simulations

2.4.1 Ignition Delay Time. Ignition delay simulations were conducted with a closed homogeneous ignition delay model with constant volume in Ansys Chemkin-Pro. Initial temperatures ranged from 400 K to 1000 K and initial pressures from 0.5 bar to 20 bar, and reactions were modelled for a duration of 200 ms. Mixtures of air and the fuels in Table 5 were modelled at $\phi = 0.5$. Ignition delay was defined by a 50 K temperature rise to detect the relatively small temperature rises caused by LTHR [5, 8]. A reduced Lawrence Livermore National Laboratory gasoline surrogate mechanism that had 165 species and 839 reactions [31] was employed.

2.4.2 0D Engine Modelling. A multi-zone HCCI model in Ansys Chemkin-Pro was validated to match the geometry and thermodynamic conditions of the engine (Table 1). The dimensionless heat transfer correlation was used with the Woschni Correlation for Gas Velocity [30]. Engine settings and fuels were chosen to match the experimental study (Tables 4 and 5).

2.5 Data Analysis

Combustion analysis was performed during post-processing with a MATLAB-based procedure. Cylinder volume was calculated from the engine geometry whilst cylinder temperature was calculated using the ideal gas law with measured pressure, calculated volume, and estimated trapped cylinder mass.

2.6 Quantifying LTHR Intensity

The LTHR intensity of each test run was quantified by measuring the exhaust CO concentration with the FTIR. This method is only possible because of the isolated nature of LTHR in these experiments—there are no HTHR reactions to generate CO, hence the sole source is the low temperature reactions that are also responsible for LTHR. Using CO as an indicator of LTHR is a well-established practice [2] because the relationship between exhaust CO concentration and heat released from LTHR is highly linear [29].

3. RESULTS

3.1 Low Temperature Heat Release of PRF Blends

The LTHR intensity for PRF0, PRF50 and PRF75 (as indicated by exhaust CO concentration) can be seen in Figure 1. No LTHR is observed for any fuel for the T_{in} = 40 °C cases. The non-zero CO concentration indicates signs of LTHR at the T_{in} = 60, 80 and 100 °C cases for PRF0, PRF50 and PRF75 respectively. Then, LTHR intensity monotonically increased with inlet temperature for all fuels tested. No data was collected for n-heptane at T_{in} = 120 °C or higher as these inlet conditions caused n-heptane to undergo HTHR. Such HTHR would have led to engine damage from knocking so was avoided. Some of the test points, such as PRF50 at T_{in} = 100 °C, exhibit relatively large variation in CO exhaust concentration and hence LTHR intensity; this can be attributed to the imperfect control of—and hence the variation in inlet temperature occurring at conditions where LTHR intensity increases rapidly with increasing inlet temperature. From the trends shown in Figure 2, the effect of blending iso-octane into n-heptane is apparent: increasing iso-octane content always decreased LTHR intensity, regardless of the conditions. This was particularly apparent for PRF100 (i.e. pure iso-octane), where LTHR was not exhibited under any conditions.

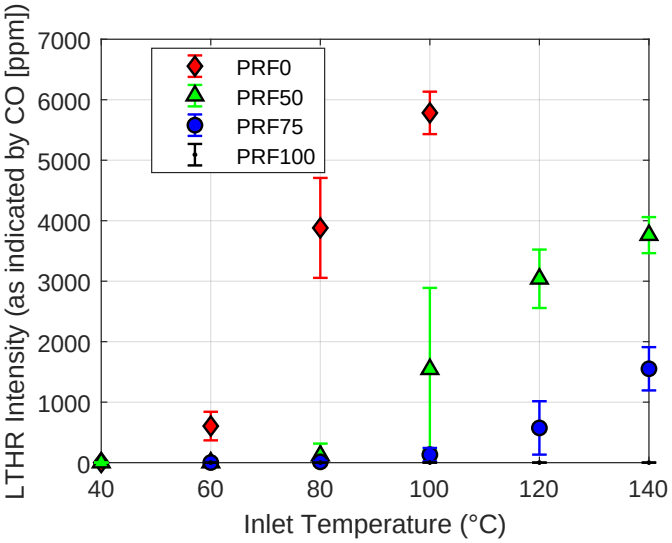

FIGURE 1: LTHR (AS INDICATED BY EXHAUST CO CONCENTRATION) FOR FOUR PRF BLENDS AT A RANGE OF INLET TEMPERATURES

The LTHR intensity results for PRFs in Figure 1 can be explained by examining the thermodynamic state of the mixture

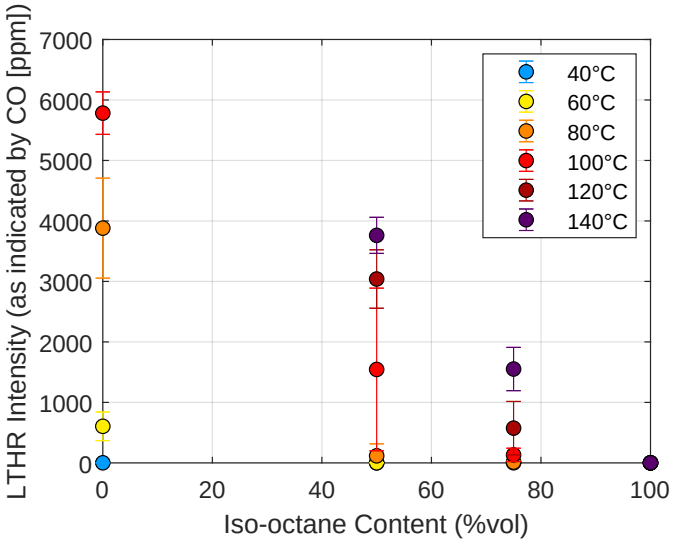

FIGURE 2: THE EFFECT OF ISO-OCTANE CONTENT IN PRF BLENDS ON LTHR (AS INDICATED BY EXHAUST CO CONCENTRATION) FOR DIFFERENT INLET TEMPERATURES

in relation to the mixture's ignition delay contour. Figures 3, 4 and 5 show experimental pressure-temperature (P-T) trajectories superimposed onto ignition delay contours, for first stage ignition as defined by a 50 K rise in temperature, generated from many ignition delay simulations with varying initial pressure and temperature. The colour of the contour represents the ignition delay time of the mixture at a given starting condition and is indicative of the reactivity of the mixture with respect to LTHR. For LTHR to occur, the mixture must have reached its first stage ignition delay time on average. Hence, the more time a mixture spends in a short ignition delay—high reactivity region, the more likely LTHR is to be observed experimentally. The plots display ignition delay time between 1 and 100 ms, with 1 ms equating to 6.6 crank angle degrees at the engine test speed of 1100 rpm. As inlet temperature increases so does the temperature trajectory throughout the cylinder, pushing the thermodynamic state of the mixture into the LTHR region. Figure 3 shows P-T trajectories of PRF0 at the four inlet temperatures. LTHR is apparent in T_{in} = 80 °C and T_{in} = 100 °C cases, where heat released causes temperature rise, unlike in the two lower inlet temperature cases, where expansion temperature is lower than compression temperature due to heat losses to heat transfer.

For the cases that exhibit moderate to high amounts of LTHR, a positive feedback effect appears to occur: as heat starts to be released, mixture temperature increases, moving the mixture into an even more reactive pressure-temperature space—enabling further heat release and temperature rise. This occurs until either fuel is depleted or temperature increases so much that the state of the mixture is pushed into the NTC zone where reactivity decreases with temperature (this behaviour was first explained in work by Splitter *et al.* [8]), halting LTHR. This feedback effect explains the points in Figure 1, such as PRF50 at T_{in} = 100 °C, where LTHR intensity increases rapidly with increasing inlet temperature—causing a relatively small temperature variation to produce a wide error bar on LTHR intensity. Figure 4 shows obvious LTHR for only T_{in} = 100 °C and higher cases for PRF50—which is consistent with Figure 1, meanwhile in Figure 5 the effect of LTHR is only apparent for PRF75 at the T_{in} = 140 °C case. Using the contours in Figures 3, 4 and 5 to compare ignition delay time across the three fuels reveals that, whilst the contour shape is very similar, the value of ignition delay increases with iso-octane content—because neat iso-octane's ignition delay is longer than n-heptane's for any given temperature. Hence LTHR reactivity is lower and therefore the different fuel mixtures that traverse the same pressure-temperature space will exhibit less LTHR. This decreased reactivity is ultimately the cause of the trends in Figure 2. This also explains why PRF100 exhibited no LTHR at any conditions—its first stage ignition delay time at the temperatures and pressures experienced by the mixture was too long for any LTHR reactions to occur.

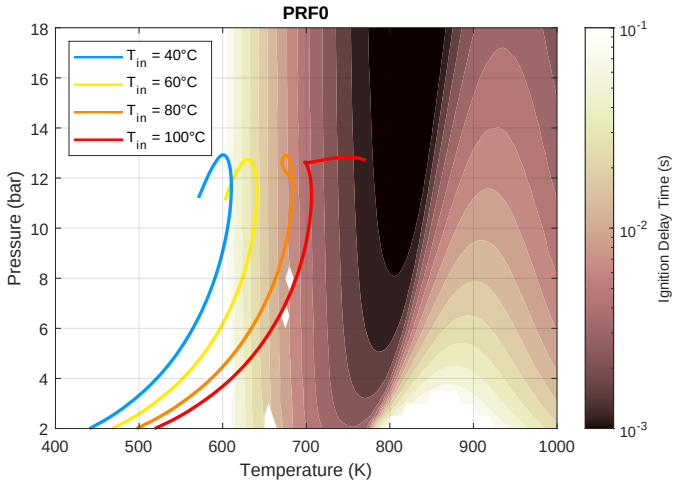

FIGURE 3: PRESSURE-TEMPERATURE TRAJECTORIES OF CYCLES FROM AN ENGINE MOTORED WITH PRF0 AT A RANGE OF INLET TEMPERATURES SUPERPOSED ONTO AN IGNITION DELAY CONTOUR FOR PRF0, DEFINED BY 50 K RISE IN TEMPERATURE

3.2 Low Temperature Heat Release of blends of ethanol and n-heptane

The LTHR intensity for PRF0, EH10, EH20 and EH50 (as indicated by exhaust CO concentration) can be seen in Figure 6. The occurrence of LTHR started at T_{in} = 60 °C for EH10 and T_{in} = 80 °C for EH20, meanwhile no LTHR was observed for EH50 at any conditions. Figure 7 illustrates how rapidly LTHR intensity decreases with ethanol content. Particularly compared to PRF50 in Figure 2. This is because, whilst iso-octane is known to undergo LTHR (albeit with a lower reactivity than n-heptane at the same conditions), ethanol not only does not undergo LTHR but is capable of actively inhibiting LTHR by consuming the OH radicals involved in the low-temperature oxidation of n-heptane [32, 33]. Again, PRF0 was not tested above T_{in} = 100 °C in order to avoid engine damage.

As with the PRFs, examining the ignition delay contours in Figures 8, 9 and 10 can explain the trends observed in LTHR of EH blends. For the EH10 and EH20 cases with the higher inlet

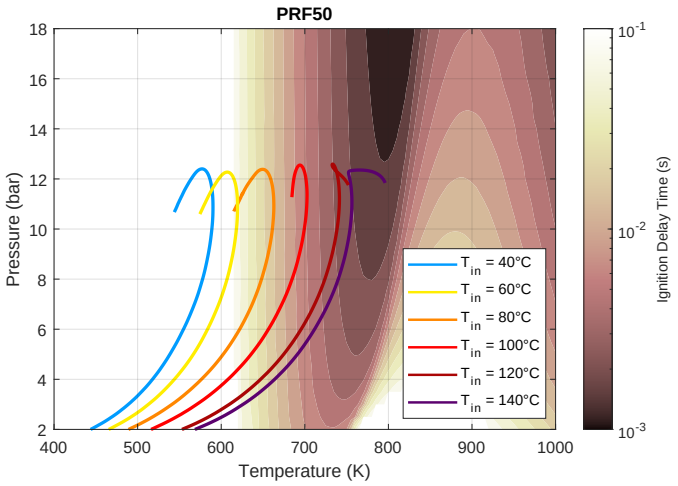

FIGURE 4: PRESSURE-TEMPERATURE TRAJECTORIES OF CYCLES FROM AN ENGINE MOTORED WITH PRF50 AT A RANGE OF INLET TEMPERATURES SUPERPOSED ONTO AN IGNITION DELAY CONTOUR FOR PRF50, DEFINED BY 50 K RISE IN TEMPERATURE

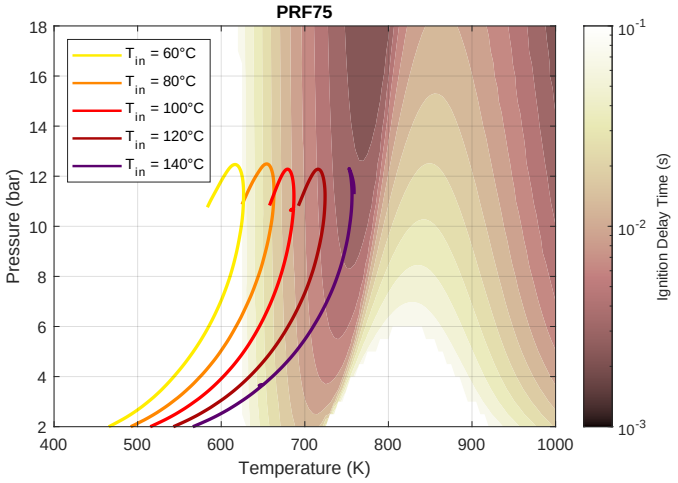

FIGURE 5: PRESSURE-TEMPERATURE TRAJECTORIES OF CYCLES FROM AN ENGINE MOTORED WITH PRF75 AT A RANGE OF INLET TEMPERATURES SUPERPOSED ONTO AN IGNITION DELAY CONTOUR FOR PRF75, DEFINED BY 50 K RISE IN TEMPERATURE

temperatures, their P-T trajectory moves the mixture into the most reactive region (i.e. the regions with the shortest ignition delay), explaining why LTHR was high for these cases. For the T_{in} = 120 °C and T_{in} = 140 °C cases for EH10, the LTHR intensity is very high and the pressure-temperature trajectories show very sharp rises in both temperature and pressure as LTHR occurs. Such conditions put PRF0 at risk of knocking in the experimental engine, though this did not occur for EH10—likely due to ethanol's high resistance to autoignition. This suggests that, despite its inhibiting effects, blending in small proportions of ethanol could help create safe, high LTHR conditions for advanced combustion regimes by inhibiting the knocking associated with fuel components (such as n-heptane) that are required to induce LTHR. Examining the contours reveals that increasing ethanol content has a significant effect on ignition delay. Moving from 0% to

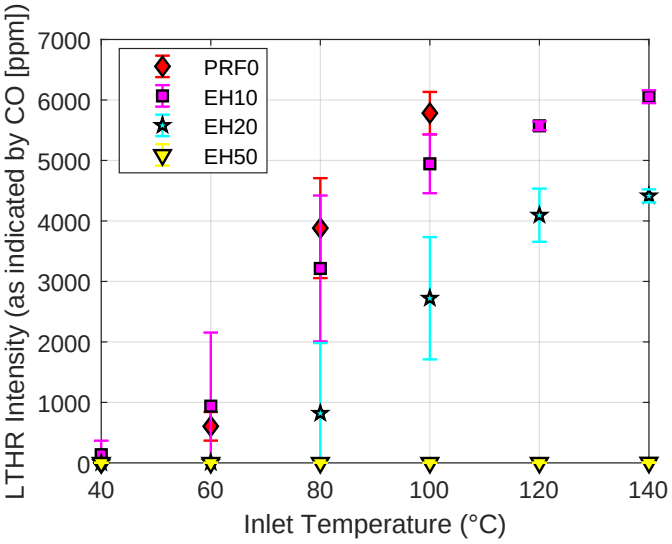

FIGURE 6: LTHR (AS INDICATED BY EXHAUST CO CONCENTRATION) FOR FOUR EH BLENDS AT A RANGE OF INLET TEMPERATURES

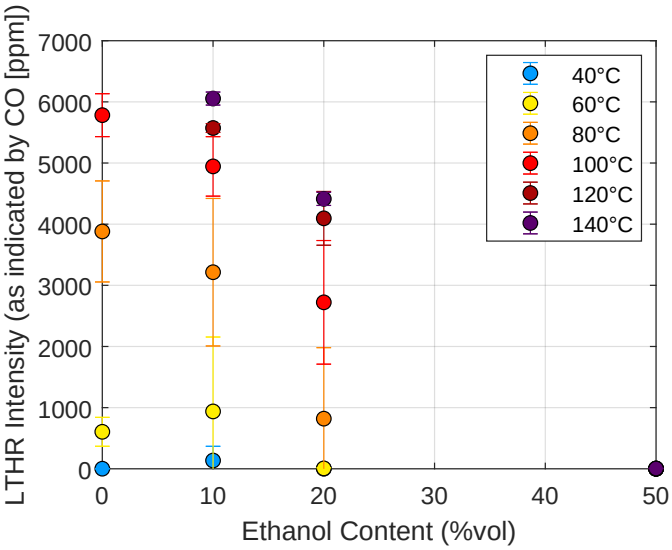

FIGURE 7: THE EFFECT OF ETHANOL CONTENT IN EH BLENDS ON LTHR (AS INDICATED BY EXHAUST CO CONCENTRATION) FOR DIFFERENT INLET TEMPERATURES

50% ethanol pushes the 100 ms ignition delay time region nearly 50 K higher, and the 1 ms region disappears rapidly with ethanol content. The EH50 trajectories in Figure 10 show meaningful change in shape as inlet temperature increases, which is consistent with the observed LTHR intensity. This is ultimately caused by ethanol's consumption of OH radicals strongly reducing the low-temperature reactivity of the mixture.

3.3 Effect of Residuals on Low Temperature Heat Release

Figure 11 shows the average AHRR for the non-firing cycles in the skip-fire test, and an AHRR trace at the same conditions for the standard isolated LTHR method. The skip-fire cycles are separated into two average traces: an average of the cycles

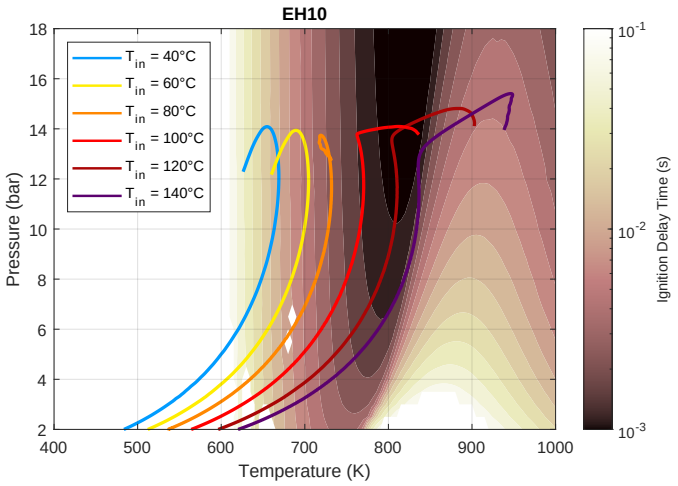

FIGURE 8: PRESSURE-TEMPERATURE TRAJECTORIES OF CYCLES FROM AN ENGINE MOTORED WITH EH10 AT A RANGE OF INLET TEMPERATURES SUPERPOSED ONTO AN IGNITION DELAY CONTOUR FOR EH10, DEFINED BY 50 K RISE IN TEMPERATURE

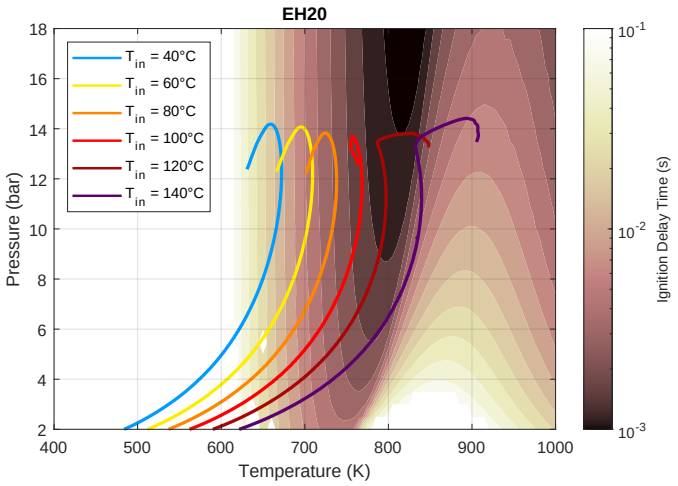

FIGURE 9: PRESSURE-TEMPERATURE TRAJECTORIES OF CYCLES FROM AN ENGINE MOTORED WITH EH20 AT A RANGE OF INLET TEMPERATURES SUPERPOSED ONTO AN IGNITION DELAY CONTOUR FOR EH20, DEFINED BY 50 K RISE IN TEMPERATURE

immediately following the fired cycle ("1 after") and an average of the cycles that were two cycles after the fired cycle ("2 after").

Compared to the regular isolated LTHR cycles ("many after") and despite the engine coolant control, both skip fire cycle sets will have experienced slightly elevated cylinder temperatures due to the high temperatures generated by the HTHR cycle. Furthermore, the temperature of the residuals in the "1 after" cycle will be hotter. This explains the intensity and the phasing of the AHRR traces in Figure 11, with both skip-fire cycles experiencing approximately 15% higher heat release rate peaks compared to the standard isolated case.

However, only the "1 after" cycles will have had a cylinder containing residuals from high temperature, complete combustion. Of the HTHR residuals, the species likely to have the biggest impact on LTHR behaviour is nitric oxide (NO). Whilst there is

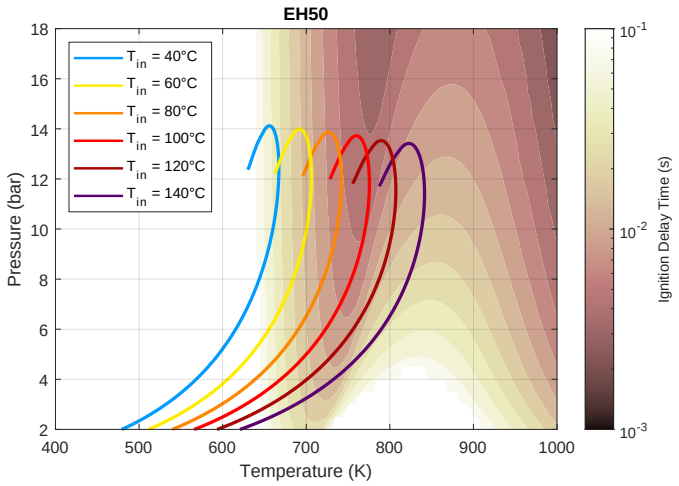

FIGURE 10: PRESSURE-TEMPERATURE TRAJECTORIES OF CYCLES FROM AN ENGINE MOTORED WITH EH50 AT A RANGE OF INLET TEMPERATURES SUPERPOSED ONTO AN IGNITION DELAY CONTOUR FOR EH50, DEFINED BY 50 K RISE IN TEMPERATURE

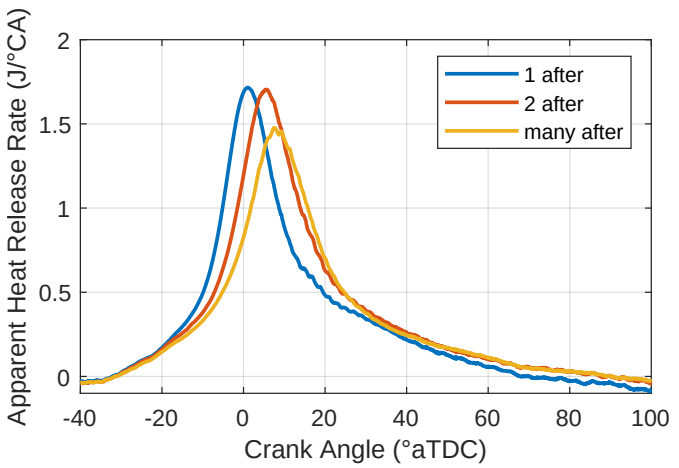

FIGURE 11: APPARENT HEAT RELEASE RATE OF ISOLATED LTHR FOR THE SKIP FIRING AND REGULAR CASES WITH PRF80

relatively little and sometimes conflicting evidence in the literature on the effect of NO on LTHR, small amounts of NO have been shown to increase ignition delay time (and hence decrease reactivity) of PRF mixtures at relatively low temperatures [28]; this would provide an inhibiting effect on LTHR [34]. This is likely to be the explanation as to why the "2 after" cycles were observed to have a higher total LTHR intensity (i.e. they released more heat) than the "1 after" cycles in Figure 12.

3.4 Emissions/Chemical Products of Isolated Low Temperature Heat Release

Exhaust emissions measurements from the FTIR exhaust analyser and predictions from the 0D HCCI model are presented in this section. Whilst the species and concentrations are discussed and presented here as "exhaust emissions" due to the isolated LTHR methodology; they would ordinarily be considered intermediate species, or more accurately, the products of LTHR.

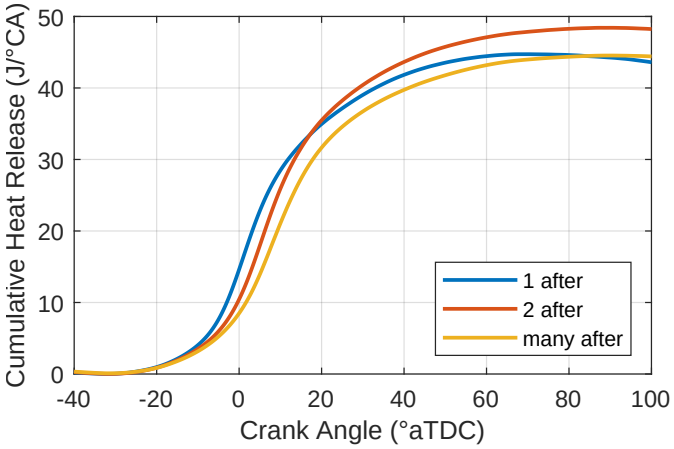

FIGURE 12: CUMULATIVE HEAT RELEASE OF ISOLATED LTHR FOR THE SKIP FIRING AND REGULAR CASES WITH PRF80

These would be present in end gas and subsequently consumed by HTHR (either deflagration or high temperature autoignition), making them very difficult to quantify. As discussed in the introduction, these species are of significant interest because they determine the knocking behaviour in engine cycles where LTHR occurs. The HCCI model provided satisfactory results at inlet temperatures of T_{in} = 100 °C and above, but performed relatively poorly for T_{in} = 80 °C and lower, predicting no LTHR.

3.4.1 Formaldehyde. Formaldehyde is the simplest aldehyde and a highly toxic (carcinogenic) pollutant emission. It is known to be a product of low temperature oxidation of PRFs [19, 20] and is seen in very large quantities compared to standard combustion. However, it is easily consumed by HTHR and further removed by exhaust aftertreatment so its presence in the emissions from vehicles is very low—its presence here is a function of the isolated LTHR methodology being used and not representative of a vehicle exhaust emission [35]. Figure 13a shows the very strong relationship between CO and hence LTHR intensity. Formaldehyde can be considered a good marker for the occurrence of LTHR during firing engine cycles because it is consumed by HTHR. It also has much lower concentrations during typical deflagration and it has a very strong relationship to CO concentration (a very robust indicator of isolated LTHR [29]). Figure 13b shows predicted formaldehyde concentration against CO concentration from the 0D simulation. The first observation to note is that, whilst the overall trend is in very good agreement with the results in Figure 13a, the absolute values for CO concentration were overpredicted by around 40% and the formaldehyde concentration was overpredicted by the model by around 30%; this suggests that the LTHR chemistry is modelled reasonably accurately but with a small overprediction of the extent of LTHR intensity. The points corresponding to the highest concentration of CO have associated formaldehyde concentrations that do not fit with the monotonically increasing trend seen in the rest of the predictions and in the experimental data—this also applies to C_3H_6 in Figure 14b (discussed in more depth later). Unsurprisingly, these points corresponded to highest temperature cases, which suggests two possible explanations: either the higher temperatures caused these species to further decompose in the model towards CO and CO_2, or the higher temperatures favoured low-temperature oxidation pathways in the model that were less favourable to their production in the first instance.

3.4.2 CO_2 and H_2O. CO_2 is a greenhouse gas and a product of complete combustion, alongside H_2O. For complete combustion at ϕ = 0.5, exhaust CO_2 concentration would be expected to be around 65,000 ppm. Clearly, the CO_2 concentrations presented in Figure 13a are significantly lower than would be expected from complete combustion, though it is still present. All measurements show a baseline measurement of about 440 ppm, i.e. the CO_2 concentration in a well-ventilated lab environment. Figure 13b shows the predicted final CO_2 against LTHR intensity, as indicated by CO concentration. Compared to the experimental data, CO_2 concentration is significantly underpredicted by around 60%. One plausible explanation for this is that whilst the simulation results capture the behaviour as soon as exhaust valves open, in the experimental studies there is an opportunity for CO to oxidise to CO_2 before sampling, potentially via the water-gas shift reaction, which would also account for some of the disagreement in CO measurements. For H_2O, the measurements in Figure 13a and HCCI predictions in Figure 13b are in very good agreement. While, initially there might seem to be some fuel-dependent difference in baseline H_2O in the measured data (most notably with PRF75), this is almost certainly due to different humidity on the days of the tests (intake humidity was not measured or controlled in these experiments)—this also explains why no baseline concentration is present in the predictions.

3.4.3 Ethanol. The measured exhaust ethanol concentration for the EH blends is plotted in Figure 13a. The data reveals a very significant conclusion—there is considerable consumption of ethanol as LTHR occurs. This, however, does not suggest that ethanol contributes to the heat release from LTHR, rather, ethanol is consumed whilst it inhibits LTHR by reacting with OH radicals. Comparing the measurements to the predictions in Figure 13b reveals good agreements between them—aside from EH50. In this case, it is the measurement that is inaccurate, it disagrees with the theoretical calculation of initial concentration, which is over 10x the range of the exhaust analyser. This is the only test case in which the authors do not have confidence in the above-specification emissions measurements, as discussed in the methodology.

3.4.4 (Unburned) Hydrocarbons: C_2H_4, C_3H_6, C_4H_6. Ethylene (C_2H_4), Propylene (C_3H_6) and 1,3-Butadiene (C_4H_6) are all considered to be unburned hydrocarbons (UHCs) and pollutant emissions. They are produced during LTHR as products of the beta decomposition of larger hydrocarbons [19, 20] and would ordinarily be almost entirely consumed by deflagration. Figure 14a shows that there is a strong, proportional relationship between both C_2H_4 and C_3H_6, and LTHR (as indicated by exhaust CO concentration). The concentrations are also noted to be very high compared to what would be expected from standard deflagration combustion (HTHR), particularly when considering the mixture was lean of stoichiometric. The measured exhaust concentration of C_4H_6 was much reduced compared to the smaller hydrocarbons. Furthermore, there was

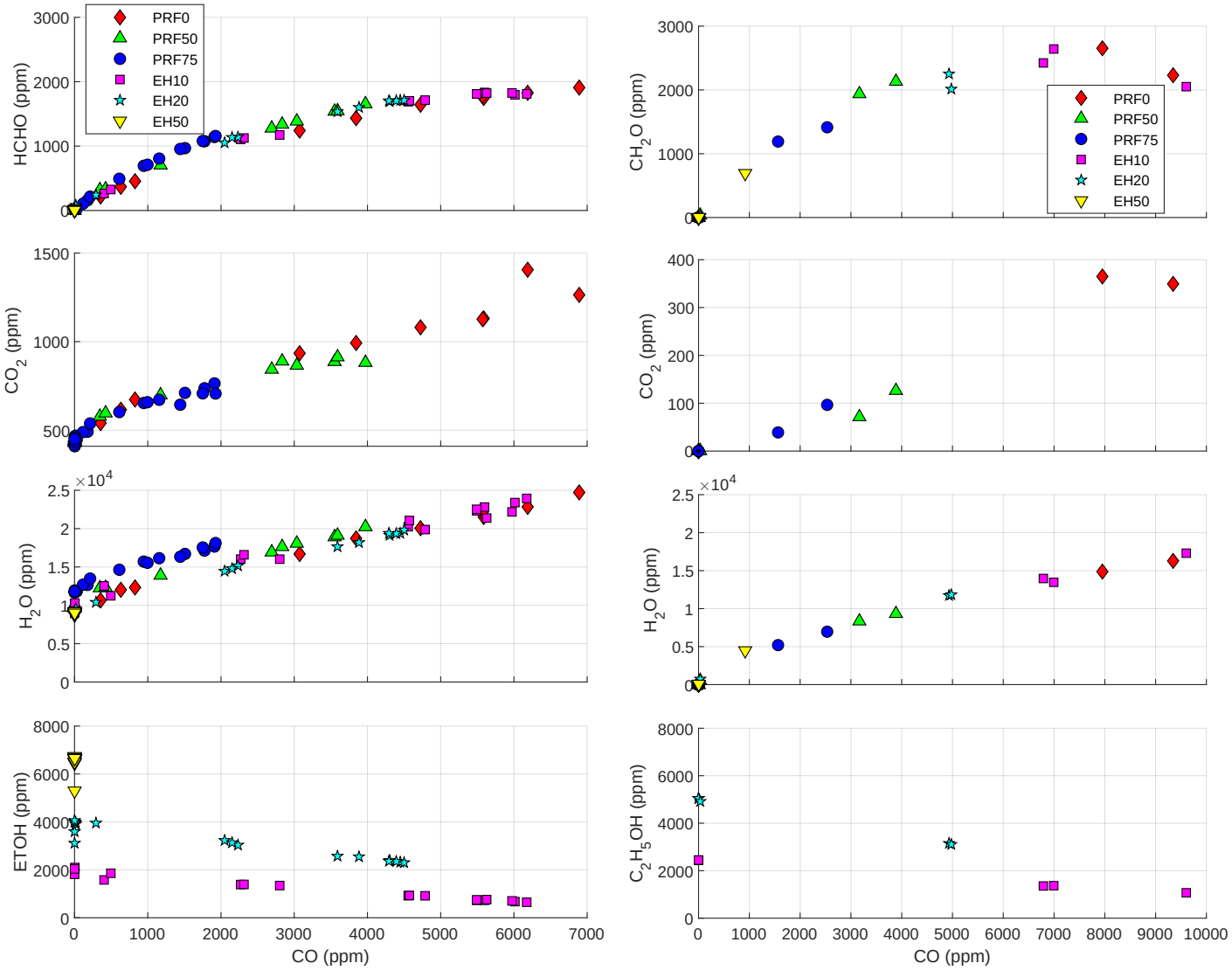

(a) Exhaust species against CO (an LTHR indicator) concentrations as measured in the exhaust gas of the experimental tests

(b) Exhaust species against CO (an LTHR indicator) as predicted by the 0D HCCI model (note - different axes to experiments)

FIGURE 13: COMPARISON OF EXPERIMENTAL MEASUREMENTS AND HCCI MODEL PREDICTIONS OF EXHAUST GAS SPECIES FOLLOWING ISOLATED LTHR

a clear, highly proportional and fuel-dependent trend for PRF50 (green) and PRF75 (blue), with different ratios depending on the fuel's iso-octane content; C_4H_6 were negligible for PRF0. This trend is also present but less apparent in the C_3H_6 emissions and the C_2H_4 emissions are slightly lower for PRF50 and PRF75 than for the fuels that did not contain any iso-octane. The results from the 0D engine modelling of LTHR emissions of C_2H_4, C_3H_6 and C_4H_6 are presented in Figure 14b. Generally, the trends are less apparent than in the experimental results and there is significant disagreement in the magnitude of the concentrations—in particular, the C_2H_4 concentrations are predicted to be 4x more than the experimental exhaust measurements. Further oxidation of C_2H_4, whether it occurs during the engine cycle or in the exhaust, does not seem to be captured by the model. The disagreement for C_4H_6 is even more apparent, with an approximately 20x overprediction; the fuel-dependent behaviour is also absent. It is not entirely clear why and further analysis would be required to establish the cause of the disparity.

Considering all of the emissions reported in this section, including CO suggests that most of the products of LTHR are still unaccounted for. For the highest LTHR intensity case, just 1.5% of the potential CO_2 was formed (compared to complete combustion). The remaining carbon atoms from the fuel appear approximately as 10% CO, 3% formaldehyde and 5% in the UHCs that were detected—this leaves over 80% of the carbon atoms unaccounted for; some of this will be original fuel, but in high LTHR intensity cases where the majority of the fuel is consumed, there must therefore be a large mix of UHCs of various sizes remaining as LTHR products. These UHCs are not detected by the FTIR but would be detected by a conventional exhaust

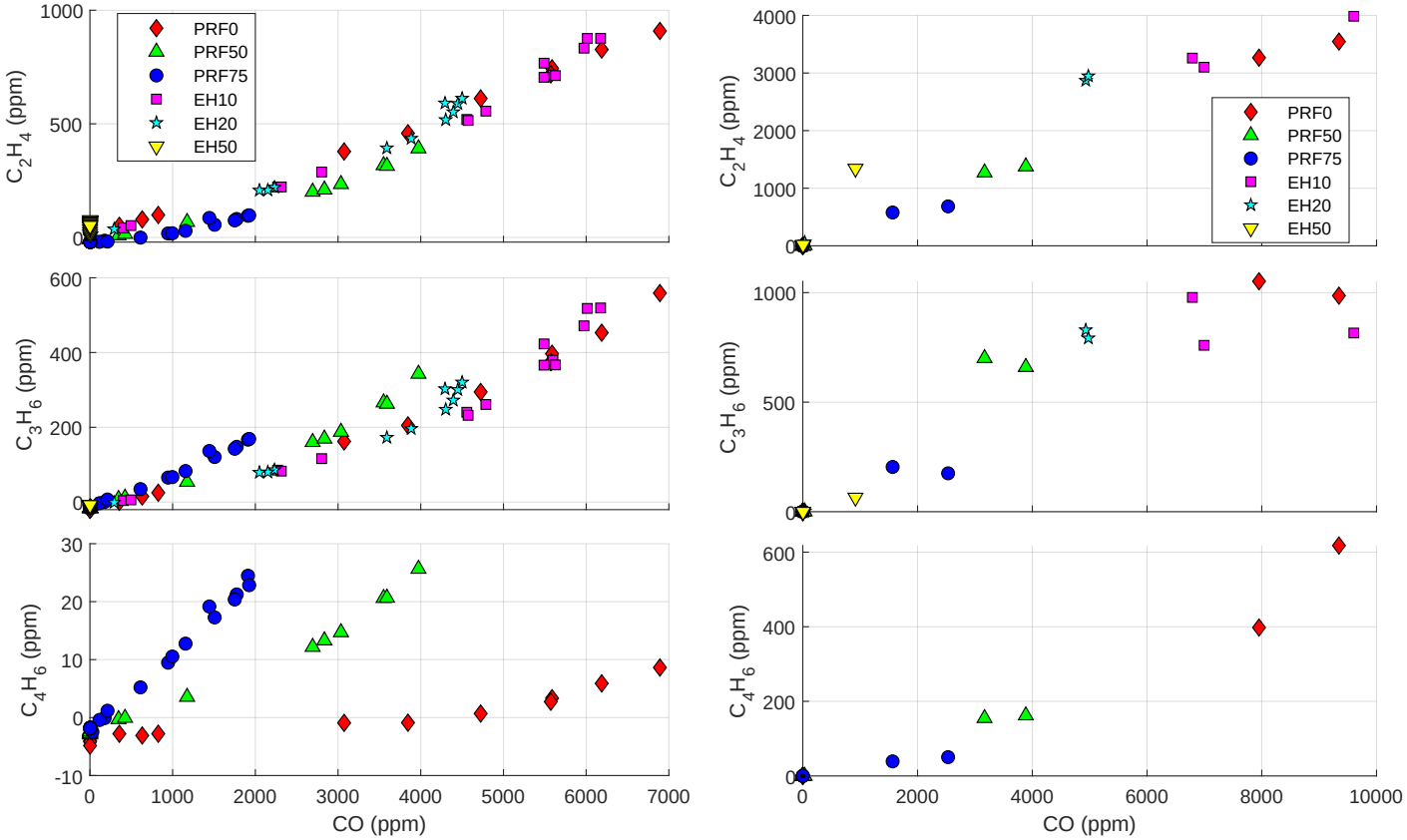

(a) Exhaust species against CO (an LTHR indicator) concentrations as measured in the exhaust gas of the experimental tests

(b) Exhaust species against CO (an LTHR indicator) as predicted by the 0D HCCI model (note - different axes to experiments)

FIGURE 14: COMPARISON OF EXPERIMENTAL MEASUREMENTS AND HCCI MODEL PREDICTIONS

analyser such as a flame ionisation detector—and this will be checked in future work.

3.5 Relative Fuel Component Consumption During LTHR

Figure 15 shows the fraction of each component in the fuel blends that was consumed in the T_{in} = 120 °C cases. Clearly, n-heptane dominates, with 75-95% consumption for cases that exhibited LTHR, with consumption (unsurprisingly) increasing monotonically with LTHR intensity. In both sets of blends, despite being the most reactive component, and the only component to exhibit LTHR in its neat form at these conditions, n-heptane was not the only component of the blends to be consumed. The low temperature oxidation process for iso-octane is essentially the same as it is for n-heptane [19, 20], hence the OH radicals that are produced in the low temperature chain branching of n-heptane could feasibly abstract hydrogen from iso-octane, initiating the low temperature reactions in iso-octane that wouldn't otherwise be seen at the pressures and temperatures tested. Likewise, as ethanol actively inhibits LTHR, it is consumed as it reacts with the OH radicals produced by low temperature chain branching [33]. Note that the ethanol consumption of approximately 40% is in reasonable agreement with the FTIR emissions data in Figure 13a (with the exhaust of the reacting cases containing 50%–60% of the ethanol measured in the cases where LTHR did not occur). Whilst this analysis highlights how much of each component was consumed, it cannot be used to trace back and quantify the heat release contributions of each component.

4. CONCLUSIONS

In this work, a motored engine was used to collect experimental data on the effect of different binary blends of iso-octane & n-heptane and ethanol & n-heptane on isolated low temperature heat release (LTHR) behaviour at different inlet temperatures. The experimental tests were also simulated in an HCCI engine to compare exhaust product predictions and to determine the consumption of each fuel blend component as LTHR occurred. Finally, a skip-fire setup was used to examine the effects of high temperature combustion residuals on LTHR. The experimental results were analysed alongside ignition delay simulations which were presented as contours. The results show:

- PRF blends up to 75% iso-octane exhibited LTHR at elevated inlet temperatures. However, PRF100 did not at the conditions tested. LTHR intensity always reduced as iso-octane content increased in the blend with n-heptane.
- Similarly, ethanol content reduced LTHR intensity when blended with n-heptane, having a much more dramatic effect than iso-octane, due to OH scavenging by ethanol.

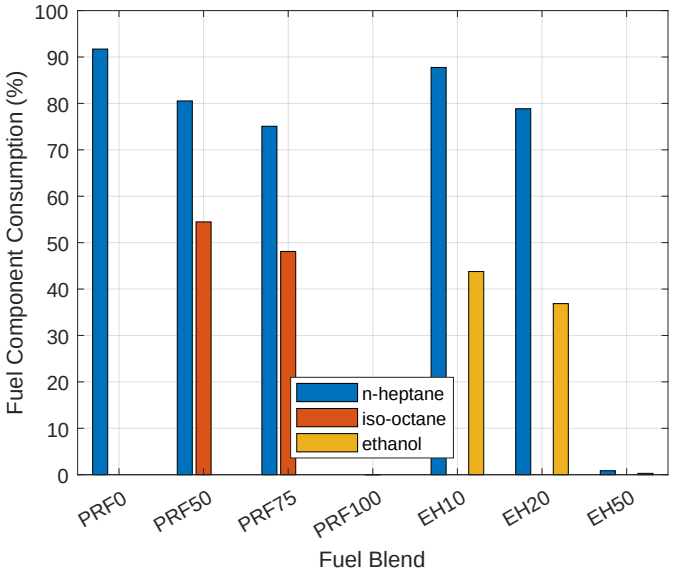

FIGURE 15: HCCI MODEL PREDICTION OF FUEL COMPONENT CONSUMPTION FOR T_{in} = 120 °C

- The effect of inlet temperature on isolated LTHR depends on the specific fuel's ignition delay characteristics, and the pressure and temperature conditions that the mixture traverses throughout its cycle. The more time the mixture resided in the short ignition delay (by 50 K rise) region, the more energy was released by LTHR.
- Experimental exhaust emissions measurements showed very high concentrations of formaldehyde in exhaust from LTHR cycles, with formaldehyde concentration having a strong correlation with LTHR intensity. Such emissions would likely not be present in vehicle emissions, nevertheless as they are a combustion intermediate.
- Complete combustion products (CO_2 and H_2O) were present in much lower quantities than would be seen for complete combustion. The unburned hydrocarbons ethene and propene were measured in relatively high concentrations whilst 1,3-butadiene was not.
- 0D HCCI modelling tended to overpredict exhaust species concentrations compared to the experimental results, though the trends were in broad agreement—with the exception of 1,3-butadiene which was hugely overpredicted by the model.
- HCCI modelling indicated that, despite iso-octane's reducing effect on LTHR and it not exhibiting any LTHR in its single component form, approximately 50% of the iso-octane was consumed during LTHR of PRF50 and PRF75. Similar behaviour was indicated with ethanol with approximately 40% consumption in the EH10 and EH20 blends.
- Residual effects from firing cycles had mixed effects on LTHR behaviour in PRF80. The slightly elevated engine temperatures increased peak heat release and advanced LTHR phasing but the residual gases reduced overall LTHR intensity by approximately 10% for LTHR cycles that immediately followed firing cycles.

5. ACKNOWLEDGEMENTS

This research was supported by an Engineering and Physical Sciences Research Council Prosperity Partnership, grant number EP/T005327/1. For the purpose of Open Access, the authors have applied a CC BY public copyright license to any Author Accepted Manuscript (AAM) version arising from this submission. The Prosperity Partnership is a collaboration between JLR, Siemens Digital Industries Software, the University of Bath, and the University of Oxford. This publication also arises in part from research funded by the John Fell Oxford University Press Research Fund. The authors would like to thank the Dept. of Engineering Science technicians and maintenance teams for facilities support.

REFERENCES

[1] Senecal, Kelly and Leach, Felix C. P. *Racing Toward Zero: The Untold Story of Driving Green*. SAE International (2021).

[2] Leppard, William R. "The Chemical Origin of Fuel Octane Sensitivity." *SAE Technical Paper* No. 902137 (1990).

[3] Saisirirat, P., Foucher, F., Chanchaona, S. and Mounaïm-Rousselle, C. "Effects of Ethanol, n-Butanol n-Heptane Blended on Low Temperature Heat Release and HRR Phasing in Diesel-HCCI." *SAE Technical Paper* No. 2009-24-0094 (2009).

[4] Shibata, Gen, Oyama, Koji, Urushihara, Tomonori and Nakano, Tsuyoshi. "The Effect of Fuel Properties on Low and High Temperature Heat Release and Resulting Performance of an HCCI Engine." *SAE Technical Paper* No. 2004-01-0553 .

[5] Szybist, James P. and Splitter, Derek A. "Pressure and temperature effects on fuels with varying octane sensitivity at high load in SI engines." *Combustion and Flame* Vol. 177 (2017): pp. 49–66.

[6] Splitter, Derek, Kaul, Brian, Szybist, James and Jatana, Gurneesh. "Engine Operating Conditions and Fuel Properties on Pre-Spark Heat Release and SPI Promotion in SI Engines." *SAE International Journal of Engines* Vol. 10 No. 3 (2017): pp. 1036–1050.

[7] Waqas, Muhammad Umer, Hoth, Alexander, Kolodziej, Christopher P., Rockstroh, Toby, Gonzalez, Jorge Pulpeiro and Johansson, Bengt. "Detection of low Temperature heat release (LTHR) in the standard Cooperative Fuel Research (CFR) engine in both SI and HCCI combustion modes." *Fuel* Vol. 256 (2019): p. 115745.

[8] Splitter, Derek A., Gilliam, Arthur, Szybist, James and Ghandhi, Jaal. "Effects of pre-spark heat release on engine knock limit." *Proceedings of the Combustion Institute* Vol. 37 No. 4 (2019): pp. 4893–4900.

[9] Urushihara, Tomonori, Yamaguchi, Koichi, Yoshizawa, Koudai and Itoh, Teruyuki. "A Study of a Gasoline-fueled Compression Ignition Engine Expansion of HCCI Operation Range Using SI Combustion as a Trigger of Compres-

sion Ignition ." *SAE Technical Papers* No. 2005-01-0180 (2005).

[10] Ma, Xiao, Wang, Zhi, Jiang, Changzhao, Jiang, Yizhou, Xu, Hongming and Wang, Jianxin. "An optical study of in-cylinder CH2O and OH chemiluminescence in flame-induced reaction front propagation using high speed imaging." *Fuel* Vol. 134 (2014): pp. 603–610.

[11] Hu, Zongjie, Zhang, Junjie, Sjöberg, Magnus and Zeng, Wei. "The use of partial fuel stratification to enable stable ultra-lean deflagration-based Spark-Ignition engine operation with controlled end-gas autoignition of gasoline and E85." *International Journal of Engine Research* Vol. 21 No. 9 (2020): pp. 1678–1695.

[12] Martz, J.B., Kwak, H., Im, H.G., Lavoie, G.A. and Assanis, D.N. "Combustion regime of a reacting front propagating into an auto-igniting mixture." *Proceedings of the Combustion Institute* Vol. 33 No. 2 (2011): pp. 3001–3006.

[13] White, Samuel P., Bajwa, Abdullah U. and Leach, Felix C. P. "Isolated Low Temperature Heat Release in Spark Ignition Engines." *SAE International Journal of Advances and Current Practices in Mobility* Vol. 6 No. 2 (2023): pp. 827–840.

[14] "ASTM D2699-19e1, Standard Test Method for Research Octane Number of Spark-Ignition Engine Fuel." Standard. ASTM International, West Conshohocken, PA. 2019.

[15] "ASTM D2700-19e1, Standard Test Method for Motor Octane Number of Spark-Ignition Engine Fuel." Standard. ASTM International, West Conshohocken, PA. 2019.

[16] Fan, Qinhao, Wang, Zhi, Qi, Yunliang and Wang, Yingdi. "Investigating auto-ignition behavior of n-heptane/iso-octane/ethanol mixtures for gasoline surrogates through rapid compression machine measurement and chemical kinetics analysis." *Fuel* Vol. 241 (2019): pp. 1095–1108.

[17] Bogin, Gregory E., Luecke, Jon, Ratcliff, Matthew A., Osecky, Eric and Zigler, Bradley T. "Effects of iso-octane/ethanol blend ratios on the observance of negative temperature coefficient behavior within the Ignition Quality Tester." *Fuel* Vol. 186 (2016): pp. 82–90.

[18] Singh, Eshan, Waqas, Muhammad, Johansson, Bengt and Sarathy, Mani. "Simulating HCCI Blending Octane Number of Primary Reference Fuel with Ethanol." *SAE Technical Paper* No. 2017-01-0734 (2017).

[19] Curran, H.J., Gaffuri, P., Pitz, W.J. and Westbrook, C.K. "A Comprehensive Modeling Study of n-Heptane Oxidation." *Combustion and Flame* Vol. 114 No. 1 (1998): pp. 149–177.

[20] Curran, H. J., Gaffuri, P., Pitz, W. J. and Westbrook, C. K. "A comprehensive modeling study of iso-octane oxidation." *Combustion and Flame* Vol. 129 No. 3 (2002): pp. 253–280.

[21] Tang, Qinglong, Liu, Haifeng, Li, Mingkun and Yao, Mingfa. "Optical study of spray-wall impingement impact on early-injection gasoline partially premixed combustion at low engine load." *Applied Energy* Vol. 185 (2017): pp. 708–719.

[22] Manzetti, Sergio and Andersen, Otto. "A review of emission products from bioethanol and its blends with gasoline. Background for new guidelines for emission control." *Fuel* Vol. 140 (2015): pp. 293–301.

[23] Shankar, Varun and Leach, Felix. "Effects of oxygenate and aromatic content on engine-out aldehyde emissions from pure, binary, and ternary mixtures of ethanol, toluene, and iso-octane." *SAE Technical Paper* No. 2023-32-0029 (2023).

[24] Guo, Hengjie, Torelli, Roberto, Szybist, James P and Som, Sibendu. "CFD modeling of pre-spark heat release in a boosted direct-injection spark-ignition engine." *International Journal of Engine Research* Vol. 24 No. 1 (2023): pp. 3–15.

[25] Guo, Hengjie, Torelli, Roberto, Szybist, James and Som, Sibendu. "Three-Dimensional CFD Investigation of Pre-Spark Heat Release in a Boosted SI Engine." *SAE Technical Paper* No. 2021-01-0400 (2021).

[26] DelVescovo, Dan A., Splitter, Derek A., Szybist, James P. and Jatana, Gurneesh S. "Modeling pre-spark heat release and low temperature chemistry of iso-octane in a boosted spark-ignition engine." *Combustion and Flame* Vol. 212 (2020): pp. 39–52.

[27] Yang, Can, Wang, Weiye, Li, Yuhang and Cheng, Xiaobei. "Experimental and kinetic study of NO/NO2 chemical effects on n-heptane high temperature auto-ignition." *Combustion and Flame* Vol. 249 (2023): p. 112604.

[28] Fang, Ruozhou, Saggese, Chiara, Wagnon, Scott W., Sahu, Amrit B., Curran, Henry J., Pitz, William J. and Sung, Chih-Jen. "Effect of nitric oxide and exhaust gases on gasoline surrogate autoignition: iso-octane experiments and modeling." *Combustion and Flame* Vol. 236 (2022): p. 111807.

[29] Bajwa, Abdullah U., White, Samuel P. and Leach, Felix C. P. "Low Temperature Heat Release and phi-Sensitivity Characteristics of Iso-Octane/Air Mixtures." *Combustion Science and Technology* Vol. 0 No. 0 (2023): pp. 1–23.

[30] Heywood, John .B. *Internal Combustion Engine Fundamental*. McGraw-Hill (1988).

[31] Wu, Y., Pal, P., Som, S. and Lu, T. "A skeletal chemical kinetic mechanism for gasoline and gasoline/ethanol blend surrogates for engine CFD applications." *International Conference on Chemical Kinetics*. 2017.

[32] Singh, Eshan, Tingas, Efstathios-Al., Goussis, Dimitris, Im, Hong G. and Sarathy, S. Mani. "Chemical Ignition Characteristics of Ethanol Blending with Primary Reference Fuels." *Energy & Fuels* Vol. 33 No. 10 (2019): pp. 10185–10196.

[33] White, Samuel P., Bajwa, Abdullah U. and Leach, Felix C. P. "Effect of Ethanol and Iso-octane Blends on Isolated Low Temperature Heat Release in a Spark Ignition Engine." *SAE International Journal of Fuels and Lubricants* Vol. 17 No. 3 (2024).

[34] White, Samuel P., Bajwa, Abdullah U. and Leach, Felix C. P. "Effects of Nitric Oxide on Isolated Low Temperature Heat Release in Spark Ignition Engines." *Combustion and Flame* (2024).

[35] Shankar, Varun, Usen, Ime, Molden, Nick, Willman, Christopher and Leach, Felix. "Comparing Real Driving Emissions from Euro 6d-TEMP Vehicles Running on E0 and E10 Gasoline Blends." *SAE Technical Paper* No. 2023-01-1662 (2023).

Statement of Authorship for joint/multi-authored papers for PGR thesis

To appear at the end of each thesis chapter submitted as an article/paper

The statement shall describe the candidate's and co-authors' independent research contributions in the thesis publications. For each publication there should exist a complete statement that is to be filled out and signed by the candidate and supervisor **(only required where there isn't already a statement of contribution within the paper itself).**

Title of Paper	Isolated Low Temperature Heat Release from Binary Blends of iso-Octane, n-Heptane and Ethanol in a Spark Ignition Engine
Publication Status	Submitted for Publication
Publication Details	White, S. P. & Leach, F. C. P. Isolated Low Temperature Heat Release from Binary Blends of iso-Octane, n-Heptane and Ethanol in a Spark Ignition Engine ASME 2024 ICE Forward Conference (2024).

Student Confirmation

Student Name:	Samuel P. White		
Contribution to the Paper	• Idea • Experimental design • Implementation (all) • Data analysis (all) • Writing (all)		
Signature 		Date	12 April, 2024

Supervisor Confirmation

By signing the Statement of Authorship, you are certifying that the candidate made a substantial contribution to the publication, and that the description described above is accurate.

Supervisor name and title: Felix Leach, Associate Professor of Engineering Science		
Supervisor comments I agree with Sam's comments.		
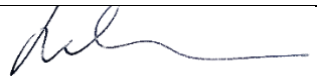	Date	12-4-24

This completed form should be included in the thesis, at the end of the relevant chapter.

The results from this paper showed that whilst iso-octane didn't undergo LTHR on its own at the conditions tested, it did when blended with n-heptane, and 0D modelling suggests that iso-octane was consumed and therefore involved in the process. Ethanol was found to have strongly inhibited LTHR—significantly more so than iso-octane for a given volume blended with n-heptane. This paper initiated the study of combustion residuals, finding that they reduced LTHR intensity, though further analysis is required as to what exactly is causing the behaviour and why; hence, this topic is explored in greater depth in Section 3.3.

Note that Figure 12 in this paper presents cumulative heat release (CHR) traces that appear to drop later on in the cycle. In the published version of this paper, the traces should have been curtailed at their maximum. The apparent reduction in CHR is caused by imperfect isolation of heat transfer effects as opposed to any chemical heat absorption phenomena.

3.2 Effect of Ethanol and Iso-octane Blends on Isolated Low Temperature Heat Release in a Spark Ignition Engine

Following on from the previous study, this work also investigated the effect of ethanol, but in blends that more closely resemble market fuels for spark ignition engines (at least in terms of octane number). To take the analysis a step further, a sensitivity analysis is introduced, to determine the root cause of the effect ethanol has on PRF LTHR.

This work was presented at the SAE Energy & Propulsion Conference & Exhibition where it won the 2023 SAE Excellence in Oral Presentation Award.

Contributions

- Ethanol was blended into iso-octane at different ratios to experimentally investigate its effect on LTHR behaviour at a range of inlet conditions.
- Benefits and drawbacks of two LTHR indicators—exhaust carbon monoxide concentration and pressure-derived heat release measurements—were demonstrated.
- A sensitivity analysis on first-stage ignition delay time is carried out to explain the effect of ethanol on LTHR of iso-octane.

ARTICLE INFO
Article ID: 04-17-03-0016

doi:10.4271/04-17-03-0016

Effect of Ethanol and Iso-Octane Blends on Isolated Low-Temperature Heat Release in a Spark Ignition Engine

Samuel Philip White,[1] Abdullah Umair Bajwa,[2] and Felix Leach[1]
[1]*University of Oxford, Engineering Science, UK*
[2]*Southwest Research Institute, USA*

Abstract

Low-temperature heat release (LTHR) is of interest for its potential to help control autoignition in advanced compression ignition (ACI) engines and mitigate knock in spark ignition (SI) engines. Previous studies have identified and investigated LTHR in both ACI and SI engines before the main high-temperature heat release (HTHR) event and, more recently, LTHR in isolation has been demonstrated in SI engines by appropriately curating the in-cylinder thermal state during compression and disabling the spark discharge. Ethanol is an increasingly common component of market fuel blends, owing to its renewable sources. In this work, the effect of adding ethanol to iso-octane (2,2,4-trimethylpentane) blends on their LTHR behavior is demonstrated. Tests were run on a motored single-cylinder engine elevated inlet air temperatures and pressures were adjusted to realize LTHR from blends of iso-octane and ethanol without entering the HTHR regime. The blends were tested with inlet temperatures of 40°C–140°C at equivalence ratios of 0.5, 0.67, and 1.0 with boosted (1.5 barA) conditions. The measured LTHR decreased with increasing ethanol content for all conditions tested; iso-octane–ethanol blends with above 20% ethanol content (by volume) showed minimal LTHR under engine conditions. These net effects resulted from the combination of thermal effects (charge cooling) and chemical effects (reactivity changes at low temperatures). The effect of temperature, pressure, fuel composition, and equivalence ratio on ignition delay times calculated from chemical kinetic modeling are presented alongside pressure–temperature trajectories of the in-cylinder gases to explain the trends. The underlying cause of the trends is explained by using a sensitivity analysis to determine the contribution of each reaction within the chemical kinetic mechanism to first-stage ignition, revealing the effect of introducing ethanol on the OH radical pool and resulting LTHR intensity.

History
Received: 27 Feb 2024
Revised: 27 Mar 2024
Accepted: 01 May 2024
e-Available: 17 May 2024

Keywords
Low-temperature heat release, Ethanol, Iso-octane

Citation
White, S., Bajwa, A., and Leach, F., "Effect of Ethanol and Iso-Octane Blends on Isolated Low-Temperature Heat Release in a Spark Ignition Engine," *SAE Int. J. Fuels Lubr.* 17(3):2024, doi:10.4271/04-17-03-0016.

ISSN: 1946-3952
e-ISSN: 1946-3960



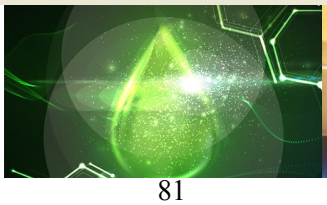


1. Introduction

The contribution to global CO_2 emissions from light-duty vehicles (LDVs) must be reduced as quickly and effectively as possible to mitigate the effect of climate change. At present, the vast majority of LDVs are propelled by the internal combustion engine (ICE) [1]. One route to reduce net CO_2 emissions from ICEs is the adoption of low-carbon and carbon-neutral fuels such as biofuels and efuels. Bioethanol is produced from biogenic matter and contains carbon originating from CO_2 absorbed from the atmosphere during photosynthesis. Its uptake is increasing due to its ability to aid decarbonization from the existing vehicle fleet, for example in the UK where standard gasoline moved from E5 to E10 (i.e., 5 to 10 %vol ethanol) in 2021. Despite its slightly lower energy density, ethanol is a suitable candidate for a drop-in fuel to replace or displace crude oil fractions thanks to its high octane rating and lower combustion temperatures—this allows for higher efficiency through the use of high compression ratios, optimized ignition timing, and reduced emissions [1, 2, 3].

Lean combustion, where the air–fuel ratio is weak of stoichiometric, has the potential to increase the efficiency of ICEs by 10–20% by improving the ratio of specific heats of the mixture and reducing wall heat losses [4]. However, the widespread adoption of lean operation in modern spark ignition (SI) engines has been inhibited by its associated challenges with ignition, combustion stability, and compatibility with three-way catalysts to treat NO_x emissions. Problems with NO_x emissions have been mostly solved with either an advanced in-cylinder technique [5] or an on-board aftertreatment system—which comes with an associated efficiency penalty. Ignition and combustion control issues are exaggerated during ultra-lean operation—a subset of lean operation where the equivalence ratio (ϕ) is (here defined as) less than 0.5 [6].

One potential remedy for the combustion control and ignition problems with lean mixtures is low-temperature heat release (LTHR); this is the phenomenon in which some of the fuel–air mixture undergoes a slower, exothermic reaction at relatively lower temperatures, producing intermediate species prior to the main combustion event. These intermediate species may have different combustion characteristics to the original fuel, therefore harnessing and controlling the underlying reactions could be key to improving lean combustion. LTHR is in contrast to high-temperature heat release (HTHR) in the main combustion event—where the chemistry differs and far more energy is released. HTHR is required for practical engine applications of combustion, whether it be caused by the second stage of autoignition or a positive ignition source such as a spark plug.

The source of LTHR is heat released from the first-stage of two-stage autoignition, which is often associated with fuel blends that exhibit negative temperature coefficient (NTC) behavior. A fuel mixture that exhibits NTC behavior has a non-monotonically decreasing relationship between ignition delay time and mixture temperature at certain pressures. In certain temperature ranges (depending on fuel), mixture reactivity decreases due to unfavorable equilibrium rates of radical forming reactions, ultimately leading to an ignition delay time that increases with temperature [7].

Fuels that exhibit strong NTC behavior include iso-octane (2,2,4-trimethylpentane) and n-heptane, the two components of the primary reference fuels (PRFs), which are used in the standard research octane number (RON) and motor octane number (MON) tests [8, 9]. Alkane fuels, particularly straight-chained alkanes, are most likely to exhibit this behavior, unlike alkenes and aromatics, which have different low-temperature chemistry [7, 10].

Unlike iso-octane and n-heptane, ethanol does not exhibit NTC behavior and therefore does not exhibit two-stage autoignition; however, iso-octane–ethanol blends of up to 20 %vol ethanol have been shown to exhibit NTC behavior in an ignition quality tester [11]. In other studies, introducing ethanol into iso-octane blends in a homogeneous charge compression ignition (HCCI) engine running at 600 and 900 rpm was shown to reduce LTHR peaks [12]. Furthermore, ethanol has been observed to be more effective at radical scavenging than iso-octane [13].

The occurrence of LTHR in HCCI engines and gasoline compression ignition (GCI) engines has been well reported [14, 15, 16, 17]. In these engines, the occurrence of LTHR has been taken advantage of to control combustion heat release rate via partial fuel stratification [18]. Furthermore, LTHR has been studied in reactivity-controlled compression ignition (RCCI) engines, where the low-temperature reactions can have an important role in curating varying degrees of charge reactivity and therefore help control HTHR [19, 20, 21].

More recently, LTHR has been shown to also occur in SI engines, occurring before the spark under certain conditions—where it is termed pre-spark heat release (PSHR) [22]. The occurrence of LTHR has been found to make knock onset less sensitive to inlet temperature by moving the mixture's thermodynamic state into a long ignition delay (low reactivity) region [22]. In other circumstances, the frequency and intensity of low-speed pre-ignition have been found to correlate with LTHR magnitude [23]. It has been hypothesized that LTHR-induced changes in mixture composition increase its laminar flame speed, which accelerates combustion [24], this could ultimately lead to improved combustion efficiency, particularly for ultra-lean operation where low flame speeds can be a limiting factor.

The effect of engine and mixture parameters on LTHR have been explored in previous studies [25, 26]:

- Increased inlet pressure generally encourages the occurrence of LTHR onset and increases its magnitude as higher pressures reduce ignition delay time.
- Increasing compression time by reducing engine speed increases the magnitude of heat release by LTHR, by allowing more time for chain-branching exothermic reactions to occur. Increasing the compression time too far allows the mixture sufficient time to progress to the second stage of two-stage autoignition, resulting in HTHR.

- The effect of increasing engine inlet temperature and therefore compression temperature is nonlinear and depends on many other factors. LTHR is more prominent with increasing temperature until the compression temperatures reach the NTC ignition delay region, at which point LTHR intensity decreases. The more time spent at temperatures corresponding to low first-stage ignition delay (usually defined by a 50 K temperature rise), the more prominent LTHR is. Hence, increasing compression temperature can either increase or decrease the strength of LTHR, depending on the starting conditions.
- LTHR magnitude increases as equivalence ratio increases due to reactivity enhancement, up until a certain limit in direct injection engines, where the thermal cooling effects of fueling overpower reactivity enhancement, and LTHR is abruptly quenched.

To date, much research on LTHR has predominantly centered around iso-octane and n-heptane, because they are the two components of PRFs. However, these compounds, with their pronounced NTC characteristics, do not comprehensively represent all elements of contemporary gasoline blends. Octane sensitivity defines the difference between RON and MON and therefore is implicitly tied to the NTC behavior of iso-octane and n-heptane; fuels with the highest octane sensitivity have demonstrated superior performance in some tests, especially those mirroring modern engine conditions [27] where LTHR was also present. Consequently, there is a pressing need for a more nuanced understanding and quantification of fuel performance that takes into account modern engines and incorporates the effects of LTHR.

The chemistry of LTHR can be studied both experimentally and computationally, via chemical kinetics simulations of engines and ignition delay times in software packages such as CHEMKIN.

In the past, investigating the effect on LTHR in SI engines, of variables such as those above or others such as fuel blends, has been challenging—pressure-derived heat release analysis techniques cannot distinguish between LTHR and other concurrent sources of heat release, such as HTHR from deflagration. A recently developed technique [25] is employed in this work to investigate the effects of blending ethanol with iso-octane on the occurrence of LTHR in isolation.

2. Methodology

2.1. Experimental Facility

The experimental investigations employed a single-cylinder, gasoline direct injection engine based on a Ricardo Hydra bottom end with technical specifications as detailed in Table 1. The engine was connected to a 57 kW AC motoring dynamometer (Vascat MAC-Q) that controlled speed (±1 rpm). Fuel injection settings including timing, duration, and fuel rail pressure were controlled with a Schaeffler Protronic ECU

TABLE 1 Engine specifications.

Bore [mm]	83.0
Stroke [mm]	92.0
Displacement [cm³]	500.0
Compression ratio	10.56.1
Fuel injection system	Production direct injector centrally mounted in cylinder head

using an ETAS INCA interface and the spark plug was disabled. Intake pressure was maintained at desired levels using an external boosting rig, with the throttle kept wide open throughout. Intake air was heated using an electric heater installed upstream of the throttle. Engine coolant and oil temperatures were maintained at 90°C.

Inlet temperature and pressure were measured around 350 mm upstream of the inlet ports using a Druck UNIK 5000 pressure sensor and a 3 mm type K thermocouple, respectively. The fuel flow rate was measured using a Coriolis Mass Flow Meter (Siemens FC Mass 2100) and the airflow rate was measured with a hot wire (Sierra-CP Airtrak 628S) flow meter. Exhaust composition was measured with a Horiba MEXA-ONE emissions analyzer. These parameters were recorded at 1 Hz using a Sierra-CP CADET system for 30 s per test. A water-cooled piezoelectric transducer (Kistler-6041B) was used to measure cylinder pressure at a resolution of 0.1°CA using an AVL Indiset data acquisition system; these high-speed measurements were recorded for 300 cycles at a time. Data was post-processed with AVL Concerto and bespoke MATLAB scripts. Further details about the test cell can be found in previous publications [26, 28, 29].

2.2. Isolating LTHR

LTHR was induced by pressurizing and heating the inlet air of the engine (which had SI geometry), as described in [25]. LTHR was isolated by disabling the spark, so as not to cause deflagration, which would interfere with the heat release phenomena and intermediate species. Boosting, inlet heating, and speed were monitored so as not to induce HTHR from the second stage of two-stage autoignition, in order to preserve the engine (and because HTHR is not of interest for this study).

2.3. Operating Conditions

Tests were performed at a constant speed of 1500 rpm and inlet pressure of 1.5 bar (absolute). A broad range of inlet temperatures (40–140°C) were tested to maximize the compression temperature range explored by the fuel–air mixtures. Equivalence ratios of 0.5, 0.67, and 1.0 were chosen in order to investigate the behavior at stoichiometric and lean conditions, where the consequences of LTHR chemistry are relevant.

Equivalence ratios were calculated from fuel and air flow measurements, and verified from exhaust emissions using the "Spindt" method [30] up to $\phi \approx 0.55$. Beyond that, the exhaust unburned hydrocarbon sensor started to saturate and only

TABLE 2 Engine settings.

IVO [°CA aTDC]	−352
IVC [°CA aTDC]	−165
EVO [°CA aTDC]	159
EVC [°CA aTDC]	359
Speed [rpm]	1500
Injection pressure [bar]	140
Injection timing [°CA aTDC]	−300
Inlet temperature [°C]	40, 60, 80, 100, 120, 140
Inlet pressure (P_{in}) [bar]	1.5
Equivalence ratio (ϕ)	0.5, 0.67, 1.0

the air and fuel flow measurements were used for determining ϕ. Inlet temperatures were maintained within ±2°C and pressure within ±0.01 bar. Engine settings are listed in Table 2.

2.4. Test Fuels

Table 3 shows the four two-component test fuels that were blended from iso-octane and ethanol (both 99.5+% purity). Fuels were coded (and will subsequently be referred to) using "OE" and their %vol of ethanol: OE05 is 5% ethanol, for example. Blends simulated computationally followed the same rule, with the range of ethanol percentages extended. Blends above 20% ethanol were not studied as this was the detectable limit for LTHR in the conditions. The fuel system was manually drained and then flushed for 25 minutes between test runs with different fuels in order to avoid contamination.

2.5. Quantifying LTHR

To quantify the amount of energy released from LTHR, net apparent heat release rate (AHRR), $\frac{dQ_n}{d\theta}$ (defined as the heat release rate $\frac{dQ_{hr}}{d\theta}$ less than the heat transfer rate $\frac{dQ_{ht}}{d\theta}$) was calculated in MATLAB using the crank angle, θ, based pressure, p, and cylinder volume, V (calculated from engine geometry) traces according to Equation 1 [31], using a constant ratio of specific heats $\gamma = 1.35$:

$$\frac{dQ_n}{d\theta} = \frac{dQ_{hr}}{d\theta} - \frac{dQ_{ht}}{d\theta} = \frac{\gamma}{\gamma - 1} p \frac{dV}{d\theta} + \frac{1}{\gamma - 1} V \frac{dp}{d\theta} \quad \text{Eq. (1)}$$

To distinguish heat release Q_{hr} measurements originating from isolated LTHR from heat transfer Q_{ht} effects and other assumptions, the calculated AHRR trace for a corresponding unfueled, motored case was subtracted from the fueled case. The start and end of LTHR were determined by finding points around top dead center (TDC) where the AHRR of the fueled case (with motoring case subtracted) deviated from zero. The isolated LTHR methodology (as introduced by White et al. [25]) meant that no HTHR was present and hence any heat release from the calculated trace was deemed to be LTHR. The AHRR was then integrated between the start and end boundaries to find the total heat release in Joules per cycle.

Cylinder temperature was calculated using the ideal gas law with measurements of cylinder pressure, cylinder volume, and estimations of cylinder contents.

TABLE 3 Test fuels.

Fuel	OE00	OE05	OE10	OE20
Iso-octane [%vol]	100.0	95.0	90.0	80.0
Ethanol [%vol]	0.0	5.0	10.0	20.0
Ethanol [%mass]	0.0	5.7	11.3	22.2
Ethanol [%mol]	0.0	13.0	24.0	41.5

2.6. Chemical Kinetics Modeling and Sensitivity Analysis

Ignition delay simulations were performed in CHEMKIN using the closed homogeneous ignition delay model with a constant volume. The simulations modeled reactions for 200 ms, and reported ignition delay defined by a 50 K rise in temperature, in order to detect the relatively small rises in temperature caused by LTHR, as in [22, 27]. Mixtures of air and iso-octane were modeled at $\phi = 0.5$ and $\phi = 1.0$ using a reduced Lawrence Livermore National Laboratory (LLNL) gasoline surrogate mechanism with 165 species and 839 reactions [32]. The contribution of each reaction within the mechanism to LTHR was determined by performing a brute force sensitivity analysis, modifying the rate constant, k, of each reaction in turn and determining the subsequent effect on ignition delay time, τ. The sensitivity coefficient, S, was calculated using Equation 2 [33], where the + and − subscripts correspond to the cases with increased and decreased rate constants, respectively. The simulations were run in CHEMKIN, controlled by a version of Pysens [34], modified to run on Windows 10.

$$S = \frac{\log_{10}\left(\tau_+ / \tau_-\right)}{\log_{10}\left(k_+ / k_-\right)} \quad \text{Eq. (2)}$$

2.7. CO as an Indicator of LTHR

Before discussing the effect of ethanol content on LTHR, the most effective metric for quantifying LTHR was determined. Traditionally, pressure-derived apparent heat release methods (as described in Section 2.5) have been used, and often lead to satisfactory estimates when test points are similar and LTHR is strong. However, when thermal effects are significant and LTHR is weak (but present), this method ceases to give perfectly accurate measurements. This is because heat transfer effects are not fully ruled out and the precise methodology regarding the start and end of LTHR can be subjective.

Reactions involved in LTHR lead to the formation of carbon monoxide (CO), and hence the extent to which CO is

FIGURE 1 Exhaust carbon monoxide measurements versus total heat released by LTHR according to the pressure-based methodology described in [25], for all fuels and inlet temperatures.

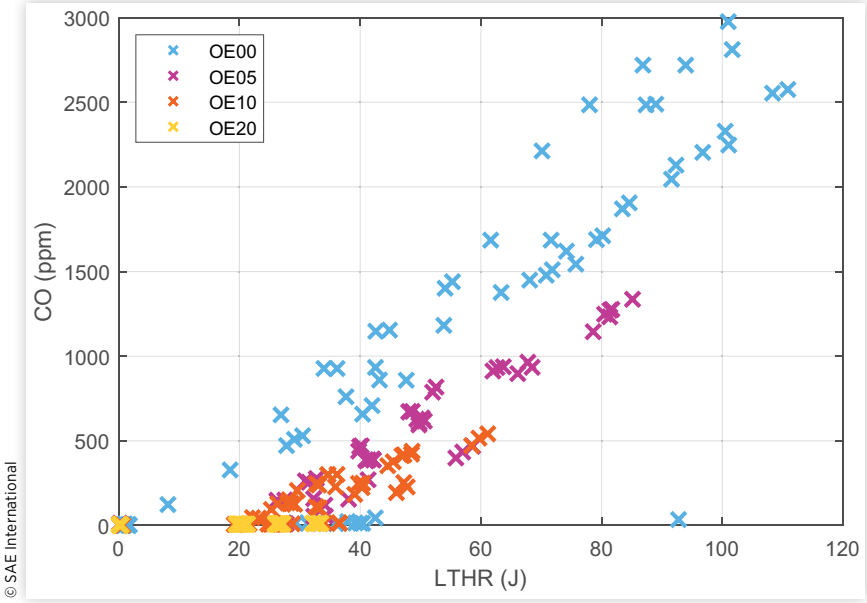

present in exhaust gases has been shown to provide a good, proportional, proxy for the intensity of LTHR when using the isolated LTHR methodology [26]; note that this is not the case when HTHR occurs alongside or after LTHR as the CO will be oxidized during complete combustion.

Figure 1, which shows direct exhaust CO measurements against estimated heat release using the pressure-derived method, demonstrates the issue. It is particularly noticeable in the fuels with higher ethanol content. In fact, test points that showed no signs of LTHR (such as some OE10 test points and all OE20 test points) led to erroneous readings of over 20 J. These readings are a result of differences in apparent heat release traces between pure air and the non-reacting air–fuel mixture, which stem from thermodynamic properties of mixtures, such as heat capacities, and differing initial temperatures stemming from charge cooling.

In fact, the linear CO-LTHR relationship that is typically observed can also be seen in this data, once it is split up into separate fuel and equivalence ratio groups. Figure 2 shows this, with the constant offset measurement error in LTHR for the various combinations; OE20 is omitted as no signs of LTHR were measured. The likely cause of this constant overestimation in pressure-derived LTHR measurement is explained above. This overestimate also applied to OE00 points (at ϕ = 0.67 and ϕ = 1.0) that didn't experience any LTHR, hence they were not included in the linear fitting process.

When this error (the x-intercept for each fuel equivalence ratio combination in Figure 2) is plotted against the energy "lost" to charge cooling (which itself is a function of fuel and equivalence ratio) an approximate doubling trend is observed (Figure 3). Charge cooling energy was calculated by multiplying the measured mass of fuel injected by the enthalpy of vaporization, using data from [35]. This did not apply to the pure iso-octane data set, where the error was minimal (0 to −5 J)—apart from the stoichiometric case where increased uncertainty in the pressure-derived measurements stopped the correction method from working effectively.

The effect of this correction is shown in Figure 4 and serves to demonstrate that carbon monoxide is a more effective indicator for LTHR intensity in this work.

3. Results

3.1. Effect of Ethanol on Measured LTHR Intensity

Figure 5 shows an overview of the experimental results at all the conditions tested. LTHR behavior of iso-octane is consistent with trends in the literature; at the low equivalence ratio point, LTHR occurred at all inlet temperatures, with the lower inlet temperatures proving favorable. As the equivalence ratio increased to 0.67, LTHR ceased at the lowest inlet temperature and peaked around T_{in} = 80°C. The inlet temperature for which LTHR ceased decreased to around T_{in} = 60°C for the stoichiometric case. This relatively sudden cutoff has been attributed to the effect of charge cooling on the pressure–temperature history and therefore autoignition chemistry of fuel–air mixtures [6].

OE05 displays a similar trend to iso-octane, albeit with only around half the LTHR intensity; the LTHR peak also occurs at higher temperatures—the precise reason for this will be explained in Section 3.3. OE10 continues this trend,

FIGURE 2 Demonstration of the linear relationship between exhaust carbon monoxide measurements and total heat released by LTHR (according to the pressure-based methodology), grouped up by equivalence ratio and test fuel for OE00, OE05, and OE10.

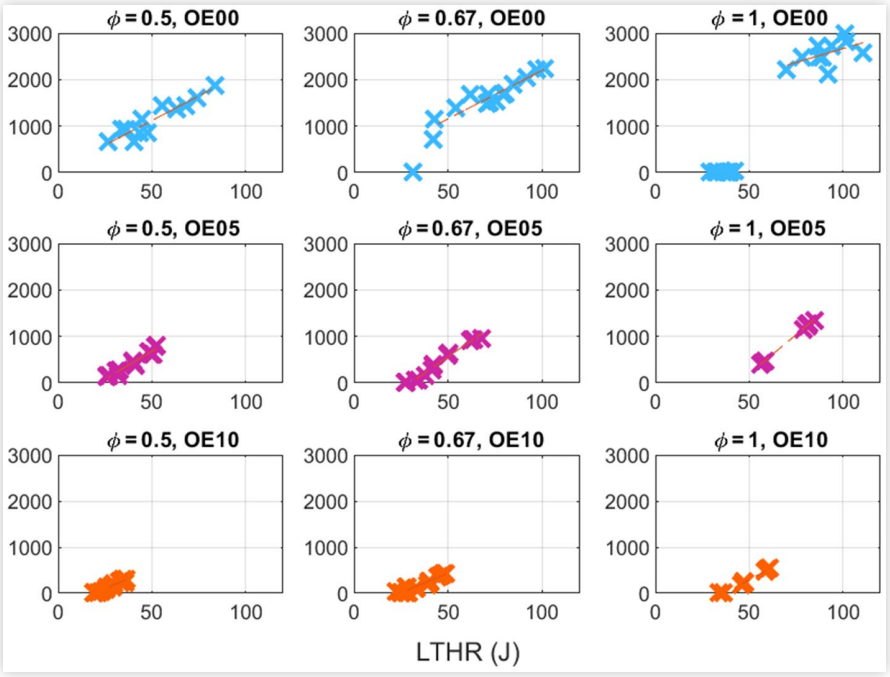

FIGURE 3 The measurement error of the thermodynamic LTHR quantifying methodology (as implied by linear CO measurements) plotted against calculated charge cooling energy for OE05 and OE10 test points.

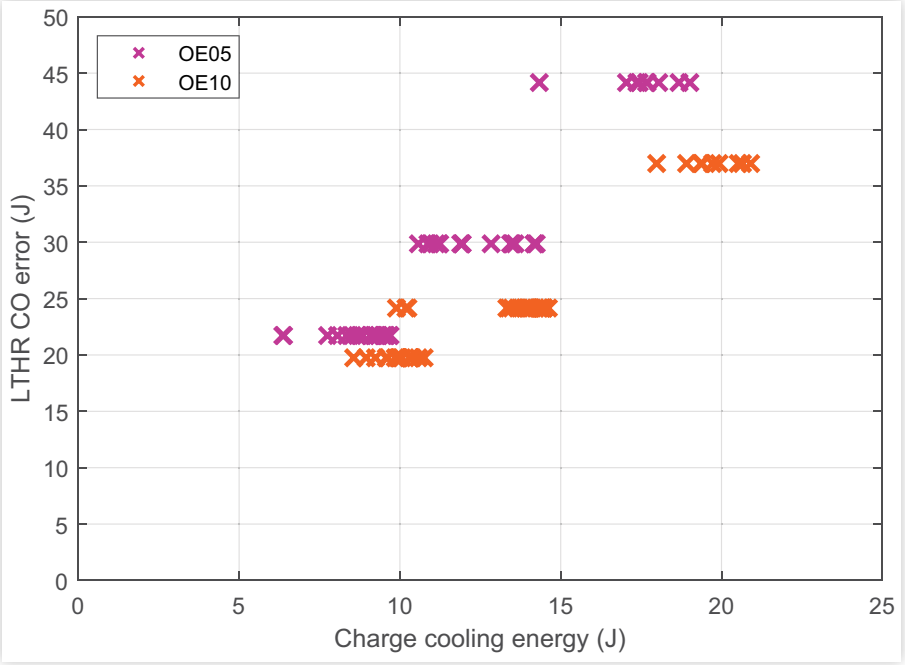

FIGURE 4 Exhaust carbon monoxide measurements versus total heat released by LTHR according to the pressure-based methodology described—incorporating a correction offset, for all test points.

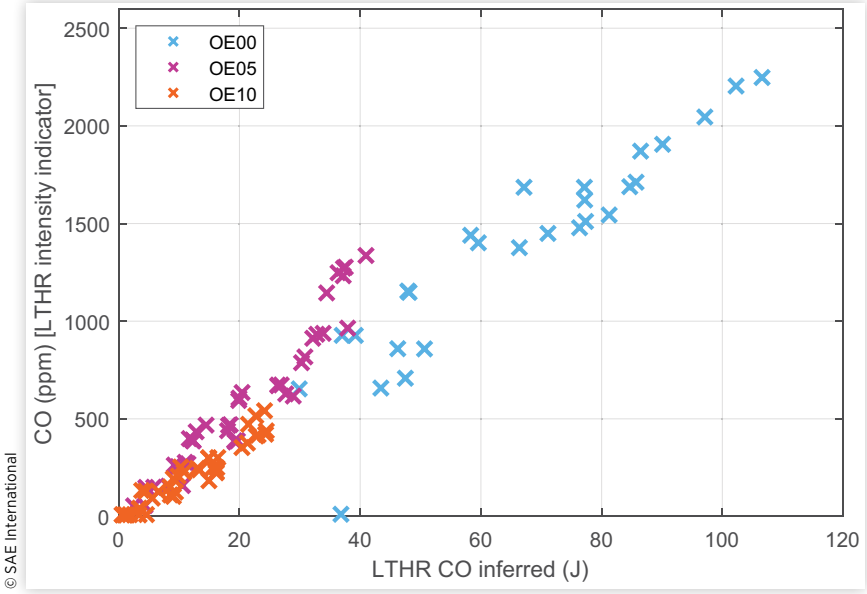

with increasing inlet temperatures for maximum LTHR intensity, with approximately half the LTHR occurring as indicated by the exhaust CO.

Increasing the ethanol content in the fuel always decreased the amount of LTHR observed for every test point; this trend can clearly be seen in Figures 6 and 7. $\phi = 0.5$ and $T_{in} = 120°C$ were chosen for plotting as they contained the most data points, and the trends observed are representative of all data that were collected. OE20 displayed no signs of LTHR for any combination of inlet temperature or equivalence ratio. The results are stark—the reduction in LTHR is far greater than can be accounted for by the displacement of iso-octane with a non-LTHR-exhibiting fuel in the blend. Instead, the observed behavior must be accounted for by chemical and physical effects resulting from the introduction of ethanol into the iso-octane blends.

3.2. Effect of Ethanol on LTHR Phasing

Increasing ethanol content was found to retard the phasing of LTHR, as shown in Figure 8; a 10 %vol increase in ethanol content delayed the CA50 of LTHR by as much as 15°CA. $\phi = 0.5$ has been shown here as it contained the most data points at different operating conditions; the other equivalence ratios exhibited the same trends. The first-stage ignition delay times for these blends are of the same order of magnitude of the time the mixtures spend at elevated cylinder pressures and temperatures, hence LTHR phasing is dependent on ignition delay time and engine speed. Increasing ethanol content in the blend increases first-stage ignition delay time, hence LTHR occurs later for the higher ethanol blends.

Comparison of Figures 5(c) and 8 suggest a strong relationship between LTHR intensity and phasing, which is confirmed in Figure 9. LTHR is too slow and commencing too late for high ethanol blends. This also explains the advancing-then-retarding nature of the phasing as inlet temperature increases.

3.3. Ignition Delay Analysis

LTHR originates from the heat released by fuels during the first stage of autoignition, so ignition delay simulations can be combined into an ignition delay contour, which represents how reactive (with respect to LTHR) a given fuel–air mixture is at different temperatures and pressures. The rate of progress toward first-stage autoignition depends on the current thermodynamic state of a mixture—this changes rapidly in a motoring engine, but in general, the further a mixture progresses into the short ignition delay region—and the more time it spends there—the more progress can be made toward first-stage autoignition, the more heat will be released by LTHR. In this section, specific cases for different fuels at a range of equivalence ratios are analyzed.

The OE00 trends observed in Figure 5(a) can be further explained by analyzing the pressure–temperature trajectories (from inlet valve closing to 10°aTDC) in Figure 10, which are overlaid onto an ignition delay contour of OE00 at $\phi = 1.0$. In these plots, the temperature and pressure axes refer to both the temperature (and pressure) of the experimental data (in the pressure–temperature trajectories) and the initial temperature (and pressure) for each ignition delay simulation. The three higher temperature cases penetrate the LTHR region—the pressure–temperature space with relatively short ignition delays. The effect of heat released from LTHR can be seen

FIGURE 5 Exhaust CO concentration (as a proxy for LTHR intensity) plotted for different fuel inlet temperatures and equivalence ratios.

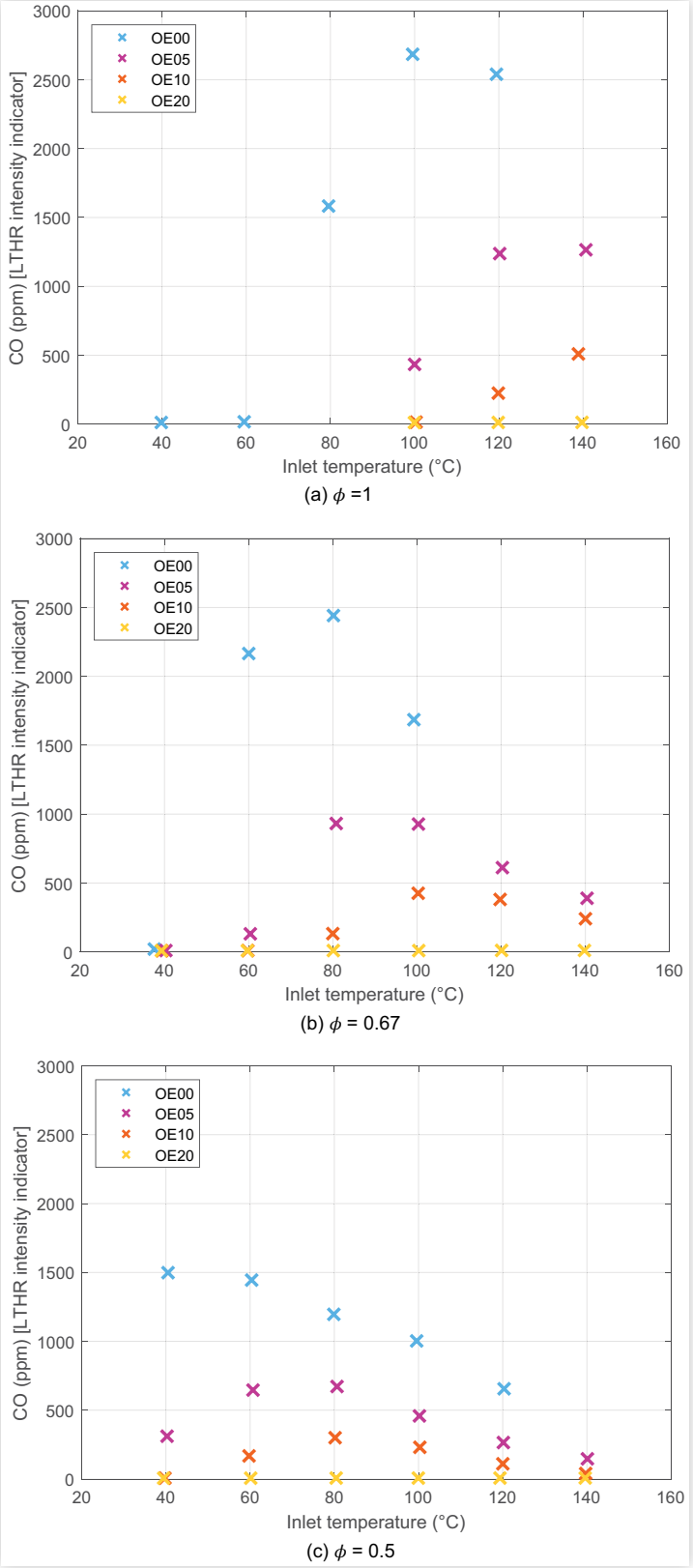

8

FIGURE 6 Exhaust CO concentration plotted against fuel ethanol content (%vol) for T_{in} = 120°C.

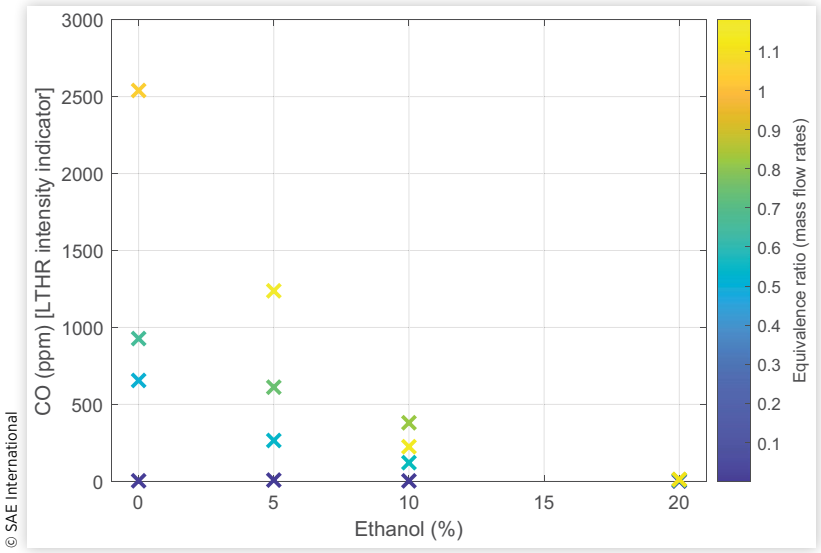

directly in the trajectories—there is a sharp temperature increase at around 32 bar, caused by the temperature rise associated with LTHR. The T_{in} = 100°C and T_{in} = 120°C cases traverse the regions with the shortest ignition delay, explaining why these points exhibited the greatest LTHR intensity in Figure 5(a).

Similarly, the OE05 trends observed in Figure 5(c) can be explained by analyzing Figure 11, which shows cylinder pressure–temperature trajectories overlaid onto an ignition delay contour of OE05 at ϕ = 0.5. The trajectories corresponding to inlet temperatures of T_{in} = 60°C and T_{in} = 80°C traverse the region with the shortest ignition delay, i.e., the most reactive low-temperature region—this explains why the T_{in} = 60°C and T_{in} = 80°C cases exhibited the greatest LTHR for OE05 at this equivalence ratio. The effect of the heat release from LTHR can be observed in the trajectories directly: the T_{in} = 40°C and T_{in} = 100°C and greater cases display a "hooking" shape, where cylinder temperature is lower after TDC than it was at the corresponding compression pressure due to heat transfer losses. Meanwhile, the T_{in} = 60°C and T_{in} = 80°C cases approximately trace back on themselves, suggesting that the heat released by LTHR approximately balances heat losses to heat transfer at the walls.

In Figure 12 the three trajectories 100°C, 120°C, and 140°C increase their penetration into the LTHR region with increasing inlet temperature. LTHR is only observed for the two highest inlet temperature cases for OE10 in Figure 5(a), which is consistent with these trajectories.

FIGURE 7 Exhaust CO concentration plotted against fuel ethanol content (%vol) for ϕ = 0.5.

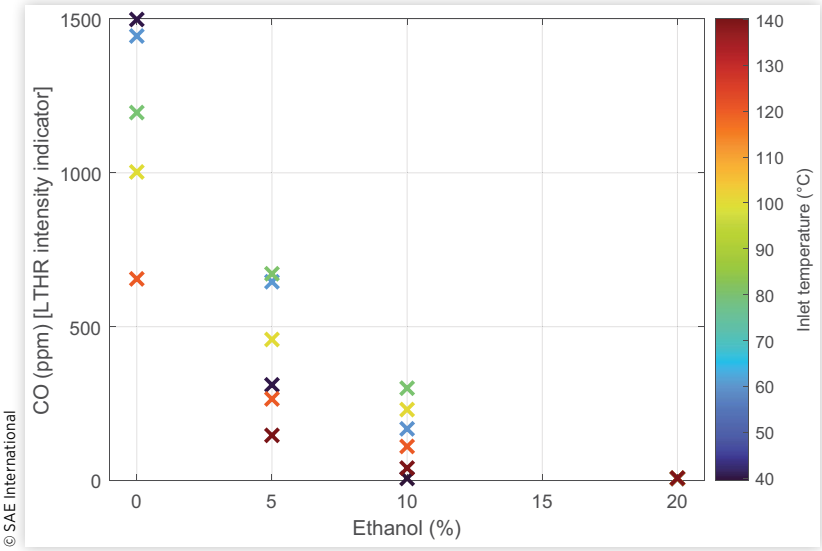

FIGURE 8 LTHR CA50 plotted for different fuels and inlet temperatures at ϕ = 0.5.

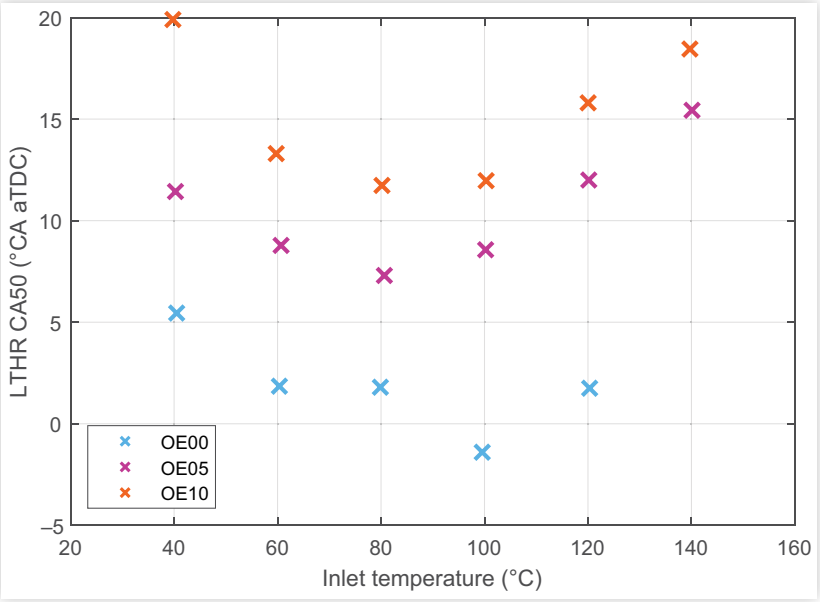

The pressure–temperature trajectories for OE20 all show the hooking behavior consistent with non-reacting cases. The ignition delay contour for OE20 lacks the large LTHR region displayed by the lower ethanol content fuels and hence none of the trajectories reach regions where the ignition delay is less than 0.01 s; the lack of LTHR observed in Figure 5(c) is not surprising (Figure 13).

To compare the reactivity and thermodynamic differences in the fuels directly, pressure–temperature trajectories of the four fuel blends are shown in Figure 14; a (dashed) line of constant ignition delay (10 ms) is also plotted for each fuel to compare their reactivity. A total of 10 ms was chosen as it corresponds to 90°CA at 1500 rpm—i.e., 45°CA either side of TDC, where pressures and temperatures are raised. The dashed lines show the decrease in reactivity as ethanol content increases, with the 10 ms line for OE20 being out of reach of the pressure–temperature trajectory at T_{in} = 80°C, ϕ = 0.5. The trends shown at these inlet conditions are representative of the full dataset.

The effects of charge cooling (which increases with ethanol content) can be seen in Figure 14(a) with the trajectories of the high ethanol fuels coming in at slightly reduced temperatures, though this behavior is not entirely consistent and its effect is smaller than the reactivity differences, with a

FIGURE 9 LTHR CA50 plotted against exhaust CO concentration at ϕ = 0.5.

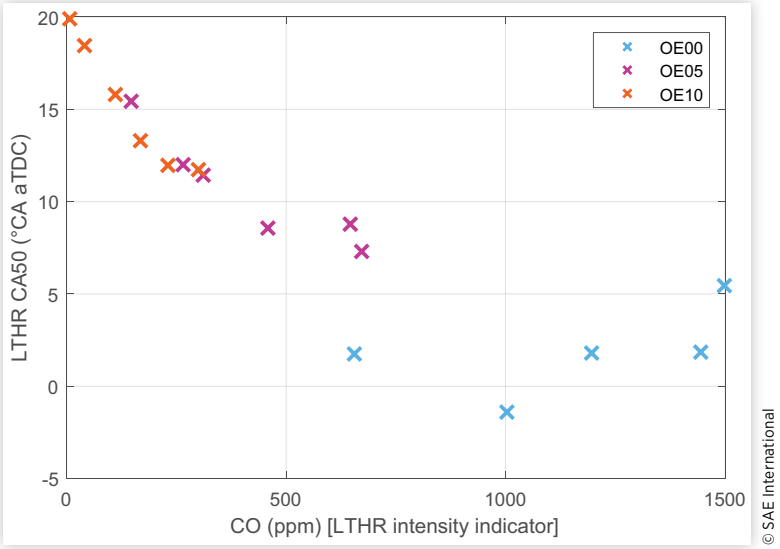

FIGURE 10 Pressure–temperature trajectories for OE00 test points with varying inlet temperatures from T_{in} = 40°C to T_{in} = 120°C, superimposed onto an ignition delay contour (defined by a 50 K rise in temperature) for OE00 at ϕ = 1.

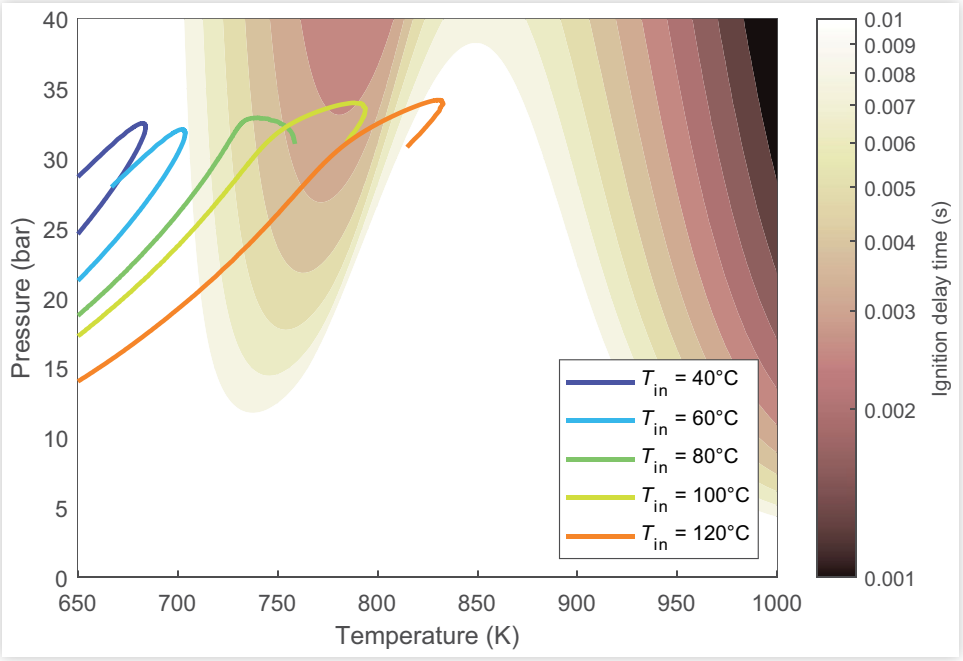

FIGURE 11 Pressure–temperature trajectories for OE05 test points with varying inlet temperatures from T_{in} = 40°C to T_{in} = 140°C, superimposed onto an ignition delay contour (defined by a 50 K rise in temperature) for OE05 at ϕ = 0.5.

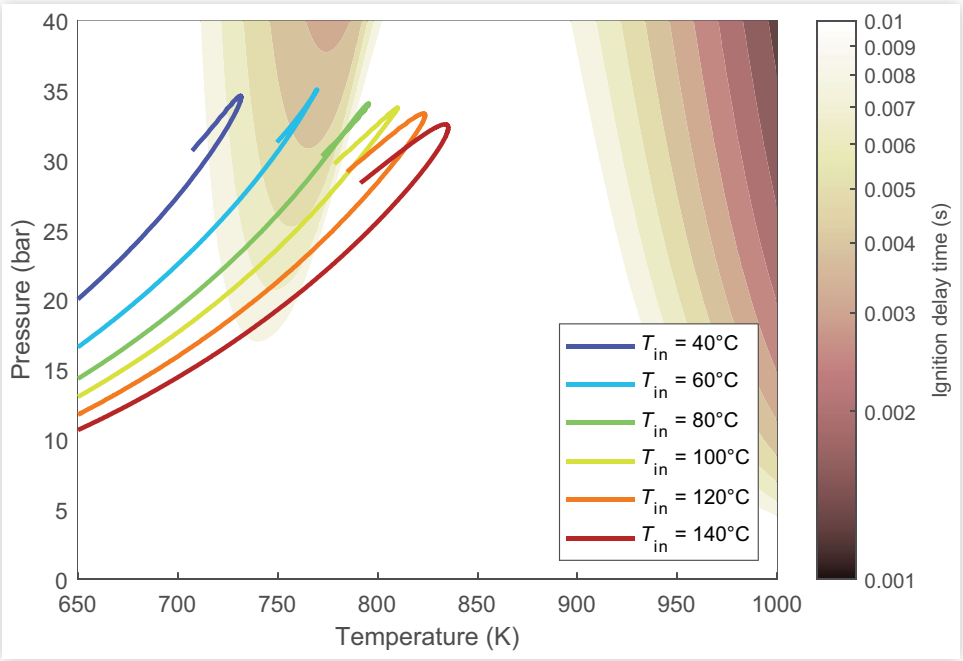

FIGURE 12 Pressure–temperature trajectories for OE10 test points with varying inlet temperatures from T_{in} = 100°C to T_{in} = 140°C, superimposed onto an ignition delay contour (defined by a 50 K rise in temperature) for OE10 at ϕ = 1.

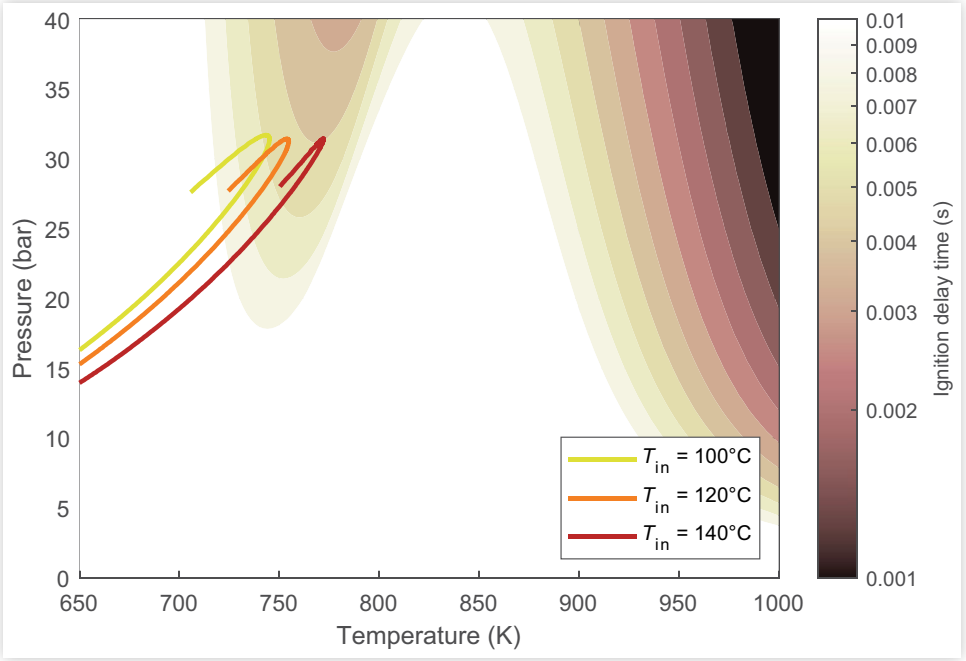

FIGURE 13 Pressure–temperature trajectories for OE20 test points with varying inlet temperatures from T_{in} = 40°C to T_{in} = 140°C, superimposed onto an ignition delay contour (defined by a 50 K rise in temperature) for OE20 at ϕ = 0.5.

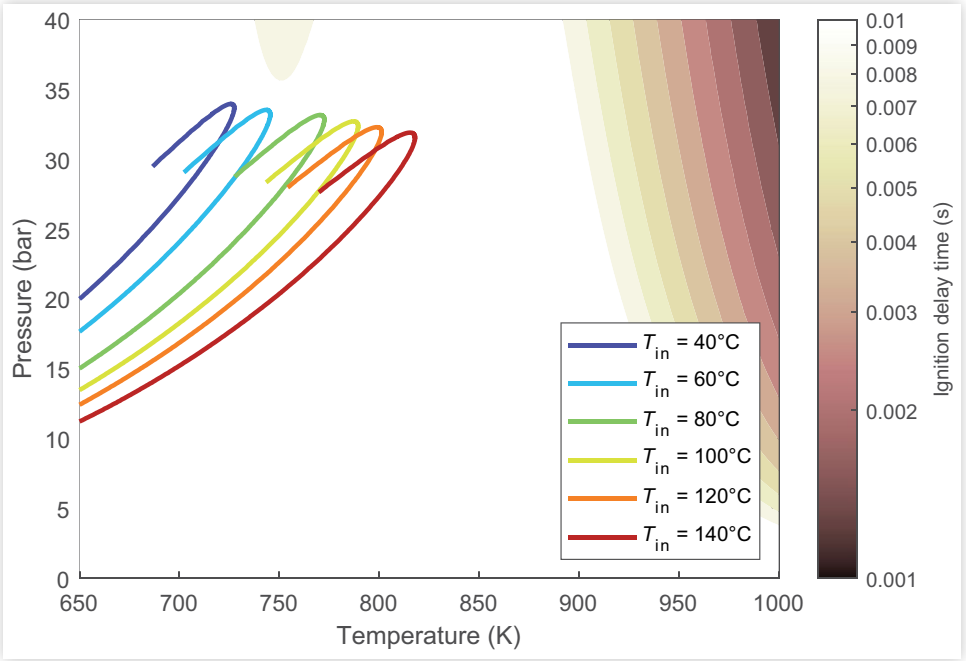

FIGURE 14 Pressure–temperature trajectories of test points for each fuel, displayed on top of corresponding dashed lines of constant ignition delay of 10 ms.

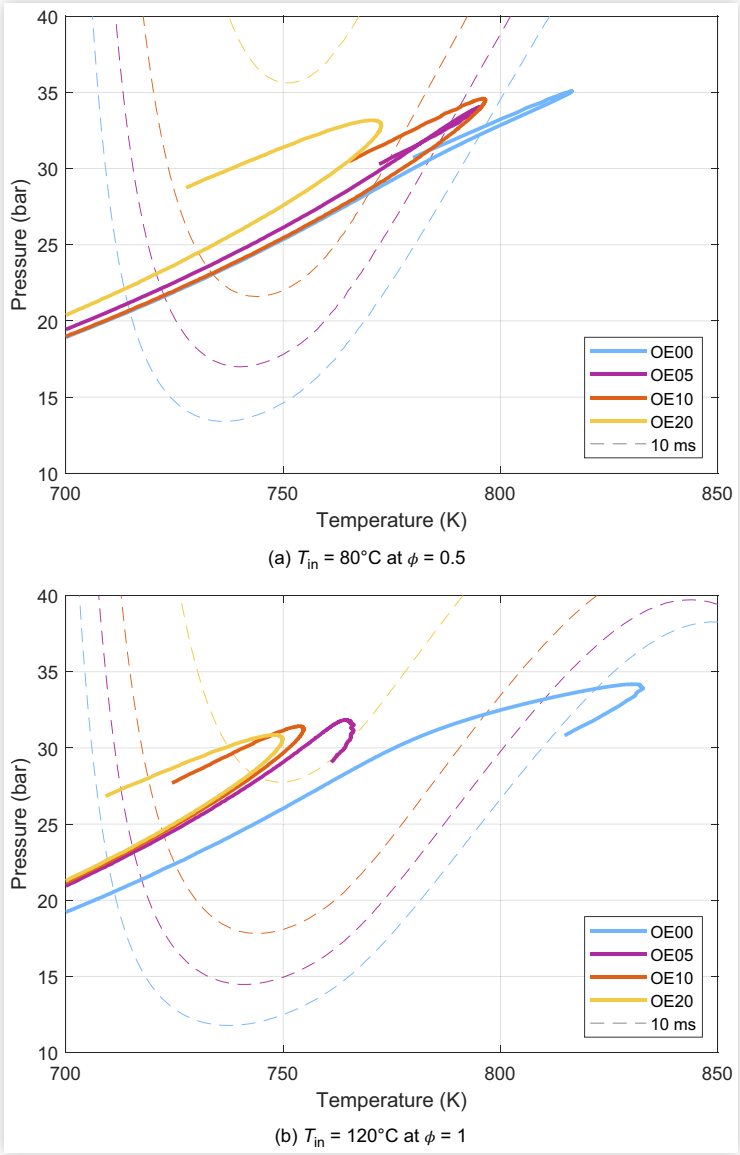

decreasing fraction of each fuel's pressure–temperature trajectory residing in the sub-10 ms region as ethanol content increases. Comparing the two sets of inlet conditions showed that the effect of ethanol at T_{in} = 120°C at ϕ = 1 seemed to be more significant. This is because, despite the high inlet temperature, the charge cooling associated with more mass injected reduces temperatures overall throughout the cycle, giving only the lowest ethanol blends the opportunity to undergo first-stage autoignition.

While the above plots show which parts of the LTHR region the pressure–temperature trajectories interact with, they do not directly measure time resided in these regions. In a system where the thermodynamic conditions and therefore the ignition delay is nonconstant, the Livengood–Wu (LW) integral (Equation 3) can be used to quantify progress toward the continuously changing target of ignition delay time for a given fuel–air mixture.

$$\mathrm{LW} = \int_0^t \frac{\mathrm{d}t}{\tau\left(T(t),P(t)\right)} \qquad \text{Eq. (3)}$$

Figure 15 shows a scatter plot of the evaluation of this integral between the times corresponding to intake valve closing (IVC) and exhaust valve opening (EVO), against the measured exhaust CO concentration. A value of unity corresponds to the mixture reaching its first-stage ignition delay on average, and the plot shows that all data points with a LW score of greater than one show significant LTHR intensity—in

FIGURE 15 Ignition delay progress, as calculated by the Livengood–Wu integral between IVC and EVO, plotted against exhaust CO concentration.

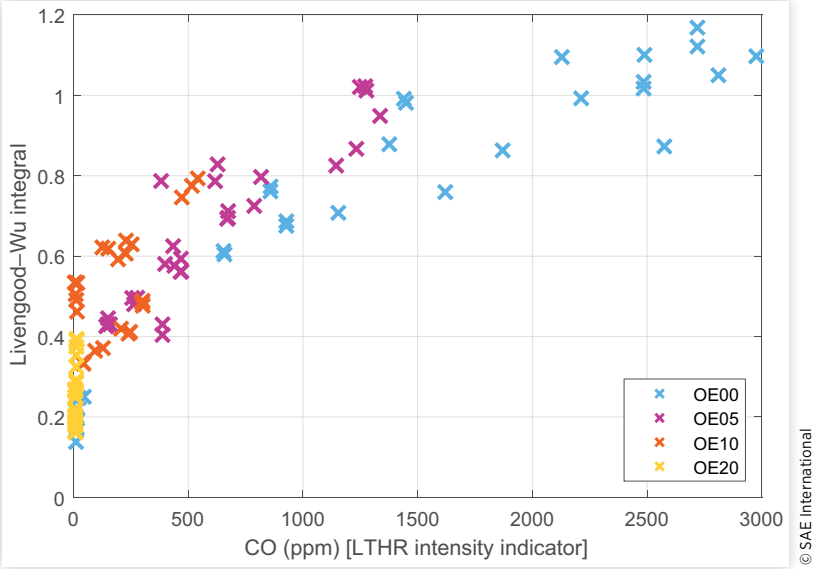

fact, every point with a score above 0.6 shows some LTHR as indicated by CO. Conversely, points with a score of less than 0.4 show little-to-no LTHR behavior. It is not entirely surprising that test cases with scores between 0.6 and 1 show some LTHR behavior; this can be attributed to two reasons: slight inhomogeneities in-cylinder temperatures and equivalence ratios, and more importantly, the fact that some heat is released prior to reaching the peak of first-stage autoignition.

Figure 16 shows an example time series of temperature during an ignition delay simulation. For OE00 to OE10, two distinct rises in temperature are clearly seen. For maximum LTHR intensity, it is necessary to move the thermodynamic stage of a mixture into a region with very short first-stage ignition delay—however, the second-stage ignition delay (defined by the steepest rise in temperature) must also be relatively long, to minimize the chances of the LTHR developing into undesirable HTHR, such as in White et al. [25].

The regions of pressure–temperature space where the difference between first-stage and second-stage ignition delays are greatest (but first stage is still short enough for LTHR to

FIGURE 16 Ignition delay time series simulations for the four fuels in a constant volume reactor with T_0 = 775°C and P_0 = 28 bar.

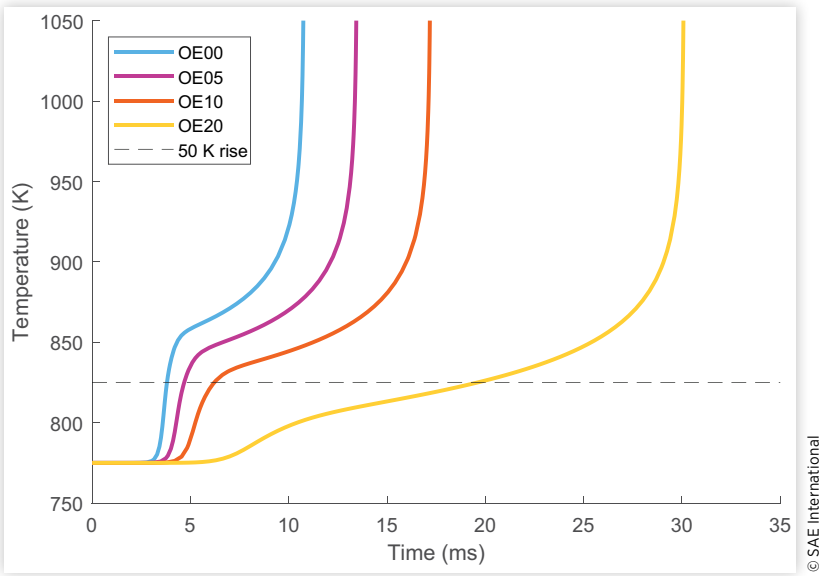

FIGURE 17 A contour showing the difference between first- and second-stage ignition delay time for OE00 at $\phi = 1$.

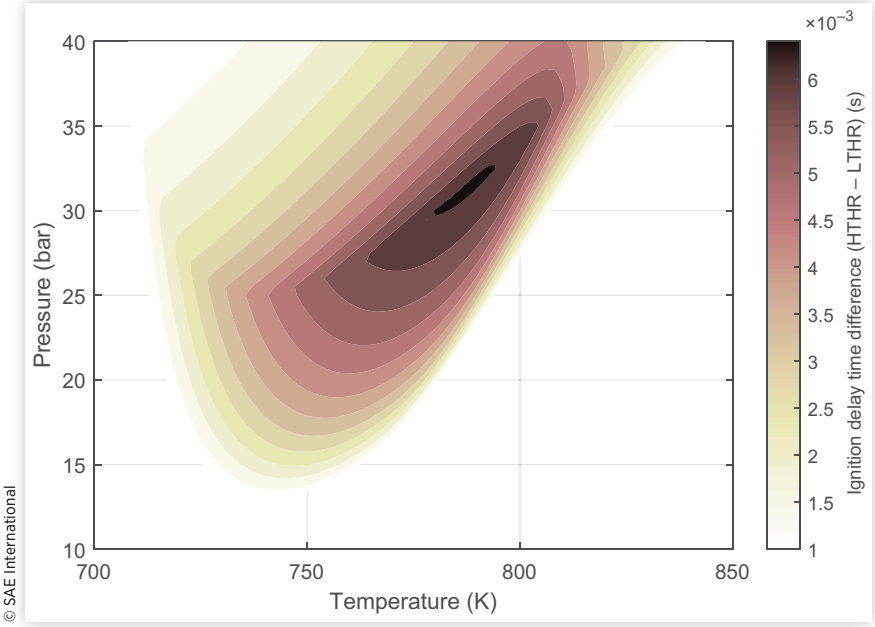

occur in engine timescales) are shown in Figure 17; the key region for LTHR in OE00 is 760–800 K, 26–33 bar, which is chosen for further exploration with an ignition delay time (brute force) sensitivity analysis.

3.4. Chemical Mechanism Analysis

A sensitivity analysis can be used to explain the fundamental cause of the results seen in this work. The most sensitive reactions are shown in Figure 18. A positive sensitivity coefficient means increasing the reaction rate increases the ignition delay time, which is not conducive to LTHR. Meanwhile, a negative sensitivity coefficient means that increasing reaction rate leads to a shorter wait for a 50 K rise, hence making a positive contribution to the occurrence of LTHR.

The four equations for hydrogen abstraction from iso-octane by a hydroxyl radical (reaction R.1) are among the reactions with the highest sensitivity coefficients (appearing first, third, sixth, and eight from the top in Figure 18):

$$iC_8H_{18} + OH \Leftrightarrow xC_8H_{17} + H_2O \qquad \text{Eq. (R.1)}$$

The x represents the four distinct sites for hydrogen abstraction. A and D are the 1° carbon atoms (first and fifth along the chain, respectively), B corresponds to the 2° carbon atom, and C represents the 3° carbon atom.

Reaction R.2, hydrogen abstraction from ethanol (fifth from the top), also has a large sensitivity coefficient:

$$C_2H_5OH + OH \Leftrightarrow sC_2H_4OH + H_2O \qquad \text{Eq. (R.2)}$$

Reaction R.3 (second from the top of Figure 18) forms an OH radical alongside a carbonyl hydroperoxide molecule form the isomerization of the peroxy–alkylhydroperoxide (O_2QOOH) radical [36]. It is known to have a strong negative sensitivity due to its involvement in the low-temperature chain-branching process—the carbonyl hydroperoxide molecule subsequently decomposes to form a carbonyl radical and a second OH radical, i.e., two radicals from a stable molecule.

$$aC_8H_{16}OOH\text{-}bO_2 \Leftrightarrow iC_8ketab + OH \qquad \text{Eq. (R.3)}$$

Meanwhile, reaction R.4 (fourth from top), the decomposition of a hydroperoxyalkyl radical (QOOH) to a cyclic ether and OH radical is known to have a strong positive sensitivity coefficient because it does not promote the route to chain-branching reactions such as reaction R.3 [36].

$$aC_8H_{16}OOH\text{-}b \Leftrightarrow iC_8eterab + OH \qquad \text{Eq. (R.4)}$$

Reaction R.5 (seventh from top), alkylperoxy radical isomerization to a hydroperoxyalkyl radical ($RO_2 \Leftarrow \Rightarrow$ QOOH), does not directly involve OH radicals, but is a precursor to reaction R.3 and the subsequent chain branching and hence has a strong negative sensitivity coefficient [36].

$$aC_8H_{17}O_2 \Leftrightarrow aC_8H_{16}OOH\text{-}b \qquad \text{Eq. (R.5)}$$

As ethanol content in the fuel increases, the positive sensitivity of hydrogen abstraction from ethanol (reaction R.2) increases; meanwhile the negative sensitivities of the hydrogen abstraction of iso-octane by OH reactions increase (reaction R.1), alongside reaction R.3. This suggests that there is competition for the OH radical and that by introducing ethanol into the fuel blend, the OH radical pool is reduced, slowing down the low-temperature reactions (as evidenced by their

FIGURE 18 Sensitivity coefficients for the sensitivity of ignition delay time (by 50 K rise) to reactions in the chemical kinetics mechanism that was used to simulate the four fuels in a constant volume reactor with T_0 = 775°C and P_0 = 28 bar.

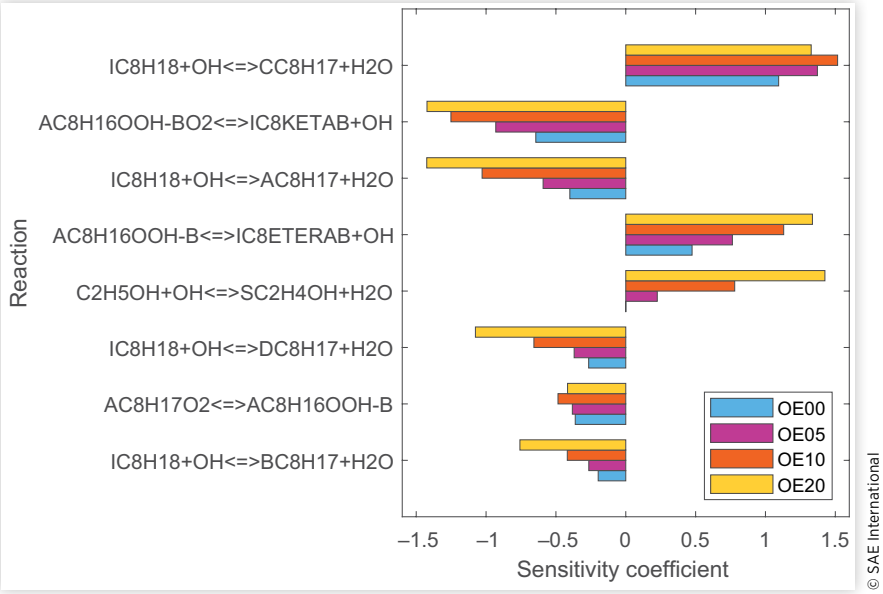

increasing ignition delay times) until ultimately they are longer than the time fuel–air mixtures spent at high compression temperatures and pressures, resulting in the observed behavior of LTHR being strongly inhibited in the motoring engine.

The C version of the hydrogen abstraction from iso-octane by a hydroxyl radical (reaction R.1) had a significant positive sensitivity but did not show a significant effect on ethanol ratio. This is in contrast with the three other hydrogen abstraction reactions, which had negative sensitivity coefficients that increased with ethanol content. The site of initial hydrogen abstraction has implications further on in the low-temperature oxidation of iso-octane; in the absence of any ethanol, the four sites are effectively in competition with each other for OH radicals. The C-type reaction involves an internal carbon, and some of the subsequent reactions, such as alkyl radical decomposition (reaction type 3 in reference [36]) have a higher activation energy than for A-, B-, and D-type reactions, which is less conducive to LTHR—but not dependent on the presence of ethanol.

4. Conclusions

In this work, experimental LTHR results of binary mixtures of iso-octane and ethanol were obtained using a motored engine with inlet temperatures of 40°C to 140°C at equivalence ratios of 0.5, 0.67, and 1.0 with boosted (1.5 barA) conditions. Both pressure-derived and carbon monoxide emission measurements were used to determine LTHR intensity. These experimental results were analyzed with the help of ignition delay contours, and a sensitivity analysis, obtained from accompanying chemical kinetics modeling.

The results show that:

- Exhaust carbon monoxide concentration is proportional to the heat released from LTHR for each fuel and equivalence ratio group.
- Blending ethanol into iso-octane in relatively small quantities has drastic inhibiting effects on the blend's LTHR behavior—much more than can be accounted for by the displacement of iso-octane molecules by non-LTHR exhibiting molecules. Blends of 20 %vol ethanol exhibited no LTHR at the conditions tested.
- The LW integral has been shown to be a good predictor of LTHR occurrence, given the pressure–temperature history of a mixture.
- The differences in first-stage ignition delay times of the fuels—and ultimately the behavior observed in this work—can be explained by the effect of ethanol's introduction on the pool of OH radicals, which are heavily involved in the initiation of low-temperature oxidation of iso-octane (by hydrogen abstraction) and the subsequent chain-branching reactions related to LTHR.

Contact Information

Felix Leach, corresponding author
felix.leach@eng.ox.ac.uk

Nomenclature

ACI - Advanced compression ignition
AHRR - Apparent heat release rate
AI - Autoignition
°CA - Crank angle degrees
CA50 - CA location at 50% heat release point
CAI - Controlled autoignition
CHR - Cumulative heat release
CO - Carbon monoxide
EVC - Exhaust valve closing
EVO - Exhaust valve opening
GCI - Gasoline compression ignition
HCCI - Homogenous charge compression ignition
ICE - Internal combustion engine
IVC - Intake valve closing
IVO - Intake valve opening
k - Chemical reaction rate
LTHR - Low-temperature heat release
LW - Livengood–Wu progress variable
NTC - Negative temperature coefficient
OExx - Iso-octane–ethanol blend with xx %vol ethanol
P - Pressure
PRF - Primary reference fuel
SI - Spark ignition
T - Temperature
TDC - Top dead center
V - Volume
ϕ - Fuel–air equivalence ratio
τ - Ignition delay time

Acknowledgements

This research was supported by an Engineering and Physical Sciences Research Council Prosperity Partnership, grant number EP/T005327/1. For the purpose of Open Access, the authors have applied a CC BY public copyright license to any Author Accepted Manuscript (AAM) version arising from this submission. The Prosperity Partnership is a collaboration between JLR, Siemens Digital Industries Software, the University of Bath, and the University of Oxford. The authors would also like to thank the Dept. of Engineering Science technicians and maintenance teams for facilities support.

References

1. Leach, F., Kalghatgi, G., Stone, R., and Miles, P., "The Scope for Improving the Efficiency and Environmental Impact of Internal Combustion Engines," *Transportation Engineering* 1 (2020): 100005, doi:https://doi.org/10.1016/j.treng.2020.100005.
2. Iodice, P. and Cardone, M., "Ethanol/Gasoline Blends as Alternative Fuel in Last Generation Spark-Ignition Engines: A Review on CO and HC Engine Out Emissions," *Energies* 14, no. 13 (2021): 4034.
3. Kim, S. and Dale, B., "Ethanol Fuels: E10 or e85 – Life Cycle Perspectives (5 pp)," *The International Journal of Life Cycle Assessment* 11, no. 2 (2006): 117-121, doi:https://doi.org/10.1065/lca2005.02.201.
4. Senecal, K. and Leach, F., *Racing Toward Zero: The Untold Story of Driving Green* (Warrendale, PA: SAE International, 2021)
5. Attard, W. and Blaxill, H., "A Lean Burn Gasoline Fueled Pre-Chamber Jet Ignition Combustion System Achieving High Efficiency and Low NOx at Part Load," SAE Technical Paper 2012-01-1146 (2012), doi:https://doi.org/10.4271/2012-01-1146.
6. Bajwa, A.U., Leach, F.C.P., and Davy, M.H., "Prospects of Controlled Auto-Ignition Based Thermal Propulsion Units for Modern Gasoline Vehicles," *Energies* 16, no. 9 (2023): 3887, doi:https://doi.org/10.3390/en16093887.
7. Leppard, W., "The Chemical Origin of Fuel Octane Sensitivity," SAE Technical Paper 902137 (1990), doi:https://doi.org/10.4271/902137.
8. ASTM, "Standard Test Method for Research Octane Number of Spark-Ignition Engine Fuel," ASTM D2699-19e1, ASTM International, West Conshohocken, PA, 2019.
9. ASTM, "Standard Test Method for Motor Octane Number of Spark-Ignition Engine Fuel," ASTM D2700-19e1, ASTM International, West Conshohocken, PA, 2019.
10. Battin-Leclerc, F., "Detailed Chemical Kinetic Models for the Low-Temperature Combustion of Hydrocarbons with Application to Gasoline and Diesel Fuel Surrogates," *Progress in Energy and Combustion Science* 34, no. 4 (2008): 440-498, doi:https://doi.org/10.1016/j.pecs.2007.10.002.
11. Bogin, G.E., Luecke, J., Ratcliff, M.A., Osecky, E. et al., "Effects of Iso-Octane/Ethanol Blend Ratios on the Observance of Negative Temperature Coefficient Behavior within the Ignition Quality Tester," *Fuel* 186 (2016): 82-90, doi:https://doi.org/10.1016/j.fuel.2016.08.021.
12. Singh, E., Waqas, M., Johansson, B., and Sarathy, M., "Simulating HCCI Blending Octane Number of Primary Reference Fuel with Ethanol," SAE Technical Paper 2017-01-0734 (2017), doi:https://doi.org/10.4271/2017-01-0734.
13. Singh, E., Tingas, E.-A., Goussis, D., Im, H.G. et al., "Chemical Ignition Characteristics of Ethanol Blending with Primary Reference Fuels," *Energy & Fuels* 33, no. 10 (2019): 10185-10196, doi:https://doi.org/10.1021/acs.energyfuels.9b01423.
14. Shibata, G., Oyama, K., Urushihara, T., and Nakano, T., "Correlation of Low Temperature Heat Release with Fuel Composition and HCCI Engine Combustion," SAE Technical Paper 2005-01-0138 (2005), doi:https://doi.org/10.4271/2005-01-0138.

15. Mehl, M., Pitz, W., Sjöberg, M., and Dec, J., "Detailed Kinetic Modeling of Low-Temperature Heat Release for PRF Fuels in an HCCI Engine," SAE Technical Paper 2009-01-1806 (2009), doi:https://doi.org/10.4271/2009-01-1806.
16. Shibata, G., Oyama, K., Urushihara, T., and Nakano, T., "The Effect of Fuel Properties on Low and High Temperature Heat Release and Resulting Performance of an HCCI Engine," SAE Technical Paper 2004-01-0553 (2004), doi:https://doi.org/10.4271/2004-01-0553.
17. Truedsson, I., Cannella, W., Johansson, B., and Tuner, M., "Engine Speed Effect on Auto-Ignition Temperature and Low Temperature Reactions in HCCI Combustion for Primary Reference Fuels," SAE Technical Paper 2014-01-2666 (2014), doi:https://doi.org/10.4271/2014-01-2666.
18. Yang, Y., Dec, J.E., Dronniou, N., and Sjöberg, M., "Tailoring HCCI Heat-Release Rates with Partial Fuel Stratification: Comparison of Two-Stage and Single-Stage-Ignition Fuels," *Proceedings of the Combustion Institute* 33, no. 2 (2011): 3047-3055, doi:https://doi.org/10.1016/j.proci.2010.06.114.
19. Saxena, M.R., Rana, S., and Maurya, R.K., "Analysis of Low- and High-Temperature Heat Release in Dual-Fuel RCCI Engine and its Relationship with Particle Emissions," *Journal of Energy Resources Technology* 144, no. 9 (2022): 091201, doi:https://doi.org/10.1115/1.4053517.
20. Willems, R., Willems, F., Deen, N., and Somers, B., "Heat Release Rate Shaping for Optimal Gross Indicated Efficiency in a Heavy-Duty RCCI Engine Fueled with e85 and Diesel," *Fuel* 288 (2021): 119656, doi:https://doi.org/10.1016/j.fuel.2020.119656.
21. Kokjohn, S.L., Hanson, R.M., Splitter, D.A., and Reitz, R.D., "Fuel Reactivity Controlled Compression Ignition (RCCI): A Pathway to Controlled High-Efficiency Clean Combustion," *International Journal of Engine Research* 12, no. 3 (2011): 209-226, doi:https://doi.org/10.1177/1468087411401548.
22. Splitter, D.A., Gilliam, A., Szybist, J., and Ghandhi, J., "Effects of Pre-Spark Heat Release on Engine Knock Limit," *Proceedings of the Combustion Institute* 37, no. 4 (2019): 4893-4900, doi:https://doi.org/10.1016/j.proci.2018.05.145.
23. Splitter, D., Kaul, B., Szybist, J., and Jatana, G., "Engine Operating Conditions and Fuel Properties on Pre-Spark Heat Release and SPI Promotion in SI Engines," *SAE Int. J. Engines* 10, no. 3 (2017): 1036-1050, doi:https://doi.org/10.4271/2017-01-0688.
24. Yamakawa, M., Youso, T., Fujikawa, T., Nishimoto, T. et al., "Combustion Technology Development for a High Compression Ratio SI Engine," *SAE Int. J. Fuels Lubr.* 5, no. 1 (2012): 98-105, doi:https://doi.org/10.4271/2011-01-1871.
25. White, S., Bajwa, A., and Leach, F., "Isolated Low Temperature Heat Release in Spark Ignition Engines," *SAE Int. J. Adv. & Curr. Prac. in Mobility* 6, no. 2 (2024): 827-840, doi:https://doi.org/10.4271/2023-01-0235.
26. Bajwa, A., White, S., and Leach, F., "Low Temperature Heat Release and Phi-Sensitivity Characteristics of Iso-Octane/Air Mixtures," *Combustion Science and Technology* (2023): 1-23.
27. Szybist, J.P. and Splitter, D.A., "Pressure and Temperature Effects on Fuels with Varying Octane Sensitivity at High Load in SI Engines," *Combustion and Flame* 177 (2017): 49-66, doi:https://doi.org/10.1016/j.combustflame.2016.12.002.
28. Leach, F., Davy, M., and Peckham, M., "Cyclic NO_2: NO_x Ratio from a Diesel Engine Undergoing Transient Load Steps," *International Journal of Engine Research* 22, no. 1 (2021): 284-294, doi:https://doi.org/10.1177/1468087419833202.
29. Papaioannou, N., Leach, F.C., Davy, M.H., Weall, A. et al., "Evaluation of Exhaust Gas Recirculation Techniques on a High-Speed Direct Injection Diesel Engine Using First Law Analysis," *Proceedings of the Institution of Mechanical Engineers, Part D: Journal of Automobile Engineering* 233, no. 3 (2019): 710-726, doi:https://doi.org/10.1177/0954407017749110.
30. Bresenham, D., Reisel, J., and Neusen, K., "Spindt Air-Fuel Ratio Method Generalization for Oxygenated Fuels," SAE Technical Paper 982054 (1998), doi:https://doi.org/10.4271/982054.
31. Stone, C.R., *Introduction to Internal Combustion Engines*, 4th ed. (London: Macmillan International Higher Education, 2012)
32. Wu, Y., Pal, P., Som, S., and Lu, T., "A Skeletal Chemical Kinetic Mechanism for Gasoline and Gasoline/Ethanol Blend Surrogates for Engine CFD Applications," in *International Conference on Chemical Kinetics*, Chicago, IL, 2017.
33. Burke, U., Metcalfe, W.K., Burke, S.M., Heufer, K.A. et al., "A Detailed Chemical Kinetic Modeling, Ignition Delay Time and Jet-Stirred Reactor Study of Methanol Oxidation," *Combustion and Flame* 165 (2016): 125-136, doi:https://doi.org/10.1016/j.combustflame.2015.11.004.
34. Weber, B., "High Pressure Ignition Chemistry of Alternative Fuels," Ph.D. thesis, University of Connecticut, 2014
35. Chen, L. and Stone, R., "Measurement of Enthalpies of Vaporization of Isooctane and Ethanol Blends and Their Effects on PM Emissions from a GDI Engine," *Energy & Fuels* 25, no. 3 (2011): 1254-1259, doi:https://doi.org/10.1021/ef1015796.
36. Curran, H., Gaffuri, P., Pitz, W., and Westbrook, C., "A Comprehensive Modeling Study of Iso-Octane Oxidation," *Combustion and Flame* 129, no. 3 (2002): 253-280, doi:https://doi.org/10.1016/S0010-2180(01)00373-X.

Statement of Authorship for joint/multi-authored papers for PGR thesis

To appear at the end of each thesis chapter submitted as an article/paper

The statement shall describe the candidate's and co-authors' independent research contributions in the thesis publications. For each publication there should exist a complete statement that is to be filled out and signed by the candidate and supervisor **(only required where there isn't already a statement of contribution within the paper itself).**

Title of Paper	Effect of ethanol and iso-octane blends on isolated low temperature heat release in a spark ignition engine.
Publication Status	Submitted for Publication
Publication Details	White, S. P., Bajwa, A. U. & Leach, F. C. P. Effect of ethanol and iso-octane blends on isolated low temperature heat release in a spark ignition engine. SAE International Journal of Fuels and Lubricants (2024).

Student Confirmation

Student Name:	Samuel P. White		
Contribution to the Paper	• Idea • Experimental design • Implementation (computational modelling and sensitivity analysis) • Data analysis (all) • Writing (all) • Conference presentation		
Signature 		Date	12 April, 2024

Supervisor Confirmation

By signing the Statement of Authorship, you are certifying that the candidate made a substantial contribution to the publication, and that the description described above is accurate.

Supervisor name and title: Felix Leach, Associate Professor of Engineering Science		
Supervisor comments I agree with Sam's comments.		
	Date	12-4-24

This completed form should be included in the thesis, at the end of the relevant chapter.

In this section, the limitations of the AHRR-based methodology discussed in Section 2.1.1 are very apparent in this work, and hence the value of the exhaust carbon monoxide concentration-based method, first demonstrated in Section 2.2 can clearly be seen. When exhaust composition data can be measured, the CO-based method would be highly preferred for making accurate comparisons between test points with little in common with each other, for example different fuels, equivalence ratios and inlet pressures. The primary drawback of the method is that it does not quantify the heat released in Joules, so it would require calibration from another technique in such circumstances.

Results relating to the effect of ethanol are consistent with the results in Section 3.1. The sensitivity analysis in this work showed the increasing significance of the competition between ethanol and iso-octane molecules for OH radicals, this behaviour is highly likely to also occur with n-heptane (since the low temperature oxidation mechanism is the same).

3.3 Effects of Nitric Oxide on Isolated Low Temperature Heat Release in Spark Ignition Engines

Following on from the initial residuals experiment in Section 3.1, an alternative approach is employed, focusing on nitric oxide (NO), which is directly seeded into inlet air in this study. This study also takes advantage of the sensitivity analysis, as used in the previous paper, to delve deeper towards the chemical reactions that determine the behaviour observed in experiments. Furthermore, since the topic of NO and iso-octane has not been well studied or modelled, the study includes a test of the behaviour of three popular chemical kinetic mechanisms that contain NO_x sub-models under LTHR relevant conditions.

Contributions

- The effect of seeding nitric oxide into the inlet air on isolated LTHR from iso-octane is investigated experimentally and computationally.
- The performance of popular gasoline surrogate chemical kinetic mechanisms were assessed at LTHR relevant conditions.
- A sensitivity analysis on first-stage ignition delay time is carried out to explain the effect of nitric oxide concentration on the LTHR of iso-octane.

Combustion and Flame 273 (2025) 113921

Contents lists available at ScienceDirect

Combustion and Flame

journal homepage: www.sciencedirect.com/journal/combustion-and-flame

Effects of nitric oxide on Isolated low temperature heat release in spark ignition engines

Samuel P. White[1], Abdullah U. Bajwa[1], Felix C.P. Leach[*]

Department of Engineering Science, Parks Road, Oxford, OX1 3PJ, UK

ARTICLE INFO

Keywords:
Nitric oxide
Iso-octane
LTHR
Ignition delay

ABSTRACT

Low temperature heat release (LTHR) is a phenomenon of interest in both spark ignition (SI) engines and in advanced compression ignition (ACI) engines. Previous studies have demonstrated and investigated LTHR in both ACI and SI engines before the main heat release event and recently, LTHR has been isolated in SI engines by modifying the in-cylinder thermal state during compression and disabling the spark discharge. Nitric Oxide (NO) is a common by-product of combustion in engines. It is formed mostly by oxidation of nitrogen from the air at high temperatures and has been shown to be one of the most reactive residual gas components since it can affect hydrocarbon combustion in small quantities (as low as 30 ppm). In this work, isolated LTHR has been studied under varying levels of NO. Tests were performed on a motored single-cylinder spark ignition engine with inlet air temperatures and pressures adjusted to realise isolated LTHR from mixtures of air, iso-octane (2,2,4-trimethylpentane) and NO. The mixtures were tested with inlet temperatures of 60 °C and 100 °C at an equivalence ratio (ϕ) of 0.5 with boosted (1.5 barA) inlet air conditions.

The results show that, contrary to most other published work, the LTHR decreased with increasing NO concentrations for all but one condition tested and NO was shown to inhibit LTHR entirely at higher concentrations. The effect of temperature, pressure, and NO concentration on ignition delay times calculated using a recently developed chemical mechanism are presented alongside experimental pressure-temperature trajectories of the in-cylinder gases to explain the trends. The underlying cause of the trends is explained by using sensitivity analysis to determine the contribution of each reaction within the chemical kinetic mechanism to first-stage ignition, revealing the effect of introducing nitric oxide on the reaction pathways, radical consumption and therefore resulting ignition delay contours and ultimately, LTHR intensity.

Novelty and significance statement

The effect of nitric oxide (NO) on low temperature heat release (LTHR) has been studied in models but rarely experimentally. Previously, NO was thought to promote LTHR in internal combustion engines. However, this work, looking at the effect of NO on LTHR from iso-octane (2,2,4-Trimethylpentane)-air mixtures at different inlet temperatures, shows that, in general, NO inhibits LTHR. Different chemical kinetics mechanisms are used to explore this behaviour and a recent mechanism from Fang et al. is shown to capture well the behaviour observed experimentally.

1. Introduction

Low-temperature heat release (LTHR), refers to exothermic reactions taking place at relatively low (<850 K) mixture temperatures. Reactions taking place at higher temperatures (>1200 K) are characterised as high-temperature heat release (HTHR) [1]. LTHR reactions influence the composition of combustion mixtures in internal combustion engines and consequently the phasing and intensity of chemical energy release [2]. They can also trigger abnormal combustion events like end-gas auto-ignition (“knocking”) [3] or stochastic preignition (“superknock” or “low-speed pre-ignition (LSPI)”) [4].

Understanding the thermo-chemical phenomena that occur during these early, and background, heat release events is thus essential for precisely controlling their effect on overall combustion and therefore on engine performance, efficiency, and emissions. LTHR behaviour depends on a combination of mixture reactivity (which is commonly indexed by the ignition delay (ID) time), pressure and temperature.

* Corresponding author.
E-mail address: felix.leach@eng.ox.ac.uk (F.C.P. Leach).
[1] These authors contributed equally to this work.

https://doi.org/10.1016/j.combustflame.2024.113921
Received 21 June 2024; Received in revised form 11 December 2024; Accepted 12 December 2024
Available online 24 December 2024

Typically, ID decreases monotonically as fuel-air mixture temperatures increase. However, for certain fuels, this relationship is non-monotonic due to the presence of a negative temperature coefficient (NTC) region [5]. It is these fuels that exhibit LTHR.

The predominant thermal propulsion system for light duty vehicles is the gasoline engine, which makes up approximately 80% of the global fleet [6]. Improved combustion control in gasoline engines, thus, presents an opportunity for significant CO_2 and pollutant emissions reduction. The potential of tailoring or managing LTHR in such engines has been revealed in previous gasoline LTHR work, for example, it can enable stable ultra-lean combustion [7], mitigate knock (provided the fuel has significant NTC behaviour) [8] and improve compression ignition control [9,10]. In particular, the effects of fuels and ignition delay on knock mitigation have been studied comprehensively by Kalaskar et al. [11] and Boehman et al. [12]. A strong determinant of gasoline LTHR intensity are residual combustion species in the reacting mixture.

With regards to the effect of LTHR on LSPI initiation, pre-ignition events can be made more likely by a reduction in ignition delay in the relatively low temperatures around a hot spot, hence strong NTC behaviour can make pre-ignition events more likely. This can be from the fuel (if it exhibits LTHR chemistry, likely due to NTC behaviour) and/or from lubricants that often have long carbon chain components that exhibit NTC behaviour. Once a pre-ignition event has occurred, the state of the end gas determines whether the pre-ignition events will lead to end gas auto-ignition (superknock) or not - end gas NTC characteristics can affect this and determine whether the subsequent combustion would be deflagrative or detonative [4,13].

The current work investigates the effect of nitric oxide (NO), a common residual gas species, concentration on LTHR in gasoline engines under different thermal conditions. Nitric oxide is formed mostly (at least when there is no fuel-bound nitrogen) by oxidation of nitrogen from the air at high temperatures via the thermal (Zeldovich) mechanism [14]. It is found in significant quantities in the products of engine combustion which, via internal or external exhaust gas recirculation (EGR), make it a part of pre-combustion mixtures [15]. The quantity, composition, and thermal state of EGR affect combustion and emission formation reactions. The net effect of EGR results from interplays between its dilution, heat capacity, chemical, and charge heating influences [16]. These effects can manifest via HTHR and/or through LTHR reactions. For example, Sjöberg et al. [17] found that fuel reformation reactions in partially firing cycles increased residual mixture reactivity and strengthened LTHR in succeeding cycles.

NO present in residual mixtures has been shown to have a strong reactivity-promoting, and consequently LTHR-promoting, effect on hydrocarbon combustion, even when it is present in small (<100 ppm) quantities [15,18–21]. LTHR promotion refers to the shortening of the first-stage (LTHR) ID, which serves to weaken the NTC behaviour of two-stage chemistry fuels [20,22,23]. This is qualitatively illustrated in Fig. 1.

The intensity of NO's influence on LTHR depends on mixture temperature and NO concentration, and to a lesser extent on the pressure and equivalence ratio (ϕ) of the mixture [19,20,23].

Moréac et al. [18] looked at air/iso-octane mixtures in a jet-stirred reactor at different conditions (10 bar, 550–1000 K, ϕ = 1, 50 ppm NO), and found that NO addition did not affect heat release until 750 K, after which it promoted iso-octane oxidation. In a recent study in a jet-stirred reactor, Tang et al. [24] added up to 500 ppm of NO to air/iso-octane mixtures at 1 bar and a range of temperatures (600–1100 K) and equivalence ratios ($\phi = 0.2$ *to* 1.5). NO addition enhanced fuel reactivity, however, the enhancement effect saturated at around 200 ppm NO and became slightly weaker as mixtures became richer. Am Ano and Dryer investigated NO and NO_2 addition to methane-air mixtures. They found that even small (ppm) quantities of NO improved the autoignition and oxidative behaviour of methane but that chemical mechanisms struggled to describe the behaviour [21]. Song et al. [20] studied the effect of NO (up to 1000 ppm) in EGR on iso-octane

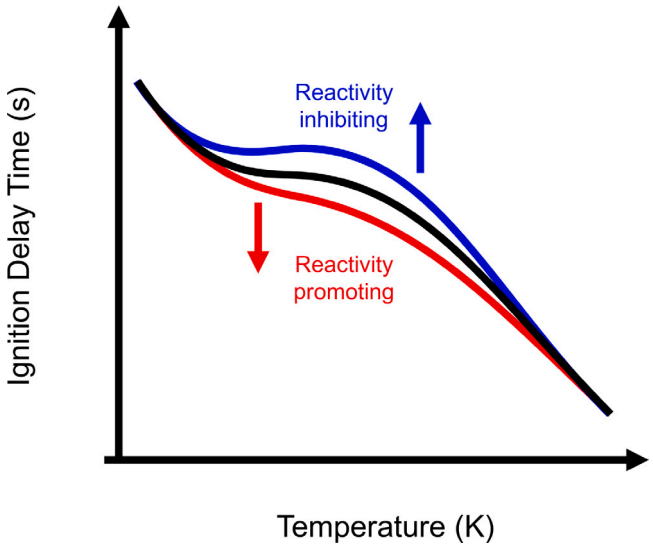

Fig. 1. Qualitative illustration of LTHR reactivity promoting and inhibiting effects of NO addition. Based on results in [20,23].

reactivity in a rapid compression machine at a range of conditions (20–30 bar, 600–950 K, ϕ = 0.6–1.4). NO addition enhanced reactivity slightly in the LTHR region (667–732 K) and much more at higher temperatures. Moreover, increasing NO concentration amplified the promotion effect.

In these studies, the chain-propagating reaction R1 has been found to be a key reactivity-promoting reaction [15,18,20]. In it, NO oxidises to NO_2, and converts less reactive hydroperoxyl radicals to highly reactive hydroxyl radicals.

$$NO + HO_2^{\bullet} \iff NO_2 + OH^{\bullet} \quad \text{(R1)}$$

Reaction R1 is more active at high temperatures where it is also supported by high $HO_2^{\bullet}$ availability. Increased production of H and O radicals at high temperatures helps initialise hydrocarbon fuel oxidation and generate $HO_2^{\bullet}$ via H-abstraction [19,20]. At low temperatures, $HO_2^{\bullet}$ radicals can be produced by reactions between the hydrocarbon fuel and OH radicals, with intermediate reactions between O_2 and alkyl-hydroperoxy groups that also generate OH [25]. The intensity of the reactivity-promoting effect of NO has been reported to decrease for mixtures with increased NTC characteristics as the drop in temperature significantly reduces reaction R1 activity, which has relatively high activation energy [26]. The NO_2 produced in reaction R1 can also promote mixture reactivity by reacting with H atoms [18].

Fang et al. [19] studied the effects of low concentrations (<70 ppm) of NO in air/iso-octane mixtures using a rapid compression machine. At 20 bar and low temperatures (<646 K), first stage decreased when NO concentration was increased up to 30 ppm, however, an inhibiting effect (i.e. an increase in ignition delay time) was observed with NO concentrations greater than 30 ppm. This suggests that it could be possible for NO to have an LTHR-inhibiting effect. At 640 to 750 K mixture temperatures, NO addition had a non-monotonic reactivity-promoting effect resulting from a trade-off between two NO-consuming reactions, reaction R1 and reaction R2. Excess NO reacted with $RO_2^{\bullet}$ via reaction R2. $RO_2^{\bullet}$ is an important intermediate species for $HO_2^{\bullet}$ production. Thus, $HO_2^{\bullet}$ production and reaction R1 activity reduced.

$$RO_2^{\bullet} + NO \iff RO^{\bullet} + NO_2 \quad \text{(R2)}$$

Contino et al. [23] studied the effects of NO addition (30-400 ppm) computationally at high pressures (40 bar) for a range of air/iso-octane mixtures (ϕ = 0.3, 650–1100 K) in a constant volume chamber. NO strongly promoted reactivity between 750 and 950 K, and

less strongly beyond 1000 K. Reaction R1 was the major reactivity-promoting pathway, consuming 75% of the total NO at 800 K (200 ppm NO).

In internal combustion engines, rather than in reactors, thermo-chemical conditions cannot be controlled independently and precisely as in various combustion reactors. To highlight the net effects of NO addition in gasoline engines, a few examples of engine studies are presented next.

Iso-octane fuelled HCCI engine experiments by Contino et al. [23] mixed up to 500 ppm of NO with the fresh charge. A stronger, monotonic reduction in ID was observed upon increasing NO concentration than in comparable experiments with n-heptane. Across iso-octane experiments, NO-induced reactivity promotion was stronger when LTHR was weak ("cool flame to main flame ratio" was low). Masurier et al. [27] experimentally observed significant reactivity enhancement in an iso-octane HCCI engine when 20 ppm of NO was introduced. Supporting chemical kinetics modelling showed a reduction in ID throughout the temperature range (666 to 1000 K) studied. The reduction was most pronounced between 750 and 850 K.

Chen et al. [28] experimentally studied the effect of NO addition (up to 800 ppm) on knocking at multiple inlet temperatures (52 to 200 °C) and a range of equivalence ratios ($\phi = 0.7$ *to* 1.1) in a CFR engine fuelled by iso-octane. The reactivity enhancement effect of NO addition manifested as advanced knock onset, and was generally stronger for leaner mixtures and higher temperatures. The enhancement was maximum for lean mixtures at low NO levels (25 ppm) while for richer mixtures, reactivity increased with increasing NO concentration.

In motored engine experiments, Yu et al. [25] dosed a hydrocarbon fuel (propane, up to 4000 ppm) and NO (up to 500 ppm) to the inlet air, and tracked NO to NO_2 conversion via reaction R1. Increasing NO concentration up to 300 ppm increased reaction R1 activity, and thus encouraged LTHR. This registered as an increase in exhaust NO_2 concentration. Beyond 300 ppm NO, exhaust NO_2 concentration dropped rapidly. This was attributed to low HC:NO ratio, which led to insufficient production of $HO_2^{\bullet}$ radicals by fuel oxidation. Formaldehyde and CO, which are common by-products of reactions in the reaction R1 chain, were also measured and were found to exhibit similar trends as NO_2. DelVescovo et al. [22] performed extensive chemical kinetics modelling of iso-octane pre-spark heat release to complement experimental engine investigations. They found that doubling the concentration of NO in the residual gas fraction from 1421 ppm had an LTHR reactivity-promoting effect.

As shown by the above-referenced examples, the effects of NO on reactivity have been studied using rapid compression machines [19,20], shock tubes [29], jet-stirred reactors [18], constant volume spray chambers [15], and reciprocating engines [23,25]. While these combustion apparatuses can generate high-fidelity chemical reaction data, they cannot be readily used for isolated investigations into the chemical effects of NO addition at engine-relevant conditions and time scales. Use of motored engines to investigate the relationship between knock onset and fuel chemistry is not new. Sturgis investigated this as long ago as 1955 [30] and Szybist et al. examined diesel-like fuels albeit with combined LTHR and HTHR [31]. A recently developed engine-based isolated LTHR investigation technique [32] can help bridge this gap. It achieves isolated LTHR by motoring (without ignition) a gasoline direct injection engine at high intake temperatures and pressures to realise LTHR without triggering HTHR.

Previous iso-octane LTHR investigations using this technique have explored the effects of changing mixture temperature, pressure, and composition [32,33]. This work builds on those studies and investigates the effect of adding NO to mixtures exhibiting LTHR in direct-injected gasoline engines, including at conditions relevant for boosted engines. The technique is well-suited for such an investigation because it allows holding boundary conditions constant while only changing NO concentration. This permits the study of the chemical effects of NO on iso-octane LTHR in engines without confounding effects from non-chemical (dilution/thermal) influences.

Table 1
Engine specifications.

Bore [mm]	83.0
Stroke [mm]	92.0
Displacement [cm^3]	500.0
Compression ratio	10.56:1
IVO [°CA aTDC]	−352
IVC [°CA aTDC]	−165
EVO [°CA aTDC]	159
EVC [°CA aTDC]	359
Fuel injection system	Production direct injector centrally mounted in cylinder head

Table 2
Engine instrumentation.

Measured quantity	Sensor
Cylinder pressure	Kistler 6041B piezoelectric transducer
Exhaust pressure	Kistler 4045a piezoresistive transducer
Inlet pressure	Druck UNIK 5000
Exhaust emissions	Horiba MEXA-ONE, Horiba FTX-ONE
Inlet/exhaust NO conc.	Cambustion CLD500
Fuel flow rate	Siemens SITRANS F C MASSFLO MASS2100
Air flow rate	Sierra CP Airtrak 620S-L06-M1-EN2-V4-DD-0
Inlet/exhaust temperature	3 mm k-type thermocouples

Supporting chemical kinetics modelling is used to identify key chemical pathways for different fuel/NO/air mixtures. Iso-octane is selected as a single-component, gasoline surrogate fuel because it has been extensively characterised [9,22]. The experimental data obtained is useful for validating and testing chemical kinetics models for NO-fuel interactions at low temperatures and filling knowledge gaps [19].

2. Methodology

In this work, a recently developed LTHR isolation methodology is applied to mixtures of air and nitric oxide using iso-octane as the fuel. The isolation methodology involves motoring the engine whilst fuel is injected, but with the ignition system disabled, so as not to trigger HTHR deflagration [32]. The isolated method allows for not only a specific focus on LTHR, but also removes uncertainty associated with NO residuals that would be generated from firing cycles, allowing the concentration to be precisely and accurately controlled whilst still subjecting the mixture to engine-relevant temperatures and pressures.

2.1. Experimental facility

The engine used in this study is a gasoline direct injection, single-cylinder research engine, with combustion geometry based on a production engine, which has been used in previous LTHR investigations [32,33]. Relevant specifications of the engine are listed in Table 1 and instrumentation in Table 2.

A Cambustion CLD500 high-speed ($t_{10–90\%}$ = 2 ms) chemiluminescence based NO analyser was used to measure NO concentration in the inlet and the exhaust. This instrument has an uncertainty of <1% full scale. Sampling heads were connected 27 cm and 16 cm upstream and downstream of the inlet and exhaust ports, respectively. To minimise measurement error from calibration drift, both the heads were recalibrated after every five test points. Exhaust gas samples were also sent to a Fourier-transform infrared (FTIR) analyser (Horiba FTX-ONE) to track LTHR markers, namely CO, formaldehyde and acetaldehyde in addition to measuring standard species measured by a standard 5-gas analyser (Horiba MEXA-ONE). These instruments have an uncertainty of <0.5% (MEXA-ONE) and <1% (FTX-ONE) full scale. Background FTIR spectrum calibration was performed every hour. The Horiba MEXA-ONE also measured exhaust NO_2 concentration to monitor NO

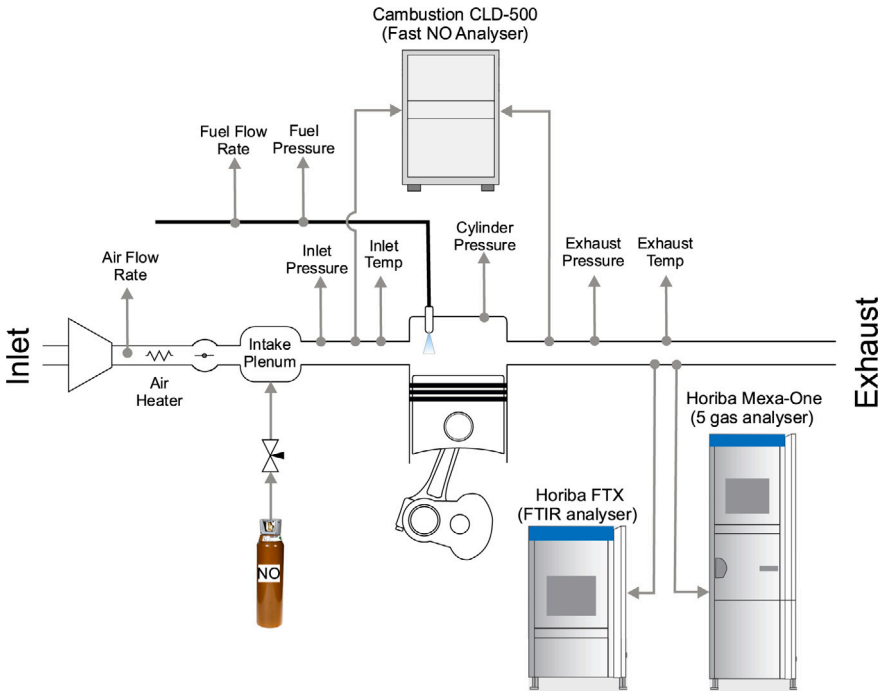

Fig. 2. Schematic of the experimental setup showing the NO dosing and measurement system.

Table 3
Measured inlet and exhaust species.

Species	Measured by	Measurement range (ppm)
CO	FTX-ONE, MEXA-ONE	0–5000
NO (inlet)	CLD500	0–5000
NO (exhaust)	CLD500, FTX-ONE, MEXA-ONE	0–10000
NO_2	MEXA-ONE	0–10000

to NO_2 oxidation. The schematic of the experimental setup shown in Fig. 2 identifies the location of relevant sensors. Table 3 includes the details of the measured species reported on in the results of this work.

Low-speed data (inlet pressure, temperatures, FTX-ONE, and MEXA-ONE) was recorded at 1 Hz for 30 s using a *Sierra-CP CADET* system. High-speed data (cylinder and exhaust pressure, high-speed NO) was logged every 0.1 °CA using an *AVL Indiset* data acquisition system for 300 cycles. Data post-processing was carried out using custom *MATLAB* scripts.

2.2. Operating conditions

Experiments were performed at a single engine speed (1500 rpm) and equivalence ratio ($\phi = 0.5$) at a boost pressure of 1.5 bar (absolute). These were chosen as reasonably strong LTHR was observed for such mixtures in a previous study [33]. The inlet NO concentration levels were varied between 0 ppm and 1000 ppm in increments detailed in Table 4, and two inlet temperature conditions (60 and 100 °C) were tested. The NO concentration levels were selected to cover the typical range of NO concentrations found in compression stroke (trapped) mixtures, these could be resulting from both internal and external EGR. These values have also been widely used in the literature [23–25]. Other operating conditions and parameters are summarised in Table 4. Three repeats were performed at each test point except for the 1500 ppm NO point where only one repeat could be performed because of limited NO availability.

2.3. NO addition

A bottle of 100% concentration NO (1.22 litre, 30.8 bar) was used to supply the NO into the inlet air via a metering needle valve that permitted precise flow control (Fig. 2). During NO addition experiments, the engine was initially motored without any fuel injection at the required inlet temperature and pressure conditions, and the needle valve was gradually opened to permit NO to flow. The inlet NO concentration measured by the high-speed NO analyser was monitored and the valve was opened until the required concentration was achieved. During this time, exhaust NO concentration, measured by the second high-speed NO channel and MEXA-ONE, served as calibration checks—where they all reported similar NO concentration values. The inlet NO concentration drifted slightly, especially for the high NO consumption cases, because of drop in the NO supply pressure as NO was consumed from the bottle. Next, with NO supply continuing at the required flow rate, fuel injection duration was increased from 0 ms (i.e. motoring) to deliver the fuel needed to create a $\phi = 0.5$ mixture. The inlet NO concentration stayed the same during injection while exhaust NO concentration changed because of fuel injection and in-cylinder LTHR reactions. Data was recorded once the system reached steady operation, marked by the stabilisation of exhaust emissions and temperature readings.

2.4. Quantifying LTHR intensity

The LTHR intensity of each test run was quantified by using the exhaust CO concentration, measured with the FTIR and MEXA-ONE, as an indicator of LTHR intensity. This method is made possible by the isolated nature of LTHR in these experiments—there are no HTHR reactions to generate CO, hence the sole source of CO is the low temperature reactions that are also responsible for LTHR. Using CO as not only an indicator of LTHR but also to quantify the magnitude of LTHR is a long-established practice [5,34,35], and more recently, the relationship between exhaust CO concentration and apparent heat release rate methods was shown to be highly linear [33]. The possibility of NO reactions consuming some of the CO and effecting the use of this method was investigated comprehensively. Where NO is converted to a

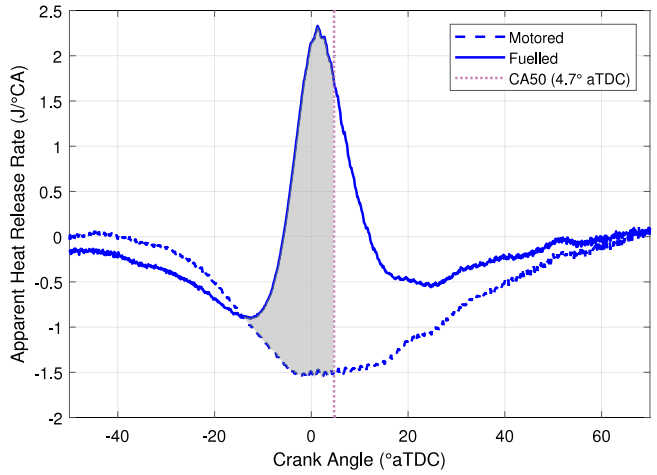

Fig. 3. Comparison of AHRR between motoring and fuelled cases.

Table 4
Engine operating conditions.

Parameters	Values
Fuel	iso-octane (>99% purity)
Injection pressure [bar]	140
Injection timing [°CA aTDC]	−300
Equivalence ratio (ϕ)	0.5
Target NO concentration (ppm)	0, 200, 500, 1000, 1500
Inlet temperature [°C]	60, 100
Inlet pressure (P_{in}) [bar]	1.5
Speed [rpm]	1500

substance other than NO_2, which is the only other nitrogen substance that can be measured, the modelling indicates that it is converting to CH_3NO_2, HONO, and $HONO_2$, none of which consume CO. This method was chosen over the AHRR-based indexing method because it is not affected by heat transfer between the combustion volume and the surroundings, making it considerably more accurate and precise for conditions where the pressure rise as a result of LTHR is very difficult to distinguish from other contributions to cylinder pressure. However, to obtain other combustion parameters such as the angle of 50% mass fraction burned (CA50) the AHRR method was used. It is likely that LTHR will initiate at the same temperature, for a given set of conditions, and therefore engine crank angle — meaning that CA50 will be a measure of combustion duration for a given set of engine conditions. A comparison of AHRR between motoring and fuelled (exhibiting LTHR) cases is shown in Fig. 3, which shows how CA50 (in this case) is obtained — being the angle at which 50% of the total heat from LTHR has been released. Further discussion of this is included in Bajwa et al. [33].

2.5. Chemical kinetic modelling and sensitivity analysis

2.5.1. Single-zone HCCI modelling

A single-zone HCCI model (Ansys Chemkin-Pro) was validated to match the geometry and thermodynamic conditions of the engine (Table 1). The dimensionless heat transfer correlation was employed with the Woschni correlation for gas velocity [14]. Inlet conditions and valve timings were set to match the experiments, as in Table 4, whilst inlet NO concentration was swept from 0 ppm to 1500 ppm in 50 ppm increments.

A single-zone model was employed rather than a multi-zone model due to computational limitations—particularly to allow for detailed mechanisms with a very large number of reactions. The aim of the HCCI simulation was to compare trends between the mechanisms, as opposed to achieving a precise match with the experimental data, hence one zone was deemed sufficient.

Table 5
Selected chemical kinetic mechanisms for HCCI model.

Mechanism	Ren [36]	C3MechV3.3 [37]	Fang [19]
Species	178	3761	1543
Reactions	758	16,522	8725
NOx Submechanism	GRIv3.0	NUIGMechv1.1	Fang
Year	2017	2022	2022

The three mechanisms tested are summarised in Table 5. The first, a reduced mechanism, developed by Ren et al. was chosen for its satisfactory performance in the PSHR modelling study by DelVescovo et al. [22]. The second, C3MechV3.3 (referred to herein as simply "C3") was chosen for its complexity and inclusion of NO_x chemistry for gasoline surrogates. Finally, a mechanism developed by Fang et al. was chosen for its specific focus on iso-octane and its low temperature interactions with NO_x [19].

2.5.2. Ignition delay analysis

Corresponding ignition delay calculations were used to analyse the experimental data. Ignition delay simulations were performed in Ansys Chemkin-Pro using the closed homogeneous ignition delay model with a constant volume. The simulations modelled reactions for 200 ms and reported first stage ignition delay (τ), which was defined by a 50 K rise in temperature in order to detect the relatively small rises in temperature caused by LTHR. This is consistent with commonly adopted values in the literature [2,8]. Mixtures of air and iso-octane were modelled at $\phi = 0.5$ with initial temperatures between 650 K and 1000 K and initial pressures of 0.5 bar to 40 bar for inlet NO concentrations of 0, 200, 500 and 1000 ppm.

Experimental pressure-temperature trajectories were generated using measured cylinder pressure ($P(t)$) and calculated average cylinder temperature ($T(t)$). The cylinder temperature was calculated using the ideal gas law with measured cylinder pressure, calculated cylinder volume, and estimated trapped cylinder mass. To aid with the ignition delay analysis of the experimental data, the Livengood-Wu (LW) integral (Eq. (1)) was used to quantify progress though time (t) towards the continuously changing ignition delay time (τ) for a given mixture [38]. The integral used calculated ignition delay times (from the preceding paragraph) for the corresponding experimental pressure and temperature data.

$$\mathrm{LW} = \int_0^t \frac{dt}{\tau\left(T(t), P(t)\right)} \tag{1}$$

2.5.3. Sensitivity analysis

A brute force sensitivity analysis was used to determine the contribution of each reaction within a mechanism to LTHR. The rate constant k of each reaction was modified in turn to determine the subsequent effect on ignition delay time τ. The sensitivity coefficient, S, is calculated according to Eq. (2) [39], where the + and − subscripts correspond to the cases with increased and decreased rate constants respectively. The simulations were performed in CHEMKIN, controlled by a version of Pysens [40] (a Python-based Chemkin-Pro sensitivity analysis tool), modified to run on Windows 10 and handle an expanded range of mechanism formats.

$$S = \frac{\log_{10}\left(\tau_+/\tau_-\right)}{\log_{10}\left(k_+/k_-\right)} \tag{2}$$

3. Results and discussion

3.1. Effect of inlet nitric oxide concentration on LTHR intensity

Fig. 4 shows the effect of seeding nitric oxide into the inlet air on low temperature heat release (as indicated by CO) at different

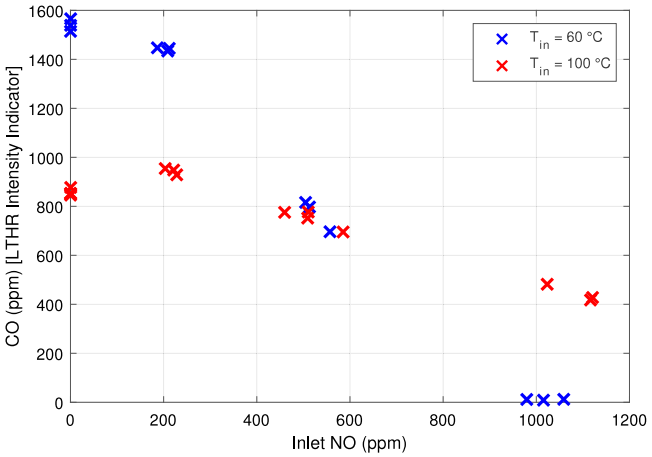

Fig. 4. Exhaust CO concentration (as a proxy for LTHR intensity) plotted for different concentrations of seeded nitric oxide in inlet air.

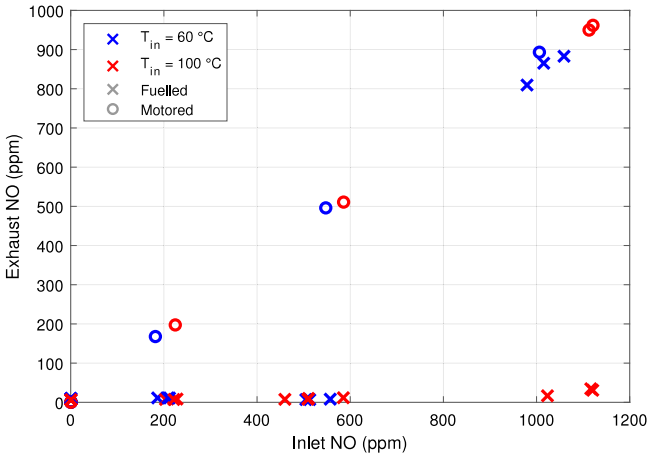

Fig. 5. Exhaust nitric oxide composition.

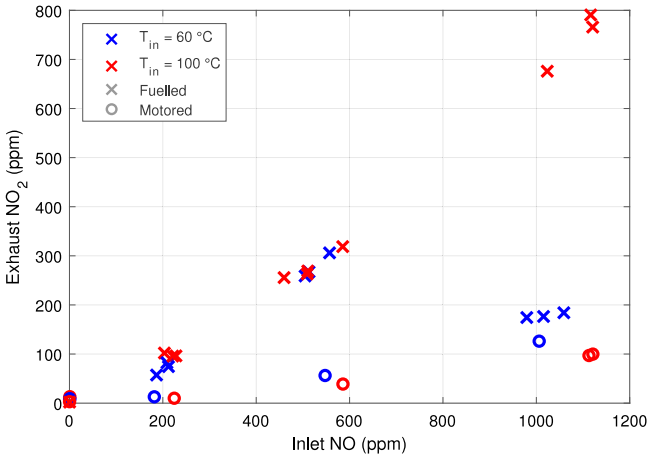

Fig. 6. Exhaust nitrogen dioxide composition.

concentrations for inlet temperatures of T_{in} = 60 °C and T_{in} = 100 °C. For all but one condition (200 ppm NO, T_{in} = 100 °C), introducing nitric oxide inhibits LTHR, which is in contrast to models of similar behaviour in the literature [22]. Examining the T_{in} = 100 °C case, there is a slight promoting effect observed when comparing the zero NO case to 200 ppm case, however beyond this, NO serves to inhibit the amount of LTHR observed, reducing the intensity of LTHR to half when inlet concentration reached 1000 ppm. The trend in the T_{in} = 60 °C case is more pronounced. LTHR intensity drops slightly at the 200 ppm case, then rapidly to half its neat value when seeded NO concentration reached 500 ppm. Furthermore, increasing seeded NO concentration to 1000 ppm inhibited LTHR entirely, with all experimental indicators pointing to no reactions occurring.

3.2. LTHR and oxidation of nitric oxide

To gain further insight into which reactions inhibit LTHR, the consumption and conversion of NO to NO_2 can be examined. These species are particularly relevant; NO_x reactions occur in hot air and NO:NO_2 ratios are known to be affected by the presence of hydrocarbons [41].

Examining the motoring case (circular markers, Fig. 5) for NO-out vs NO-in shows that, without fuel present, most NO remains. This confirms that it does not convert to NO_2 early in the cycle and hence it is likely to be NO and not NO_2 involved with the initial interaction with the fuel.

On the other hand, in the presence of fuel (cross markers, Fig. 5), in all but one of the test points, nearly all of the NO is consumed. This is consistent with past work from Leach et al. which examined NO in the presence of hydrocarbons [41] and suggests that NO consumption is directly involved in the inhibiting of low-temperature oxidation of iso-octane, and subsequently LTHR, at these conditions.

One point stands out: the T_{in} = 60 °C, 1000 ppm NO case, where no LTHR occurred (Fig. 4). For this test point, the presence of NO has fully inhibited LTHR (as indicated by CO), but this time — unlike all others observed — without any significant consumption of NO (i.e. it appears in line with the motoring cases in Fig. 5). This suggests that the presence of NO affects both the initial low temperature oxidation reactions (i.e. hydrogen abstraction from iso-octane) as well as later stages such as the low temperature chain branching reactions where NO is likely to be consumed. In this case, the inhibiting effects are so strong that the low temperature oxidation process cannot get started and hence there is minimal opportunity at the chain branching stage for NO to be consumed.

Regardless of whether or not fuel is present, NO is known to convert to NO_2 in the presence of air and particularly at elevated temperatures. Examining the NO_2 out vs NO in plots in Fig. 6 shows that, when motored, approximately 10% of NO was converted to NO_2 for the T_{in} = 60 °C case, and less (about 7%), was converted for the T_{in} = 100 °C case, assuming there was no conversion before plenum measurement).

Meanwhile, the fuelled cases exhibit a strong linear trend where conversion to NO_2 is approximately 50%, consistent across both inlet temperatures, aside from the 1000 ppm T_{in} = 60 °C case where conversion is much lower, but slightly (and significantly enough) above the motoring case, suggesting that a small amount of NO is still converted to NO_2 as part of the inhibiting process. These trends are similar to those seen in work by Krutzsch et al. [42,43].

3.3. Effect of inlet nitric oxide concentration on LTHR phasing

LTHR is linked to the first stage ignition delay of a mixture—these ignition delay times are often on engine timescales, hence examining the phasing of LTHR can give an indication of the effect on ignition delay time, with more advanced phasing suggesting shortened ignition delay times and vice versa. Here, heat release phasing is indicated by CA50—the crank angle at which 50% of the heat from LTHR (as indicated by the AHRR analysis method) has been released.

Fig. 7 shows the effect of NO seeding on CA50. In general, higher concentrations of NO slowed down the combustion process—giving later combustion phasing. However, at small concentrations of NO—increasing inlet NO concentration from zero to 200 ppm—the heat release phasing is advanced for both inlet temperature cases, despite having a mixed effect on LTHR intensity.

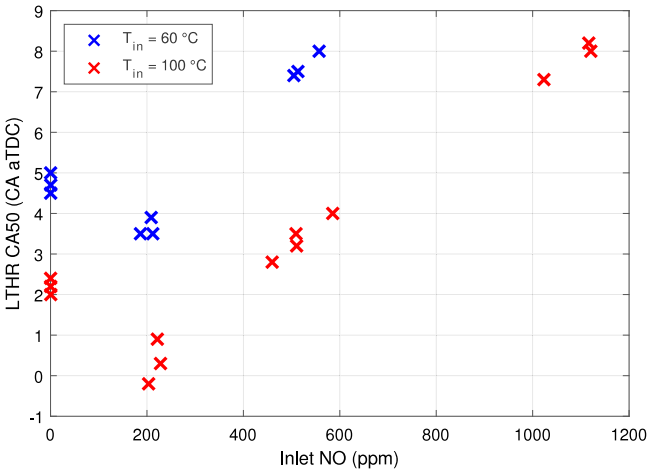

Fig. 7. The effect of inlet NO concentration on LTHR phasing.

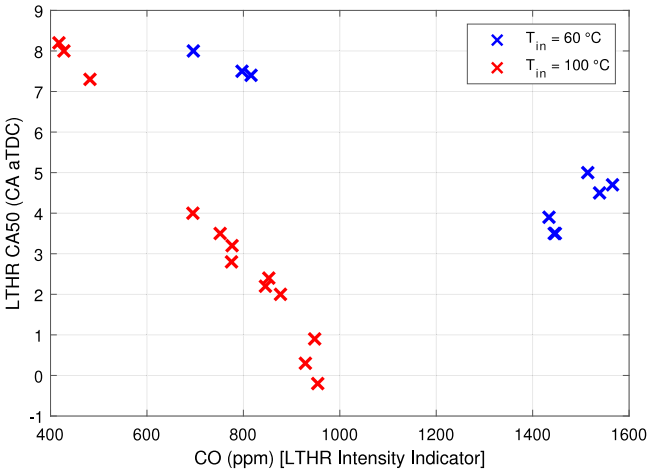

Fig. 8. Relationship between LTHR phasing and LTHR intensity.

Plotting CA50 against LTHR (Fig. 8) shows a very strong link between the amount of LTHR and LTHR phasing for the T_{in} = 100 °C case. This is less strong for cold cases. This trend has been seen in previous work when considering other factors that affect LTHR and first stage ignition delay of mixtures [44]. Lower reactivity leads to longer first stage ignition delay, which results in LTHR starting later, giving the mixture less time and opportunity at peak temperatures and pressures for low temperature reactions to occur, resulting in less LTHR being observed overall.

3.4. Chemical kinetic mechanism comparisons

In order to better understand the experimental results that were obtained, the conditions tested experimentally were evaluated in a single-zone model comparing three chemical mechanisms: Ren et al. [36], the C3 Mechanism V3.3 [37], and Fang et al. [19]. Fig. 9 shows the results of the model comparison. The y-axis shows total heat chemical heat release (i.e. LTHR) at the end of the cycle and the data points have been normalised by the 0 ppm NO case for Fang. There is a clear contrast to the experimental results from Fig. 4, where in the T_{in} = 60 °C case, LTHR intensity decreased rapidly and was fully inhibited at 1000 ppm, and in the T_{in} = 100 °C case where LTHR increased at 200 ppm before also slowly reducing as inlet NO concentration increased up to 1000 ppm.

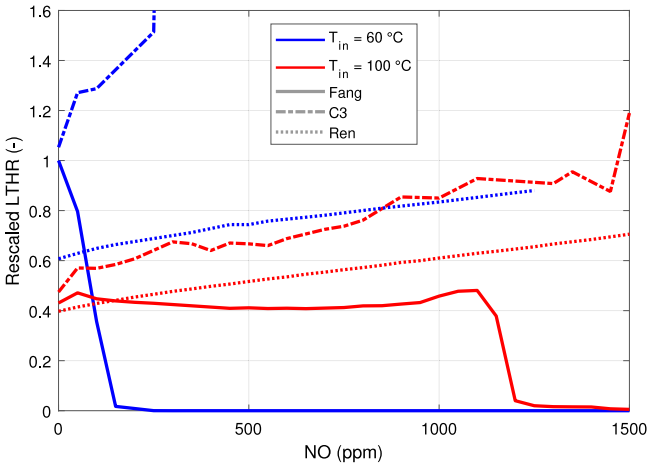

Fig. 9. Three significant chemical kinetic mechanisms tested in an HCCI engine model. The plot shows (normalised) predicted LTHR against inlet NO concentration.

Both the C3 and Ren mechanisms predicted that NO increases LTHR. The Ren mechanism predicted a gradual, steady increase for both inlet temperatures tested, whilst C3 predicted larger LTHR intensity rises than Ren for T_{in} = 60 °C and a very dramatic rise at T_{in} = 100 °C, to the point where, beyond 250 ppm, HTHR was predicted. This is entirely different from the behaviour observed in the experimental study (as shown in Fig. 4). Meanwhile, results from the simulations that used Fang's mechanism showed opposite predictions on the effect of NO concentration on LTHR, which are much closer to resembling the experimental results in Fig. 4. The cessation of LTHR for T_{in} = 60 °C case can be seen albeit at a lower concentration than the experiments. The T_{in} = 100 °C case does not show an LTHR promoting trend, instead showing a peak at 50 ppm, followed by a gradual fall until around 600 ppm, before a gradual rise until 1100 ppm where LTHR then sharply declines.

Whilst a single zone HCCI model is clearly too simple to expect accurate reproductions of experimental results (the main issue being temperature stratification, which causes differences in reaction progress throughout the cylinder, resulting in heat release events that are less intense and take place over a longer period of time), the purpose of this figure is to demonstrate the clear difference in trends between the mechanisms. Whilst the Fang mechanism and 0D engine model clearly would require further calibration and a more sophisticated engine model to reproduce the results accurately, it was the only mechanism that correctly models the inhibiting effect of NO on LTHR intensity.

The stark differences in predictions in Fig. 9 can be explained by examining the effect of nitric oxide on the ignition delay time of representative mixtures, as calculated by the three models, shown in Fig. 10. The IDT solutions for the 0 ppm case were not in precise agreement between the three mechanisms hence, for clarity, the relative differences between the 0 ppm and 200 ppm solutions for each mechanism have been plotted as ratios ($\frac{\tau_{200}}{\tau_0}$) where a ratio of less than 1 represents a 200 ppm ignition delay time that is shorter than the 0 ppm case, corresponding to a supposed promoting effect of NO on LTHR.

Once again, there is a clear difference between Fang and the other two models. For all temperatures tested, Ren and C3 predicted a shorter ignition delay time when NO concentration was increased to 200 ppm from 0 ppm (as shown by the $\frac{\tau_{200}}{\tau_0}$ ratio of less than one) meanwhile Fang's mechanism predicts the opposite, i.e. a longer ignition delay and therefore inhibition of LTHR at temperatures below 715 K.

Mechanisms, such as C3 and Ren (which have been employed in past studies modelling LTHR and adjacent topics [22]) are not able to accurately model the effect of NO on LTHR because they do not account for the inhibiting effect that NO has on iso-octane ignition chemistry at

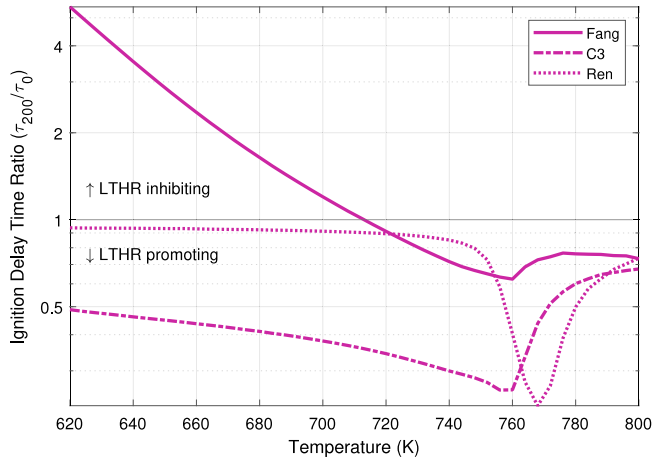

Fig. 10. The effect on ignition delay time (τ) of increasing mixture NO concentration to 200 ppm from 0 ppm, plotted as a ratio $\frac{\tau_{200}}{\tau_0}$ for temperatures between 620 and 800 K, for three different chemical kinetic mechanisms.

relatively low temperatures. This has important ramifications for the whole combustion model since NO is almost always present and the presence (or lack thereof) of LTHR can significantly impact combustion behaviour later on in the cycle—for example, the knocking limit [8].

3.5. Ignition delay analysis

The underlying causes of the behaviour observed in the experiments (Fig. 4) can be explained by examining the relevant ignition delay contours. Fig. 11 shows pressure-temperature (P-T) trajectory of the cylinder contents from the experimental work (each contour contains representative trace for each test point), superimposed onto first stage ignition delay contour generated from the ignition delay simulations with the Fang et al. mechanism [19]. The colour of the contour represents ignition delay time at a given pressure and temperature. The ignition delay is related to the reactivity of the mixture: the shorter the ignition delay, the more reactive it is, and the more progress can be made towards first stage ignition (and hence low temperature heat release) whilst at those conditions. The plots show the dramatic difference the presence of nitric oxide has on the reactivity of iso-octane and air mixtures.

The effect of heat release from LTHR can be seen in P-T trajectory of experimental data. For high LTHR cases (T_{in} = 60 °C, 0 ppm and 200 ppm) there is a rightward bend in the trajectory, as the heat release causes a temperature rise. Conversely, for the low and no LTHR cases, the heat loss effects can be seen as the trajectory is at a significantly lower temperature for a given pressure either side of TDC.

The effect NO concentration ultimately has on LTHR intensity can be explained by examining the penetration of the mixture's P-T state into the high reactivity—low first stage ignition delay—region: in the T_{in} = 60 °C case, the P-T trajectory is very deep into the low ignition delay space (here defined as an ignition delay of less than 10 ms—corresponding to 90° CA at the test speed of 1500 rpm) for the low NO concentration cases but almost entirely outside of it for the 1000 ppm case. Meanwhile in the T_{in} = 100 °C case, the differences are less obvious, but the P-T trajectory appears to pass through the most low reactivity regions in the 200 ppm case, consistent with the LTHR maxima at the same concentration in the experimental results (Fig. 4).

Figs. 12(a) and 12(b) show P-T trajectories of the experiments at T_{in} = 60 °C and T_{in} = 100 °C inlet, superimposed onto a plot of dashed lines of constant ignition delay of 10 ms and 5 ms respectively. These illustrate the drastic effect that the seeded NO concentration has on ignition delay across the P-T space.

In Fig. 12(a), between 680 K and 750 K, above 20 bar, the increasing seeded NO concentration from 0 to 1000 ppm pushes the high reactivity, 10 ms region rightwards, towards higher temperatures, by nearly 50 K. In the same plot, at around 720 K, the 200 ppm line drops to the lowest pressure, suggesting that moderate (i.e. 200 ppm) concentrations have a LTHR promoting effect around the 12–15 bar, 710–740 K region. The T_{in} = 100 °C cases and 5 ms lines show a similar effect, with increasing NO shifting the low temperature reactivity region to the right.

Looking rightward, from approximately 750 K onward, the effect of NO concentration reverses. The higher NO cases show 10 ms ignition delay at considerably lower pressures, with the presence of NO reducing the NTC behaviour of the mixture. Examining the experimental P-T traces, as NO concentration increases, the traces decreasingly penetrate into the low ignition delay region due to decreasing cumulative LTHR increasing mixture temperatures during the cycle, resulting in a two-fold effect with respect to reduced LTHR.

For the T_{in} = 100 °C cases in Fig. 4, maximum LTHR was lower than the colder cases, and the range of LTHR intensities were smaller. This is also reflected by the similarity in the P-T traces in Fig. 12(b). The trajectory through low temperatures — where NO decreases reactivity — mostly balances the trajectory through intermediate temperatures where NO has the effect of increasing reactivity. The lower dip of the 200 ppm 5 ms ignition delay line can be seen again here and is the most likely explanation for the LTHR intensity peaking at 200 ppm NO in Fig. 4—the P-T trace of the 200 ppm case passes through the very low ignition delay (5 ms) regions the most.

The significant and characteristic effect that NO seeding has on the ignition delay time of iso-octane points to the existence of a "critical temperature" [15]—the temperature at which NO switches from having an inhibiting effect on ignition chemistry to a promoting effect. Whilst this behaviour was reproduced in only one of the three chemical kinetics mechanisms tested in Fig. 10, there is evidence from fundamental studies of this behaviour. For example, in experiments by Fang et al. in a rapid compression machine with iso-octane at ϕ = 1, 20 bar, NO concentrations above 30 ppm inhibited ignition chemistry, leading to a delayed first stage ignition delay time, up to 737 K [19]. Furthermore, Contino et al. reported a similar inhibiting effect with iso-octane below 700 K, when 400 ppm NO was introduced [23].

This effect has been observed more frequently with n-heptane, for example Moreac et al. reported an inhibiting effect "to the point of extinction" (much like the T_{in} = 60 °C case in Fig. 4) persisting up to 600 K with 50 ppmv NO and 670 K with 500 ppmv in a jet-stirred reactor at 10 atm, ϕ = 1, with a residence time of 1 s [18]. However, in these tests, the same effect was not observed for iso-octane. The critical temperature phenomenon is not unique to iso-octane and n-heptane, with other alkanes such as n-pentane [45] and propane [29] also exhibiting lengthened ignition delay times at low temperatures when exposed to nitric oxide.

Whilst Figs. 11 and 12 show which parts of the LTHR region the pressure-temperature trajectories interact with, they do not directly measure time resided in these regions. In scenarios where the thermodynamic conditions and therefore ignition delay is non-constant, the Livengood-Wu (LW) integral (Eq. (1)) can be used to quantify progress towards the continuously changing ignition delay time for a given mixture.

Fig. 13 presents the experimental data in a scatter plot of the evaluation of this integral between the times corresponding to intake valve closing (IVC) and exhaust valve opening (EVO), against LTHR intensity as indicated by the measured exhaust CO concentration; the inlet NO concentration for each test point is indicated by the colour scale. A value of unity corresponds to the mixture reaching its first stage ignition delay on average—though the intensity of LTHR would not necessarily be expected to be correlated with the value evaluation of the LW integral. In the plot, all of the points with a score of greater than 1 showed clear LTHR; there was only one case where LTHR did

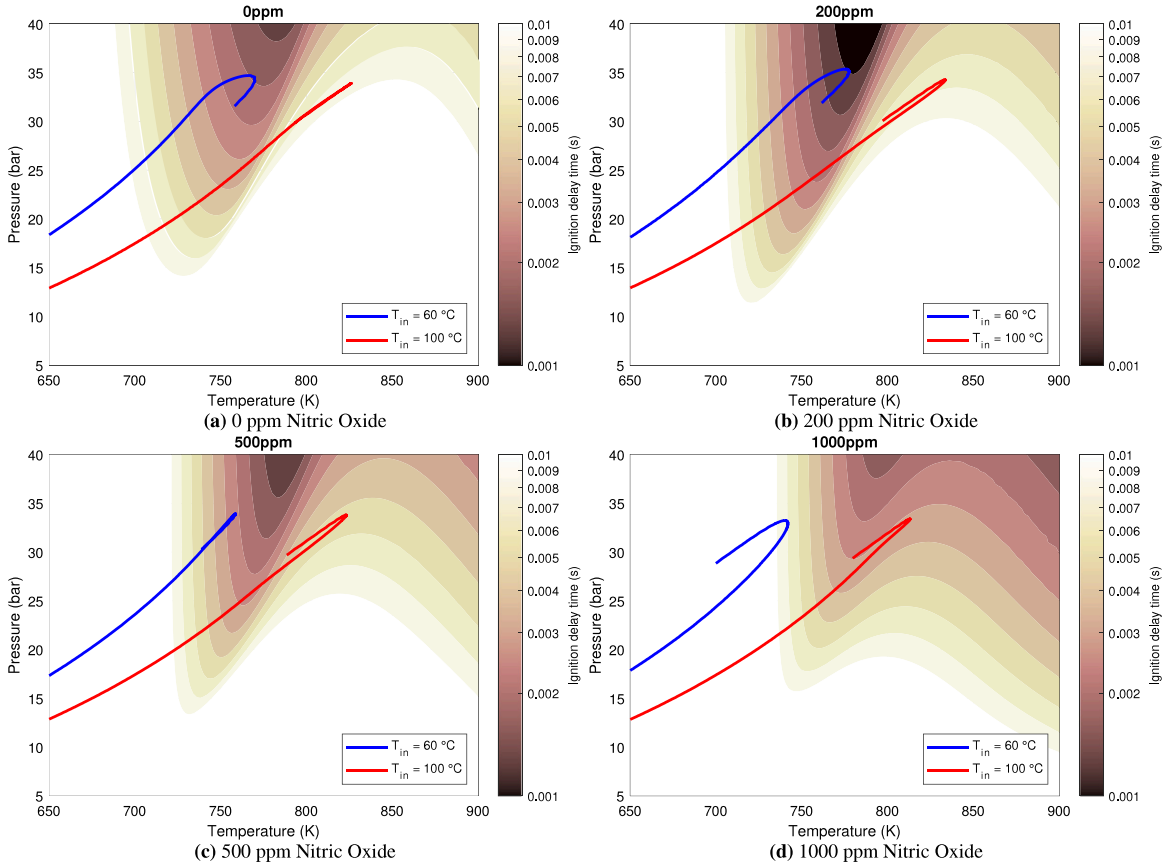

Fig. 11. Experimental pressure-temperature trajectories (from IVC to 10° aTDC) plotted over first stage ignition delay (as defined by a 50 K temperature rise) contours for the iso-octane, air and nitric oxide mixtures at $\phi = 0.5$. (For interpretation of the references to colour in this figure legend, the reader is referred to the web version of this article.)

not occur, and that had a very low LW score of approximately 0.3. For the intermediate scores (0.7 to 1.0) it is not entirely surprising that LTHR is observed, as heat is released by LTHR soon before 1st stage ID is reached, and there may also have been small temperature and equivalence ratio inhomogeneities in the cylinder.

3.6. Chemical mechanism analysis

A sensitivity analysis can be used to determine the chemical reactions that have the most significant impact on the behaviour seen in the results of the experiments in this work. This was carried out at with ignition delay calculations using the Fang et al. mechanism [19] at 740 K and 32 bar—conditions where the pressure-temperature trajectories of the $T_{in} = 60$ °C cases traversed. The twelve most sensitive reactions are shown in Fig. 14. A positive sensitivity coefficient corresponds to an increased reaction rate causing the ignition delay time to increase, which is not conducive to LTHR. Meanwhile, a negative sensitivity coefficient means that increasing reaction rate leads to a shorter wait for the 50 K rise, hence the reaction would promote the occurrence of LTHR.

By looking at these reactions, they can be categorised into two groups based on the behaviour they contribute to: competition for the CH_3O radical and NO influence on low temperature oxidation reactions. Each of these groups is then considered.

3.6.1. Competition for CH_3O

Three of the reactions in Fig. 14 do not directly involve large iso-octane-based radicals and instead directly compete with each other for the CH_3O radical. The first of these, reaction R3 (4th from the top) involves the seeded nitric oxide and has a positive sensitivity coefficient. Its product, CH_3ONO can only be consumed by reacting it with an OH radical (which are in high demand in the low temperature oxidation process) to produce a relatively unreactive methanol [19]. Hence occurrence of this reaction reduces the OH radical pool. It also directly competes with reactions R4 and R5 (7th and 10th in Fig. 14), which have negative sensitivity coefficients as a result. Furthermore, reaction R4 produces a HO_2 radical, which aids low temperature oxidation of iso-octane, hence its more negative sensitivity coefficient compared to reaction R5.

$$CH_3O + NO\,(+M) \Longleftrightarrow CH_3ONO\,(+M) \quad \text{(R3)}$$

$$CH_3O + O_2 \Longleftrightarrow CH_2O + HO_2 \quad \text{(R4)}$$

$$CH_3O\,(+M) \Longleftrightarrow CH_2O + H\,(+M) \quad \text{(R5)}$$

In effect, the NO that was introduced is competing with O_2 for CH_3O to favour a reaction that ultimately inhibits LTHR rather than promoting it.

3.6.2. Effect of NO on low temperature oxidation reactions

The remaining significant reactions centre around the reaction R2, and the influence of the reaction site on the reaction and its subsequent effects. In general, the presence of NO steers the iso-octane intermediates away from the usual chain branching reactions that occur in absence of any NO.

The first reaction in this process is hydrogen abstraction of iso-octane by hydroxyl radical to form iso-octanyl radical plus water, reaction R6. The hydrogen abstraction site is denoted by x, which represents the number of the carbon along iso-octane's carbon chain.

$$iC_8H_{18} + OH \Longleftrightarrow xC_8H_{17} + H_2O \quad \text{(R6)}$$

It appears in Fig. 14 as the 1st, 6th, and bottom two reactions in the format IC8+OH=IC8-xR+H2O. This reaction class is significant because it is the first step of low-temperature oxidation of iso-octane,

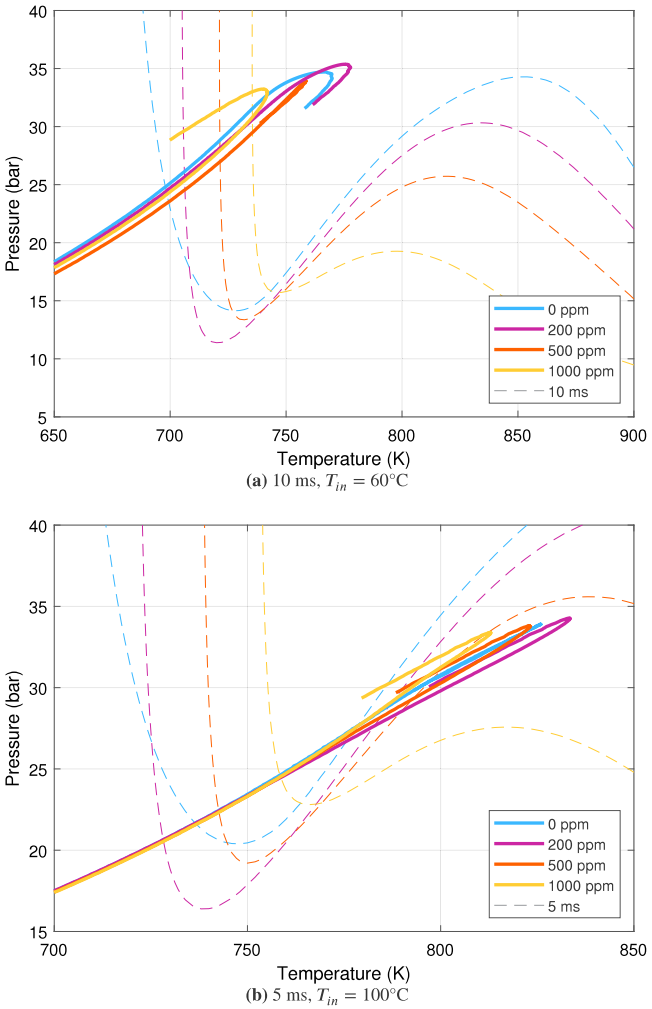

(a) 10 ms, $T_{in} = 60°C$

(b) 5 ms, $T_{in} = 100°C$

Fig. 12. Lines of constant ignition delay.

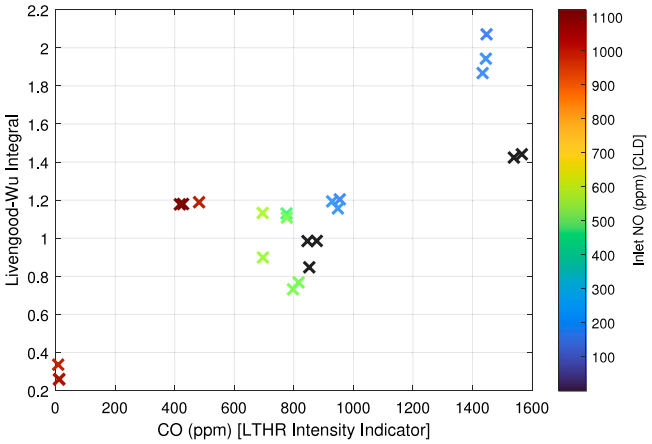

Fig. 13. Experimental Ignition delay progress, as calculated by the Livengood-Wu integral between IVC and EVO, plotted against exhaust CO concentration. Inlet NO concentration for each test point is indicated by the colour scale. (For interpretation of the references to colour in this figure legend, the reader is referred to the web version of this article.)

and specifically because the four different abstraction reactions (for the four distinct carbons from which hydrogen can be abstracted) compete and have different consequences. With increasing NO concentration, the sensitivity for three reactions (1,3 and 5 carbon) become more positive. The opposite occurs for carbon 4 for the reasons outlined below.

The next step in the low temperature oxidation process is the first addition of O_2 to the iso-octanyl radical to create an iso-octylperoxy radical. Ordinarily (i.e. without NO present), the third step would be iso-octylperoxy radical isomerisation, which subsequently leads to a second O_2 addition and then finally the low temperature chain branching reactions that result in LTHR. However, with NO present, a different reaction can occur: oxygen abstraction from the iso-octylperoxy radical by NO to create iso-octane alkoxy radicals and NO_2 (reaction R7, 3rd 8th and 9th in Fig. 14); this is a subset of reaction type R2 discussed in the introduction:

$$xC_8H_{17}O_2 + NO \iff xC_8H_{17}O + NO_2 \quad \text{(R7)}$$

These reactions directly compete with the alkyl peroxy radical isomerisation, steering the pathway away from low temperature chain branching—hence the three reactions that appear in Fig. 14 all have positive sensitivity coefficients when NO is present.

When reacted with NO, the $x = 1$, $x = 3$ and $x = 5$ isomers of the iso-octane alkoxy radical subsequently undergo beta scission, and the products of all three reactions do not lead to low temperature chain branching reactions, hence why the sensitivity coefficients for the hydrogen abstraction reactions (R6) become increasingly positive with increasing NO concentration.

The same cannot be said for the $x = 4$ isomer, whose beta scission product—a neopentyl radical, can still undergo a low temperature chain branching reaction that yields two OH radicals from one OH radical [46,47]. Hence two reactions from the low temperature oxidation of neopentane appear in Fig. 14: reactions R8 and R9. Since OH radicals are critical in the low temperature oxidation of iso-octane, the net effect is that the $x = 4$ pathway slightly promotes LTHR—and the reactions associated with that pathway have a negative sensitivity coefficient in the presence of NO. Most notably, the $x = 4$ hydrogen abstraction from iso-octane reaction has a sensitivity coefficient that becomes strongly negative with increasing NO concentration; this is due to the competition between the four carbon sites for the hydrogen abstraction to occur (and the subsequent reaction pathways that they lead to).

$$neoC_5ket \iff neoC_5ketox + OH \quad \text{(R8)}$$

$$neoC_5H_{10}OOH + O_2 \iff neoC_5H_{10}OOH{-}O_2 \quad \text{(R9)}$$

Finally, it is worth noting that reaction R1 did not appear to be a significant reaction, according to the sensitivity analysis. This is likely due to the lack of HO_2 radicals caused by the inhibiting effects of the other reactions discussed above [19].

4. Conclusions

In this work, a motored engine was used to collect experimental data on the effect of nitric oxide (NO) on the isolated low temperature heat release (LTHR) behaviour (as indicated by exhaust CO concentration) of iso-octane (2,2,4-Trimethylpentane)-air mixtures at different inlet temperatures. Three chemical kinetic mechanisms were simulated in an HCCI engine to determine their ability to reproduce experimental trends. The experimental results were analysed alongside ignition delay simulations and a sensitivity analysis, modelled using a recently developed mechanism [19].

The results show that:

- Contrary to modelling predictions in the literature, introducing moderate to high concentrations of nitric oxide into iso-octane and air mixtures almost always strongly reduced LTHR intensity, and in one case prevented it entirely at the conditions tested in this work.

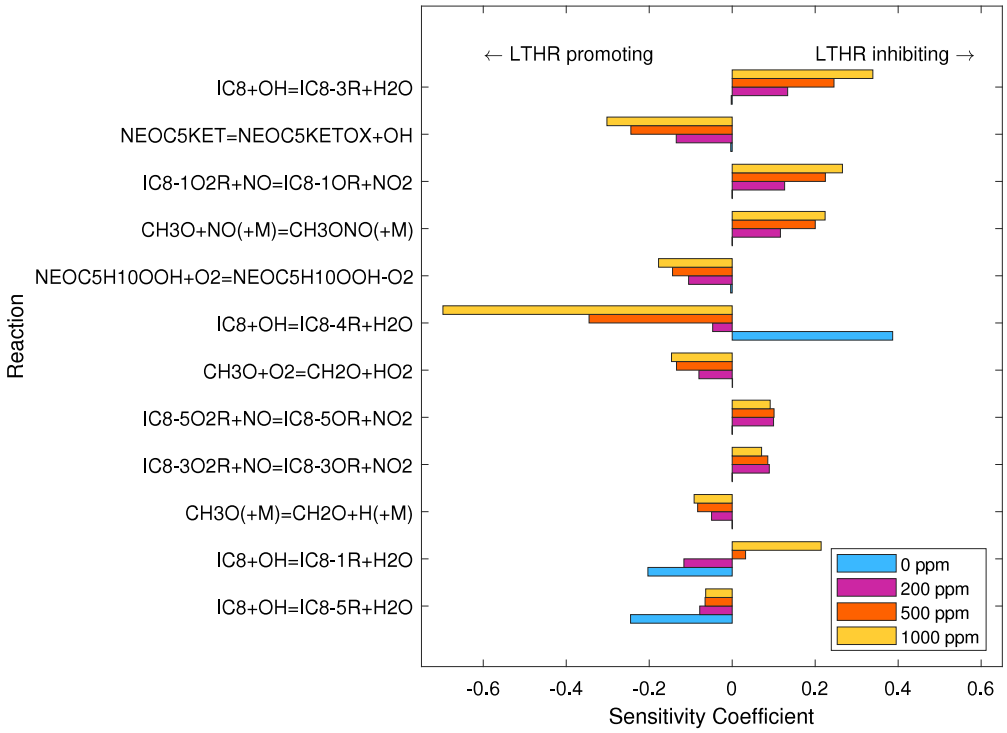

Fig. 14. Sensitivity coefficients for the sensitivity of ignition delay time (by 50 K rise) to reactions in the chemical kinetics mechanism that was used to simulate the four iso-octane/air/NO mixtures in a constant volume reactor with $T_0 = 740$ °C and $P_0 = 32$ bar.

- Exhaust NO and NO_2 concentrations showed strong conversion of NO to NO_2 whilst LTHR was being reduced but not totally inhibited. This conversion reduced back to near motoring levels when LTHR was entirely inhibited.
- Moderate levels of NO advance LTHR phasing but high levels of NO substantially retard LTHR phasing, due to the close link between LTHR phasing and LTHR intensity.
- Many gasoline surrogate mechanisms do not correctly predict the trends observed in the experimental data, instead predicting that NO promotes LTHR. These incorrect predictions stem from the mechanism not modelling the inhibiting behaviour of NO seen at low temperatures. Inaccurately modelling LTHR has ramifications for the whole engine cycle due to the effect LTHR can have on mixture composition and autoignition chemistry. However, at other engine operating conditions (specifically NO concentration and temperature), beyond those tested in this work, the models do still suggest trends different to that observed in this work. This would need to be verified with experiments at those conditions.
- The observed LTHR behaviour can be explained by examining pressure-temperature trajectories on ignition delay contours. The shape of these contours are strongly affected by modifying the concentration of seeded nitric oxide.
- LTHR inhibiting effects are observed overall, despite mixtures surpassing the critical temperature where NO promotes LTHR—only a detailed ignition delay analysis can be used to fully explain engine cases.
- The Livengood-Wu integral was shown to be a good predictor of LTHR occurrence for all NO concentrations.
- A sensitivity analysis showed that, at the conditions tested, nitric oxide primarily affects LTHR chemistry through oxygen abstraction from the iso-octylperoxy radical by NO to create iso-octane alkoxy radicals—steering the reaction pathway away from low temperature chain branching, and through competition with O_2 for CH_3O radicals causing a knock-on reduction in OH radical production.
- With sufficient NO concentrations present, low-temperature chain branching reactions can be almost entirely halted, preventing LTHR from occurring.

Nomenclature

ACI	Advanced compression ignition
°CA	Crank angle degrees
CA50	CA location at 50% heat release point
CO	Carbon monoxide
EGR	Exhaust gas recirculation
EVC	Exhaust valve closing
EVO	Exhaust valve opening
HCCI	Homogenous charge compression ignition
HTHR	High temperature heat release
IVC	Intake valve closing
IVO	Intake valve opening
k	Chemical reaction rate
LTHR	Low temperature heat release
LW	Livengood-Wu progress integral
NO	Nitric oxide
NTC	Negative temperature coefficient
P	Pressure
PSHR	Pre-spark heat release
S	Sensitivity coefficient
SI	Spark ignition
T	Temperature
TDC	Top dead centre
ϕ	Fuel-air equivalence ratio
τ	Ignition delay time

CRediT authorship contribution statement

Samuel P. White: Writing – original draft, Methodology, Formal analysis, Data curation, Conceptualization. **Abdullah U. Bajwa:** Writing – review & editing, Methodology, Investigation, Data curation. **Felix C.P. Leach:** Writing – review & editing, Methodology, Investigation, Funding acquisition, Formal analysis, Conceptualization.

Declaration of competing interest

The authors declare that they have no known competing financial interests or personal relationships that could have appeared to influence the work reported in this paper.

Acknowledgements

This research was supported by an Engineering and Physical Sciences Research Council Prosperity Partnership, grant number EP/T005327/1. For the purpose of Open Access, the authors have applied a CC BY public copyright license to any Author Accepted Manuscript (AAM) version arising from this submission. The Prosperity Partnership is a collaboration between JLR, Siemens Digital Industries Software, the University of Bath, and the University of Oxford. The authors would like to thank the Dept. of Engineering Science technicians and maintenance teams for facilities support.

References

[1] M.U. Waqas, A. Hoth, C.P. Kolodziej, T. Rockstroh, J.P. Gonzalez, B. Johansson, Detection of low temperature heat release (LTHR) in the standard cooperative fuel research (CFR) engine in both SI and HCCI combustion modes, Fuel 256 (2019) 115745.

[2] J.P. Szybist, D.A. Splitter, Pressure and temperature effects on fuels with varying octane sensitivity at high load in SI engines, Combust. Flame 177 (2017) 49–66.

[3] G. Kalghatgi, Fuel/Engine Interactions, SAE International, 2013.

[4] K. Rönn, A. Swarts, V. Kalaskar, T. Alger, R. Tripathi, J. Keskiväli, O. Kaario, A. Santasalo-Aarnio, R. Reitz, M. Larmi, Low-speed pre-ignition and super-knock in boosted spark-ignition engines: A review, Prog. Energy Combust. Sci. (2023).

[5] W.R. Leppard, The chemical origin of fuel octane sensitivity, 902137, SAE International, 1990,

[6] K. Senecal, F.C.P. Leach, Racing Toward Zero: The Untold Story of Driving Green, SAE International, 2021.

[7] A. Iijima, M. Tanabe, K. Yoshida, H. Shoji, N. Itoh, A. Terashima, T. Tojo, Visualization and spectroscopic measurement of knocking combustion accompanied by cylinder pressure oscillations in an HCCI engine, SAE Int. J. Engines 6 (4) (2013) 2150–2163.

[8] D.A. Splitter, A. Gilliam, J. Szybist, J. Ghandhi, Effects of pre-spark heat release on engine knock limit, Proc. Combust. Inst. 37 (2019) 4893–4900.

[9] D.L. Pintor, J.E. Dec, G.R. Gentz, Φ-Sensitivity for ltgc engines: understanding the fundamentals and tailoring fuel blends to maximize this property, SAE Tech. Pap. (2019) 2019-01-0961.

[10] A.U. Bajwa, F.C.P. Leach, M.H. Davy, Prospects of controlled auto-ignition based thermal propulsion units for modern gasoline vehicles, Energies 16 (9) (2023).

[11] V. Kalaskar, D. Kang, A.L. Boehman, Impact of fuel composition and intake pressure on lean autoignition of surrogate gasoline fuels in a CFR engine, Energy Fuels 31 (2017) 11315–11327.

[12] A.L. Boehman, J. Luecke, L. Fouts, M. Ratcliff, B.T. Zigler, R.L. McCormick, Ignition delay measurements of four component model gasolines exploring the impacts of biofuels and aromatics, Proc. Combust. Inst. 38 (2021) 5549–5555.

[13] D. Peng, Q. Chengken, C. Zheng, Effects of initial temperature on autoignition and detonation development in dimethyl ether/air mixtures with temperature gradient, Proc. Combust. Inst. 36 (3) (2017) 3643–3650.

[14] J.B. Heywood, Internal Combustion Engine Fundamental, McGraw-Hill, 1988.

[15] B.A. Eraqi, S.S. Nagaraja, E.-t. Es-sebbar, S.M. Sarathy, Spray ignition of n-alkanes in diesel and jet fuels: Effects of temperature, pressure, and N2 and NO addition, Fuel 355 (2024) 129430.

[16] N. Ladommatos, S. Abdelhalim, H. Zhao, The effects of exhaust gas recirculation on diesel combustion and emissions, Int. J. Engine Res. 1 (1) (2000) 107–126.

[17] M. Sjöberg, J.E. Dec, A. Babajimopoulos, D. Assanis, Comparing enhanced natural thermal stratification against retarded combustion phasing for smoothing of HCCI heat-release rates, SAE Int. J. Engines 113 (2004) 1557–1575.

[18] G. Moréac, P. Dagaut, J. Roesler, M. Cathonnet, Nitric oxide interactions with hydrocarbon oxidation in a jet-stirred reactor at 10 atm, Combust. Flame 145 (3) (2006) 512–520.

[19] R. Fang, C. Saggese, S.W. Wagnon, A.B. Sahu, H.J. Curran, W.J. Pitz, C.-J. Sung, Effect of nitric oxide and exhaust gases on gasoline surrogate autoignition: Iso-octane experiments and modeling, Combust. Flame 236 (2022) 111807.

[20] Y. Song, Y. He, Y. Yu, B. Moreau, F. Foucher, Effect of exhaust gas recirculation and NO on ignition delay times of iso-octane in a rapid compression machine, Energ Fuel 34 (7) (2020) 8788–8795.

[21] F.L.D. Toshiji Am Ano, Effect of dimethyl ether, NOx, and ethane on CH4 oxidation: High pressure, intermediate-temperature experiments and modeling, Symp. (Int.) Combust. 27 (1) (1998) 397–404.

[22] D.A. DelVescovo, D.A. Splitter, J.P. Szybist, G.S. Jatana, Modeling pre-spark heat release and low temperature chemistry of iso-octane in a boosted spark-ignition engine, Combust. Flame 212 (2020) 39–52.

[23] F. Contino, F. Foucher, P. Dagaut, T. Lucchini, G. D'Errico, C. Mounaïm-Rousselle, Experimental and numerical analysis of nitric oxide effect on the ignition of iso-octane in a single cylinder HCCI engine, Combust. Flame 160 (8) (2013) 1476–1483.

[24] W. Tang, Y. Zhai, Q. Wang, C. Shao, I. Gorbatenko, S. Gail, A. Nicolle, S.M. Sarathy, An experimental and kinetic modeling study of the impact of nitric oxide and hydrogen on iso-Octane combustion, Combust. Flame 260 (2024) 113196.

[25] X. Yu, S. Yu, M. Zheng, Hydrocarbon impact on NO to NO_2 conversion in a compression ignition engine under low-temperature combustion, Int. J. Engine Res. 20 (2) (2019) 216–225.

[26] P. Roberts, C. Sheppard, The influence of residual gas NO content on knock onset of iso-octane, PRF, TRF and ULG mixtures in SI engines, SAE Int. J. Engines 6 (4) (2013) 2028–2043.

[27] J.-B. Masurier, F. Foucher, G. Dayma, P. Dagaut, Investigation of iso-octane combustion in a homogeneous charge compression ignition engine seeded by ozone, nitric oxide and nitrogen dioxide, Proc. Combust. Inst. 35 (3) (2015) 3125–3132.

[28] Z. Chen, H. Yuan, T.M. Foong, Y. Yang, M. Brear, The impact of nitric oxide on knock in the octane rating engine, Fuel 235 (2019) 495–503.

[29] A.A. El-Sabor Mohamed, A.B. Sahu, S. Panigrahy, M. Baigmohammadi, G. Bourque, H. Curran, The effect of the addition of nitrogen oxides on the oxidation of propane: An experimental and modeling study, Combust. Flame 245 (2022) 112306.

[30] B.M. Sturgis, Some concepts of knock and antiknock action, SAE Tech. Pap. (1955) 550149.

[31] J.P. Szybist, A.L. Boehman, D.C. Haworth, H. Koga, Premixed ignition behavior of alternative diesel fuel-relevant compounds in a motored engine experiment, Combust. Flame 149 (2007) 112–128.

[32] S.P. White, A.U. Bajwa, F.C.P. Leach, Isolated low temperature heat release in spark ignition engines, SAE Int. J.-Adv. Mobil. 6 (2) (2023) 827–840.

[33] A.U. Bajwa, S.P. White, F.C.P. Leach, Low temperature heat release and phi-sensitivity characteristics of iso-octane/air mixtures, Combust. Sci. Technol. 197 (2) (2025) 440–462.

[34] H. Li, D. Miller, N. Cernansky, A study on the application of a reduced chemical reaction model to motored engines for heat release prediction, SAE Tech. Pap. (1992) 922328.

[35] J.P. Szybist, B.G. Bunting, Cetane number and engine speed effects on diesel hcci performance and emissions, SAE Tech. Pap. (2005) 2005-01-3723.

[36] S. Ren, S.L. Kokjohn, Z. Wang, H. Liu, B. Wang, J. Wang, A multi-component wide distillation fuel (covering gasoline, jet fuel and diesel fuel) mechanism for combustion and PAH prediction, Fuel 208 (2017) 447–468.

[37] S. Dong, S.W. Wagnon, L. Pratali Maffei, G. Kukkadapu, A. Nobili, Q. Mao, M. Pelucchi, L. Cai, K. Zhang, M. Raju, T. Chatterjee, W.J. Pitz, T. Faravelli, H. Pitsch, P.K. Senecal, H.J. Curran, A new detailed kinetic model for surrogate fuels: C3mechv3.3, Appl. Energy Combust. Sci. 9 (2022) 100043.

[38] J. Livengood, P. Wu, Correlation of autoignition phenomena in internal combustion engines and rapid compression machines, Symp. (Int.) Combust. 5 (1) (1955) 347–356.

[39] U. Burke, W.K. Metcalfe, S.M. Burke, K.A. Heufer, P. Dagaut, H.J. Curran, A detailed chemical kinetic modeling, ignition delay time and jet-stirred reactor study of methanol oxidation, Combust. Flame 165 (2016) 125–136.

[40] B. Weber, High Pressure Ignition Chemistry of Alternative Fuels (Ph.D. thesis), University of Connecticut, 2014.

[41] F. Leach, V. Shankar, M. Davy, M. Peckham, The influence of cycle-to-cycle hydrocarbon emissions on cyclic NO:No2 ratio from a HSDI diesel engine, J. Eng. Gas Turbines Power 143 (9) (2021) 091016.

[42] B. Krutzsch, G. Wenninger, M. Weibel, P. Stapf, et al., Reduction of NOx in Lean Exhaust by Selective NOx-Recirculation (SNR-Technique) Part I: System and Decomposition Process, SAE Tech P 982592, 1998.

[43] E. Chaize, D. Webster, B. Krutzsch, G. Wenninger, et al., Reduction of NOx in Lean Exhaust by Selective NOx-Recirculation (SNR-Technique) Part I: System and Decomposition Process, SAE Tech P 982593, 1998.

[44] S.P. White, A.U. Bajwa, F.C.P. Leach, Effect of ethanol and iso-octane blends on isolated low temperature heat release in a spark ignition engine, SAE Int. J.-Fuels Lubr. 17 (3) (2024) 243–260.

[45] H. Zhao, L. Wu, C. Patrick, Z. Zhang, Y. Rezgui, X. Yang, G. Wysocki, Y. Ju, Studies of low temperature oxidation of n-pentane with nitric oxide addition in a jet stirred reactor, Combust. Flame 197 (2018) 78–87.

[46] S. Wang, D.L. Miller, N.P. Cernansky, H.J. Curran, W.J. Pitz, C.K. Westbrook, A flow reactor study of neopentane oxidation at 8 atmospheres: Experiments and modeling, Combust. Flame 118 (3) (1999) 415–430.

[47] H.J. Curran, P. Gaffuri, W.J. Pitz, C.K. Westbrook, A comprehensive modeling study of iso-octane oxidation, Combust. Flame 129 (3) (2002) 253–280.

Statement of Authorship for joint/multi-authored papers for PGR thesis

To appear at the end of each thesis chapter submitted as an article/paper

The statement shall describe the candidate's and co-authors' independent research contributions in the thesis publications. For each publication there should exist a complete statement that is to be filled out and signed by the candidate and supervisor **(only required where there isn't already a statement of contribution within the paper itself).**

Title of Paper	Effects of nitric oxide on isolated low temperature heat release in spark ignition engines
Publication Status	Submitted for Publication
Publication Details	White, S. P., Bajwa, A. U. & Leach, F. C. P. Effects of nitric oxide on isolated low temperature heat release in spark ignition engines. Submitted for Publication (2024)

Student Confirmation

Student Name:	Samuel P. White		
Contribution to the Paper	• Idea • Experimental design • Implementation (joint effort for experimental setup, solo effort for computational work) • Data analysis (all) • Writing (joint effort for introduction and methodology, solo effort for the rest of the manuscript) • Editing		
Signature 		Date	12 April, 2024

Supervisor Confirmation

By signing the Statement of Authorship, you are certifying that the candidate made a substantial contribution to the publication, and that the description described above is accurate.

Supervisor name and title: Felix Leach, Associate Professor of Engineering Science		
Supervisor comments I agree with Sam's comments.		
	Date	12-4-24

This completed form should be included in the thesis, at the end of the relevant chapter.

Chapter Summary

Ethanol was shown to actively inhibit LTHR from PRFs in Section 3.1, and the underlying cause of this was showed by further study in Section 3.2, where a sensitivity analysis revealed the effect of ethanol on OH radicals, which in turn affects the initiation of low temperature oxidation of PRF components. The effect of residuals was first examined in Section 3.1 where it was suggested that the presence of residuals could inhibit LTHR. This effect was examined in great depth in Section 3.3 where nitric oxide was shown to have a strong inhibiting effect on LTHR.

The findings from this chapter, and Chapter 2 enable the progression to finding alternative methods for observing LTHR in engines without having to rely on cylinder pressure measurements or exhaust gas measurements from isolated LTHR—as targeted in the objectives of this thesis (Section 1.4.1). The learnings surrounding pressure, temperature, speed, equivalence ratio and fuel blend effects provide a relatively large number of parameters that can each be varied to curate isolated LTHR across a wide range of engine conditions. Furthermore, the FTIR measurements in Section 3.1 inform the options in terms of chemical indicators to look for when trying to track LTHR.

Chapter 4

Planar Laser-Induced Fluorescence Imaging of Low Temperature Heat Release

4.1 Observing Simultaneous Low Temperature Heat Release and Deflagration in a Spark Ignition Engine Using Formaldehyde Planar Laser Induced Fluorescence

This final chapter revolves around the second overarching aim of this thesis—to develop a new technique, that does not rely on pressure-derived apparent heat release measurements, to observe LTHR in SI engines—then apply it to a fired engine where LTHR is likely but currently is unobservable with current techniques (Section 1.4.1). The findings from the two previous chapters helped inform the choice of fuel and inlet conditions for these experiments, aiming to maximise LTHR intensity and minimise the risk of knocking for the fired tests. Furthermore, results in Section 3.1 provided confidence that formaldehyde would be present in high enough quantities to design a methodology around its detection using optical methods.

Contributions

- The planar laser-induced fluorescence signal intensity is compared to LTHR intensity of a cycle-by-cycle basis.
- Planar laser-induced fluorescence of formaldehyde is used to track LTHR progression within a cycle.
- Demonstration of simultaneous volumetric low temperature heat release and deflagration in a spark ignition for the first time engine when other methods (i.e. pressure-derived heat release analysis) are unable to observe LTHR.

Applications in Energy and Combustion Science 21 (2025) 100321

Contents lists available at ScienceDirect

Applications in Energy and Combustion Science

journal homepage: www.elsevier.com/locate/jaecs

Observing simultaneous low temperature heat release and deflagration in a spark ignition engine using formaldehyde planar laser induced fluorescence

Samuel P. White, Christopher Willman, Felix C.P. Leach *

Department of Engineering Science, Parks Road, Oxford, OX1 3PJ, UK

ARTICLE INFO

Keywords:
PLIF
Formaldehyde
LTHR
PRF

ABSTRACT

Low temperature heat release (LTHR) and its underlying chemistry is of particular interest for its potential to mitigate knock in spark ignition (SI) engines and enable advanced combustion strategies that rely on end gas autoignition. It has been proposed that, in SI engines, LTHR can occur volumetrically in the end gas, after ignition, whilst deflagration occurs elsewhere in the cylinder, however, current pressure-based heat release metering techniques are unable to distinguish such LTHR from high temperature heat release (HTHR) due to the overlapping pressure rise characteristics. Planar laser-induced fluorescence (PLIF) of formaldehyde, a known product of LTHR which is consumed during HTHR, offers an opportunity to detect end gas LTHR simultaneously with deflagration but is challenging to implement, as end gas is often located closer to cylinder walls and away from typical optically accessible locations. An optically accessible SI engine was used to show formaldehyde PLIF signal intensity under motored conditions is well correlated to cumulative LTHR intensity, using a recent method to isolate LTHR in SI engine conditions. An alternative ignition method using four side-mounted spark plugs was implemented to generate end gas close to the cylinder axis. This enabled measurement of LTHR within the end gas during the deflagration process of a SI engine, demonstrating the utility of formaldehyde PLIF to optically measure LTHR under conditions where pressure-based diagnostics cannot isolate the contribution of LTHR.

1. Introduction

The overall CO_2 emissions of light-duty vehicles can be reduced by increasing internal combustion engine efficiency and using fuels and fuel sources that are less carbon-intensive [1]. Knocking, unwanted and uncontrolled autoignition of end gas (the portion of the fuel-air mixture ahead of the flame), is one of the main factors limiting engine operation and efficiency [2]. The high-frequency, high-pressure oscillations associated with the occurrence of knock can cause significant damage to many different engine components, hence it must be avoided. Knocking can occur when the pressure and temperature of the end gas spend enough time above a certain threshold, leading to spontaneous autoignition [3]. The specific delay time, pressure and temperature at which autoignition occurs depends on the composition of the mixture and therefore the choice of fuel and any intermediate reactions that have occurred in the meantime.

Leppard showed that, for alkane fuels, the autoignition chemistry is dominated by negative temperature coefficient (NTC) behaviour [4]. This is where, at certain conditions, the reaction rate is inversely proportional to temperature. This leads to two distinct stages of the ignition process. Low temperature heat release (LTHR) is followed by the NTC region (characterised by a pause in heat release) and subsequently, high temperature heat release (HTHR), where knocking can occur. Since then, LTHR has been observed in homogeneous charge compression ignition (HCCI) engines [5–7].

The low temperature reaction pathways that cause LTHR in the two primary reference fuels (PRFs), iso-octane and n-heptane, were examined in depth by Curran in comprehensive modelling studies [8, 9]. At low temperatures the PRFs first undergo hydrogen abstraction by OH, then two additions of O_2 and isomerisation reactions to form carbonylhydroperoxide species, which subsequently undergo low temperature chain branching, producing OH radicals. Alongside this, beta-decomposition of the various intermediate species leads to the formation of significant amounts of formaldehyde.

More recently, LTHR has been shown in SI engines, [10–12] where it is seen before the spark and hence termed pre-spark heat release (PSHR). Szybist and Splitter observed that PSHR was more likely to be seen in fuels with low octane sensitivity and at high load conditions with elevated inlet temperatures. Furthermore, Splitter et al. used elevated intake temperatures to show PSHR is related to knocking

* Corresponding author.
E-mail address: felix.leach@eng.ox.ac.uk (F.C.P. Leach).

https://doi.org/10.1016/j.jaecs.2025.100321
Received 25 September 2024; Received in revised form 17 December 2024; Accepted 15 January 2025
Available online 22 January 2025

chemistry [13]. They found that when PSHR occurred, the knock-limited combustion phasing was insensitive to intake temperature, with higher intake temperatures not requiring retarded ignition timings as they otherwise would. The occurrence of LTHR (as PSHR) caused the end gas to move into a thermodynamic state with a long ignition delay, which inhibited knock.

In SI engines (and unlike in HCCI engines), HTHR combustion occurs as a pre-mixed flame deflagration process which need not necessarily be preceded by the low-temperature pathways that exhibit LTHR, however, if it is, the chemical and thermodynamic properties of the end gas will have changed—changing the autoignition properties, including knocking. Hence, if LTHR can be understood better — and ultimately controlled — it has the potential to increase engine efficiency by extending the knocking limit [13] or by enabling high-efficiency advanced combustion strategies that involve spark-triggered flame propagation causing auto-ignition without triggering engine knock [14–17]. These advanced combustion strategies rely on curating specific chemical conditions in the end gas [18].

Splitter et al. used ignition delay analysis in a PSHR study to show that it is possible that, for some conditions that do not exhibit PSHR, as deflagration occurs the end gas region will traverse the same region in pressure-temperature space as cases that do exhibit PSHR, suggesting that bulk gas LTHR reactions in the end gas is probable [13]. Since these reactions change the species composition ahead of the flame, understanding them could be critical for understanding knocking behaviour in SI engines. However, as these authors highlighted, conventional pressure-based heat release analysis techniques are unable to experimentally observe end gas LTHR as its contribution to pressure rise would be indistinguishable from that of the heat released from deflagration. The aim of this work is to use alternatives to pressure-based diagnostic techniques to determine whether LTHR can occur in end gas at the same time as deflagration (elsewhere in the cylinder), for conditions with no observable PSHR. Hence an alternative method of experimentally observing LTHR must be determined.

Through past experimentation and work developing chemical kinetic mechanisms for the primary reference fuels, the reaction indicators and products of the low temperature oxidation pathways are relatively well known [8]. Indicators include the OH and HO_2 radicals and significant products include CO, H_2O_2, and CH_2O. The latter two are particularly significant as they are present in much larger quantities as products of first stage autoignition compared to as HTHR products [10,19], so have the potential to be used as markers for LTHR. Spatially and temporally resolved measurement of formaldehyde would therefore enable in-cylinder detection of the progression of LTHR processes within the end gas.

Optical diagnostic techniques enable gas-phase measurements within challenging environments, where measurements with physical sensors are either impossible or impractical [20–23].

For two-dimensional measurements, Laser-Induced Fluorescence (LIF) is widely used for species detection, using a laser sheet to excite the target species to a higher energy state and imaging the fluorescence emitted as the species returns to the ground state [24]. Selective detection of species is often achieved by utilising features in either the absorption or emission spectra of the target species, which allows multiple species to be detected simultaneously, such as OH, CH and formaldehyde, in flame reaction zone studies [25].

In the case of formaldehyde, absorption features around 355 nm overlap with the conveniently-accessible 3rd harmonic output of an Nd:YAG laser. While more efficient excitation is possible, targeting alternative excitation lines (e.g. 353.07 nm with a tuneable dye laser), the higher output energy of a tripled Nd:YAG typically more than compensates for the lower excitation efficiency [26,27] and allows for a simpler experimental setup.

Excitation of in-cylinder end gas at 355 nm may excite a range of LTHR products whose fluorescence cannot be distinguished from formaldehyde using broad spectral filters [28]. Multi-band filters can provide more selective detection of formaldehyde emission [29]; however, if the intention is to detect LTHR products, exact identification of the other fluorescing species is not necessary, only that they are generated during LTHR and consumed during HTHR [27]. This permits the use of LIF primarily targeting formaldehyde to investigate the end gas of SI engines to infer spatial temperature variations [30] and to identify sites of autoignition [31].

Formaldehyde LIF has been used to investigate the first stage of the ignition process in HCCI engines [27,32,33]. For PRF blends of iso-octane and n-heptane which exhibit NTC behaviour, LTHR in HCCI engines typically occurs earlier than, and distinct from, HTHR [34], enabling the use of either optical or pressure-based measurement techniques similarly to PSHR in SI engines [35]. Graf et al. used LIF to measure formaldehyde concentration in “cool-flame” (LTHR) events in an SI engine with PRF50 under HCCI conditions [36]. Their work is similar to this work in some ways, but measures LTHR prior to ignition with a centrally mounted spark plug. LTHR in end-gas is unobserved in their work.

LTHR processes continuing during deflagration has been observed using formaldehyde LIF in a Rapid Compression Machine (RCM) under Spark Induced Compression Ignition (SICI) conditions [37], however a significant pressure rise due to LTHR was observed before the main HTHR pressure rise, putting these SICI conditions in a similar regime to partially developed PSHR, which may also be measured using pressure-based methods [35].

This work uses formaldehyde LIF to demonstrate that LTHR occurring simultaneously with deflagration in an SI engine may be measured optically under conditions in which pressure-based measurement techniques cannot distinguish between the pressure rises associated with LTHR and HTHR processes.

Recent work by White et al. [38–40] and Bajwa et al. [41] introduced a methodology to isolate LTHR in a spark ignition engine by maintaining LTHR- and PSHR-prone inlet conditions whilst avoiding HTHR by disabling the ignition system. This can be used to test techniques for detecting LTHR with optical methods that observe non-pressure-based markers by comparing them to standard LTHR markers observed using the isolated methodology.

In this study, we seek to expand the understanding of the occurrence of LTHR in SI engines through the use of a formaldehyde LIF-based optical diagnostic method. 2D PLIF images will be analysed alongside measured apparent heat release rate and high-speed flame imaging to detect LTHR both in isolation and in end gas while deflagration is occurring elsewhere in the cylinder. LIF signals and LTHR measurements will be analysed to determine the efficacy of LIF as a diagnostic tool for observing LTHR in SI engines. In a fired engine, the ignition system is modified to produce central, optically accessible end gas, and formaldehyde PLIF is used to examine said central end gas during deflagration. The results of this study highlight the ability of non-pressure-derived diagnostic techniques to detect LTHR and subsequently answer the question of whether or not bulk gas LTHR reactions occur in the end gas concurrently with deflagration in SI engines.

2. Methodology

2.1. Experimental facility

Optical and pressure-based measurements of LTHR were performed in a single cylinder, optically accessible direct injection SI engine during motored and fired operation with two non-fluorescing fuels: n-heptane and a mixture of 15% (v/v) n-heptane and 85% 2,2,4-trimethylpentane (iso-octane) — PRF85. The specifications of the optically accessible engine are given in Table 1 and details of the instrumentation are supplied in Table 2.

Optical access to the engine (for imaging) was provided through a 60 mm central piston window. Considering the nature of this work — to image LTHR in the unburnt end gas — the last portion of the cylinder

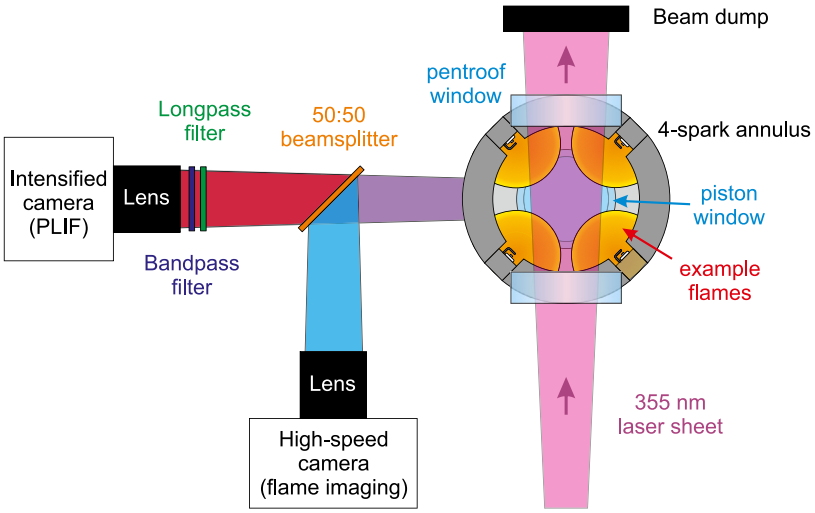

Fig. 1. Optical layout for formaldehyde PLIF and high-speed flame imaging. A 355 nm laser sheet passes through a pair of opposed pentroof windows. A 4-spark annulus ensures centrally-located end gas. The cylinder is imaged from below through a piston crown window, with a 50:50 beamsplitter enabling simultaneous PLIF and flame imaging with an intensified and high-speed camera respectively.

Table 1
Engine specifications.

Bore [mm]	85
Stroke [mm]	90
Fuel injection system	Direct injection
Injection pressure [bar]	200
Inlet valve actuation	Single valve (of two)
Dynamometer	DC, 40 kW

Table 2
Engine instrumentation.

Measured quantity	Sensor
Cylinder pressure	Kistler 6043A60
Barrel pressure	Kistler 4075A10 (with cooling adapter Kistler 7505B)
Inlet pressure	Kistler 4043A5
Manifold pressure	Druck PDCR 820-0800
Exhaust pressure	Kistler 4075A10 (with switching cooling adapter Kistler 7533A)
Air flow rate	Roots meter model 1.5 M125
Inlet temperature	Exposed junction K-type thermocouple
Engine speed	Leine and Linde crank encoder 632006911

to be reached by deflagration would be the central, optically accessible portion. In a typical ignition setup, where charge motion and spark plug placement are optimised for combustion speed and efficiency, the spark is usually centrally mounted, with the flame propagating out from the centre to the cylinder walls—this is incompatible with the objectives of this work. Hence an annulus with four simultaneously triggered spark plugs was designed, in order to produce four flame fronts that travel from the edges of the cylinder inwards. High levels of swirl motion were obtained by disabling the flywheel-side intake valve (Schaeffler UniAir Continuously-Variable Valve Train system) and this setup successfully produced central end gas.

The optical setup to perform PLIF measurements of the central end gas, simultaneously with high-speed imaging of the flame luminosity, is detailed in Fig. 1.

The 3rd harmonic (355 nm) of a 10 Hz, ns-pulse Nd:YAG laser (Continuum Surelite I-10), which had a fluence of 0.05 J/cm^2, was used in combination with sheet forming optics (Thorlabs LK1283L1-A, f = −40 mm cylindrical lens; Thorlabs LA4579-UV-ML, f = 300.0 mm spherical lens) to pass a laser sheet through opposing pentroof windows. This illuminated a horizontal plane within the engine, 3 mm above the firing deck, with approximate dimensions 30 mm × 50 mm × 1 mm, which were determined by using the sheet to illuminate a scale target. The pulse energy at 355 nm was 14 mJ.

A circular piston crown window and a 45-degree mirror within the Bowditch extended piston enabled both formaldehyde fluorescence from the PLIF measurement plane and light emission from the flame to be imaged from below. A 50:50 plate beamsplitter (Thorlabs BSW27) was used to direct light from the engine onto the two detection arms. The beamsplitter's wide range coating (350–1100 nm, as opposed to a typical visible coating range of 400–700 nm) was necessary to avoid ghosting on the flame luminosity images due to partial reflection of light above 800 nm from the rear surface of the beamsplitter.

One detection arm consisted of a high-speed camera (Phantom VEO 710L) using a Nikkor 105 mm lens at f/2.5 to image the flame luminosity at one frame per crank angle. The formaldehyde fluorescence was imaged in the other detection arm using a UV-compatible intensified camera (Andor iStar sCMOS 18U-E4, with a Nikkor 85 mm lens at f/2) which incorporates a WE-AGT photocathode and a fast-decay P46 phosphor (200 ns decay time to 10%), using an intensifier gate time of 1 μs. A bandpass filter (UQG optics CDB-5051) and a longpass filter (UQG optics FGG-39550) were used to transmit the formaldehyde fluorescence with >75% transmission between 400 nm and 470 nm onto the intensified camera, while blocking elastic scatter from the 355 nm excitation sheet with an effective optical density of >10^5.

During the preliminary testing with n-heptane, cylinder head features were visible on the PLIF images, having been illuminated by the fluorescence emission from the measurement plane. Image processing steps in Section 2.3.2 partially mitigated this effect for the n-heptane runs but for all subsequent datasets the cylinder head was painted black to minimise the intensity of these background features.

2.2. Operating conditions

To isolate LTHR, fuel was injected into the motored engine with the ignition system disabled and the inlet air heated, as described by White et al. [38]. Table 3 summarises the operating conditions for the three sets of tests. n-heptane was chosen for the initial motored tests because of its strong LTHR behaviour and hence maximised signal intensity. PRF85 was chosen for the fired tests to maximise LTHR intensity with its n-heptane content but minimise the possibility of engine knock with its relatively high octane rating. The fuels were injected early to give as homogeneous as possible a mixture at the point of LTHR, and previous work has shown that there is a near homogeneous mixture in this engine at this injection timing (albeit at a different operating

Table 3
Engine operating conditions.

Study	Cycle-based	Intra-cycle	Firing
Fuel	n-heptane	PRF85	
Inlet temperature (°C)	60, 100	120	
Ignition timing (°CA aTDC)	N/A		−30, −15
Injection timing (°CA aTDC)	−280		
Engine speed (rpm)	1180		
Equivalence ratio (ϕ)	0, 0.5	0.5	
Inlet pressure (kPa)	80		
Injection pressure (bar)	200		
Air mass flow rate (g/s)	2.75		

point) [42]. With PRF85, the inlet temperature was increased from 100 to 120 °C to account for its lower LTHR propensity. The engine speed was selected to synchronise with the LIF excitation laser's repetition rate of just under 10 Hz (9.83 Hz) — enabling the same crank angle to be imaged cycle-to-cycle. The laser and cameras were triggered from the engine crank at the desired crank angle. To maximise the runtime of the optical engine under fired conditions, the coolant temperature was set to 25 (°C).

The equivalence ratio of $\phi = 0.5$ was chosen to give the best chance of observing LTHR at engine conditions compatible with the optical engine. An equivalence ratio higher than 0.5 would have required increased cylinder pressures and temperatures that exceed the pressure limits of the engine with optical components fitted, but the LTHR behaviour observed in this work at $\phi = 0.5$ would be expected to generalise to higher equivalence ratios, including stoichiometric [35, 41].

As this engine is a direct injection engine, it should be noted that the direct injection causes charge cooling which in turn reduces temperatures and therefore LTHR intensity [41]. At lean equivalence ratios where LTHR was present, ignition was unstable, causing somewhat unreliable combustion that presented itself as alternating firing and misfiring cycles. While nominal fuel and air flow rates were maintained between motored and fired cases, the residuals in the chamber after a failed combustion event made the equivalence ratio of the subsequent cycle slightly richer but ultimately enabled the required sustained combustion within that cycle. Increasing the equivalence ratio in an attempt to reliably fire the engine every cycle was attempted but caused cylinder temperatures to be too low for LTHR to occur due to the additional charge cooling. When analysing the data, fired cycles were filtered and presented.

2.3. Data analysis

2.3.1. Engine data processing

Combustion analysis was performed during post-processing with a MATLAB-based procedure. Cylinder pressure was calibrated with concurrent barrel pressure measurements to avoid drift, and cylinder volume was calculated from the engine geometry. Apparent heat release rate (AHRR) was calculated on a per-cycle basis according to Stone [43]. A median filter was applied to each AHRR cycle before the mean trace was calculated to remove noise. To calculate cumulative heat release (also referred to as LTHR intensity), AHRR for unfuelled, motored, cases were subtracted to account for an approximation for most heat transfer effects.

2.3.2. Image processing

A calibration grid, placed in line with the laser plane, was imaged with all windows installed in the engine and used to transform and spatially calibrate the intensified camera images and high-speed flame images using MATLAB. For the n-heptane tests, the cylinder head was unpainted and strongly illuminated by scattered light and PLIF emission from the laser sheet region, leading to background cylinder head structure being clearly visible in the PLIF frames which could not be removed by subtraction of, for example, the mean image from a non-fuelled run without LTHR due to the PLIF-dependent contribution to the apparent background intensity. To mitigate this, individual PLIF frames (in Fig. 4) were divided by the mean illuminated image to minimise the visibility of the background cylinder head structure and partially correct for spatial variation in laser plane intensity. For the remainder of test points in this work, the cylinder head was painted black and this image correction via division did not need to be applied. Three regions, either could not be painted or were still highly reflective during the tests and were therefore masked out of the images presented in the results; these appear as an annulus around the centrally mounted spark (which was disabled), the area around the pressure transducer and an oval-shaped patch at around (−10, −10).

Regions of formaldehyde were detected in the PLIF images using a MATLAB procedure that applied a median filter, then applied morphological close and open filters to remove speckles and finally applied adaptive thresholding to create a binary image, with the threshold based on the overall brightness of the image. Adaptive thresholding was required due to the nature of scattering—the dark gaps in the plane that did not contain formaldehyde were brighter in bright cycles due to the omnidirectional nature of fluorescence and subsequent scatter. The same method was applied for flame detection without the need for adaptive thresholding. The flame images are presented in this work as flame history images, calculated by taking the maximum pixel intensity for each pixel for the range up to a specified crank angle. This was to ensure that early, bright flame regions that later become dark are taken into account when comparing them to the effects of the flames in the PLIF images.

PLIF signal intensity was calculated by using the above method to identify fluorescing pixels, then summing their intensity and dividing that sum by the number of fluorescing pixels to calculate the mean fluorescing pixel intensity. This was required so that the gaps caused by formaldehyde consumption did not affect indicated LTHR intensity. Shot-to-shot variation in laser intensity and laser sheet spatial inhomogeneity were not corrected for.

For the n-heptane data, the cameras were triggered before the output of the laser had fully stabilised. So, to correct for laser warm-up which manifested as an increase in PLIF intensity over time due to increasing laser pulse energy, a logarithmic curve was fitted to, and subsequently subtracted from, the intensity data. Then, a moving window correlation was calculated by finding the Pearson correlation coefficient, r, between the PLIF and LTHR intensity traces for each pair of cycles and their immediate neighbours.

3. Results and discussion

3.1. Cycle-based PLIF

3.1.1. Qualitative analysis

To qualitatively investigate the effect of LTHR on the PLIF signal, initial tests were carried out with n-heptane, using the isolated LTHR methodology [38] at two inlet temperatures—one where minimal LTHR would be expected and one where relatively high LTHR intensity is common. The apparent heat release rate traces are presented in Fig. 2 and mean PLIF signal images are presented in Fig. 3; baseline traces and images for cases with the injection turned off (i.e. unfuelled motored cases) are also presented, to help distinguish any non-LTHR related signal strength. Examining the baseline AHRR traces reveals them to be effectively identical. Since no fuel is present in these cases, the net heat release — which is negative — can be attributed solely to the effects of heat transfer from the compression-heated air to the walls at lower temperatures. The $T_{in} = 60$ °C case where fuel was injected still shows net negative heat release, though it is up to 0.25 J/°CA more positive than the unfuelled cases, suggesting that LTHR is likely to be occurring, but with very low intensity. Finally, the fuelled $T_{in} = 100$ °C case shows the clear isolated LTHR that has been observed in previous

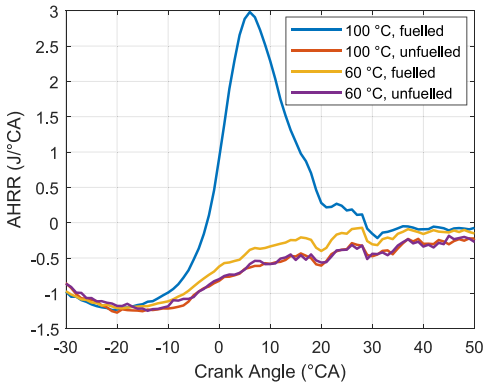

Fig. 2. Apparent heat release rate data for a fuelled and unfuelled engine, motored operation with n-heptane at two inlet temperatures.

studies [38]—with peak AHRR reaching 3 J/°CA.

The four PLIF images presented in Fig. 3 are mean averages of images from over 200 consecutive cycles for each test point; each individual image was taken at 20 °CA aTDC. Formaldehyde is known to be formed during LTHR [9], and under motored conditions, there is no cause for it to be consumed so formaldehyde accumulates in the cylinder until it exits through the exhaust valves. Hence, images captured at 20 °CA aTDC would be expected to show fluorescence from formaldehyde that has accumulated over the course of the cycle. The first thing to note is that the images for the unfuelled cases (i.e. "Injection Off") are not entirely dark — even where no laser sheet structure is present, the shape of the cylinder head can be distinguished. This non-zero PLIF signal may be attributed to background light of a similar wavelength (blue visible) to formaldehyde fluorescence, or to small amounts of fluorescence and subsequent scatter from contaminants such as gasket sealing compound within the pent roof window recesses.

Examining the mean image for the $T_{in} = 60$ °C case where fuel was injected reveals a slightly brighter signal, most evident in the enhanced visibility of the cylinder head structure; however, the structure of the laser sheet is still not present. The small increase in brightness relative to the unfuelled cases is consistent with Fig. 2 — there is likely very weak LTHR intensity that leads to the formation of relatively small, but non-zero, concentrations of formaldehyde at 20 °CA aTDC. The direct fluorescence is too weak to distinguish but has the effect of raising the overall brightness of the image. Finally, the image for the fuelled $T_{in} = 100$ °C case is significantly brighter than all other cases. Furthermore, the outline (and to some extent, the structure) of the laser sheet is apparent. This is consistent with the high LTHR intensity AHRR in Fig. 2. Due to scatter, and the fact that the cylinder head surface had not been painted black during these preliminary tests, the brightness in the raw PLIF images does not exclusively correlate with spatial formaldehyde concentration. Hence a strong overall illumination effect is observed for the whole cylinder. Nevertheless, the pair of figures serve as evidence that formaldehyde PLIF can be used to detect the presence of LTHR over averaged cycles—i.e. signal brightness is qualitatively correlated with LTHR.

3.1.2. Individual snapshots

16 individual example frames from the set of images that were used to make the $T_{in} = 100$ °C image in Fig. 3 are presented in Fig. 4. As described in Section 2.3.2, each snapshot image has been divided by the mean image to partially correct for both laser plane intensity and the contribution from the cylinder head structure. The spatially calibrated frames have been masked to isolate the laser sheet area and are presented in the order in which they were captured. Gas structure is apparent in many of the images, in particular cycle numbers 70, 100, 130 and 190, though some show almost no signs of it, for example, cycle numbers 110, 160 and 200. The cause of the gas-like structures is likely due to inhomogeneities within the temperature and species distributions of the turbulent in-cylinder flow. The hottest regions with the highest local reactivity will experience the most LTHR and produce the most formaldehyde—then, turbulent cylinder flows will transport this formaldehyde around the cylinder and LTHR continues to occur elsewhere. The clarity of these detailed structures within the PLIF images is characteristic of the planar nature of PLIF measurements, as opposed to line-of-sight integrated techniques such as natural light imaging. It is apparent on inspection of the chronologically ordered PLIF images that there is a trend for image brightness to increase over time (cycles). Rather than any gradual increase in LTHR intensity, this can be attributed to laser warm-up for this preliminary dataset. Laser warm-up effects were avoided in the subsequent datasets of Section 3.2 onwards.

3.1.3. Semi-quantitative analysis

Section 3.1.1 demonstrated a qualitative link between LTHR intensity and the brightness of the formaldehyde PLIF signal. The images and thermodynamic data captured at $T_{in} = 100$ °C can be further analysed to attempt to gain semi-quantitative insights into the relationship between the strength of the PLIF signal and the corresponding LTHR intensity.

The PLIF signal across each image (see Fig. 4) is first spatially averaged, then corrected for gradual laser warm-up by fitting a logarithmic trend to the spatially-averaged brightness vs. cycle number (time) of the set of over 200 PLIF signals for each run. This enables the relative brightness between adjacent cycles to be compared in order to investigate the correlation of PLIF signal intensity with LTHR intensity (note that these tests are isolated LTHR so there is no contribution from deflagration). Fig. 5 shows a representative subset of the min–max normalised cumulative heat release for each cycle, i.e. the LTHR intensity (the blue solid line), alongside the corrected PLIF signal intensity (the black dash-dotted line).

There is an apparent similarity between the two traces—as well as some clear differences. Direct comparison of the two measurements is non-trivial due to the inherent differences in spatial averaging between the whole-cylinder pressure-based technique and single-plane optical technique. However, it is reasonable to expect cycles with more LTHR to have a higher likelihood of having high concentrations of formaldehyde within the PLIF measurement plane, leading to brighter PLIF signals.

This potential relationship is assessed with a rolling correlation coefficient using a window size of three. This describes the local similarity in trends of LTHR and PLIF signal intensities for adjacent cycles (one cycle ahead and one behind). The background of Fig. 5 is coloured according to the calculated correlation coefficient for each cycle, highlighting the strong similarity between LTHR intensity and PLIF signal intensity for the majority of this data subset; as well as notable differences around cycles 39, 48 and 52.

The rolling correlation coefficients for all cycles are summarised in Fig. 6. Over 37% of the total are 0.9 or above and 77% are positive, suggesting that there is a positively correlated relationship between LTHR intensity and PLIF signal from formaldehyde within the measurement plane on a cycle-by-cycle basis.

This is particularly compelling, considering that the PLIF measurement plane represents a very small portion of the cylinder volume (2% at 20 °CA aTDC), the formaldehyde distribution is not homogeneous (as seen in gas structure frames in Fig. 4), and PLIF signal intensity is not expected to be linear with LTHR.

3.2. Ensemble-averaged intra-cycle PLIF

The principal aim of this work is to demonstrate the use of PLIF to detect, and track the progress of LTHR for application in conditions where a pressure-derived method of LTHR tracking cannot be applied. Hence it is necessary to determine whether PLIF signal intensity can

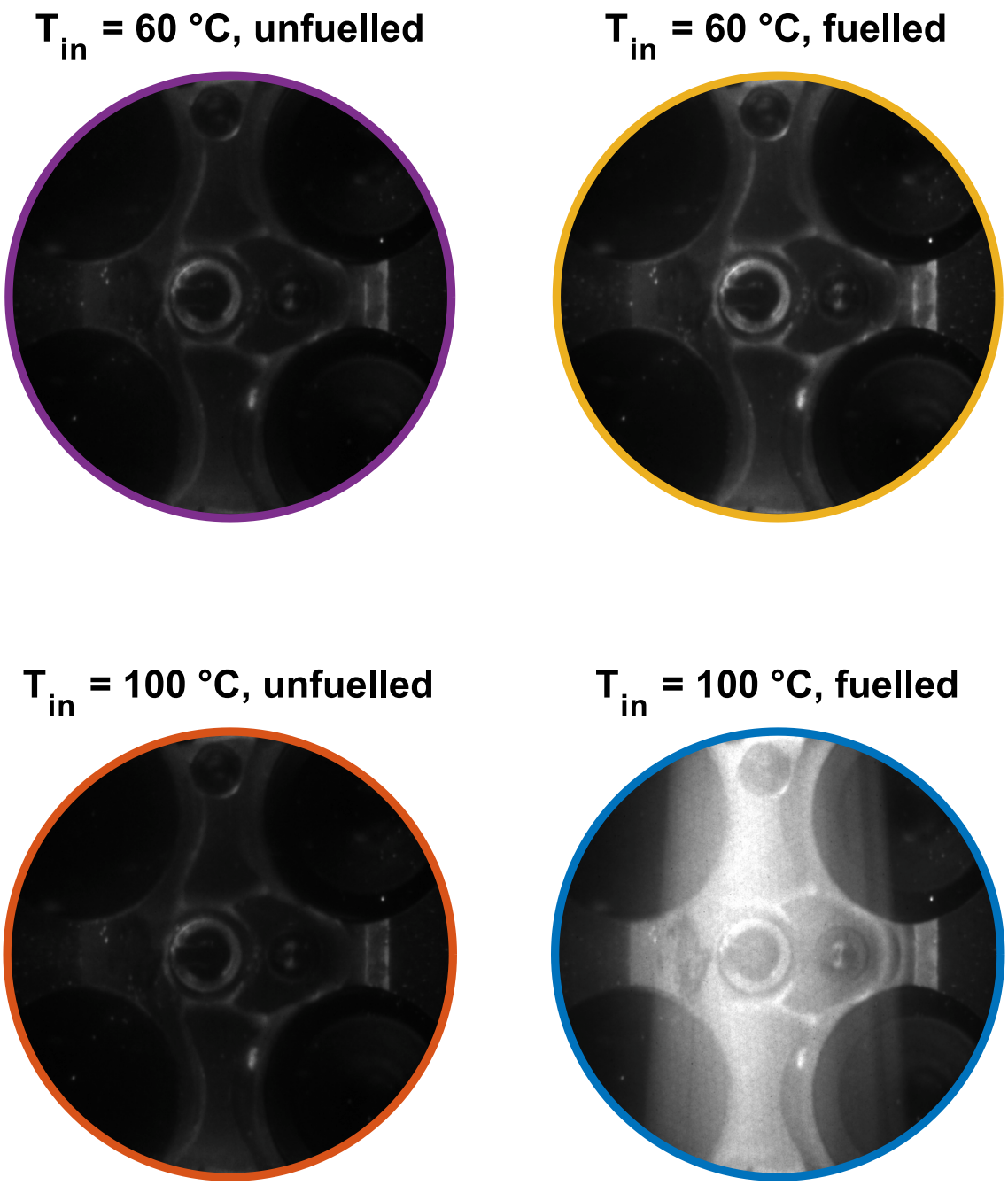

Fig. 3. Average PLIF images captured at 20 °CA aTDC for the four cases in Fig. 2. (For interpretation of the references to colour in this figure legend, the reader is referred to the web version of this article.)

be related to LTHR progress within a cycle. The laser employed was limited to one shot per cycle, so investigations within a single cycle were not possible and ensemble-averaged PLIF and LTHR data were studied instead. A motored test condition producing repeatable pressure-derived LTHR traces (PRF85 at T_{in} = 100 °C) was selected and PLIF images were captured over a wide range of crank angles over sequential cycles.

Formaldehyde formation is used as a marker for LTHR intensity (i.e. the rate of heat release from LTHR) and, in the absence of deflagration, there is no cause for it to be consumed, so for motored cases formaldehyde should accumulate throughout the cycle. Interpretation of the PLIF images as a measure of formaldehyde is complicated by the change in volume as a function of crank angle. This leads to the number density of formaldehyde at each crank angle depending both on the creation and the subsequent compression of formaldehyde created at all preceding crank angles of the cycle. The PLIF signal may also depend on the variation of pressure and temperature as a function of crank angle.

To investigate qualitative relationships, for the range of crank angles near TDC of interest in this work where volume changes are a small (but not negligible) fraction of the total swept volume, corrections for volume, pressure and temperature effects were not attempted.

Fig. 7 shows averaged PLIF images every 5 °CA. The PLIF images show a trend of increasing image brightness with time, despite volume, pressure and temperature trends reversing around TDC. This is especially apparent in the −5 °CA to 10 °CA region where volume, pressure and temperature variation is minimised.

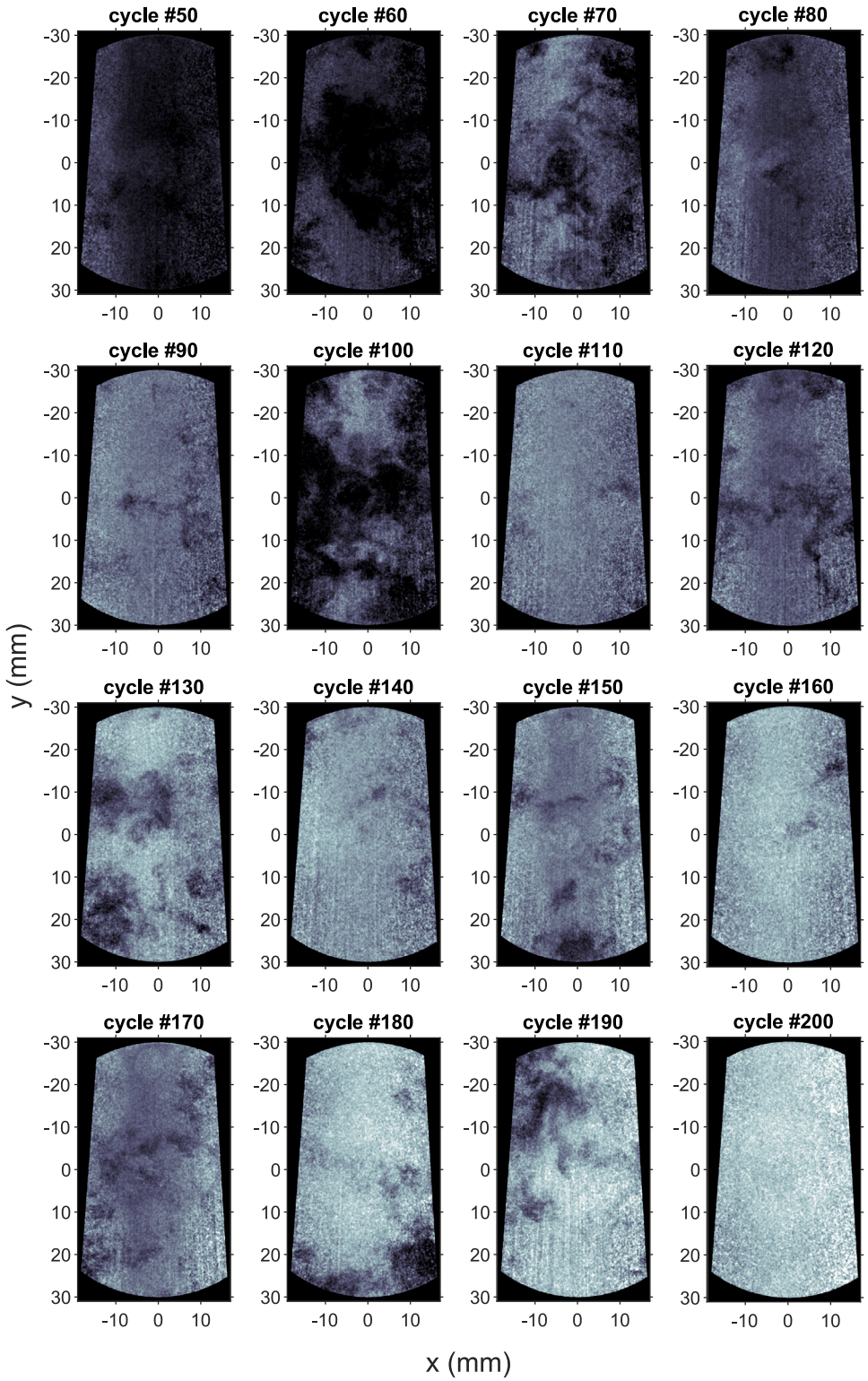

Fig. 4. 16 example PLIF images captured at 20 °CA aTDC, for the engine motored with n-heptane at T_{in} = 100 °C.

Calculating the average cumulative heat release from the pressure traces gives a second accumulating measure of LTHR. If PLIF signal intensity is suitable to use for tracking LTHR processes, there should be a qualitative match between the trends of PLIF signal intensity and cumulative heat release as a function of crank angle for the averaged cycle data.

Min–max normalised traces of average PLIF signal intensity and cumulative heat release are presented in Fig. 8. There is a good level of agreement, considering the cycle-to-cycle variation of the PLIF signal and the uncorrected factors influencing the PLIF signal detailed above, between the two independent methods of following heat release, particularly the timing of their respective greatest rate of change at 0 °CA,

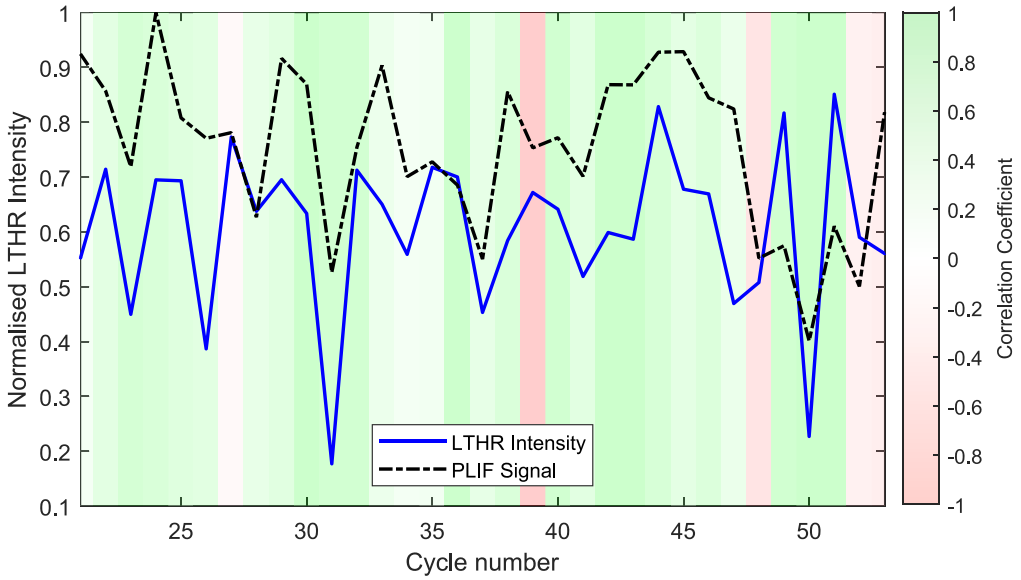

Fig. 5. Cycle-by-cycle LTHR intensity and PLIF signal intensity for a selection of consecutive cycles of motored operation with n-heptane at T_{in} = 100 °C; the similarity in the traces is illustrated with the local correlation coefficient. (For interpretation of the references to colour in this figure legend, the reader is referred to the web version of this article.)

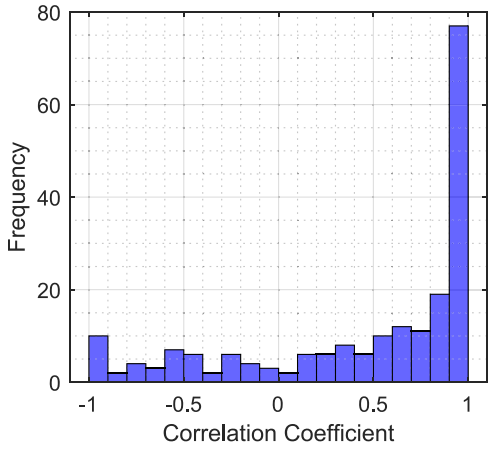

Fig. 6. Distribution of the local correlation coefficients between the LTHR intensity (pressure-based) and the PLIF data for all cycles—engine motored with n-heptane at T_{in} = 100 °C.

supporting the use of formaldehyde PLIF to track LTHR progress within a cycle.

3.3. Simultaneous LTHR and deflagration

As discussed in the introduction, it has recently been theorised that LTHR could be occurring in a volumetric manner in the unburned regions simultaneously alongside deflagration (in contrast to occurring just ahead of the flame as 'cool flame' reactions, which are well-studied). Should this occur, it would not be detectable using standard pressure-based heat release analysis techniques [13]. The deflagration results presented in this work used the four spark ignition setup as described in Section 2.1 as part of the efforts to detect such behaviour. Fig. 9 illustrates this with three apparent heat release rate traces from three different test points: AHRR from an isolated LTHR cycle (Section 3.2) is shown in blue, and AHRR for two firing cases differing only by ignition timing are shown— a later spark timing of −15° aTDC in orange and an earlier spark timing of −30° aTDC in yellow. Note that the AHRR peaks are small in magnitude and long in duration compared to typical work. This is because spark plug placement and cylinder charge motion were not optimised for combustion speed but for optical access of the end gas.

The later ignition case (orange solid line) closely resembles previous PSHR work in the literature [13], with a clear initial heat release peak around 0° aTDC, before the main HTHR from deflagration. Subtracting the AHRR trace of the isolated LTHR case from the later ignition case results in a virtual AHRR trace (orange dashed line) that approximates the HTHR contribution to the later ignition case.

The earlier ignition case (yellow solid line) shows no visible LTHR peak. This is highlighted in Fig. 9 by translating this trace 15 °CA later (yellow dashed line) where it closely resembles the approximated HTHR trace of the later spark timing case. AHRR traces similar to the early spark timing case exhibit no clear signs of LTHR in the pressure trace, so when analysing the formaldehyde PLIF signals for the −30° aTDC ignition case, one might not necessarily expect to see any signals indicating LTHR.

Fig. 10 presents PLIF images from the −30° aTDC spark timing condition and shows that, in fact, there are indications of the occurrence of LTHR in the form of mean PLIF signal intensities which show a notable increase around 0 °CA (top row). These mean PLIF images resemble the isolated LTHR condition of Fig. 7, albeit with reduced intensities at later crank angles.

These reduced mean PLIF intensities are a consequence of the flame intersecting the PLIF measurement plane at later crank angles and consuming the formaldehyde. The middle row of Fig. 10 displays an example single-shot PLIF image for each crank angle and the simultaneous natural light flame history images are presented in the bottom row.

From 10° aTDC onwards, dark regions in the otherwise bright PLIF images qualitatively overlap with the bright flame emission regions in the natural light images. For the example PLIF image at 30° aTDC, the flame has almost completely consumed the formaldehyde within the PLIF measurement plane, leaving only a small bright region to contribute to the mean PLIF image of the top row.

The intensity of these PLIF signals are quantified in Fig. 11, which compares the fired case signal intensity to the motored case from Fig. 8 (the traces are min–max normalised together). To account for the "burnt" regions, the regions of each image where formaldehyde is present were identified and only these regions were used to calculate intensity (as described in Section 2.3.2).

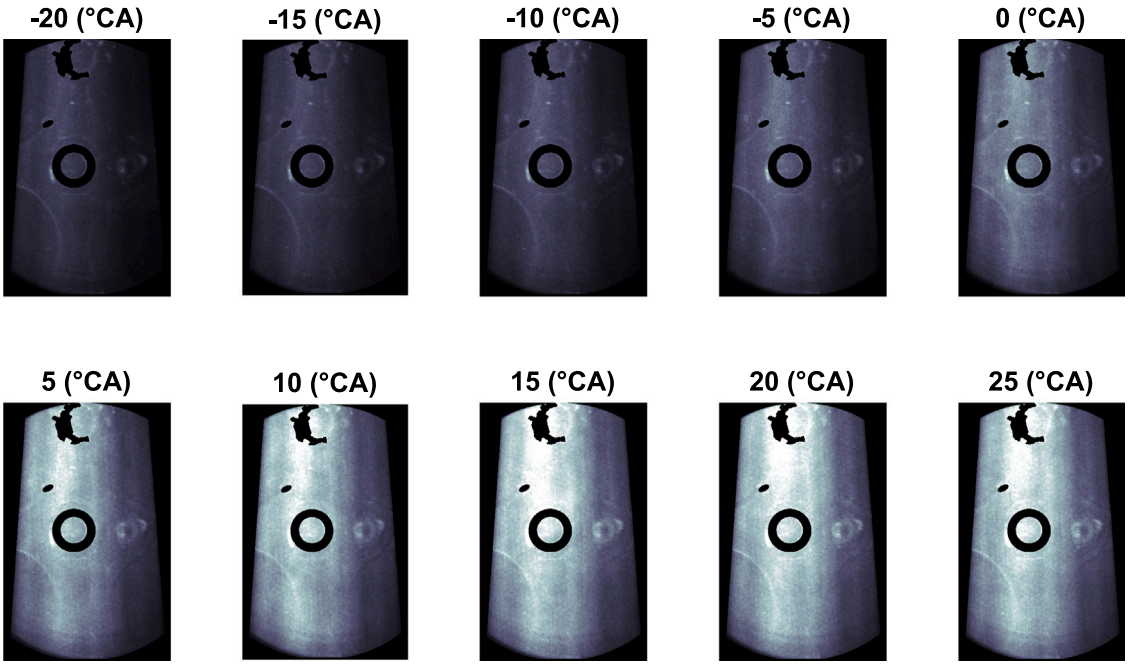

Fig. 7. Average PLIF images captured at 5 °CA increments, for the engine motored with PRF85 at T_{in} = 120 °C in order to induce isolated LTHR.

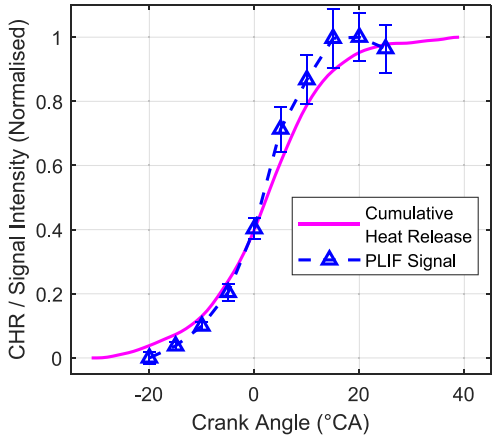

Fig. 8. Min–max normalised cumulative heat release and PLIF signal intensity (of the images in Fig. 7) for an engine motored with PRF85 at T_{in} = 120 °C in order to induce isolated LTHR.

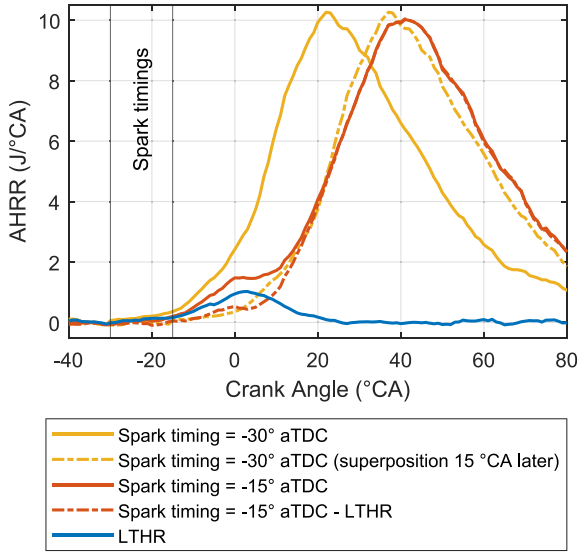

Fig. 9. Apparent heat release rate (AHRR) traces for fired cases at two different spark timings, one with a visible LTHR peak (red) and one without (yellow), compared to a motored case with a visible LTHR peak (blue). (For interpretation of the references to colour in this figure legend, the reader is referred to the web version of this article.)

The two traces exhibit some key similarities and differences. Both cases show a clear sigmoidal shape rise in intensity from −20° aTDC to on or after 20° aTDC, which (as shown in Fig. 8) is consistent with cumulative heat release from LTHR. On the other hand, there is an approximately constant difference in intensity — 0.2 units on the normalised scale — suggesting increased formaldehyde concentration in the motored case compared to the fired case. This can be attributed to a baseline concentration of formaldehyde from residuals present in the motored case, that are not present in the fired case because they are consumed by deflagration. Furthermore, the error bars on the fired case (which correspond to one standard deviation of PLIF signal intensity) are considerably wider for data points at −5° aTDC and later, owing to the cyclic variability caused by combustion—particularly in this setup which was not optimised for combustion speed and stability. The increasing PLIF signal intensity during flame propagation indicates that LTHR is occurring in unburnt regions whilst deflagration contributes to heat release elsewhere in the cylinder. To the best of the authors' knowledge, this is the first time it has been demonstrated in an SI engine. A key implication of these findings is that the chemical composition of the end gas that the flame propagates into will be different to that of the original fuel-air mixture—hence combustion properties such as knocking propensity will be different as a result.

The variations in flame progression inevitably result in cyclic variation in combustion phasing and speed and hence variation in pressure (and temperature) rises. Higher cylinder pressures and certain temperatures (i.e. below the NTC region) are conducive to LTHR. For the PLIF images collected, the cases where deflagration initiated sooner and flames developed earlier often showed large dark patches, but with the remaining signal tending to be brighter due to the elevated pressures and temperatures. This observation is presented semi-quantitatively in Fig. 12, which shows the test cases grouped into three by the start of

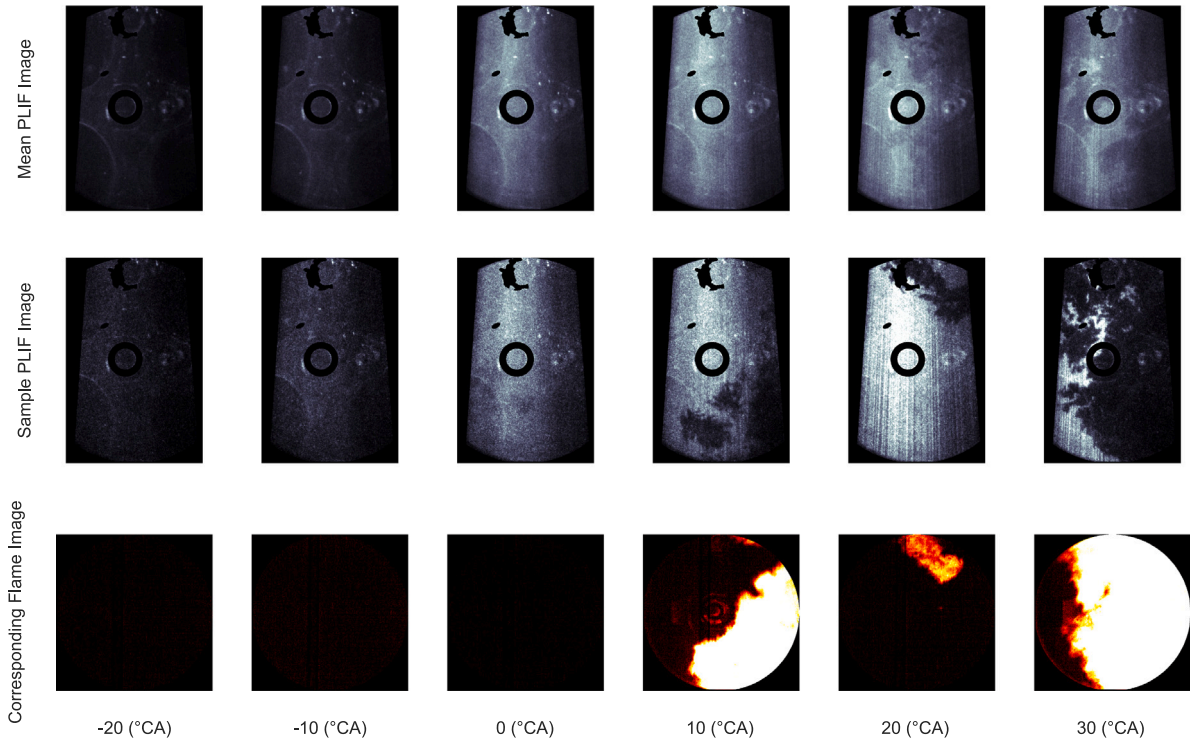

Fig. 10. PLIF and flame history images at a range of crank angles for cycles fired with −30° aTDC spark timing—average PLIF images are presented on the top row, individual sample PLIF frames on the middle row and corresponding flame history images on the bottom row. (For interpretation of the references to colour in this figure legend, the reader is referred to the web version of this article.)

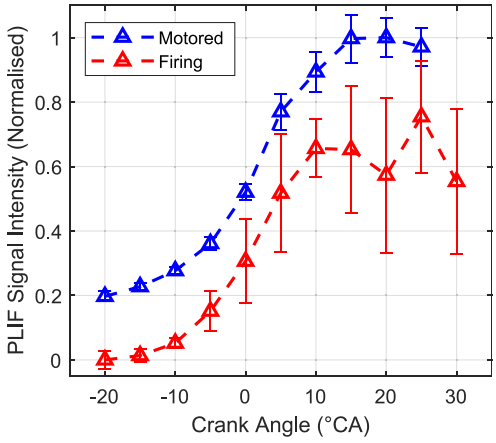

Fig. 11. PLIF Signal intensity for motored, isolated LTHR cycles (blue) and fired cycles (red) with −30° aTDC spark timing. (For interpretation of the references to colour in this figure legend, the reader is referred to the web version of this article.)

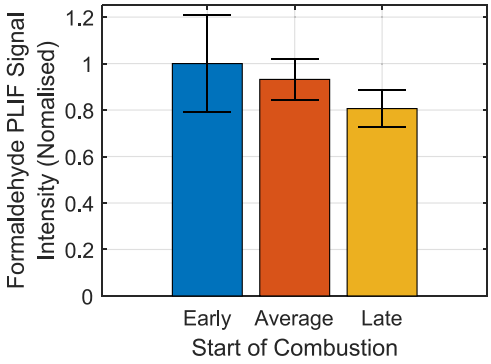

Fig. 12. Effect of combustion phasing (as indexed by start of combustion) on the PLIF signal intensity of the formaldehyde zones in PLIF images from fired cycles with −30° aTDC spark timing.

combustion (defined by the crank angle at which 10% of fuel is burnt) plotted against the intensity of the remaining patches of fluorescence in the PLIF images. It should be clarified that these trends are specific to this engine but indicative of more fundamental behaviour that can be generalised. It was the case that in these tests, the occurrence of the earlier stages of deflagration modified the pressure and therefore temperature of the end gas into conditions that are conducive to LTHR. In other engines, the same phenomena could, for example, increase the temperature too much, such that it enters the NTC region and therefore reduces LTHR intensity.

The link between the dark patches within the formaldehyde PLIF images and the flames was qualitatively demonstrated in Fig. 10 — this relationship was quantified, as demonstrated in Fig. 13.

The left-hand side column depicts four example PLIF frames with the dark patches (the gaps in fluorescence) outlined in orange. As in previous images, portions of the cylinder head paint that failed to reduce scatter (such as around the spark plug and pressure transducer) are masked out and appear black. The right-hand side shows the corresponding flame history images, generated by taking the maximum pixel intensity until the time the PLIF image was captured. This is to ensure early bright regions that become dark by the time the PLIF image is taken are still taken into account. This does assume an overall charge motion that is slow relative to the flame propagation speed. Gas velocities were not measured in this work, but the results of Fig. 14 (discussed later) are consistent with this assumption. Flame history is then detected and outlined in cyan. In the centre column, both the dark zones from the PLIF images (orange) and the flame history zones (cyan) are presented for direct comparison and overlaid on a grayscale image of the flame history.

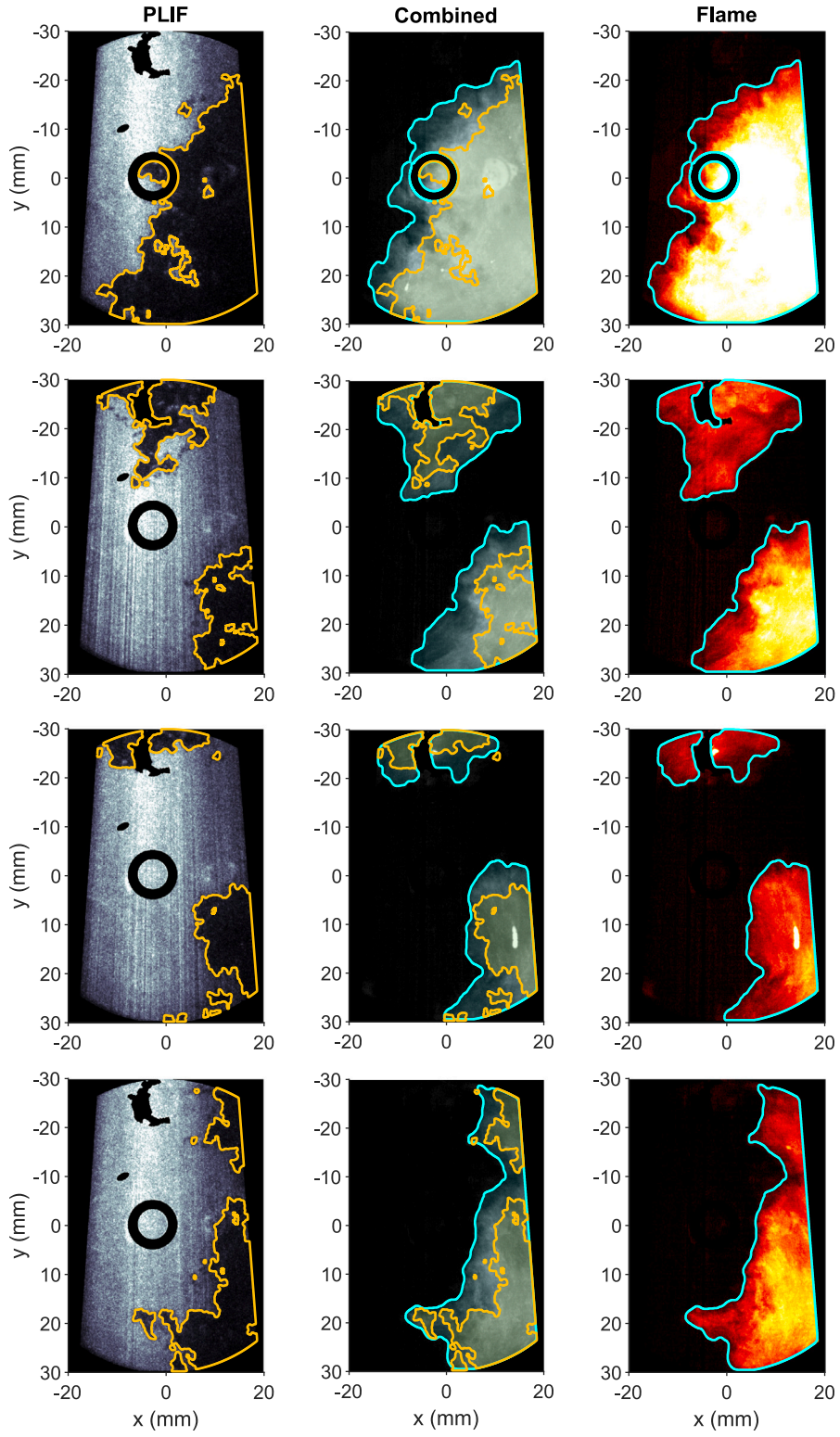

Fig. 13. Spatially calibrated formaldehyde PLIF (left column) and flame history images (right column) captured simultaneously for fired cycles with −30° aTDC spark timing—burnt zones are highlighted and compared in the middle column. (For interpretation of the references to colour in this figure legend, the reader is referred to the web version of this article.)

The independently determined zones show significant similarity — the formaldehyde gaps (highlighted in orange) are almost exclusively located within the flame history zone. This is not entirely surprising as the flame images are line-of-sight integrated whilst the PLIF image samples a relatively thin plane within the cylinder. Any flame activity outside of the laser plane will be detected in the natural light imaging

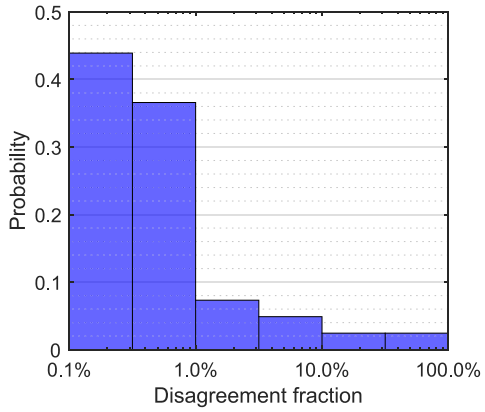

Fig. 14. Distribution of 'Disagreement fraction'—the fraction of the burnt zone in the PLIF images that appear outside of the burnt zone in the flame history images.

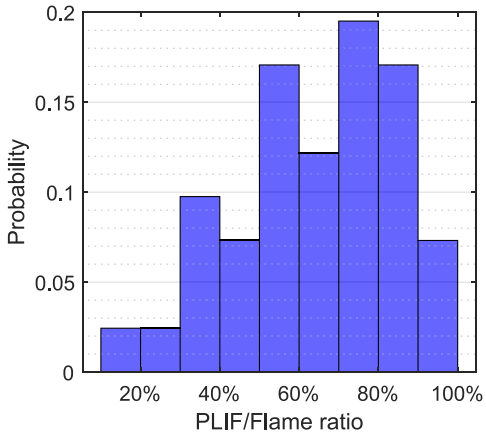

Fig. 15. The ratio of the number of pixels in the burnt zone of the PLIF images to the number of pixels in the burnt zone of the flame history images, plotted as a distribution.

but will not consume the formaldehyde within the plane and hence will not cause a dark patch in the PLIF image. On the other hand, if a dark patch appears in the PLIF image, it will almost certainly have been caused by flame presence and hence that portion of the flame will be detected in the natural light imaging.

Fig. 13's middle column qualitatively shows good agreement between zones from the two independent imaging techniques for the example images presented. The overall similarity between the full set of cycles imaged is quantified in Figs. 14 and 15.

The extent to which the PLIF dark patches (the gaps in fluorescence signal indicating lack of formaldehyde presence) appear outside of the flame zone can be described as the disagreement fraction — the fraction of dark patch pixels that appear outside of the flame zone region. A histogram plot of the disagreement fraction can be seen in Fig. 14. In 80% of cases, the disagreement fraction is 1% or less, suggesting that across the images, the gaps in visible formaldehyde fluorescence can be attributed to formaldehyde consumption by the flame with very high confidence. It is also consistent with the earlier assumption that overall charge motion was slow relative to the flame propagation speed.

The proportion of flame zone occupied by the PLIF dark patches (by number of pixels) is defined as the 'PLIF/Flame' ratio and is presented in Fig. 15. Typically, the dark patches occupied a large proportion of the flame zone, with three-quarters of the image pairs having a ratio of over 50%, and the modal ratio was in the range 70%–80%. Again, this shows good similarity between the methods, considering it would not be expected to be too close to 100% since the PLIF images were planar and flame history images were line-of-sight integrations.

4. Conclusions

In this work, n-heptane and PRF85 were injected into a motored, optically accessible, engine to determine the utility of formaldehyde planar laser-induced fluorescence (PLIF) for observing and tracking low temperature heat release (LTHR) without relying on pressure measurement-based methods. The engine was then fired with four side-mounted spark plugs in order to observe the end gas through the engine's piston window. PLIF was used to track the progression of LTHR occurring in the end gas while high speed natural light flame imaging was used to track the progress of deflagration.

The results show that:

1. For motored conditions, a strong formaldehyde PLIF signal is present when isolated LTHR occurs but not otherwise.
2. Cycle-based PLIF signal intensity within the selected 2D measurement plane is well correlated with total heat released from LTHR on a cyclic basis, despite the relatively small sampling area of the PLIF images.
3. Formaldehyde PLIF signal intensity can be used to track LTHR progression within a cycle due to its strong relationship with cumulative heat release, as evaluated using ensemble-averaged data.
4. Formaldehyde in the end gas, produced by LTHR is consumed by deflagration, which makes the presence of flames visible in PLIF images as dark regions. There was good agreement between formaldehyde PLIF images of firing cycles and natural light flame history images, as measured independently by a high speed camera.
5. The PLIF technique was able to observe LTHR in firing engine cycles where the apparent heat release data exhibited no distinguishable indications of LTHR.

This work has shown simultaneous volumetric low temperature heat release and deflagration in a spark ignition engine for the first time when other methods (i.e. pressure-derived heat release analysis) are unable to observe LTHR. The occurrence of this end gas LTHR has important implications for combustion behaviour, namely that the chemical composition of the end gas that the flame propagates into will be different to that of the original fuel-air mixture, hence combustion characteristics such as knocking propensity will differ.

Nomenclature

°CA	Crank angle degrees
HCCI	Homogeneous charge compression ignition
LTHR	Low temperature heat release
NTC	Negative temperature coefficient
P	Pressure
PLIF	Planar laser-induced fluorescence
PSHR	Pre-spark heat release
SI	Spark ignition
SICI	Spark induced compression ignition
T	Temperature
TDC	Top dead centre
ϕ	Fuel-air equivalence ratio

CRediT authorship contribution statement

Samuel P. White: Writing – original draft, Visualization, Methodology, Investigation, Formal analysis, Conceptualization. **Christopher Willman:** Writing – original draft, Methodology, Investigation, Data curation. **Felix C.P. Leach:** Writing – review & editing, Supervision, Project administration, Funding acquisition, Conceptualization.

Declaration of competing interest

The authors declare that they have no known competing financial interests or personal relationships that could have appeared to influence the work reported in this paper.

Acknowledgements

This research was supported by an Engineering and Physical Sciences Research Council Prosperity Partnership, UK, grant number EP/T005327/1. For the purpose of Open Access, the authors have applied a CC BY public copyright license to any Author Accepted Manuscript (AAM) version arising from this submission. The Prosperity Partnership is a collaboration between JLR, Siemens Digital Industries Software, the University of Bath, and the University of Oxford. The authors would also like to thank Dr Priyav Shah and Professor Ben Williams for experimental setup support and the Dept. of Engineering Science technicians and maintenance teams for facilities support.

Data availability

The data that has been used is confidential.

References

[1] Leach F, Kalghatgi G, Stone R, Miles P. The scope for improving the efficiency and environmental impact of internal combustion engines. Transp Eng 2020;1:100005. http://dx.doi.org/10.1016/j.treng.2020.100005.

[2] Wang Z, Liu H, Reitz RD. Knocking combustion in spark-ignition engines. Prog Energ Combust 2017;61:78–112. http://dx.doi.org/10.1016/j.pecs.2017.03.004.

[3] Livengood J, Wu P. Correlation of autoignition phenomena in internal combustion engines and rapid compression machines. Symp (Int) Combust 1955;5(1):347–56. http://dx.doi.org/10.1016/S0082-0784(55)80047-1.

[4] Leppard WR. The chemical origin of fuel octane sensitivity. SAE Tech. Pap. 902137, 1990, http://dx.doi.org/10.4271/902137.

[5] Shibata G, Oyama K, Urushihara T, Nakano T. The effect of fuel properties on low and high temperature heat release and resulting performance of an HCCI engine. SAE Tech. Pap. 2004-01-0553, 2004, http://dx.doi.org/10.4271/2004-01-0553.

[6] Shibata G, Oyama K, Urushihara T, Nakano T. Correlation of low temperature heat release with fuel composition and HCCI engine combustion. SAE Tech. Pap. 2005-01-0138, 2005, http://dx.doi.org/10.4271/2005-01-0138.

[7] Truedsson I, Cannella W, Johansson B, Tuner M. Engine speed effect on autoignition temperature and low temperature reactions in HCCI combustion for primary reference fuels. SAE Tech. Pap. 2014-01-2666, 2014, http://dx.doi.org/10.4271/2014-01-2666.

[8] Curran HJ, Gaffuri P, Pitz WJ, Westbrook CK. A comprehensive modeling study of iso-octane oxidation. Combust Flame 2002;129(3):253–80. http://dx.doi.org/10.1016/S0010-2180(01)00373-X.

[9] Curran H, Gaffuri P, Pitz W, Westbrook C. A comprehensive modeling study of n-heptane oxidation. Combust Flame 1998;114(1):149–77. http://dx.doi.org/10.1016/S0010-2180(97)00282-4.

[10] Szybist JP, Splitter DA. Pressure and temperature effects on fuels with varying octane sensitivity at high load in SI engines. Combust Flame 2017;177:49–66. http://dx.doi.org/10.1016/j.combustflame.2016.12.002.

[11] Splitter D, Kaul B, Szybist J, Jatana G. Engine operating conditions and fuel properties on pre-spark heat release and SPI promotion in SI engines. SAE Int J Engines 2017;10(3):1036–50. http://dx.doi.org/10.4271/2017-01-0688.

[12] Waqas MU, Hoth A, Kolodziej CP, Rockstroh T, Gonzalez JP, Johansson B. Detection of low temperature heat release (LTHR) in the standard cooperative fuel research (CFR) engine in both SI and HCCI combustion modes. Fuel 2019;256:115745. http://dx.doi.org/10.1016/j.fuel.2019.115745.

[13] Splitter DA, Gilliam A, Szybist J, Ghandhi J. Effects of pre-spark heat release on engine knock limit. P. Combust Inst 2019;37(4):4893–900. http://dx.doi.org/10.1016/j.proci.2018.05.145.

[14] Urushihara T, Yamaguchi K, Yoshizawa K, Itoh T. A study of a gasoline-fueled compression ignition engine ∼ expansion of HCCI operation range using SI Combustion as a trigger of compression ignition ∼. SAE Tech. Pap. 2005-01-0180, 2005, http://dx.doi.org/10.4271/2005-01-0180.

[15] Ma X, Wang Z, Jiang C, Jiang Y, Xu H, Wang J. An optical study of in-cylinder CH_2o and OH chemiluminescence in flame-induced reaction front propagation using high speed imaging. Fuel 2014;134:603–10. http://dx.doi.org/10.1016/j.fuel.2014.06.002.

[16] Hu Z, Zhang J, Sjöberg M, Zeng W. The use of partial fuel stratification to enable stable ultra-lean deflagration-based spark-ignition engine operation with controlled end-gas autoignition of gasoline and E85. Int J Engine Res 2020;21(9):1678–95. http://dx.doi.org/10.1177/1468087419889702.

[17] Bajwa AU, Leach FCP, Davy MH. Prospects of controlled auto-ignition based thermal propulsion units for modern gasoline vehicles. Energ 2023;16(9):3887. http://dx.doi.org/10.3390/en16093887.

[18] Martz J, Kwak H, Im H, Lavoie G, Assanis D. Combustion regime of a reacting front propagating into an auto-igniting mixture. P. Combust Inst 2011;33(2):3001–6. http://dx.doi.org/10.1016/j.proci.2010.07.040.

[19] Suzuki R, Shoji H, Yoshida K, Iijima A. Analysis of knocking in an SI engine based on in-cylinder: spectroscopic measurements and visualization. SAE Tech. Pap 2010-32-0092, 2010, http://dx.doi.org/10.4271/2010-32-0092.

[20] Eckbreth A. Laser diagnostics for combustion temperature and species. 2nd ed.. Gordon and Breach Publishers; 1996, http://dx.doi.org/10.1201/9781003077251.

[21] Zhao H, Ladommatos N. Engine combustion instrumentation and diagnostics. SAE International; 2001, URL: http://books.sae.org/r-264/.

[22] Jeffries JB, Kohse-Höinghaus K. Applied combustion diagnostics. 1st ed.. London: Taylor & Francis; 2002.

[23] Schulz C, Dreizler A, Ebert V, Wolfrum J. Combustion diagnostics. In: Tropea C, Yarin AL, Foss JF, editors. Springer handbook of experimental fluid mechanics. Springer Berlin Heidelberg; 2007, p. 1241–315. http://dx.doi.org/10.1007/978-3-540-30299-5_20.

[24] Schulz C, Sick V. Tracer-LIF diagnostics: quantitative measurement of fuel concentration, temperature and fuel/air ratio in practical combustion systems. Prog Energ Combust 2005;31(1):75–121. http://dx.doi.org/10.1016/j.pecs.2004.08.002.

[25] Sjoholm J, Rosell J, Li B, Richter M, Li Z, Bai XS, Alden M. Simultaneous visualization of OH, CH, CH_2O and toluene PLIF in a methane jet flame with varying degrees of turbulence. P. Combust Inst 2013;34(1):1475–82. http://dx.doi.org/10.1016/j.proci.2012.05.037.

[26] Carter CD, Skiba AW, Boxx I, Allison PM. Optimal approaches to formaldehyde planar laser-induced fluorescence. Combust Flame 2022;246:112431. http://dx.doi.org/10.1016/j.combustflame.2022.112431.

[27] Brackmann C, Nygren J, Bai X, Li Z, Bladh H, Axelsson B, Denbratt I, Koopmans L, Bengtsson PE, Aldén M. Laser-induced fluorescence of formaldehyde in combustion using third harmonic Nd:YAG laser excitation. Spectrochim Acta A 2003;59(14):3347–56. http://dx.doi.org/10.1016/S1386-1425(03)00163-X.

[28] Donkerbroek AJ, van Vliet AP, Somers LM, Frijters PJ, Klein-Douwel RJ, Dam NJ, Meerts WL, ter Meulen JJ. Time- and space-resolved quantitative LIF measurements of formaldehyde in a heavy-duty diesel engine. Combust Flame 2010;157(1):155–66. http://dx.doi.org/10.1016/j.combustflame.2009.07.004.

[29] Thering H, Beckmann L, Jördens C, Röder M, Dreier T, Schulz C. Formaldehyde laser-induced fluorescence imaging with a multi-band transmission filter. Opt Lett 2014;39(7):1873. http://dx.doi.org/10.1364/OL.39.001873.

[30] Schießl R, Maas U. Analysis of endgas temperature fluctuations in an SI engine by laser-induced fluorescence. Combust Flame 2003;133(1–2):19–27. http://dx.doi.org/10.1016/S0010-2180(02)00538-2.

[31] Bäuerle B, Hoffmann F, Behrendt F, Warnatz J. Detection of hot spots in the end gas of an internal combustion engine using two-dimensional LIF of formaldehyde. Symp (Int) Combust 1994;25(1):135–41. http://dx.doi.org/10.1016/S0082-0784(06)80637-5.

[32] Dubreuil A, Mounaïm-Rousselle C, Foucher F, Dagaut P. Comparison between LIF measurements and modeling predictions of OH-HCHO during HCCI mode combustion development. SAE Tech. Pap. 2007-24-0019, 2007, http://dx.doi.org/10.4271/2007-24-0019.

[33] Collin R, Nygren J, Richter M, Aldén M, Hildingsson L, Johansson B. Simultaneous OH- and formaldehyde-LIF measurements in an HCCI engine. SAE Tech. Pap. 2003-01-3218, 2003, http://dx.doi.org/10.4271/2003-01-3218.

[34] Olofsson J, Seyfried H, Richter M, Aldén M, Vressner A, Hultqvist A, Johansson B, Lombaert K. High-speed LIF imaging for cycle-resolved formaldehyde visualization in HCCI combustion. SAE Tech. Pap. 2005-01-0641, 2005, http://dx.doi.org/10.4271/2005-01-0641.

[35] Splitter DA, Gilliam A, Szybist J, Ghandhi J. Effects of pre-spark heat release on engine knock limit. P. Combust Inst 2019;37(4):4893–900. http://dx.doi.org/10.1016/j.proci.2018.05.145.

[36] Graf N, Gronki J, Schulz C, Baritaud T, Cherel J, Duret P, Lavy J. In-cylinder combustion visualization in an auto-igniting gasoline engine using fuel tracer- and formaldehyde-LIF imaging. In: International spring fuels & lubricants meeting. SAE International; 2001, http://dx.doi.org/10.4271/2001-01-1924.

[37] Strozzi C, Claverie A, Prevost V, Sotton J, Bellenoue M. HCCI and SICI combustion modes analysis with simultaneous PLIF imaging of formaldehyde and high-speed chemiluminescence in a rapid compression machine. Combust Flame 2019;202:58–77. http://dx.doi.org/10.1016/j.combustflame.2019.01.002.

[38] White SP, Bajwa AU, Leach FCP. Isolated low temperature heat release in spark ignition engines. SAE Int J Adv Curr Pr Mobil 2024;6(2):827–40. http://dx.doi.org/10.4271/2023-01-0235.

[39] White SP, Bajwa AU, Leach FCP. Effect of ethanol and iso-octane blends on isolated low temperature heat release in a spark ignition engine. SAE Int J Fuels Lubr 2024;17(3). http://dx.doi.org/10.4271/04-17-03-0016.

[40] White SP, Bajwa AU, Leach FCP. Effects of nitric oxide on isolated low temperature heat release in spark ignition engines. Combust Flame 2025. http://dx.doi.org/10.1016/j.combustflame.2024.113921.

[41] Bajwa AU, White SP, Leach FCP. Low temperature heat release and phi-sensitivity characteristics of iso-octane/air mixtures. Combust Sci Technol 2025;197:440–62. http://dx.doi.org/10.1080/00102202.2023.2245635.

[42] Williams B, Ewart P, Wang X, Stone R, Ma H, Walmsley H, Cracknell R, Stevens R, Richardson D, Fu H, Wallace S. Quantitative planar laser-induced fluorescence imaging of multi-component fuel/air mixing in a firing gasoline-direct-injection engine: Effects of residual exhaust gas on quantitative PLIF. Combust Flame 2010;157(10):1866–78. http://dx.doi.org/10.1016/j.combustflame.2010.06.004.

[43] Stone CR. Introduction to internal combustion engines, 4th ed.. Macmillan International Higher Education; 2012.

Statement of Authorship for joint/multi-authored papers for PGR thesis

To appear at the end of each thesis chapter submitted as an article/paper

The statement shall describe the candidate's and co-authors' independent research contributions in the thesis publications. For each publication there should exist a complete statement that is to be filled out and signed by the candidate and supervisor **(only required where there isn't already a statement of contribution within the paper itself).**

Title of Paper	Observing simultaneous low temperature heat release and deflagration in a spark ignition engine using formaldehyde planar laser induced fluorescence.
Publication Status	Submitted for Publication
Publication Details	White, S. P., Willman, C. & Leach, F. C. P. Observing simultaneous low temperature heat release and deflagration in a spark ignition engine using formaldehyde planar laser induced fluorescence. Submitted for Publication (2024).

Student Confirmation

Student Name:	Samuel P. White		
Contribution to the Paper	• Idea • Experimental design • Implementation (joint effort) • Data analysis (all) • Writing (joint effort for introduction and methodology, solo effort for the rest of the manuscript)		
Signature 		Date	12 April, 2024

Supervisor Confirmation

By signing the Statement of Authorship, you are certifying that the candidate made a substantial contribution to the publication, and that the description described above is accurate.

Supervisor name and title: Felix Leach, Associate Professor of Engineering Science		
Supervisor comments I agree with Sam's comments.		
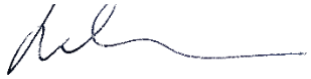	Date	12-4-24

This completed form should be included in the thesis, at the end of the relevant chapter.

Chapter Summary

This Chapter builds upon the results from the five publications in the previous two chapters to achieve the second main objective of this thesis—to develop a new technique, that does not rely on pressure-derived apparent heat release measurements, to observe LTHR in SI engines. This was achieved by testing and refining the formaldehyde PLIF method on isolated LTHR, first with n-heptane and then with PRF85, and examining the relationship between PLIF signal intensity and cumulative heat release from isolated LTHR. The method was then applied to a firing case whose apparent heat release trace showed no indications of LTHR, but the PLIF signal, indicative of the occurrence of LTHR from the presence of formaldehyde, was observed in the end gas. A full analysis of the results and implications of this work, and those of the previous chapters can be found in Chapter 5.

Chapter 5

Conclusion

This thesis has presented a collection of studies that contribute to the understanding of low temperature heat release (LTHR) in spark ignition engines. Six studies are presented as published or submitted academic papers, across three chapters based on their area of focus. The results and conclusions of each study are presented in their respective papers, with this chapter aiming to provide an overall summary and analysis of the findings from the six papers.

5.1 Summary of work

A methodology for isolating low temperature heat release in spark ignition engines, which forms the basis of this thesis, was presented in Section 2.1. It was first used to carry out studies on fundamental physical parameters of an engine, namely inlet temperature, inlet pressure and engine speed. Tests were carried out across two engines with the two single component fuels: n-heptane and iso-octane. LTHR is also presented in contrast with high temperature heat release (HTHR) for clarity. To complete the study of physical parameters, Section 2.2 presented an investigation into the effect of equivalence ratio on LTHR. To enable a comprehensive analysis of the results, Chapter 2 presented a range of techniques for observing and analysing the isolated LTHR, from apparent heat release rate and temperature traces, to ignition delay and Livengood-Wu analysis. Additionally, the study in Section 2.2 presents alternative methods for measuring LTHR, with exhaust temperature and carbon monoxide concentration measurements. The methods and results from this chapter were applied in all subsequent studies.

Chemical effects, specifically fuel composition and residual effects were studied in Chapter 3. Across the studies, binary blends of n-heptane, iso-octane and ethanol were tested to determine their effects on LTHR behaviour. Further, more comprehensive exhaust gas measurements were carried out in Section 3.1, to determine the chemical composition of the products of LTHR and to help identify a chemical indicator specific to LTHR that would help identify it using optical diagnostic techniques. The effect of combustion residuals were tested by applying a skip firing methodology in Section 3.1 and by directly seeding nitric oxide into the inlet air in Section

3.3. The studies in this chapter introduced two further techniques to analyse and explain LTHR behaviour: 0D engine modelling and sensitivities analyses on ignition delay time.

Finally, the insights from Chapters 2 and 3 surrounding fundamental inlet parameters and LTHR products (specifically, formaldehyde) were applied in Chapter 4 to develop and inform the application of an optical diagnostic technique—planar laser-induced fluorescence (PLIF) of formaldehyde, with the aim of detecting LTHR without needing to rely on pressure-derived heat release, or exhaust gas, measurements. This method was first applied and fined tuned on isolated LTHR test points, and subsequently applied to a fired cycle test case that exhibited no other measurable indications of LTHR. High speed natural light flame images were captured alongside the PLIF images to enable detection of the flames and hence the burnt and unburned zones. A non-standard annular four spark plug ignition system was employed in order to make the unburned end gas optically accessible. The findings from all six studies are presented in the following section.

5.2 Findings

5.2.1 Isolated LTHR Methodology

Section 2.1 showed that by disabling the ignition system of an SI engine, and curating the inlet temperature and pressure, it is possible to realise isolated LTHR without inducing subsequent high temperature heat release. This is one of the most significant contributions of this work, for a multitude of reasons. The methodology enables more detailed studies on the effect of various engine- and fuel-related parameters on LTHR behaviour—an important phenomenon in engines. It does not require techniques such as spline fitting to infer the amount of heat released by LTHR because it can be measured directly using various techniques. Applying the methodology enables observations of LTHR for inlet conditions where deflagration would otherwise obscure the apparent heat release data (though it is important to note that the deflagration itself will modify LTHR behaviour as it increases cylinder pressures and temperatures). As the subsequent chapters in this thesis show, the isolated LTHR methodology opens up opportunities for testing and validating chemical kinetics models, and observing LTHR using many techniques, such as exhaust emissions measurements, optical diagnostics and exhaust temperature measurements. In this thesis alone it enabled five further studies with the potential for many more. Ultimately, these studies help inform the relationship between engine thermodynamics, fuels and combustion behaviour—learning more about LTHR means learning more about knocking and hence contributing to improving internal combustion engine efficiency.

5.2.2 Effect of Pressure

The effect of inlet pressure—and therefore compression pressure—was investigated. It is particularly relevant given recent trends of engine downsizing and boosting (conditions that tend to be more knock-prone). The relationship with LTHR is relatively simple: increasing pressure increased LTHR intensity for all test points across the studies. This is a particularly useful result for advanced combustion regimes that require first-stage autoignition to have occurred, as increasing pressure is usually a relatively simple step to take. The relationship was established in the first study and was utilised in the subsequent studies to encourage the required LTHR.

5.2.3 Effect of Temperature

Temperature has a significant impact on LTHR behaviour and has a more complex relationship than pressure. Section 2.1 showed that the net effect of increasing inlet temperature for n-heptane and iso-octane was the strengthening and weakening of LTHR intensity, respectively. Furthermore, in Section 3.2 in the study on iso-octane and ethanol blends trends of increasing and subsequent decreasing LTHR intensity were observed. This appears to be counter-intuitive at first but, LTHR behaviour is in fact a function of the absolute temperature—not just the trend—because of the NTC behaviour of some fuel-air mixtures. The effect of inlet temperature (and therefore compression temperature) on isolated LTHR depends on the specific fuel's ignition delay characteristics and the temperature and pressure conditions that the mixture traverses throughout its cycle. The more time the mixture spends in a reactive pressure-temperature region, the more energy was released by LTHR.

5.2.4 Effect of Engine Speed

Engine speed affects LTHR behaviour in two ways: it reduces the time for heat losses but also for low temperature reaction progression. As a result, compression temperatures are elevated (which as discussed above, has a non-trivial effect on LTHR) with increasing engine speed. Generally, higher speed means less time at elevated pressures and temperatures and hence less opportunity for the mixture to undergo first-stage ignition delay resulting in reduced LTHR at high speeds. The main implication of this finding is that low engine speeds are most prone to exhibit LTHR behaviour.

5.2.5 Effect of Equivalence Ratio

The results from the study in Section 2.2 showed that LTHR can be induced and detected at very lean ($\phi < 0.05$) conditions. Its intensity increases proportionally as the fuel-air mixture becomes richer. However, beyond a certain ϕ limit, in direct injection engines, the proportional relationship ceases, LTHR intensity begins to decrease sharply with equivalence ratio and subsequently ceases. Equivalence ratio has a relatively small effect on ignition delay time, as defined by 50K rise (which is strongly related to LTHR intensity), though it should be noted

that the first stage ignition delay definition used throughout these studies (and beyond) does not account for the effect of dilution on temperature. In a GDI engine, the equivalence ratio can significantly impact thermal effects. For a given volume of air, an increased equivalence ratio requires increased fuel mass injected which comes with an associated increase in charge cooling—with a decreasing effect on temperature that is felt throughout the cycle and hence has a significant effect on LTHR. When the equivalence ratio is increased to the point where charge cooling effects dominate, LTHR ceases abruptly.

5.2.6 Relationship with LTHR Phasing

The relationship between LTHR intensity and its phasing is more complex than it appears upon reading the constituent studies from this thesis in isolation. The results in Sections 2.1, 3.2 and 3.3 presented trends where increasing LTHR intensity saw LTHR occurring earlier (as indicated by CA50), however Section 2.2, which focused on equivalence ratio, showed the opposite trend for the majority of the results—LTHR CA50 was linearly related to equivalence ratio, which itself was linear with LTHR intensity up until a certain equivalence ratio where the trend reversed. The relationship between LTHR intensity and phasing depends on which factor is limiting LTHR intensity: when LTHR is limited by the chemistry and thermodynamic conditions (i.e. ignition delay), not all the fuel that can undergo LTHR does. This is because a longer first-stage ignition delay time causes LTHR reactions occur to later in an engine cycle so there is less time for those reactions to occur so LTHR intensity is ultimately reduced and occurs later. Meanwhile, if the quantity of fuel is the limiting factor, LTHR reactions start at approximately the same time but finish later the more fuel there is available, causing their CA50 to be later.

5.2.7 Ignition Delay Analysis

Ignition delay analyses were employed extensively across the various studies in this thesis. The results and discussions demonstrated that it is an essential tool for understanding LTHR behaviour—because it encompasses all of the engine- and fuel-related parameters, and uses them to explain and even predict LTHR behaviour. Chemical factors (investigated in Chapter 3), such as fuel composition and residual presence define a first-stage ignition delay contour over a range of engine-relevant pressures and temperatures. Then, physical factors (Chapter 2), such as inlet pressure and charge cooling, define the path through the ignition delay space that the mixture traverses. The more time the mixture spends in the low first-stage ignition delay (i.e. high reactivity) regions, the more likely LTHR is to occur. Sections 2.1, 3.2 and 3.3 showed that progress towards LTHR can be successfully quantified by the Livengood-Wu integral. A key implication of this work is that now, given an ignition table for a fuel mixture, it would be relatively straightforward to explore the pressure-temperature area (i.e. assume polytropic compression, or use pressure-temperature trajectories from firing data) and employ

the Livengood-Wu integral to predict whether LTHR will occur, without the need for more computationally expensive engine modelling.

5.2.8 Fuel Effects: Primary Reference Fuels

The two components that make up PRFs: n-heptane and iso-octane were studied extensively in this work both as single-component gasoline surrogates and blended with other fuels. They were chosen for their strong NTC behaviour, which makes them conducive to exhibiting LTHR. Compared to n-heptane, iso-octane's NTC region occurs at higher temperatures and it has longer first-stage ignition delay times overall—explaining why it did not exhibit LTHR in the naturally aspirated engine in Sections 2.1 and 3.1 and instead required a combination of elevated pressures and boosting to realise LTHR. Section 3.1 focused on the LTHR propensity of the two components blended together in various ratios. PRF blends up to 75% iso-octane exhibited LTHR at elevated inlet temperatures, despite neat iso-octane not exhibiting it at the conditions tested. The key finding was that LTHR intensity always reduced as iso-octane content increased in the blend with n-heptane. Somewhat surprisingly, the accompanying HCCI modelling indicated that, despite iso-octane's reducing effect on LTHR, approximately 50% of the iso-octane was consumed during LTHR of PRF50 and PRF75.

5.2.9 Fuels Effects: Ethanol Content

Like iso-octane, ethanol content reduces LTHR intensity when blended with n-heptane, however, it has a more dramatic effect for a given volume fraction. HCCI modelling also indicated that, despite ethanol's reducing effect, similar consumption behaviour was indicated with ethanol with approximately 40% consumption in the 10% and 20% blends in Section 3.1. Results from the study also indicated that, despite its inhibiting effect, small amounts of ethanol may be beneficial where LTHR behaviour is required but high-temperature autoignition is a concern, owing to ethanol's low knocking propensity. Similar trends were observed when ethanol was blended into iso-octane in relatively small quantities in Section 3.2. Ethanol had drastic inhibiting effects on the blend's LTHR behaviour—much more than could be accounted for by the displacement of iso-octane molecules by non-LTHR exhibiting molecules. Blends of 20% vol ethanol exhibited no LTHR at the conditions tested in the study. Blending ethanol with n-heptane or iso-octane significantly impacts the mixture's first stage ignition delay contour. The results of the sensitivity analysis in Section 3.2 showed that introducing ethanol had a significant effect on competition for OH radicals, which are heavily involved in the initiation of low temperature oxidation of PRFs (by hydrogen abstraction) and the subsequent chain branching reactions related to LTHR.

5.2.10 Effect of Residuals

Residual effects from firing cycles were found to have mixed effects on LTHR behaviour in PRF80 in Section 3.1. The slightly elevated engine temperatures increased peak heat release and advancing LTHR phasing but the residual gases reduced overall LTHR intensity by approximately 10% for LTHR cycles that immediately followed firing cycles. This behaviour was studied in greater detail in Section 3.3, where one of the most reactive residual gases, nitric oxide was directly added to the fuel-air mixture. The results showed that, contrary to modelling predictions in the literature, introducing moderate to high concentrations of NO into iso-octane and air mixtures almost always strongly reduced LTHR intensity and in one case prevented it entirely. Exhaust NO and NO_2 concentrations showed strong conversion of NO to NO_2 whilst LTHR was being reduced but not totally inhibited; this conversion reduced back to near motoring levels when LTHR was entirely inhibited. To find the root cause of this behaviour a sensitivity analysis was carried out on ignition delay time and showed that nitric oxide primarily affected LTHR chemistry through oxygen abstraction from the iso-octylperoxy radical by NO to create iso-octane alkoxy radicals—steering the reaction pathway away from low temperature chain branching, and through competition with O_2 for CH_3O radicals causing a knock-on reduction in OH radical production. With sufficient NO concentrations present, low-temperature chain branching reactions can be almost entirely halted, preventing LTHR from occurring.

5.2.11 Emissions/Chemical Products of LTHR

The isolated LTHR methodology was taken advantage of to analyse the products of LTHR—which are usually consumed by HTHR—with an exhaust analyser. Experimental exhaust emissions measurements showed very high concentrations of carbon monoxide and formaldehyde in exhaust from LTHR cycles, with both species concentrations having a strong correlation with LTHR intensity. Complete combustion products (CO_2 and H_2O) were present in much lower quantities than would be seen for complete combustion. The unburnt hydrocarbons ethene and propene were measured in relatively high concentrations whilst 1,3-butadiene was not. The species that could be detected by the exhaust analyser in Section 3.1 only made up around 20% of the carbon atoms from the fuel, highlighting the need for further analysis and new instrumentation in this area.

5.2.12 LTHR Indicators

This thesis has presented and utilised a variety of different methods for inferring LTHR intensity, each with various benefits and drawbacks. Initially, the magnitude of heat release originating from LTHR was measured by comparing the pressure-derived AHRR measurements from a fuelled LTHR case to an unfuelled, motored case. Whilst this generally worked well for making comparisons between test cases, Section 3.2 highlighted its drawbacks in finding the absolute measurements of LTHR for certain test conditions. Sections 2.1 and

2.2 demonstrated that isolating LTHR allowed for indexing of LTHR strength using out-of-cylinder measurements such as exhaust temperature. Furthermore, multiple studies in this work demonstrated that LTHR-specific chemical species such as CO and formaldehyde made for good indicators, and the data presented in Section 2.2 showed strong evidence that exhaust carbon monoxide concentration is proportional to the heat released from LTHR, independent of other factors such as fuel (within the blends tested) and equivalence ratio.

5.2.13 0D Engine Models

0D engine models were employed as part of the analysis at various stages in this work. Given their simplicity, it was difficult (and likely impossible) to replicate experimental results precisely. However, they were particularly effective at predicting trends, assuming they were using an accurate chemical kinetic mechanism. This was highlighted in Section 3.3 where HCCI modelling was used to show that many popular gasoline surrogate mechanisms do not correctly predict trends observed experimentally (instead predicting that NO promotes LTHR). These incorrect predictions stemmed from the mechanisms not modelling the inhibiting behaviour of NO seen at low temperatures (as discussed in Section 5.2.10). These findings were particularly significant, as inaccurate modelling of LTHR will have ramifications for the whole engine cycle due to the effect LTHR can have on mixture composition and autoignition chemistry.

5.2.14 Planar Laser-induced Fluorescence Technique

Following successful exhaust emissions measurements of formaldehyde from LTHR, a Planar Laser-induced Fluorescence (PLIF) technique to observe LTHR was developed as an alternative to pressure-derived or exhaust gas measurement methods. The results from this work showed that, (despite the relatively small sampling area of the PLIF images) for motoring conditions, a strong formaldehyde PLIF signal is present when isolated LTHR occurs but not otherwise. Furthermore, formaldehyde PLIF signal intensity could be used to track LTHR progression within a cycle due to its strong relationship with cumulative heat release. The technique was tested on fired cases, where formaldehyde in the end gas is consumed by deflagration, making the presence of flames visible in PLIF images as dark regions. There was found to be good agreement between formaldehyde PLIF images of firing cycles and natural light flame history images, as measured independently by a high-speed camera.

5.2.15 Simultaneous LTHR and Deflagration

This work ultimately set out to observe simultaneous LTHR and deflagration with the preceding studies determining the feasibility of the optical diagnostic methodology and helping inform inlet conditions and fuel choices. The PLIF technique was able to observe LTHR in a firing case where the apparent heat release data

exhibited no distinguishable signs of LTHR—for the first time. The occurrence of end gas LTHR has important implications for combustion behaviour, namely that the chemical composition of the end gas that the flame propagates into will be different to that of the original fuel-air mixture, hence combustion characteristics, such as knocking propensity, will differ.

5.3 Future Work

5.3.1 Port Fuel Injection

The work in this thesis focused on LTHR in direct injection SI engines because it is the most relevant injection technology for modern production engines. However, in some of the studies, particularly those involving ethanol blends such as in Section 3.2, the thermal effects (which are now well understood) from charge cooling had a significant influence on the results. For more fundamental engine studies, port fuel injection could be employed to isolate the mixture from these effects, enabling a more focused comparison on the chemical effects of the fuels. This would be particularly useful for further studies comparing effects between fuels with large or large differences in charge cooling effects.

5.3.2 Fuels and Blends

Whilst the single component and binary blends tested in this work have much in common with market fuels (especially the iso-octane and ethanol blends) and allow for repeatable experiments that can be analysed and modelled in-depth with chemical kinetic mechanisms, there is more that can be done to simulate market fuels, derived from crude oil fractions, more closely.

There are many, slightly less common—but still highly relevant, gasoline surrogates that could and should be explored further. These include other n-alkanes and iso-alkanes such as n-octane, n-butane, n-hexane and iso-pentane; aromatics, including toluene, xylenes and 1,2,4-Trimethylbenzene; cycloalkanes such as cylcopentane and cyclohexane; alkenes and methanol [70]—which may have a similar effect to ethanol on the OH radical pool. Common fuel additives could also be studied. Whilst the lack of NTC behaviour may be established for many of the fuel components, their interactions with the NTC behaviour of PRFs, particularly in the context of an engine is yet to be established. Furthermore, there is a need to check if the ignition delay and Livengood-Wu methodology from Section 5.2.7 holds for all categories of fuel components—initial findings from unpublished research suggest that aromatic compounds may be an exception to the rule, but further work is required to establish this.

5.3.3 Residual Effects

The study of residual effects in this work centred around trapped residuals from firing— albeit with unspecified composition and nitric oxide. In reality, residuals contain a range of species, which varies depending on engine operating conditions. Notable components include CO_2, CO, water vapour, NO_2 and unburned hydrocarbons. These could be studied either by introducing isolated compounds into the inlet, as was done with NO in Section 3.3 or by employing exhaust gas recirculation (EGR) as is commonly used in mass-market engines.

5.3.4 Modelling and CFD

The results in this thesis, particularly surrounding the effect of nitric oxide on LTHR in Section 3.3 have significant implications for combustion modelling. So far, computational simulation of pre-spark heat release, or conditions where simultaneous LTHR and deflagration are likely, have not used a chemical kinetic model that correctly accounts of the effect of NO on LTHR. Recent modelling best practises have highlighted the need for chemistry to be modelled throughout the whole engine cycle (i.e. even when the valves are open) so as to account for residuals; the next logical step is to improve the NO chemistry submodel so that it correctly models the effect of NO, since it will almost certainly be present at some concentration. This should lead to tangible improvements of simulation of combustion near the knocking limit (since LTHR affects knocking behaviour)—which is of particular importance given that knocking is a key factor currently limiting ICE efficiency.

5.3.5 LTHR Chemistry

There is a clear opportunity for further species analysis of LTHR products, extending the work in Section 3.1 to analyse the approximately 80% of carbon that was not measured. This type of analysis would open up opportunities to develop and validate chemical mechanisms that model LTHR, based on their chemical products and not just thermodynamic behaviour. On a similar note, there is scope for deeper analysis on the large number of chemical reactions that take place during the LTHR process for example to discover precise reactions responsible for heat release or the reactions responsible for specific products—and how these reactions can be influenced by physical and chemical factors.

5.3.6 PLIF

Whilst the PLIF work in this thesis was only semi-quantitative, it laid the foundations for further development of the technique for LTHR measurements. Improvements that would enable a fully quantified method include designing an optical setup that can correct for variation in shot to shot intensity from the laser by using a precise and independent measurement of shot power, as well as calibrations and corrections for laser plane spatial variation. Furthermore, the setup used in this work could be further improved by using a laser system with a

higher pulse repetition rate, to capture multiple PLIF images in same cycle. Alternative optical arrangements could also be used to observe end gas LTHR, for example integrating a lens in piston window to give a wider field of view (which may negate the need for a non-standard ignition arrangement). Finally, PLIF could be used to directly measure in-cylinder temperatures, which could then be used to measure localised heat release in the end gas. This technique would likely need a temperature calibration technique, such as laser-induced grating spectroscopy.

5.3.7 LTHR-influenced Engine Design

The findings from this thesis could be used to influence future design. Specifically, the pressure-temperature trajectory of the fuel-air mixture during the compression and beginning of the expansion stroke could be controlled and optimised to take into account the influence of the mixture's specific LTHR behaviour. Boosting and inter cooling, which could adapt to upstream conditions, could be used to fine tune pressure-temperature trajectory. Of course, this would require relatively precise knowledge of the working fuel to understand the mixture's ignition delay contour.

For a fuel where LTHR reactions produce intermediates that are less knock prone, the pressure-temperature trajectory would be tuned to traverse the LTHR region, which would extend the knocking limit during traditional operation at high load (like in the work in Figure 7) and open up opportunities for controlled autoignition for increased efficiency at part load conditions without risking engine damage from autoignition. Conversely, if intermediates from LTHR are more reactive, the trajectory could be tuned to avoid the LTHR region, instead traversing through the NTC region to minimise risk of knocking at high load. At low loads the trajectory could be steered into the LTHR region to ultimately encourage end gas autoignition at conditions where it wouldn't normally occur, enabling the high efficiency, advanced combustion technique.

References

[1] Senecal, K. & Leach, F. C. P. *Racing Toward Zero: The Untold Story of Driving Green* (SAE International, 2021).

[2] Lindsey, R. If carbon dioxide hits a new high every year, why isn't every year hotter than the last? (2020).

[3] Stone, C. R. *Introduction to Internal Combustion Engines* (Macmillan International Higher Education, 2012), 4 edn.

[4] Regulation (eu) 2019/631 of the european parliament and of the council of 17 april 2019 setting co2 emission performance standards for new passenger cars and for new light commercial vehicles, and repealing regulations (ec) no 443/2009 and (eu) no 510/2011-2019 (2019).

[5] Electric vehicle outlook 2020. *BloombergNEF* (2023).

[6] Association, E. A. M. Report - vehicles in use, europe 2021: Acea - european automobile manufacturers' association (2021). URL `https://www.acea.auto/publication/report-vehicles-in-use-europe-january-2021/`.

[7] SMMT. 2020 uk automotive sustainability report (2020). URL `https://www.smmt.co.uk/reports/sustainability/`.

[8] Leach, F., Kalghatgi, G., Stone, R. & Miles, P. The scope for improving the efficiency and environmental impact of internal combustion engines. *Transportation Engineering* **1**, 100005 (2020).

[9] Heywood, J. B. *Internal Combustion Engine Fundamentals, Second Edition* (McGraw-Hill Education, New York, 2018), 2nd edition. edn. URL `https://www.accessengineeringlibrary.com/content/book/9781260116106`.

[10] Turner, J. *et al.* Ultra boost for economy: Extending the limits of extreme engine downsizing. *SAE International Journal of Engines* **7**, 387–417 (2014).

[11] Zhao, F., Lai, M.-C. & Harrington, D. Automotive spark-ignited direct-injection gasoline engines. *Progress in Energy and Combustion Science* **25**, 437–562 (1999).

[12] Iwamoto, Y., Noma, K., Nakayama, O., Yamauchi, T. & Ando, H. Development of gasoline direct injection engine. In *International Congress and Exposition* (SAE International, 1997).

[13] Blakey, S., Saunders, R., Ma, T. & Chopra, A. A design and experimental study of an otto atkinson cycle

engine using late intake valve closing. In *International Congress and Exposition* (SAE International, 1991).

[14] Fukuzawa, Y., Shimoda, H., Kakuhama, Y., Endo, H. & Tanaka, K. Development of high efficiency miller cycle gas engine (2001).

[15] Eisazadeh-Far, K. & Younkins, M. Fuel economy gains through dynamic-skip-fire in spark ignition engines. In *SAE 2016 World Congress and Exhibition* (SAE International, 2016).

[16] Wei, H., Zhu, T., Shu, G., Tan, L. & Wang, Y. Gasoline engine exhaust gas recirculation – a review. *Applied Energy* **99**, 534–544 (2012).

[17] Dennis, A. J., Garner, C. P. & Taylor, D. H. C. The effect of egr on diesel engine wear. In *International Congress and Exposition* (SAE International, 1999).

[18] Zheng, M., Reader, G. T. & Hawley, J. Diesel engine exhaust gas recirculation—a review on advanced and novel concepts. *Energy Conversion and Management* **45**, 883–900 (2004).

[19] Leach, F., Kalghatgi, G., Stone, R. & Miles, P. The scope for improving the efficiency and environmental impact of internal combustion engines. *Transportation Engineering* **1**, 100005 (2020).

[20] Ramadhas, A. S. *Alternative Fuels for Transportation* (CRC Press, 2011).

[21] Bušić, A. *et al.* Bioethanol production from renewable raw materials and its separation and purification: A review. *Food technology and biotechnology* **56**, 289–311 (2018). 30510474[pmid].

[22] Iodice, P. & Cardone, M. Ethanol/gasoline blends as alternative fuel in last generation spark-ignition engines: A review on co and hc engine out emissions. *Energies* **14** (2021). URL `https://www.mdpi.com/1996-1073/14/13/4034`.

[23] Kim, S. & Dale, B. Ethanol fuels: E10 or e85 – life cycle perspectives (5 pp). *The International Journal of Life Cycle Assessment* **11**, 117–121 (2006). URL `https://doi.org/10.1065/lca2005.02.201`.

[24] Kulzer, A. C. efuels: a further step towards sustainable mobility (2021). IMechE: Engineering fuels for the future: Climate neutral fuels for 1.5°C.

[25] Ueckerdt, F. *et al.* Potential and risks of hydrogen-based e-fuels in climate change mitigation. *Nature Climate Change* **11**, 384–393 (2021).

[26] Kokjohn, S. L., Hanson, R. M., Splitter, D. A. & Reitz, R. D. Fuel reactivity controlled compression ignition (rcci): a pathway to controlled high-efficiency clean combustion. *International Journal of Engine Research* **12**, 209–226 (2011). `https://doi.org/10.1177/1468087411401548`.

[27] Urushihara, T., Yamaguchi, K., Yoshizawa, K. & Itoh, T. A study of a gasoline-fueled compression ignition engine □ expansion of hcci operation range using si combustion as a trigger of compression ignition □. In *SAE 2005 World Congress& Exhibition* (SAE International, 2005).

[28] Ma, X. *et al.* An optical study of in-cylinder ch2o and oh chemiluminescence in flame-induced reaction

front propagation using high speed imaging. *Fuel* **134**, 603–610 (2014).

[29] Hu, Z., Zhang, J., Sjöberg, M. & Zeng, W. The use of partial fuel stratification to enable stable ultra-lean deflagration-based spark-ignition engine operation with controlled end-gas autoignition of gasoline and e85. *International Journal of Engine Research* **21**, 1678–1695 (2020).

[30] Bajwa, A. U., Leach, F. C. P. & Davy, M. H. Prospects of controlled auto-ignition based thermal propulsion units for modern gasoline vehicles. *Energies* **16** (2023).

[31] Martz, J., Kwak, H., Im, H., Lavoie, G. & Assanis, D. Combustion regime of a reacting front propagating into an auto-igniting mixture. *Proceedings of the Combustion Institute* **33**, 3001–3006 (2011).

[32] Hu, Z., Zhang, J., Sjöberg, M. & Zeng, W. The use of partial fuel stratification to enable stable ultra-lean deflagration-based spark-ignition engine operation with controlled end-gas autoignition of gasoline and e85. *International Journal of Engine Research* **21**, 1678–1695 (2020).

[33] Xu, C., Som, S. & Sjöberg, M. Large eddy simulation of lean mixed-mode combustion assisted by partial fuel stratification in a spark-ignition engine. *Journal of Energy Resources Technology* **143** (2021).

[34] Wang, Z., Liu, H. & Reitz, R. D. Knocking combustion in spark-ignition engines. *Progress in Energy and Combustion Science* **61**, 78–112 (2017).

[35] Livengood, J. & Wu, P. Correlation of autoignition phenomena in internal combustion engines and rapid compression machines. *Symposium (International) on Combustion* **5**, 347–356 (1955). URL `https://www.sciencedirect.com/science/article/pii/S0082078455800471`.

[36] Livengood, J. & Wu, P. Correlation of autoignition phenomena in internal combustion engines and rapid compression machines. *Symposium (International) on Combustion* **5**, 347–356 (1955).

[37] Astm d2699-19e1, standard test method for research octane number of spark-ignition engine fuel. Standard, ASTM International, West Conshohocken, PA (2019).

[38] Astm d2700-19e1, standard test method for motor octane number of spark-ignition engine fuel. Standard, ASTM International, West Conshohocken, PA (2019).

[39] Kalghatgi, G. Fuel anti-knock quality - part i. engine studies. In *SAE 2002 World Congress and Exhibition* (SAE International, 2001).

[40] Szybist, J. P. & Splitter, D. A. Pressure and temperature effects on fuels with varying octane sensitivity at high load in si engines. *Combustion and Flame* **177**, 49–66 (2017).

[41] Leppard, W. R. The chemical origin of fuel octane sensitivity. In *International Fuels and Lubricants Meeting and Exposition* (SAE International, 1990).

[42] Battin-Leclerc, F. Detailed chemical kinetic models for the low-temperature combustion of hydrocarbons with application to gasoline and diesel fuel surrogates. *Progress in Energy and Combustion Science* **34**, 440–498 (2008). URL `https://www.sciencedirect.com/science/article/pii/`

S0360128507000627.

[43] Saisirirat, P., Foucher, F., Chanchaona, S. & Mounaïm-Rousselle, C. Effects of ethanol, n-butanol — n-heptane blended on low temperature heat release and hrr phasing in diesel-hcci. In *9th International Conference on Engines and Vehicles* (Consiglio Nazionale delle Ricerche, 2009). URL https://doi.org/10.4271/2009-24-0094.

[44] Curran, H. J., Gaffuri, P., Pitz, W. J. & Westbrook, C. K. A comprehensive modeling study of iso-octane oxidation. *Combustion and Flame* **129**, 253–280 (2002). URL https://www.sciencedirect.com/science/article/pii/S001021800100373X.

[45] Curran, H., Gaffuri, P., Pitz, W. & Westbrook, C. A comprehensive modeling study of n-heptane oxidation. *Combustion and Flame* **114**, 149–177 (1998).

[46] Shibata, G., Oyama, K., Urushihara, T. & Nakano, T. The effect of fuel properties on low and high temperature heat release and resulting performance of an hcci engine. In *SAE 2004 World Congress& Exhibition* (SAE International, 2004).

[47] Shibata, G., Oyama, K., Urushihara, T. & Nakano, T. Correlation of low temperature heat release with fuel composition and hcci engine combustion,. *SAE Technical Paper* (2005).

[48] Mehl, M., Pitz, W., Sjöberg, M. & Dec, J. Detailed kinetic modeling of low-temperature heat release for prf fuels in an hcci engine (2009).

[49] Truedsson, I., Cannella, W., Johansson, B. & Tuner, M. Engine speed effect on auto-ignition temperature and low temperature reactions in hcci combustion for primary reference fuels. In *SAE 2014 International Powertrain, Fuels& Lubricants Meeting* (SAE International, 2014).

[50] Yang, Y., Dec, J. E., Dronniou, N. & Sjöberg, M. Tailoring hcci heat-release rates with partial fuel stratification: Comparison of two-stage and single-stage-ignition fuels. *Proceedings of the Combustion Institute* **33**, 3047–3055 (2011). URL https://www.sciencedirect.com/science/article/pii/S1540748910001999.

[51] Saxena, M. R., Rana, S. & Maurya, R. K. Analysis of Low- and High-Temperature Heat Release in Dual-Fuel RCCI Engine and Its Relationship With Particle Emissions. *Journal of Energy Resources Technology* **144**, 091201 (2022). https://asmedigitalcollection.asme.org/energyresources/article-pdf/144/9/091201/6855894/jert_144_9_091201.pdf.

[52] Willems, R., Willems, F., Deen, N. & Somers, B. Heat release rate shaping for optimal gross indicated efficiency in a heavy-duty rcci engine fueled with e85 and diesel. *Fuel* **288**, 119656 (2021).

[53] Kokjohn, S. L., Hanson, R. M., Splitter, D. A. & Reitz, R. D. Fuel reactivity controlled compression ignition (rcci): a pathway to controlled high-efficiency clean combustion. *International Journal of Engine Research* **12**, 209–226 (2011). https://doi.org/10.1177/1468087411401548.

[54] Szybist, J. P. & Splitter, D. A. Pressure and temperature effects on fuels with varying octane sensitivity at high load in si engines. *Combustion and Flame* **177**, 49–66 (2017).

[55] Splitter, D., Kaul, B., Szybist, J. & Jatana, G. Engine operating conditions and fuel properties on pre-spark heat release and spi promotion in si engines (2017).

[56] Waqas, M. U. *et al.* Detection of low temperature heat release (lthr) in the standard cooperative fuel research (cfr) engine in both si and hcci combustion modes. *Fuel* **256**, 115745 (2019). URL `https://www.sciencedirect.com/science/article/pii/S001623611931097X`.

[57] Splitter, D. A., Gilliam, A., Szybist, J. & Ghandhi, J. Effects of pre-spark heat release on engine knock limit. *Proceedings of the Combustion Institute* **37**, 4893–4900 (2019).

[58] DelVescovo, D. A., Splitter, D. A., Szybist, J. P. & Jatana, G. S. Modeling pre-spark heat release and low temperature chemistry of iso-octane in a boosted spark-ignition engine. *Combustion and Flame* **212**, 39–52 (2020). URL `https://www.sciencedirect.com/science/article/pii/S0010218019304651`.

[59] Splitter, D. A., Gilliam, A., Szybist, J. & Ghandhi, J. Effects of pre-spark heat release on engine knock limit. *Proceedings of the Combustion Institute* **37**, 4893–4900 (2019).

[60] Splitter, D., Kaul, B., Szybist, J. & Jatana, G. Engine operating conditions and fuel properties on pre-spark heat release and spi promotion in si engines. *SAE International Journal of Engines* **10**, 1036–1050 (2017). URL `https://www.jstor.org/stable/26285109`.

[61] Guo, Hengjie, Torelli, Roberto, Szybist, James & Som, Sibendu. Three-dimensional cfd investigation of pre-spark heat release in a boosted si engine. In *SAE WCX Digital Summit* (SAE International, 2021).

[62] Guo, H., Torelli, R., Szybist, J. P. & Som, S. Cfd modeling of pre-spark heat release in a boosted direct-injection spark-ignition engine. *International Journal of Engine Research* **24**, 3–15 (2023).

[63] Yamakawa, M. *et al.* Combustion technology development for a high compression ratio si engine. *SAE International Journal of Fuels and Lubricants* **5**, 98–105 (2012). URL `http://www.jstor.org/stable/26272866`.

[64] White, S. P., Bajwa, A. U. & Leach, F. C. P. Isolated low temperature heat release in spark ignition engines. *SAE International Journal of Advances and Current Practices in Mobility* (2024).

[65] Bajwa, A. U., White, S. P. & Leach, F. C. P. Low temperature heat release and phi-sensitivity characteristics of iso-octane/air mixtures. *Combustion Science and Technology* (2023).

[66] White, S. P. & Leach, F. C. P. Isolated low temperature heat release from binary blends of iso-octane, n-heptane and ethanol in a spark ignition engine. In *Proceedings of the ASME 2024 ICE Forward Conference*, Internal Combustion Engine Division Fall Technical Conference (2024).

[67] White, S. P., Bajwa, A. U. & Leach, F. C. P. Effect of ethanol and iso-octane blends on isolated low temperature heat release in a spark ignition engine. *SAE International Journal of Fuels and Lubricants*

(2024).

[68] White, S. P., Bajwa, A. U. & Leach, F. C. Effects of nitric oxide on isolated low temperature heat release in spark ignition engines. *Combustion and Flame* **273**, 113921 (2025).

[69] White, S. P., Willman, C. & Leach, F. C. Observing simultaneous low temperature heat release and deflagration in a spark ignition engine using formaldehyde planar laser induced fluorescence. *Applications in Energy and Combustion Science* **21**, 100321 (2025).

[70] Sarathy, S., Farooq, A. & Kalghatgi, G. T. Recent progress in gasoline surrogate fuels. *Progress in Energy and Combustion Science* **65**, 67–108 (2018).

In loving memory of my grandma Catherine, and my dog Tommy